



**NTNU – Trondheim**  
Norwegian University of  
Science and Technology

# Solar collectors' performance

A case study of a solar thermal heating  
system in a passive house dwelling

**Maria Jakobsons**

Master of Science in Mechanical Engineering

Submission date: July 2015

Supervisor: Hans Martin Mathisen, EPT

Co-supervisor: Magnar Berge, Høgskolen i Bergen

Norwegian University of Science and Technology  
Department of Energy and Process Engineering



EPT-M-2015-36

**MASTER THESIS**

for

Student Maria Jakobsons

Spring 2015

Solar collectors' performance  
*Solfangeres ytelse***Background**

Use of thermal solar collectors can provide a significant contribution to cover the heat demand in residential buildings with a renewable and affordable energy source, and is therefore an appropriate energy supply in low energy and passive houses. In 2008 it was installed solar systems in 28 passive houses in Løvåshagen cooperatives in Bergen, with solar collectors and accumulator/DHW tank for each apartment. These are intended to cover about 50% of the heating demand, mainly hot water.

Energy measurements going on since May 2013 show a considerably lower performance of the solar collectors than intended. It is in addition suspected a gravity driven circulation, i.e. a liquid flow because of temperature differences in the collector circuit even if the pump is not running, which leads to energy loss.

The task is to determine whether there are faults and weaknesses in the design, installation and operation and to analyze the consequences for energy performance. Based on the errors discovered and weaknesses changes will be implemented to system components and operating strategy in one apartment during the project period. Experiences from this apartment then forms the basis for a proposed list of actions for the remaining apartments.

The work was started as a specialization project and the master thesis will be in the continuation of this.

**Objective**

The objective of the work is to contribute to increased energy production from the solar plant by analyzing the existing solution by measurements and simulations, changing and adjusting the system components and control system.

**The following tasks are to be considered:**

1. Continuation of the literature survey done in the project

2. Perform simulations of the existing solution and study the influence of different parameters.
3. Compare with measured values and the extent of shading. Two flats are used for comparison.
4. Study the effect of modifications
5. Suggest new solutions and simulate the performance of these.

-- " --

Within 14 days of receiving the written text on the master thesis, the candidate shall submit a research plan for his project to the department.

When the thesis is evaluated, emphasis is put on processing of the results, and that they are presented in tabular and/or graphic form in a clear manner, and that they are analyzed carefully.

The thesis should be formulated as a research report with summary both in English and Norwegian, conclusion, literature references, table of contents etc. During the preparation of the text, the candidate should make an effort to produce a well-structured and easily readable report. In order to ease the evaluation of the thesis, it is important that the cross-references are correct. In the making of the report, strong emphasis should be placed on both a thorough discussion of the results and an orderly presentation.

The candidate is requested to initiate and keep close contact with his/her academic supervisor(s) throughout the working period. The candidate must follow the rules and regulations of NTNU as well as passive directions given by the Department of Energy and Process Engineering.


Risk assessment of the candidate's work shall be carried out according to the department's procedures. The risk assessment must be documented and included as part of the final report. Events related to the candidate's work adversely affecting the health, safety or security, must be documented and included as part of the final report. If the documentation on risk assessment represents a large number of pages, the full version is to be submitted electronically to the supervisor and an excerpt is included in the report.

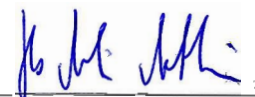
Pursuant to "Regulations concerning the supplementary provisions to the technology study program/Master of Science" at NTNU §20, the Department reserves the permission to utilize all the results and data for teaching and research purposes as well as in future publications.

The final report is to be submitted digitally in DAIM. An executive summary of the thesis including title, student's name, supervisor's name, year, department name, and NTNU's logo and name, shall be submitted to the department as a separate pdf file. Based on an agreement with the supervisor, the final report and other material and documents may be given to the supervisor in digital format.

- Work to be done in lab (Water power lab, Fluids engineering lab, Thermal engineering lab)  
 Field work

Department of Energy and Process Engineering, 14. January 2015

  
\_\_\_\_\_  
Olav Bolland  
Department Head

  
\_\_\_\_\_  
Hans Martin Mathisen  
Academic Supervisor

## Preface

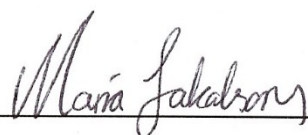
---

This master thesis was completed in spring 2015 at the Norwegian University of Science and Technology in Trondheim. It was written at the Department of Energy and Process as a part of the 5-year master's degree programme Mechanical Engineering, with a specialization in Energy and Indoor Environment.

First of all, I would like to thank my supervisor Hans Martin Mathisen for very good guidance and advice during this work. I would also like to give a special thanks to Magnar Berge from the Bergen University College, not only for providing access to measured data, but for always being available to answer questions about the examined system. I would like to express my gratitude towards Vela Solaris, who provided a free educational licence for the simulation software Polysun, to be used in this thesis. I also wish to thank John H. Skjølberg from Skjølberg Energiteknikk for contributing with his expertise on solar thermal systems, and for his comments regarding the investigated system.

I am especially grateful to my sister who spent hours reading through this master thesis, immersing herself in a topic that is far from her field of study. Without her help, this thesis would never have been finished on time.

Last, but not least, I wish to thank my boyfriend for all the support he has given me during the execution of this thesis. Thank you for repeatedly reminding me to take a break from writing, and for making sure I had a decent meal every day.



---

Maria Jakobsons

Trondheim, 10. June 2015



## Abstract

---

This study examines a solar thermal heating system consisting of evacuated tube collectors used for combined space heating and heating of domestic hot water. The investigated system belongs to one of the passive house dwellings of Løvåshagen housing cooperative, located in Bergen, Norway. Since the beginning of its operation in 2008, preliminary measurements suggest that the solar collectors are not performing as well as initially intended. The objective of this thesis was to determine potential faults and weaknesses, concerning both the design and the operation of the system, and to contribute to increased solar utilization.

For this purpose, the functioning and performance of the investigated system was studied. This was achieved by collecting and processing measured data that was available in relation to an ongoing study. In addition, a simulation model of the investigated system was created in Polysun. By comparing simulated results with measured results, an outline of the present system performance was established. Furthermore, a parametric study was performed on the simulation model, in which the influence of various design- and operation parameters on system performance was examined. The investigated parameters included collector area, inclination angle and orientation angle of the collector, tank size, insulation of pipes and tank, volumetric flow rate, as well as parameters related to the control of the system and the extent of shading. This examination provided a basis for suggesting several improved scenarios that each targeted different components. By combining these scenarios in different ways, the best possible system configuration could be obtained.

It was found that the examined system is far from achieving its initial design goals of an annual solar fraction of 47%. In 2014, the measured solar fraction was only 10,8%, whereas the corresponding simulated solar fraction was 14,3%. With the current design and operation, the monthly energy savings are minimal - even during the high-radiation periods -, thus the benefit of having solar collectors installed on the roof seems questionable. However, the results from the parametric study revealed that by correcting and improving certain design and operation parameters of the investigated system, a simulated solar fraction of almost 43% could be achieved. Even by making just a few alterations assumed to be easy and relatively inexpensive to implement, a simulated annual solar fraction of approximately 29% was obtained. Other than shading caused by nearby collectors, the most essential parameters appear to be the those related to the control of the system, as well as tank design and switch-on temperature of the auxiliary heating element.

It can be concluded that though the potential for increasing the solar utilization is considerable, any alterations must be evaluated according to additional costs. Moreover, the results demonstrate the importance of thorough research and mapping of the potential performance-reducing factors, already during the design phase. Shading by means of nearby collectors is an especially important aspect to consider. This can be achieved with the help of proper simulation tools that include a shading simulator. Lastly, once the system is installed, it is equally important to ensure proper monitoring and control of the functioning of the system.





## Sammendrag

---

I denne studien undersøkes et foreslått solfangersystem bestående av vakuumsolfangere, som brukes i et kombinert system for oppvarming av både rom og varmtvann. Systemet tilhører en av passivhusleilighetene i Løvåshagen borettslag som ligger i Bergen, i Norge. Siden oppstarten av systemets drift i 2008, har foreløpige målinger vist at utbyttet fra solfangerne er lavere enn forventet. Målet med denne oppgaven var å avgjøre om det finnes feil eller svakheter ved designet og driften av systemet, samt å bidra til økt energiutnyttelse av solfangeranlegget.

For å oppnå dette målet ble det utvalgte systemets drift og energiutnyttelse undersøkt. Dette ble gjort ved å samle og bearbeide målinger utført i forbindelse med en pågående studie. I tillegg ble det laget en modell i simuleringsverktøyet Polysun. Ved å sammenligne simulerte resultater med målte resultater fra 2014, var det mulig å evaluere systemets daværende prestasjon. Videre ble en parameterstudie utført på simuleringsmodellen, hvor effekten av diverse design- og driftsparametere ble undersøkt. De undersøkte parameterne inkluderte solfangerareal, solfangernes vinkel, orienteringsvinkel, tankstørrelse, isolasjon av rør og tank, volumstrøm, samt parametere som påvirker systemstyring og skyggenivå. Denne undersøkelsen la grunnlaget for flere foreslåtte forbedrede scenarier, som hver av dem tok for seg de viktigste komponentene i et termisk solfangersystem. Ved å kombinere disse scenariene på ulike måter, kom man fram til den mest optimale konfigurasjonen.

Gjennom undersøkelsen ble det oppdaget at det undersøkte systemet langt fra lyktes i å oppnå de opprinnelige målene for den årlige soldekningsgraden, som var satt til 47%. I 2014 var soldekningsgraden målt til å ligge på kun 10,8%, mens den tilsvarende simulerte soldekningsgraden lå på 14,3%. Med systemets nåværende design og drift, ligger den månedlige energisparingen på et minimalt nivå - selv under perioder med høy solinnstråling. Dette skaper tvil rundt det reelle utbyttet av å ha installert solfangere i de to passivhusene i Løvåshagen borettslag. På den annen side viser resultatene i parameterstudien at man, ved å korrigere og forbedre visse design- og driftsparametere i referansesystemet, kan oppnå en simulert soldekningsgrad på nesten 43%. Selv ved å gjøre kun de endringene som vurderes som enkle, samt relativt billige å gjennomføre, ble det gjennom simuleringen oppnådd en soldekningsgrad på ca. 29%. Med unntak av skyggenivå forårsaket av nærliggende solfangere, ser de viktigste parameterne ut til å være de som er tilknyttet solsystemets styring, samt designet av tanken og el-kolbens aktiveringstemperatur.

Til tross for at potensialet for økt solutnyttelse er betydelig, kan det konkluderes med at enhver endring må evalueres med tanke på tilleggskostnader. Resultatene gir dessuten et innblikk i viktigheten av å gjøre grundig forarbeid allerede under designfasen, gjennom undersøkelser og kartlegging av faktorer som potensielt kan ha en reduserende effekt på energiutnyttelsen. Skygging fra nærliggende solfangere er en spesielt viktig faktor som må tas hensyn til, og som kan unngås ved hjelp av tilstrekkelig simuleringsverktøy som tilbyr skyggesimulering. Ikke minst er det viktig å sørge for tilstrekkelig overvåking og styring av systemets drift.



## List of figures

---

Figure 1: Solar irradiation on a horizontal surface in Norway, winter (left) and summer (right) (Rindal & Salvesen, 2008) .....	23
Figure 2: Monthly solar irradiation per m <sup>2</sup> surface area. Simulated towards south at an optimum inclination angle (European Commission, 2015) .....	24
Figure 3: Solar irradiance with varying sky conditions (DGS, 2010) .....	25
Figure 4: Angles used in solar technology (DGS, 2010) .....	25
Figure 5: Monthly variation of the optimum inclination angle (°) in Bergen (European Commission, 2015) .....	26
Figure 6: Net heat demand in a building (NS3031:2014) .....	27
Figure 7: Typical energy consumption for a residential building according to different energy standards and building regulations (Andresen, 2008) .....	27
Figure 8: Graphic illustration of the criteria in Table 2 for a passive house residential building located in Bergen ( $\theta_{ym} \geq 6,3^{\circ}\text{C}$ ) with floor areas, $A_n$ , less than 250 m <sup>2</sup> .....	28
Figure 9: Variation in required heat demand and available solar energy during the course of one year (Zijdemans, 2012) .....	29
Figure 10: Schematic of a solar thermal system for preparation of hot water. Left: Direct system. Right: Indirect system (Andresen, 2008) .....	30
Figure 11: Overview of the main components of a solar thermal system .....	31
Figure 12: The main components of a flat-plate collector and the thermal processes (Quaschnig, 2005). .....	32
Figure 13: The main components and function of the evacuated tube collector with heat pipe, seen from the top and from the side (Quaschnig, 2005) .....	33
Figure 14: Collector efficiencies at different irradiances and temperature differences (Quaschnig, 2004) .....	34
Figure 15: Efficiency characteristic curves and their areas of application for different collector types. Assumed irradiated power of 1000 W/m <sup>2</sup> (DGS, 2010) .....	35
Figure 16: The variables influencing the necessary distance between two collector rows (AEE Intec, 2004) .....	36
Figure 17: Minimum row distance according to the solar altitude angle for various collector inclination angles .....	37
Figure 18: Common types of store charging with solar energy. S= temperature sensor (DGS, 2010) .....	39
Figure 19: Types of store charging with auxiliary heating (AH) S= temperature sensor (DGS, 2010) .....	39
Figure 20: Left: Stratification. Right: Uniform mixed temperature (additional heating needed) (DGS, 2010) .....	40
Figure 21: An overview of the components of a solar circuit .....	43
Figure 22: Left: Finned tube heat exchanger. Right: Plain tube heat exchanger (DGS, 2010) .....	45
Figure 23: Left: Plate heat exchanger. Right: Tubular heat exchanger (DGS, 2010) .....	46
Figure 24: A daily progression of a temperature difference controller with respect to collector temperature and heat store temperature (DGS, 2010) .....	48
Figure 25: Left: Distribution of the phases during which errors normally occur in a solar thermal heating system. Right: Distribution of common errors (DGS, 2010) .....	49
Figure 26: Function of a heat meter (Auquametro, 2015) .....	50
Figure 27: Comparison of conventional heating system and a solar heating system (Standard Norge, 2012) .....	53

Figure 28: Overview of Løvåshagen housing cooperative (Northpass, 2011) .....	54
Figure 29: Calculated monthly solar fraction (Andresen, 2008) .....	56
Figure 30: Left: A schematic illustration of the Apricus evacuated tube collector (Apricus, 2011). Right: Construction of an Apricus AP-20 tube: 1) Glazing 2) Heat-conduction metal sheet 3) Heat pipe 4) Vacuum 5) Absorber (SPF, 2004) .....	56
Figure 31: Illustration of the customized CTC tank used in the solar thermal heating system .....	57
Figure 32: Hydraulic scheme of the solar circuit. <i>Source: Skjølberg Energiteknikk</i> .....	58
Figure 33: Pictures taken of the solar thermal systems at Løvåshagen. Top and bottom left: Incomplete insulation of pipes and connections. Top and bottom right: Broken collector tubes. Photos: Magnar Berge .....	60
Figure 34: Image of the customized storage tank and the hydraulic connections .....	61
Figure 35: Modified system. <i>Source: Skjølberg Energiteknikk</i> .....	62
Figure 36: The different boundary layers for Esol, Qsol and Ssol.....	65
Figure 37: A principal sketch of the instrument setup for remote monitoring.....	67
Figure 38: Top: auxiliary energy consumption curve of the immersed electrical heating element. Bottom: Solar yield curve.....	69
Figure 39: The solar yield curve of the collectors, both before and after correction.....	70
Figure 40: Polysun horizon editor (Pressbox, 2014) .....	74
Figure 41: Open Street Map viewer in Polysun.....	75
Figure 42: Global irradiation (direct and diffuse) on a horizontal surface ( $W/m^2$ ) in Fyllingsdalen in Bergen .....	76
Figure 43: Average outdoor temperature in Fyllingsdalen in Bergen .....	76
Figure 44: Red line: The horizon for the chosen location. Yellow line: Altitude angle of the sun on June 1 <sup>st</sup> at 12:00 PM.....	77
Figure 45: Hydraulic scheme of the simulation model created in Polysun.....	78
Figure 46: Simplified sketch of the various tank component inputs in Polysun.....	80
Figure 47: Measured DHW consumption curve from 2014, imported into Polysun .....	82
Figure 48: Cold city water temperature during 2014 on an hourly basis. <i>Source: Bergen Vann KF</i> .....	82
Figure 49: Illustration of the controller inputs and outputs in Polysun .....	83
Figure 50: The twelve isothermal tank layers in Polysun (Vela Solaris, 2014).....	85
Figure 51: Monthly measured heat demand for DHW in 2014 and 2015 .....	86
Figure 52: Measured monthly heat demand for heating of bathroom floor in 2014 and 2015.....	87
Figure 53: Measured and simulated monthly solar yield .....	88
Figure 54: Measured and simulated monthly auxiliary energy supplied to the tank (immersed electrical heating element) .....	88
Figure 55: Measured and simulated energy supplied to the tank in 2014. The measured total heat demand for heating of DHW and space heating in 2014 is included with a dotted line .....	89
Figure 56: Measured and simulated monthly solar fraction .....	90
Figure 57: Comparison between the investigated solar thermal system (reference system) and the use of only conventional heating (electricity).....	91
Figure 58: Measured heat supplied to the tank, heat demand for space heating, and heating of DHW from January 1 <sup>st</sup> to May 31 <sup>st</sup> .....	92
Figure 59: Irradiated power per $m^2$ collector aperture area throughout the year. Total aperture area is $3,8 m^2$ .....	94
Figure 60: Monthly maximum irradiated power per square meter collector aperture area [ $W/m^2$ ]. .....	95
Figure 61: Simulated monthly energy transferred from the collectors to the solar circuit (collector yield), together with the corresponding irradiation onto collector (aperture) area .....	96

Figure 62: Monthly simulated collector efficiency [%].....	97
Figure 63: The efficiency curve for Apricus AP-20 for different irradiated powers ( $W/m^2$ ) .....	97
Figure 64: Monthly maximum and minimum volumetric flow rate during one year .....	98
Figure 65: Flow rate through the collectors on an hourly basis throughout the year .....	99
Figure 66: Daily maximum collector temperature during one year .....	99
Figure 67: Annual heat loss in the solar circuit in kWh.....	100
Figure 68: Monthly amount of solar energy supplied to the tank, $S_{sol}$ , together with the corresponding collector yield, $Q_{sol}$ .....	101
Figure 69: Energy flow per hour in the internal solar heat exchanger (solar coil) .....	101
Figure 70: Monthly mean tank layer temperatures.....	102
Figure 71: Tank layer temperatures from bottom layer (blue) to top layer (red).....	102
Figure 72: Operation of solar pump vs. solar energy supplied to tank.....	104
Figure 73: Daily operation (June 1 <sup>st</sup> ) of the solar pump (l/h) based on bottom tank temperature and collector outflow temperature ( $^{\circ}C$ ) .....	105
Figure 74: The effect of incorrect controller settings (June 1 <sup>st</sup> ) .....	106
Figure 75: Operation of the auxiliary heater on June 1 <sup>st</sup> .....	107
Figure 76: Illustration of solar energy flow from the collectors to the storage tank .....	107
Figure 77: Overview of the main categorization in the parametric study.....	111
Figure 78: Solar altitude diagram (yellow) for the six first months together with the horizon line (red). The pronounced peak in the middle of the horizon profile represents the impact of row-to-row shading.....	113
Figure 79: The four horizons simulated in Polysun to study the effect of shading .....	114
Figure 80: The effect of shading on monthly solar fraction for different shading conditions .....	114
Figure 81: The difference between solar irradiation, collector yield and solar energy supplied to the tank in kWh/year, both <i>with</i> and <i>without</i> shading .....	115
Figure 82: The effect of row distances 1-10 m on the horizon line (red). The yellow line represents the sun path on June 1 <sup>st</sup> .....	116
Figure 83: The effect of row-to-row distance on system performance.....	117
Figure 84: The effect of row-to-row distance on annual collector yield (left) and solar fraction (right) for collector inclination angles of $20^{\circ}$ , $40^{\circ}$ and $60^{\circ}$ .....	117
Figure 85: Effect of orientation (left) and the inclination angle (right) on system performance .....	118
Figure 86: The impact on annual solar fraction when tilting all the collectors at Løvåshagen housing cooperative at different inclination angles within the recommended range of $20^{\circ}$ - $80^{\circ}$ .....	119
Figure 87: Effect of different inclination angles on system performance when shading is eliminated..	120
Figure 88: Effect of collector area on system performance.....	121
Figure 89: The effect of solar collector (absorber) area on annual performance .....	121
Figure 90: Monthly solar fraction for different collector absorber areas, both <i>with</i> shading (left) and <i>without</i> shading (right) .....	122
Figure 91: Monthly average collector efficiency <i>with</i> and <i>without</i> shading of the collectors .....	123
Figure 92: Efficiency curves of the collectors. Left: clear, sunny day ( $1000 W/m^2$ ). Right: cloudy day ( $300 W/m^2$ ) .....	124
Figure 93: System performance for each collector type.....	125
Figure 94: Effect of tank insulation thickness on annual performance .....	126
Figure 95: Effect of tank volume on system performance .....	127
Figure 96: Effect of tank height on system performance .....	128
Figure 97: The input positions of coils and electrical heating element in the tank in Polysun. ....	129

Figure 98: Effect of tank coils- and heating element position on annual solar fraction.....	129
Figure 99: Effect of tank coils- and heating element position on annual specific delivered energy.....	130
Figure 100: Effect of solar coil height on system performance.....	131
Figure 101: Effect of solar heat exchanger area on system performance.....	132
Figure 102: The effect of pipe insulation thickness on system performance.....	134
Figure 103: The impact of pipe insulation thickness on annual heat loss in the solar circuit and on annual solar energy supplied to the storage tank.....	134
Figure 104: Effect of external pipe diameter on annual performance. Wall thickness is 1 mm .....	135
Figure 105: Left: Cross-section of the building. Right: overview of how the two collectors are installed with respect to each other on the roof .....	136
Figure 106: Top: Effect of indoor (left) and outdoor (right) pipe length on system performance. Bottom: Heat loss to indoor or outdoor room as a function of indoor or outdoor pipe lengths.....	137
Figure 107: Current collector layout (left) and suggested improved collector layout (right) .....	138
Figure 108: Effect of solar circuit pipe length on system performance.....	139
Figure 109: The various tank sensor locations that were simulated in Polysun .....	140
Figure 110: Effect of different locations of the tank sensor on monthly solar fraction.....	141
Figure 111: Solar pump control (1=ON, 0=OFF) during one week in June for the two different sensor locations.....	142
Figure 112: Energy flow in the solar coil for two different tank locations. Positive values represent energy that is supplied to the tank, whereas negative values represent energy withdrawal .....	143
Figure 113: The effect of $\Delta T$ switch-on and $\Delta T$ switch-off settings on annual system performance.....	144
Figure 114: The effect on system performance when changing the switch-on temperature of the auxiliary heater. The switch-off temperature is 2°C higher than the switch-on temperature.....	145
Figure 115: The impact of various switch-on temperatures on the amount of solar- and auxiliary energy supplied to the tank.....	145
Figure 116: Effect of volumetric flow rate (l/h) on annual system performance .....	147
Figure 117: Monthly solar fraction in May, June and July for pump speed stage 1, 2 and 3 .....	148
Figure 118: The effect of average daily DHW consumption on annual performance.....	150
Figure 119: The distribution of solar- and auxiliary energy supplied to the tank for different average daily DHW consumptions .....	150
Figure 120: Selected draw-off profiles available in Polysun .....	151
Figure 121: Effect of different draw-off profiles on annual system performance .....	152
Figure 122: Effect of annual heat demand for space heating on annual system performance .....	152
Figure 123: Distribution of auxiliary- and solar energy supplied to the tank for various annual space heating demands .....	153
Figure 124: Summary of the parametric study conducted on various design- and operation parameters .....	154
Figure 125: Annual solar fraction and specific delivered energy for improved scenarios .....	158
Figure 126: Sensitivity analysis of Scenario 18, annual solar fraction (right) and annual specific delivered energy (left) .....	161
Figure 127: Monthly share of solar- and auxiliary energy with the corresponding solar fraction (Scenario 18).....	163
Figure 128: Specific delivered energy, Reference system vs. Scenario 18 .....	164
Figure A. 1 Remote readings 2014 and 2015.....	180

<b>Figure A. 2: Daily mean air temperature, daily mean air humidity (%) and daily precipitation in Bergen for 2014 (blue) and 2015 (red) Source: Meteorologisk institutt .....</b>	<b>182</b>
<b>Figure B. 1: Test report for the Apricus AP-20 collector (SPF, 2004) .....</b>	<b>184</b>
<b>Figure B. 2: Pump curves for Wilo Star ST 20/6. 3 levels: high (max.), medium and low (min.) (Wilo, 2004) .....</b>	<b>186</b>
<b>Figure B. 3: Pre-insulated pipes (Armacell, n.d) .....</b>	<b>187</b>
<b>Figure C. 1: The effect of collector orientation (left) and inclination (right) angle on system performance .....</b>	<b>189</b>
<b>Figure C. 2: Effect of solar coil material on system performance .....</b>	<b>189</b>
<b>Figure C. 3: Effect of glycol percentage in solar liquid on system performance .....</b>	<b>190</b>

## List of tables

---

Table 1: Average monthly and annual amount of solar hours in Bergen during based on measurements from 1961-1990 (Meteorologisk Institutt, 2009) .....	24
Table 2: Norwegian passive house criteria for maximum calculated net energy demand for space heating in residential buildings (NS 3700, 2013) .....	28
Table 3: Standard values for annual hot water demand (NS3031, 2014).....	29
Table 4: Simplified estimation of required solar collector area for multi-family dwellings (Zijdemans, 2012).....	36
Table 5: Simplified dimensioning of a storage tank volume in a solar thermal heating system for multi-family dwellings (Zijdemans, 2012).....	41
Table 6: Freezing point of propylene glycol at different ratios water-glycol mix ratios [%] (Zijdemans, 2012).....	44
Table 7: Cause-effect assignment of errors in a solar thermal energy system (DGS, 2010) .....	51
Table 8: Estimated net heat demand for the passive house dwellings (Northpass, 2011).....	55
Table 9: Solar fraction of total heat supply (Northpass, 2011).....	55
Table 10: Optical collector efficiency ( $\eta_0$ ) and heat loss coefficients ( $a_1$ and $a_2$ ) for the three reference areas (SPF, 2004).....	57
Table 11: Annual delivered energy and annual specific delivered energy 2011, 2012 and 2013 (Obtained from BKK via Magnar Berge) .....	59
Table 12: Overview of each sensor type and its location on the solar thermal heating system .....	67
Table 13: Measured cold city water temperature in 2014 .....	72
Table 14: Coordinates and corresponding weather data for the location of Løvåshagen housing cooperative in Bergen, annual sums .....	75
Table 15: Shading editor inputs: Mutual shading .....	77
Table 16: Overview of component inputs .....	78
Table 17: Inputs for annual heat demand (DHW and space heating) in Polysun .....	81
Table 18: Controller inputs based on the actual controller settings in 2014.....	84
Table 19: Measured heat demand in 2014 for the investigated dwelling .....	87
Table 20: Measured (2014) and simulated annual solar fraction .....	90
Table 21: Fractional energy savings for the investigated system, annual sums .....	92
Table 22: Heat supply vs. heat demand Jan-May 2014 and Jan-May 2015 .....	93
Table 23: Irradiation onto the two collectors, annual sums.....	95
Table 24: Collector performance, annual sums.....	97
Table 25: Tank heat loss.....	103
Table 26: Operation of the solar pump, annual sums .....	104
Table 27: Effect of shading on system performance .....	115
Table 28: Potential improvement of system performance when altering the inclination angle .....	120
Table 29: Effect of one, two or three collectors on annual performance, both <i>with</i> and <i>without</i> shading .....	122
Table 30: Characteristics of the different solar collectors simulated in Polysun .....	124
Table 31: Effect of tank insulation thickness on annual performance for three cases .....	126
Table 32: Thermal conductivity of selected materials .....	133
Table 33: Simulated cases.....	138
Table 34: Annual heat loss for each case, both with and without improved collector layout.....	139
Table 35: Annual performance for five different tank sensor locations.....	141



<b>Table 36: Heat loss in the solar circuit with different tank sensor locations .....</b>	<b>143</b>
<b>Table 37: Impact of measures for Legionella protection on annual system performance.....</b>	<b>146</b>
<b>Table 38: Daily DHW demand according to different consumption levels and number of persons in the household.....</b>	<b>149</b>
<b>Table 39: Suggested improved scenarios .....</b>	<b>156</b>
<b>Table 40: Scenario 0: Limited modifications .....</b>	<b>158</b>
<b>Table 41: Fractional energy savings compared to reference system .....</b>	<b>164</b>
<b>Table 42: Summary annual values, Scenario 18.....</b>	<b>164</b>
<b>Table A. 1: Measured results from 2014 (annual sums) - Remote readings 01.01.14 - 31.12.14 .....</b>	<b>179</b>
<b>Table A. 2: Measured results from 2015 - Remote readings 01.01.15 - 31.05.15.....</b>	<b>179</b>
<b>Table A. 3: Direct readings of the meter displays during six plant visits.....</b>	<b>181</b>
<b>Table A. 4: Extracted values from Table A.3: Direct readings 11.11.13 - 19.11.14.....</b>	<b>181</b>
<b>Table A. 5: Measurements from a second passive house dwelling (28.05.2013 - 18.06.2014) .....</b>	<b>181</b>
<b>Table B. 1: Technical specification for the storage tank and the two coils.....</b>	<b>184</b>
<b>Table B. 2: Thermal properties of selected stainless steel types. Source: Norwegian Standard NS-EN 10088-1:2004, Stainless steels - Part 1: List of stainless steels .....</b>	<b>185</b>
<b>Table B. 3: Extract of technical pump data for Wilo Star ST 20/6 (Wilo, 2004) .....</b>	<b>185</b>
<b>Table B. 4: Properties of Armaflex DuoSolar Cu (Armacell, n.d).....</b>	<b>187</b>
<b>Table B. 5: Thermal properties of Tyfocor L (Tyforop, 2009).....</b>	<b>188</b>

# Table of Contents

---

<b>Preface</b> .....	<b>1</b>
<b>Abstract</b> .....	<b>3</b>
<b>Sammendrag</b> .....	<b>5</b>
<b>List of figures</b> .....	<b>7</b>
<b>List of tables</b> .....	<b>12</b>
<b>Nomenclature</b> .....	<b>19</b>
<b>Definitions</b> .....	<b>20</b>
<b>1 Introduction</b> .....	<b>21</b>
1.1 Background and objective.....	21
1.2 Structure of the report and limitations.....	21
<b>2 Potential for utilizing solar thermal energy</b> .....	<b>23</b>
2.1 Variation in solar irradiation .....	23
2.1.1 Annual solar hours .....	24
2.1.2 Local weather.....	24
2.1.3 Orientation and inclination angle of the receiving surface .....	25
2.2 Energy demand in low energy and passive house buildings .....	26
2.2.1 Space heating.....	27
2.2.2 Heating demand for heating of domestic hot water (DHW) .....	28
2.3 Heating with solar thermal energy .....	29
<b>3 Design and operation of a solar thermal system</b> .....	<b>30</b>
3.1 Solar collector .....	31
3.1.1 Flat-plate collector and evacuated tube collector.....	31
3.1.2 Collector performance and collector efficiency .....	33
3.1.3 Required solar collector area.....	35
3.1.4 Shading .....	36
3.2 Thermal heat storage.....	38
3.2.1 Types and configurations.....	38
3.2.2 Thermal stratification and energy contents of a store.....	39
3.2.3 Design and dimensioning of the storage tank.....	41

3.2.4 Temperature requirements in storage tanks.....	42
3.3 Solar circuit.....	43
3.3.1 Pipelines.....	43
3.3.2 Solar liquid .....	44
3.3.3 Solar pump.....	44
3.3.4 Solar heat exchanger .....	45
3.3.5 Return-flow prevention .....	46
3.3.6 Overheating protection .....	46
3.4 Controller .....	47
<b>4 Function and yield control of small solar thermal systems .....</b>	<b>49</b>
4.1 Function and yield control .....	50
4.2 Fault detection.....	51
4.2.1 Troubleshooting.....	51
4.2.2 Simulation-based fault detection .....	52
4.3 Evaluation of system performance.....	52
<b>5 Case description .....</b>	<b>54</b>
5.1 Løvåshagen .....	54
5.2 Heat demand and heat supply .....	55
5.3 Description of the solar thermal system.....	56
5.4 Relevant experiences and findings.....	59
5.5 Ongoing study .....	60
5.6 Visual check.....	60
5.7 Modification 2015.....	61
<b>6 Methodology .....</b>	<b>63</b>
<b>7 Description of measurements .....</b>	<b>66</b>
7.1 Devices.....	66
7.2 Reliability of devices and challenges during measurements.....	67
7.2.1 Challenges during measurements .....	68
7.2.2 Correction of measured results and stipulation of missing values.....	68

7.2.3 Estimation of annual DHW consumption curve .....	71
7.3 Volume to energy conversion .....	71
7.4 Suspicion of return-flow .....	72
<b>8 Simulation inputs .....</b>	<b>73</b>
8.1 Description of Polysun.....	73
8.2 Meteorological inputs.....	75
8.2.1 Location and climate settings .....	75
8.2.2 Horizon profile and collector field settings.....	77
8.3 Polysun model.....	78
8.3.1 Hydraulic scheme.....	78
8.3.2 Component overview .....	78
8.3.3 Comments regarding Polysun inputs vs. actual conditions .....	80
8.4 Heat demand input .....	81
8.4.1 Heating of domestic hot water and space heating.....	81
8.4.2 Annual DHW consumption profile.....	82
8.4.3 Hot and cold temperature setting .....	82
8.5 Controller inputs.....	83
8.5.1 Controller settings .....	83
<b>9 Results .....</b>	<b>86</b>
9.1 Heat demand .....	86
9.2 Energy supply .....	87
9.3 System performance.....	89
9.3.1 Solar fraction.....	89
9.3.2 Fractional energy savings.....	91
9.3.3 Original system vs. modified system .....	92
9.4 Detailed simulated results .....	93
9.4.1 Collector.....	94
9.4.2 Solar circuit .....	98
9.4.3 Storage tank.....	101

9.4.4 Controller .....	103
9.5 Discussion of measured and simulated results .....	107
<b>10 Parametric study .....</b>	<b>111</b>
10.1 Introduction .....	111
10.2 Design parameters .....	113
10.2.1 Collector .....	113
10.2.2 Tank .....	126
10.2.3 Solar circuit pipelines .....	133
10.3 Operation parameters .....	140
10.3.1 Solar pump controller .....	140
10.3.2 Control of the auxiliary heater .....	144
10.3.3 Effect of volumetric flow rate in the solar circuit .....	146
10.3.4 Effect of propylene glycol concentration of the solar liquid .....	148
10.4 Parameters related to the user .....	149
12.4.1 Effect of DHW demand .....	149
10.4.2 Effect of daily DHW consumption profiles .....	151
10.4.3 Effect of space heating demand .....	152
10.5 Summary of parametric study .....	153
10.6 Suggested improved scenarios .....	155
10.7 Sensitivity analysis of the best scenario .....	160
10.8 System performance with improved design and operation .....	162
<b>11 Discussion .....</b>	<b>165</b>
11.1 Original system .....	165
11.2 Modified system .....	168
11.3 General comments .....	170
<b>12. Conclusion .....</b>	<b>172</b>
<b>13 Future work .....</b>	<b>174</b>
<b>14 References .....</b>	<b>175</b>
<b>Appendix A – Measured data .....</b>	<b>179</b>
A.1 Remote readings .....	179

A.2 Direct readings .....	181
A.3 Weather data for 2014 and 2015 .....	182
<b>Appendix B - Detailed component specifications .....</b>	<b>183</b>
B.1 Collector .....	183
B.2 Storage tank .....	184
B.3 Solar circuit .....	185
B.3.1 Solar pump.....	185
B.3.2 Pipelines.....	187
B.3.3 Solar liquid .....	188
<b>Appendix C – Parametric study .....</b>	<b>189</b>
C.1 Design parameters .....	189
C.1.1 Effect of inclination and orientation angle of the investigated collectors .....	189
C.1.2 Effect of solar coil material.....	189
C.2.3 Effect of propylene glycol concentration in solar liquid.....	190

## Nomenclature

---

$a_1$	heat loss coefficient due to conduction and convection [ $W/(m^2K)$ ]
$a_2$	heat loss coefficient due to radiation [ $W/(m^2K^2)$ ]
$A_{abs}$	Collector absorber area
$C_{p,sl}$	Specific heat capacity of the solar liquid [ $Wh/kgK$ ]
$D$	Distance between collector rows [m]
$G$	Irradiance; irradiated power [ $W/m^2$ ]
$E_{sol}$	Solar irradiation onto total collector area [kWh]
$\Delta E$	Reduction in annual delivered energy with respect to the reference system [%]
$L$	Collector length [m]
$Q_{aux}$	Auxiliary heating requirement [kWh]
$Q_{conv}$	Energy used by conventional heating system [kWh]
$Q_{sol}$	Collector yield [kWh]
$Q_{demand}$	Total heat demand
$SF$	Solar fraction
$\Delta SF$	Increase in annual solar fraction with respect to the reference system [%]
$S_{sol}$	Solar yield; net solar energy utilized by the tank [kWh]
$T$	Temperature [ $^{\circ}C$ ]
$T_A$	Ambient temperature
$T_L$	Temperature of solar liquid in the collector manifold
$\Delta T$	Temperature difference [K]
$V$	Volume [liter]
$\dot{V}$	Volumetric flow rate in the solar circuit [l/h]
$\alpha$	Collector azimuth angle [ $^{\circ}$ ]
$\beta$	Collector inclination angle [ $^{\circ}$ ]
$\eta_{sc}$	Collector efficiency [%] or [-]
$\gamma_s$	Altitude angle of the sun [ $^{\circ}$ ]
$\lambda$	Thermal conductivity [ $W/(m \cdot K)$ ]
$\theta_{ym}$	Annual mean temperature [ $^{\circ}C$ ]
sol	solar
aux	auxiliary
DHW	Domestic Hot Water

## Definitions

---

Terms and definitions quoted from NS-EN ISO 9488 – Solar energy vocabulary (Standard Norge, 1999):

**Absorber:** component of a solar collector for absorbing radiant energy and transferring this energy as heat into a fluid

**Aperture area:** maximum projected area through which unconcentrated solar radiation enters the collector

**Auxiliary heater:** device or equipment in which heat from fuel or electric energy is supplied

**Fractional energy savings:** reduction of purchased energy achieved by the use of a solar heating system

**Irradiance:** power density of radiation incident on a surface

**Irradiation:** incident energy per unit area of surface

**Solar fraction:** energy supplied by the solar part of a system divided by the total system load

**Solar-plus-supplementary system:** solar heating system which utilizes both solar and auxiliary energy sources as an integrated way and is able to provide a specified heating service independent of solar energy

**Stagnation:** status of a collector or system when no heat is being removed by a heat transfer fluid



# 1 Introduction

---

## 1.1 Background and objective

The use of solar thermal heating systems has the potential to cover a large share of the thermal energy demand in buildings, as well as providing a renewable and affordable alternative to using fossil energy sources. This makes it especially suitable for implementation in low-energy buildings and buildings of passive house standard. Harvesting solar energy by means of solar collectors is a mature technology, and has had increasing interest in Norway in recent years.

As the number of heating systems that utilize solar thermal energy rises, the need for increased knowledge of such systems is growing accordingly. The objective of this study is to contribute to increased performance of a particular solar thermal system connected to a passive house dwelling in Bergen, which is used for both space heating and preparation of domestic hot water. This will be achieved by conducting a thorough analysis of the system, and by performing a parametric study that targets both design and operation parameters. In addition to suggesting improved solutions for the investigated system, the findings will also provide a basis for implementing alterations on similar solar thermal heating systems located in the same housing cooperative.

This master thesis is a continuation of a project study conducted autumn 2014.

## 1.2 Structure of the report and limitations

In *Chapter 2-4*, a literature review of theory relevant for this case study is provided, which is a continuation of the literature study conducted in the project work during autumn 2014. In this section, a review of the potential for utilizing solar thermal energy will first be discussed. Then, a typical solar thermal system is decomposed into its main components, and considered from a technical perspective, including discussions regarding dimensioning and important design features. This will serve as a basis for understanding and recognizing the potential of such a system. Finally, methods for detecting and identifying errors, as well as indicators used to evaluate the performance of such a system, are discussed.

In *Chapter 5. Case description*, some information and previous experiences regarding the investigated system is provided.

In *Chapter 6. Methodology*, the chosen method for evaluating the performance of the system and identifying potential errors are described.

*In Chapter 7. Description of measurements*, the measurement procedure and method for processing this data is described.

*In Chapter 8. Simulation inputs*, the chosen simulation tool for creating a simulation model of the investigated system is briefly presented, and its main features described. Then, a detailed description of the simulation model created in Polysun is provided.

*In Chapter 9. Results*, both measured and simulated results are presented

*In Chapter 10. Parametric study*, a parametric analysis of various design- and operation parameters of the investigated system is conducted. The study is based on the simulation model created in chapter 8.

*In Chapter 11. Discussion*, the findings in this study is discussed, including comments regarding previous experienced from this case study.

*Chapter 12. Conclusion*

*Chapter 13. Future work*

*Chapter 14. References*

The research question states that field work will be conducted in this study, and that a risk assessment of the work must be documented and attached in the final report. Because of extensive mapping of component data in the preliminary project study, and due to assistance from the co-supervisor, it was considered unnecessary to execute a field trip to Bergen. For this reason, field work has been omitted from the master thesis, and a risk assessment is accordingly not included in this report. Moreover, the research question states that shading will be evaluated through the comparison of two dwellings. Due to limitations in available measured data from the other dwelling, this comparison will be made in chapter *11. Discussion*, after the parametric study has been conducted.

## 2 Potential for utilizing solar thermal energy

Every year the earth receives radiation from the sun equivalent to 15.000 times the annual worldwide energy consumption of humans. In Norway, the sun provides 1500 times more energy than what is actually being consumed (Halvorsen et al., 2011). Solar energy is an environmentally friendly energy source, and with adequate solar radiation, even in a cold and northern country like Norway, there is no doubt a large potential for exploitation of solar resources also here.

There are three main principles for utilizing solar energy in buildings (Lavenergiprogrammet, 2013):

1. Passive utilization of solar energy, i.e. solar heat gains through windows
2. Solar thermal collectors that heat water to be used for either space heating or heating of domestic hot water
3. Solar cells, which convert solar radiation into electricity

Since this study targets the second option, only solar thermal utilization will be further discussed.

### 2.1 Variation in solar irradiation

In the most sunny places in the world, the annual solar irradiation can reach up to 2500 kWh/m<sup>2</sup>. In Norway, the incoming solar radiation is highly dependent on both season and latitude, spanning from approximately 700 kWh/(m<sup>2</sup>·year) in the north to 1100 kWh/(m<sup>2</sup>·year) in the south (Halvorsen et al., 2011). Figure 1 shows how irradiation on a horizontal surface in Norway varies according to both location and season.

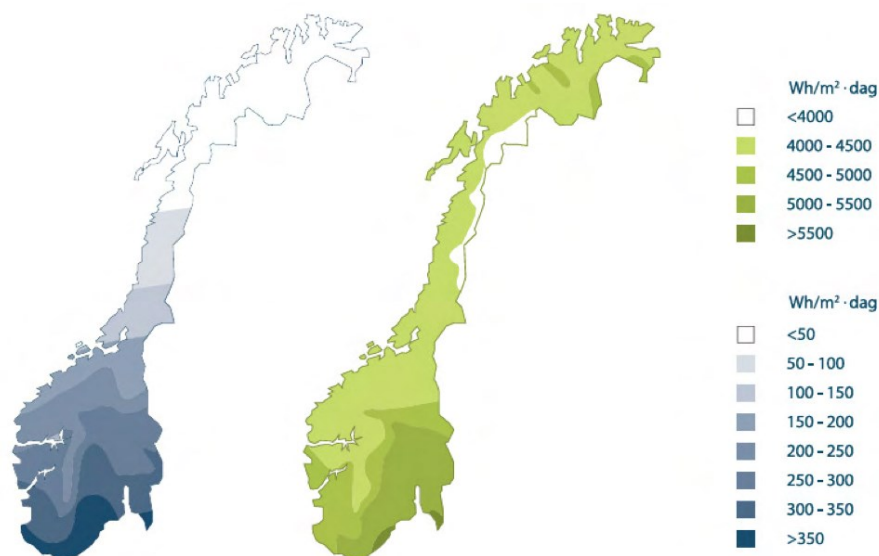


Figure 1: Solar irradiation on a horizontal surface in Norway, winter (left) and summer (right) (Rindal & Salvesen, 2008)

In Bergen, the annual solar irradiation is approximately 900 kWh/m<sup>2</sup> (European Commission, 2015). Figure 2 shows the monthly solar irradiation per square meter during one year in Bergen at an optimum inclination angle.

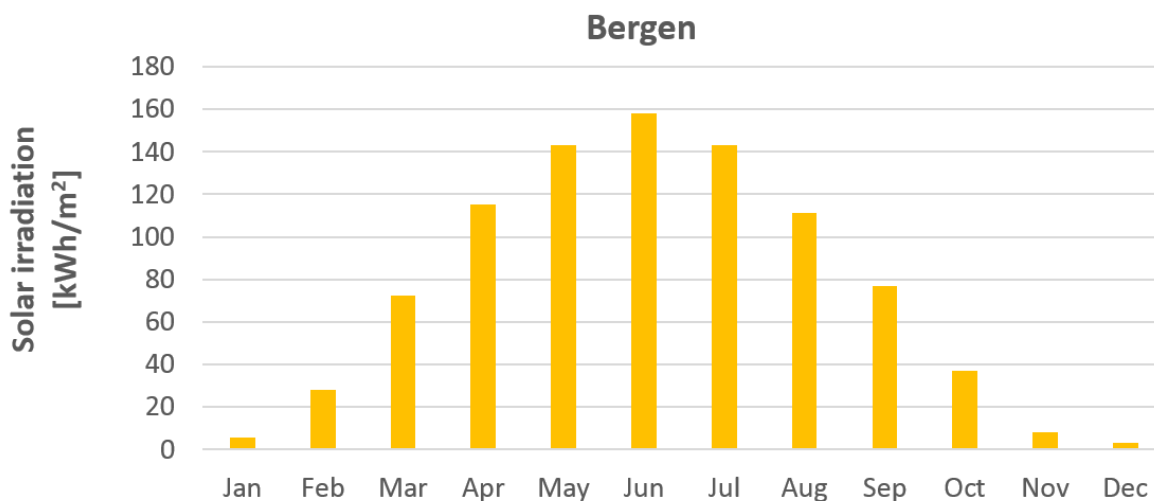


Figure 2: Monthly solar irradiation per m<sup>2</sup> surface area. Simulated towards south at an optimum inclination angle (European Commission, 2015)

The amount of solar radiation that reaches a surface depends on several factors, including the number of solar hours, the local weather conditions and on how the receiving surface is oriented according to the position of the sun (DGS, 2010).

### 2.1.1 Annual solar hours

The solar hours, i.e. the number of hours with sunshine during a particular day, varies throughout the year. Table 1 shows the monthly variation of solar hours during one year in Bergen, Norway. On average, Bergen has 1184,4 solar hours each year.

Table 1: Average monthly and annual amount of solar hours in Bergen during based on measurements from 1961-1990 (Meteorologisk Institutt, 2009)

	Jan	Feb	Mar	Apr	May	Jun	Jul	Aug	Sept	Oct	Nov	Dec	Year
<b>Solar hours [h]</b>	19,3	55,6	93,7	146,5	185,0	188,6	167,1	143,7	85,7	60,1	27,2	11,9	<b>1184,4</b>

### 2.1.2 Local weather

The local weather conditions will highly influence the amount of solar energy that reaches a surface (DGS, 2010). Figure 3 illustrates how the irradiated power (W/m<sup>2</sup>) varies with different

sky conditions: from completely covered in clouds on the left to a clear sky on the right. Furthermore, solar radiation can be separated into *direct* and *diffuse* radiation. Direct radiation from the sun is reflected, absorbed and scattered by clouds and particles in the atmosphere. This creates diffuse radiation. The sum of the two equals the *global irradiation*. Cloudy days are mainly dominated by diffuse radiation, whereas sunny days are dominated by direct radiation, which is pointed out in Figure 3.

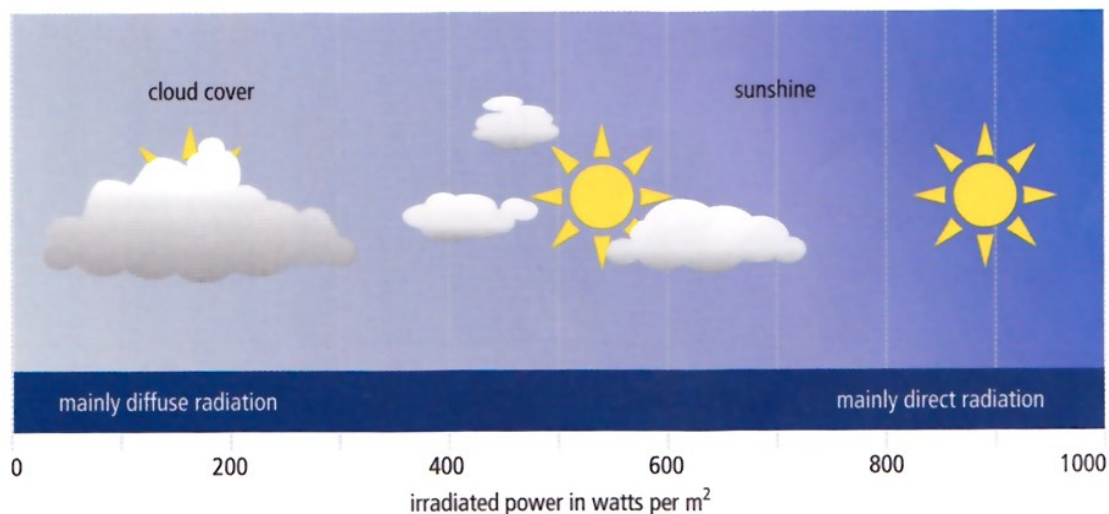


Figure 3: Solar irradiance with varying sky conditions (DGS, 2010)

### 2.1.3 Orientation and inclination angle of the receiving surface

The orientation of a receiving surface, for instance that of a solar collector, refers to two angles: the *azimuth angle*,  $\alpha$ , and the *inclination angle*,  $\beta$ , with respect to the horizontal plane. Figure 4 provides an illustration of the most important angles used in solar technology.

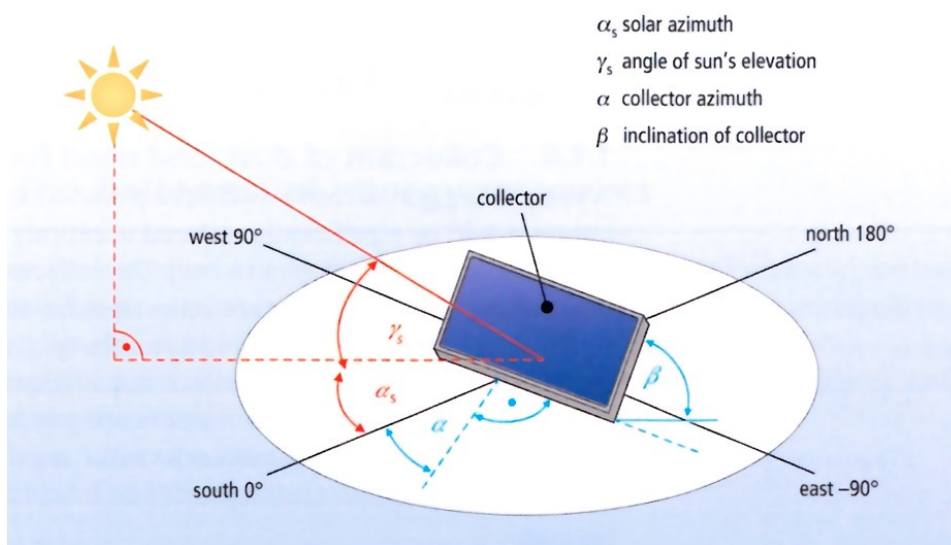


Figure 4: Angles used in solar technology (DGS, 2010)

### ***Azimuth angle***

The most ideal azimuth angle is  $0^\circ$ , i.e. when the collector is facing directly south. A southeast or a southwest orientation reduce the incoming radiation by approximately 5-15 %. Moreover, a surface that faces southwest will result in a slightly lower reduction of energy supply than a surface that faces southeast (Zijdemans, 2012).

### ***Inclination angle***

The solar beams hit a surface at an incident angle. Since this angle differs throughout the year, a solar collector should thus be tilted at a particular angle from the horizontal plane – that is, an *optimum* inclination angle - in order to obtain maximum radiation yield (DGS, 2010). Figure 5 illustrates how the optimum inclination angle varies in Bergen over the course of a year. Due to the varying elevation of the sun, this angle is larger (steeper) in the winter (during the low-radiation months) compared to in the summer (during the high-radiation months). The average optimum inclination angle in Bergen is  $34^\circ$  on an annual basis.

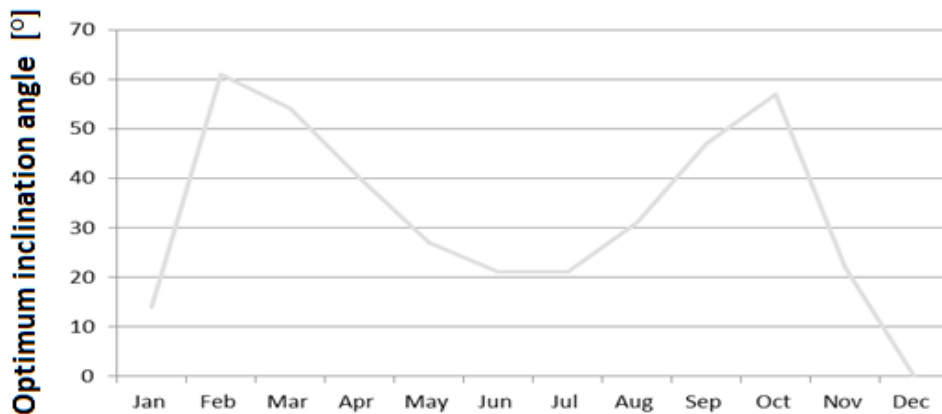


**Figure 5: Monthly variation of the optimum inclination angle (°) in Bergen (European Commission, 2015)**

However, it is important to differentiate between optimum and *recommended* inclination angle. It makes little sense to tilt the solar collector at an optimum angle, if this angle makes the collector prone to accumulation of snow or dirt. Thus, due to practical reasons, the recommended inclination angle may deviate from that of the optimum in order to ensure the highest possible radiation yield (Zijdemans, 2012).

## **2.2 Energy demand in low energy and passive house buildings**

In the Norwegian standard NS3031: 2014, the *net energy demand* is defined as the total energy demand for all the energy services in a building, including heating, cooling, domestic hot water

and lighting. The *net heat demand* is the sum of space heating, heating of ventilation air and hot water, as illustrated in Figure 6 below.

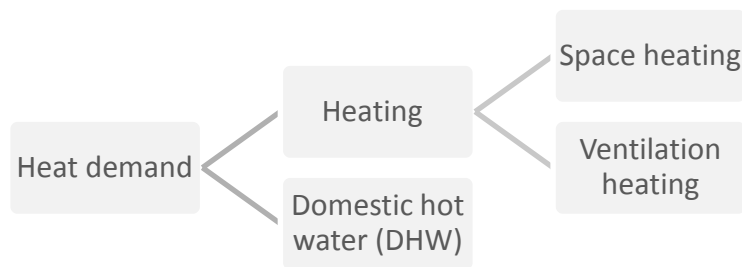


**Figure 6: Net heat demand in a building (NS3031:2014)**

### 2.2.1 Space heating

Figure 7 shows the typical energy consumption in kWh/(m<sup>2</sup>·year) for a residential building based on different energy standards and building regulations.

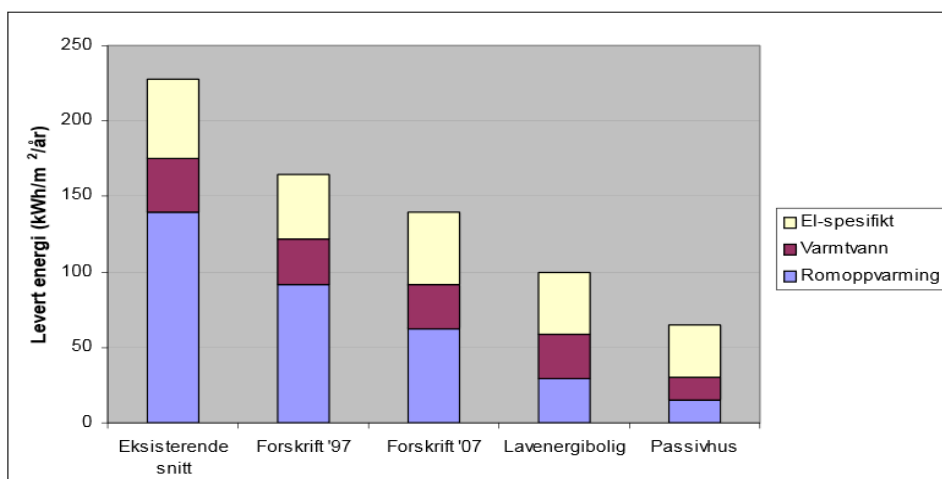


**Figure 7: Typical energy consumption for a residential building according to different energy standards and building regulations (Andresen, 2008)**

As seen in the figure, the space heating demand in low energy buildings is only 1/4 of the heat demand of existing buildings. For passive houses, the corresponding value can be as little as 1/10 (Andresen, 2008). To achieve the ambitious goals of these buildings, a special strategy should be followed: first, measures are done to reduce heat loss and electricity consumption, followed by passive utilization of solar heat (through windows and a south orientation of the building). As a final step, an energy source that are suited for the low energy demand is chosen, such as solar collectors and heat pumps (Dokka & Hermstad, 2006).

According to the Norwegian standard for passive houses and low energy residential buildings (NS 3700:2013) the maximum annual specific energy demand for space heating (kWh/(m<sup>2</sup>·year)) for a passive house dwelling can be calculated according to the equations in Table 2. A<sub>fl</sub> is the floor area [m<sup>2</sup>] and θ<sub>ym</sub> is the annual average temperature [K].

**Table 2: Norwegian passive house criteria for maximum calculated net energy demand for space heating in residential buildings (NS 3700, 2013)**

Annual mean temperature, θ <sub>ym</sub>	Maximum calculated net energy demand for space heating (kWh/m <sup>2</sup> ·year)	
	Building where A <sub>fl</sub> < 250 m <sup>2</sup>	Building where A <sub>fl</sub> > 250 m <sup>2</sup>
≥ 6,3 °C	$15 + 5,4 \times \frac{(250 - A_{fl})}{100}$	15
< 6,3 °C	$15 + 5,4 \times \frac{(250 - A_{fl})}{100} + \left( 2,1 + 0,59 \times \frac{(250 - A_{fl})}{100} \right) \times (6,3 - \theta_{ym})$	$15 + 2,1 \times (6,3 - \theta_{ym})$

Based on Table 2, the calculated specific space heating demand in Bergen (θ<sub>ym</sub> = 7,8 °C) for selected floor areas below 250 m<sup>2</sup> are shown in Figure 8. The corresponding specific space heat demand for 50 m<sup>2</sup> and 200 m<sup>2</sup> are 24,5 kWh/(m<sup>2</sup>·year) and 17,7 kWh/(m<sup>2</sup>·year), respectively.

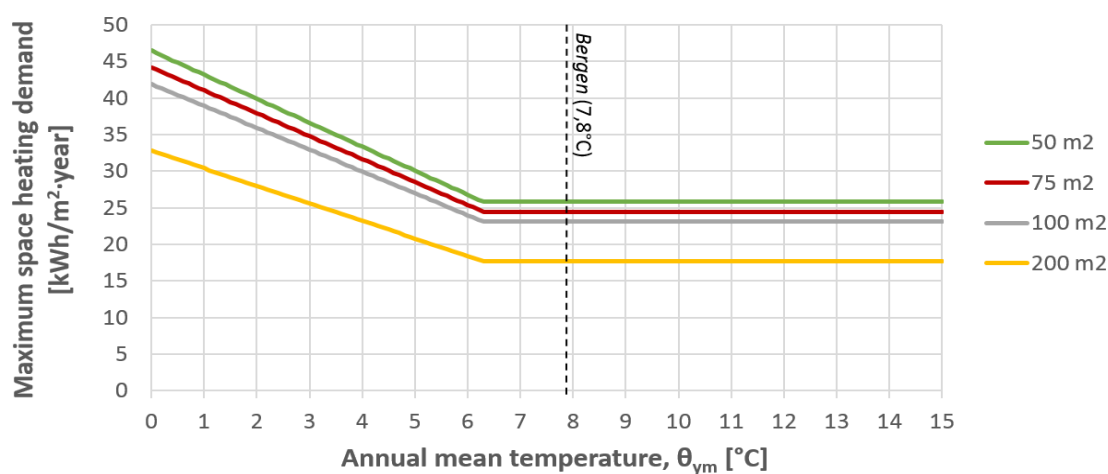


**Figure 8: Graphic illustration of the criteria in Table 2 for a passive house residential building located in Bergen (θ<sub>ym</sub> ≥ 6,3°C) with floor areas, A<sub>fl</sub>, less than 250 m<sup>2</sup>**

### 2.2.2 Heating demand for heating of domestic hot water (DHW)

The energy demand required for heating of domestic hot water can be calculated according to public standardizations. NS3031: 2014 for calculation of energy performance of buildings provides a table with annual hot water demand for different building categories. In Table 3, the values relevant for dwellings have been extracted and presented.



**Table 3: Standard values for annual hot water demand (NS3031, 2014)**

Building category	Annual hot water demand	
	[W/m <sup>2</sup> ]	[kWh/(m <sup>2</sup> year)]
Multi-dwelling building	5,1	29,8

### 2.3 Heating with solar thermal energy

In Figure 9, a typical distribution of the total heat demand for space heating and heating of DHW in a residential building is depicted. The variation within the potential for utilizing solar thermal energy is also included in the graph.

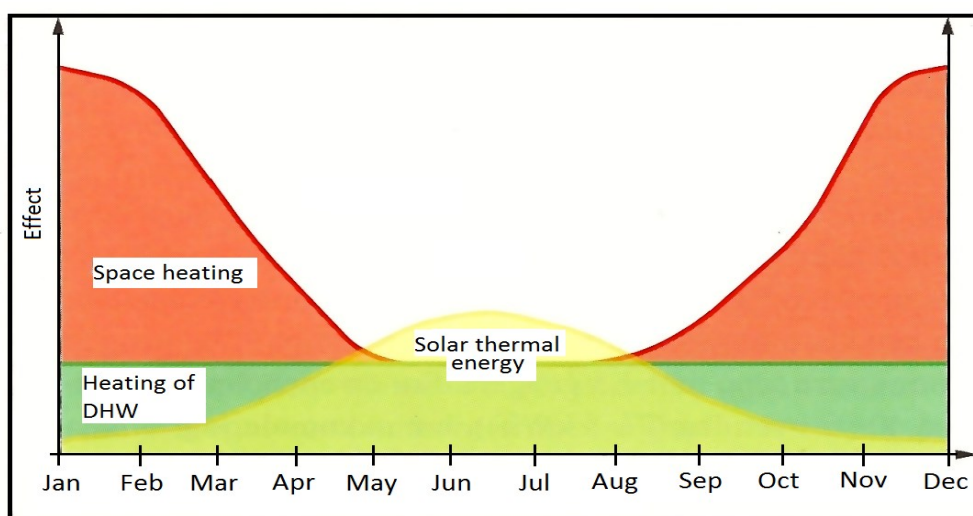


**Figure 9: Variation in required heat demand and available solar energy during the course of one year (Zijdemans, 2012)**

As can be seen from the graph, the main challenge by using solar energy as a heat source is the contradiction between the need for space heating and the availability of solar resources. During winter, the space heat demand is at its highest, while the solar irradiation is at its lowest. During summer, the opposite is the case. However, since the heat demand for preparation of DHW remains relatively stable throughout the year, there is a large potential for utilizing solar energy that could cover this demand.

From the previous subchapters, it is evident that the space heating requirements of low energy and passive house dwellings are significantly lower, compared to that of existing buildings. This fact, in light of the high performance of modern solar energy systems, encourages the supplement of space heating when utilizing solar energy. These types of systems are called *combination systems* (Halvorsen et al., 2011). Since solar collectors are unable to cover the entire heat demand, auxiliary energy is needed during the coldest months of the year, for instance from an immersed electrical heating element that is placed inside the storage tank.

### 3 Design and operation of a solar thermal system

A solar thermal heating system converts solar radiation into usable heat by using solar collectors. This heat can be utilized for heating purposes in different types of buildings (e.g. single family houses, dwellings, office buildings and hospitals), for heating of domestic hot water (DHW) and/or for space heating. A solar thermal system can also be used for generating process water for industrial processes (Halvorsen et al., 2011). This study will focus on domestic applications only.

There are different types of solar thermal systems available on the market, and it is common to differentiate between *direct* systems and *indirect* systems (Zijdemans, 2012), see Figure 10 .

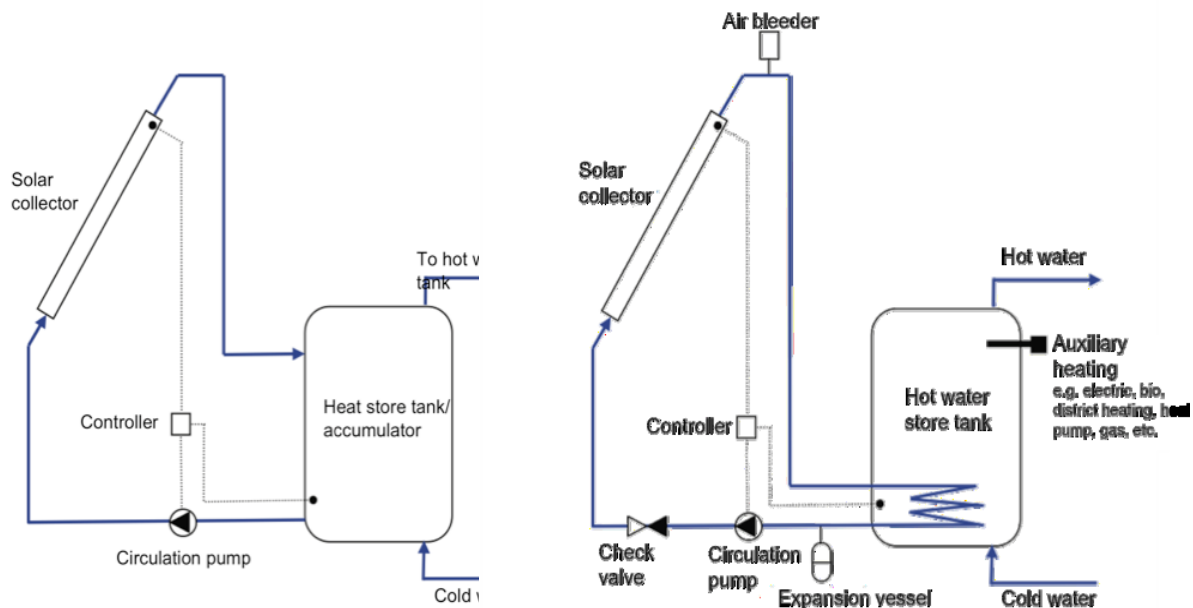


**Figure 10: Schematic of a solar thermal system for preparation of hot water. Left: Direct system. Right: Indirect system (Andresen, 2008)**

A direct system (left in Figure 10) consists of a *single-circuit system*, in which water circulates from the storage tank, flows directly through the collector, and finally returns to the storage. The use of this type is more relevant for areas with mild climates with little risk of frost. Furthermore, this system is more sensitive to unwanted Legionella growth.

An indirect system (right in Figure 10), on the other hand, has a separate solar circuit. A heat transfer fluid in the solar loop is heated by the solar collector, before transferring this heat through a heat exchanger to the domestic hot water system – often through an accumulating tank. Indirect systems are the most common type used, particularly due to the possibility of using a heat transfer medium that can handle very low temperatures, and thus protect against frost (Andresen, 2008).

In addition to the properties of the solar collector, correct dimensioning and proper construction of all the remaining components of a solar thermal heating system is essential in order to achieve a high efficiency (Zijdemans, 2012). In this chapter, a brief description of the different parts of such a system will be presented, as well as aspects related to the design and operation of the main components. Figure 11 provides an overview of these.

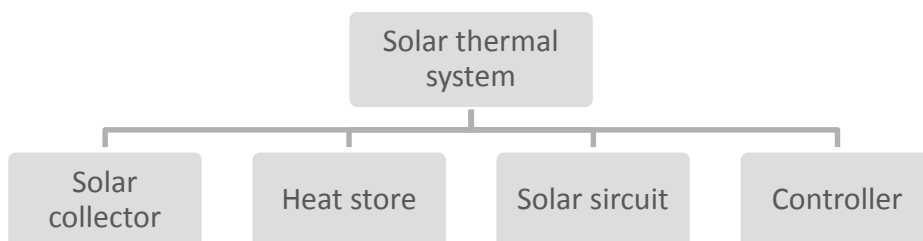


**Figure 11: Overview of the main components of a solar thermal system.**

### 3.1 Solar collector

The main task of the solar collector is to convert light into usable heat. There are many design concepts and types of collectors available on the market, all of which have different performances and costs. They range from the simplest type used for swimming pool heating, to the more sophisticated systems for high-temperature generation, such as integral storage collector systems, flat-plate collectors, evacuated flat-plate collectors and evacuated tube collectors (Quaschnig, 2004). Besides the low-temperature swimming pool collector, the most common types are glazed flat-plate collectors and evacuated tube collectors. For this reason, only glazed flat-plate collectors and evacuated tube collectors will be further discussed in this chapter.

#### 3.1.1 Flat-plate collector and evacuated tube collector

The main components of a *flat-plate collector* are the transparent front cover, the collector housing and the absorber. In the absorber, which is usually made of copper, steel or aluminium, sunlight is converted into heat and transferred in the absorber tubes. The absorber is enclosed in a box made of glass or plastic, where insulation is added to reduce thermal losses (Quaschnig, 2004). The benefits associated with this type of collector are its robustness, that snow easily slides off, and that it is aesthetically appealing. Disadvantages include relatively high heat losses and a higher degree of reflection (compared to for instance that of the evacuated tube collector) (Zijdemans, 2012). Figure 12 shows a sketch of the main components of a flat-plate collector and the thermal processes that occur.

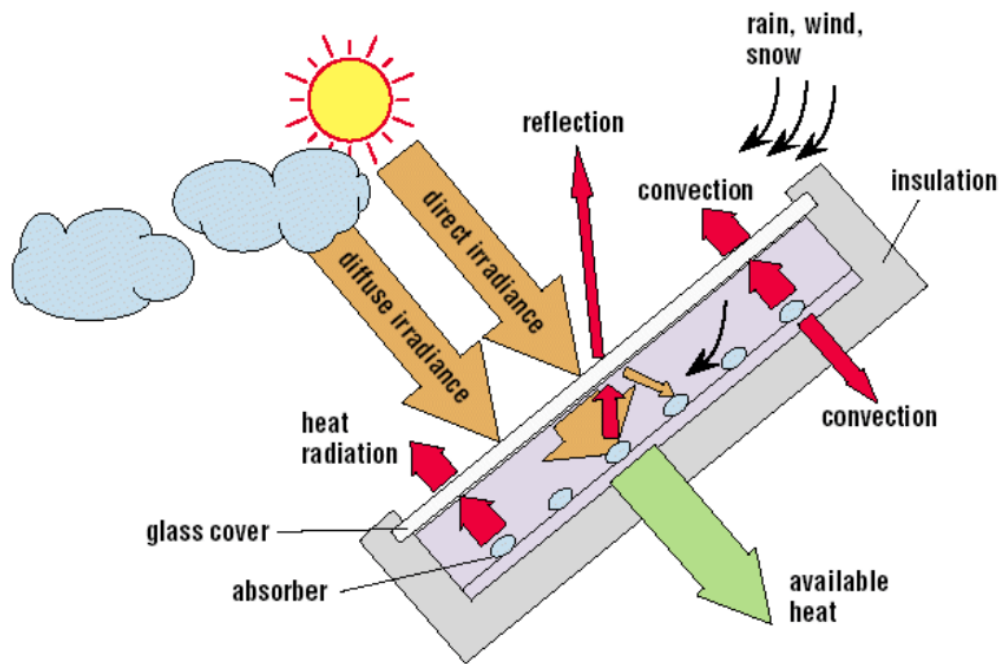
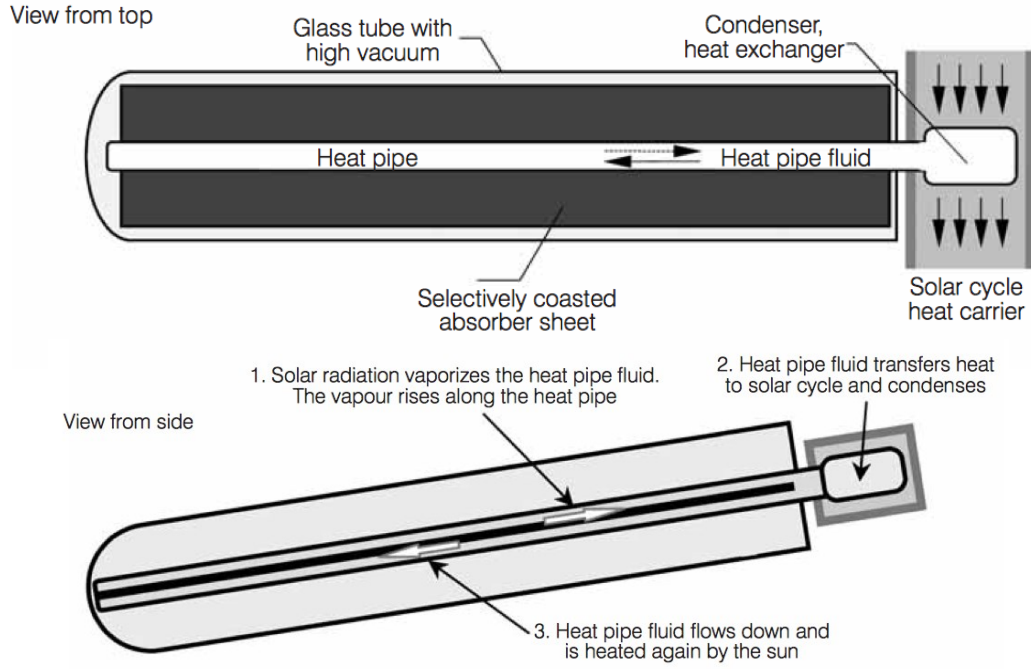


Figure 12: The main components of a flat-plate collector and the thermal processes (Quaschnig, 2005).

In the *evacuated tube collector*, the absorber is located within evacuated glass cylinders. Since the insulation properties of vacuum is much higher than that of air, the heat loss from the solar collector is kept at a minimum (Andresen, 2008). Depending on reference area and type, this type of collectors can reach efficiencies up to 30% higher than a flat-plate collector. This makes them suitable for areas of use where a high liquid temperature is necessary. Their disadvantages are that they are more expensive and have a less robust construction than the flat-plate collectors.

A common type of the evacuated tube collector is the *heat-pipe* evacuated tube collector. It consists of a copper pipe with closed ends placed inside a glass pipe. The copper pipe contains a small amount of liquid, typically water with an underpressure, which has a very low boiling point. When the pipe is heated up by the sun, the liquid inside starts to boil, which causes it to evaporate. The steam rises to the top and is cooled down by the manifold, in which cold solar circuit liquid circulates. As a result, the steam condenses and the condensate flows back to the bottom of the heat pipe. Since steam requires more space than liquid, the pressure within the copper pipe rises, subsequently causing the boiling point of the liquid to rise. This is a closed process that utilizes the heat transfer that occurs during the phase change from gas into liquid. The process is illustrated in Figure 13. To obtain this internal circulation process, the heat pipe evacuated tube collectors must be installed at a particular inclination angle, typically ranging from 20° to 70° (Zijdemans, 2012).



**Figure 13: The main components and function of the evacuated tube collector with heat pipe, seen from the top and from the side (Quaschnig, 2005).**

### 3.1.2 Collector performance and collector efficiency

The efficiency of a solar collector is defined as the ratio between useful heat production from the solar collector to the amount of solar radiation that hits the collector surface (Andresen, 2008). In other words, it describes how well the solar collector is able to utilize the incoming radiation. According to Zijdemans (2012), the efficiency of a solar collector  $\eta_{sc}$  can be calculated using equation 1.

$$\eta_{sc} = \eta_0 - a_1 \cdot \frac{(\bar{T}_L - T_A)}{G} - a_2 \cdot \frac{(\bar{T}_L - T_A)^2}{G} \quad [-] \quad (1)$$

where

$\eta_0$  is the optical efficiency, i.e. the collector efficiency without any convection and radiation losses (when there is zero temperature difference between the absorber and the ambient air) [-]

$a_1$  is the heat loss coefficient due to conduction and convection [W/(m<sup>2</sup>K)]

$a_2$  is the heat loss coefficient due to radiation [W/(m<sup>2</sup>K<sup>2</sup>)]

$T_L$  is the average liquid temperature in the solar collector (average supply – return) [K]

$T_A$  is the ambient air temperature [K]

$G$  is the solar irradiance (irradiated power) [ $W/m^2$ ]

$\eta_0$ ,  $a_1$  and  $a_2$  are based on practical measurements, and are either specified by the solar collector manufacturer or provided by an accredited testing institute. The efficiency equation expresses how the solar collector efficiency depends on the solar irradiance level and the temperatures. The temperature-dependent losses will be more dominating as the solar irradiance decreases. This is illustrated in Figure 14.

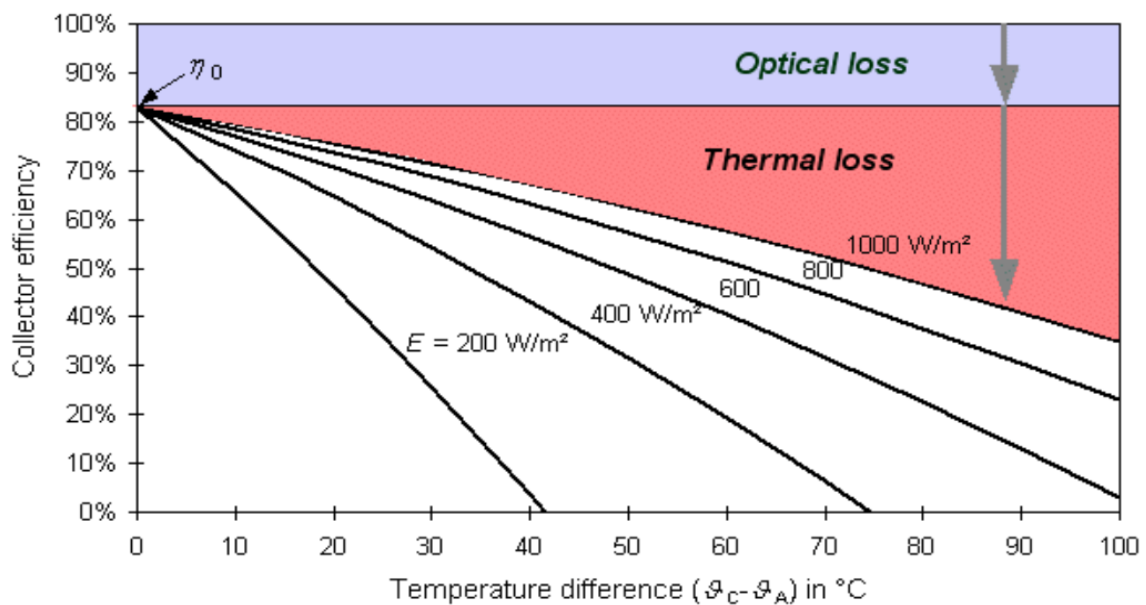


**Figure 14: Collector efficiencies at different irradiances and temperature differences (Quaschnig, 2004)**

Figure 15 below displays typical efficiency curves and areas of application for a flat plate collector, an evacuated tube collector and a low-temperature collector (swimming pool collector), with respect to different temperature differences between the surroundings and the collector. Each type reaches its highest efficiency when this temperature difference is equal to zero (optical efficiency,  $\eta_0$ ). Accordingly, the efficiency is at its lowest when the collector has reached its *stagnation temperature*, i.e. its maximum temperature limit (DGS, 2010).

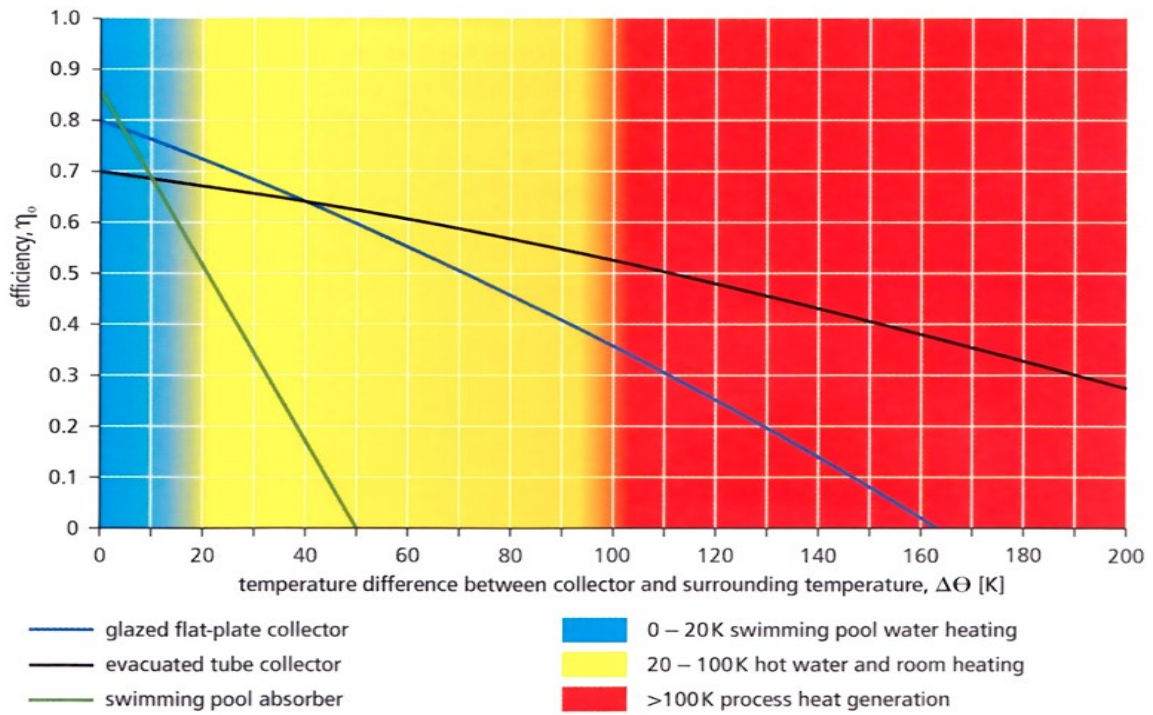


Figure 15: Efficiency characteristic curves and their areas of application for different collector types. Assumed irradiated power of  $1000 \text{ W/m}^2$  (DGS, 2010)

### 3.1.3 Required solar collector area

Zijdemans (2012) provides a simple calculation method for estimating the required solar collector area:

$$A_{abs} = \frac{Q_{demand} \cdot SF}{Q_{sol}} \quad (2)$$

where

$A_{abs}$  is the collector absorber area,  
 $Q_{demand}$  is the total heat demand,  
 $SF$  is the desired solar fraction, and  
 $Q_{sol}$  is the collector yield

As mentioned in the previous subchapter, the collector yield, or the useful thermal output of the collectors, depends on the total irradiation onto collector area and the collector efficiency.

The necessary collector area can also be estimated based on the simplifications provided in Table 4, in which the required area is stipulated based on either the number of inhabitants in each dwelling or based the number of dwellings in the building. In solar combination systems, where the collectors supply heat both for the preparation of domestic hot water (DHW) and for space heating, a larger collector area is normally required than for hot water heating only.

Table 4: Simplified estimation of required solar collector area for multi-family dwellings (Zijdemans, 2012)

	DHW heating	DHW heating + space heating
Per person in a multi-dwelling building	1 – 1,5 m <sup>2</sup>	1,5 – 2 m <sup>2</sup>
Per dwelling in a multi-dwelling building	3 – 4 m <sup>2</sup>	4 – 5 m <sup>2</sup>

### 3.1.4 Shading

When designing and planning a system that utilizes solar energy, it is important to consider the risk of shading. Other than shading from surrounding topography (hills, trees and bushes at a distance etc.), it is important to identify specific items that may block the horizon (obstructions), such as a tree, a building or another solar collector. The latter is the source of a type of shading called *mutual shading*.

Mutual shading is the shading effect that occurs when several collectors installed in rows cast shade on each other, thereby reducing the amount of radiation that hits each collector. Other than the inclination angle ( $\beta$ ), the collector length ( $L$ ) and the sun path ( $\gamma_s$ ), the distance between the collector rows ( $D$ ) affects the mutual shading (AEE Intec, 2004). These parameters and their correlation are illustrated in Figure 16.

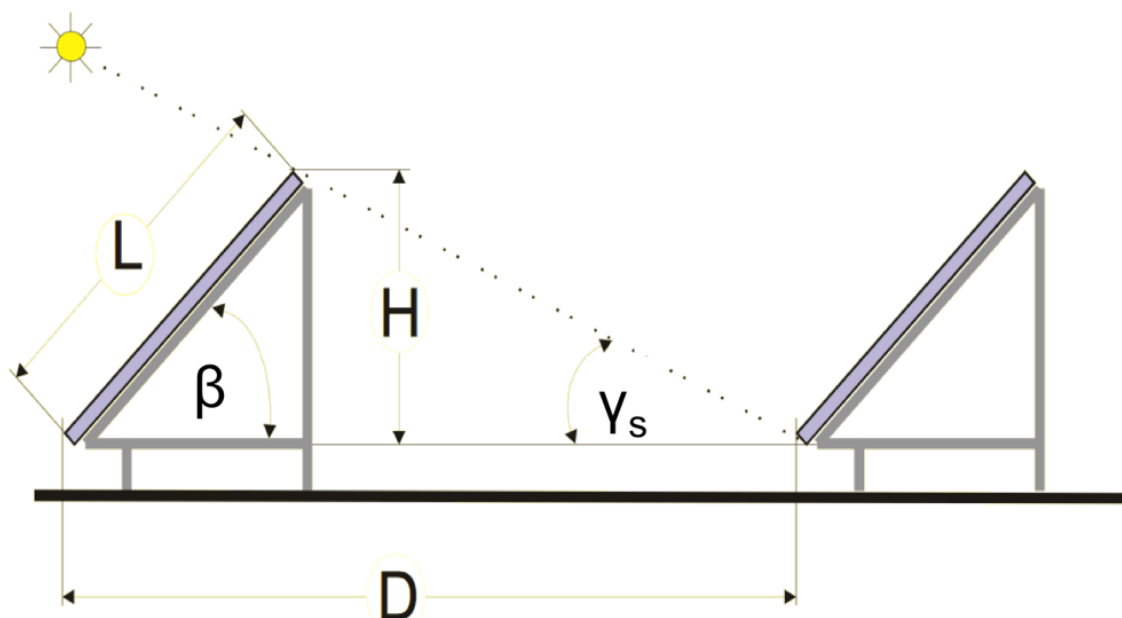


Figure 16: The variables influencing the necessary distance between two collector rows (AEE Intec, 2004)



The minimum distance needed between the collectors to avoid mutual shading can be expressed through equation 3 (AEE Intec, 2004).

$$D = \frac{L \cdot \sin(180 - (\beta + \gamma_s))}{\sin(\gamma_s)} \quad (3)$$

where

D is the distance between the rows of collectors [m],

L is the collector length [m],

$\beta$  is the collector inclination angle [°], and

$\gamma_s$  is the altitude angle of the sun [°].

Based on equation 3, the minimum row distance needed to minimize or avoid mutual shading is depicted in Figure 17 for collector inclination angles ranging from 0° to 60°. As illustrated in the graph, the difference in required row distance between the various inclination angles are smaller at large solar altitude angles.

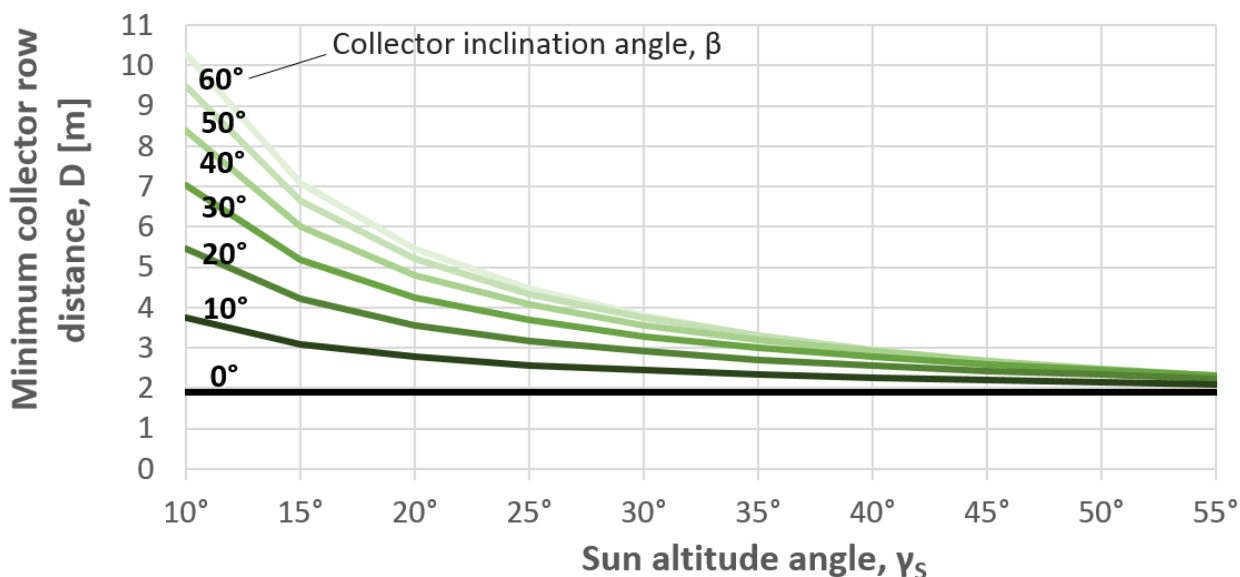


Figure 17: Minimum row distance according to the solar altitude angle for various collector inclination angles

## 3.2 Thermal heat storage

### 3.2.1 Types and configurations

As mentioned in chapter 2.3, the available solar energy does not always match the actual heat demand. Thus, the thermal energy that is generated in the collectors must be stored.

There are different storage types and configurations used for solar thermal systems, depending on their application. First of all, it is common to differentiate between the following two groups:

- Short-term heat storage systems (daily cycles)
- Long-term heat storage systems (inter-seasonal)

The short-term systems are normally only required to store heat over a period of a few days, whereas the long-term systems should be able to compensate for seasonal fluctuations. Examples of the latter are ground- and rock storage, as well as artificial storage basins.

Secondly, heat storage systems can be characterized in accordance with their temperature ranges:

- Low-temperature: below 100°C
- Medium-temperature: 100°C - 500°C
- High-temperature: above 500°C

Finally, there are different types of storage principles:

- Sensible (noticeable) heat storage
- Latent heat storage (storage due to changes in physical state)
- Thermo-chemical energy storage

(Quaschnig, 2005). This study will only focus on short-term, low-temperature storage systems by means of sensible heat, which uses water as the storage material.

In Figure 18, the most common principles of charging a water store with solar energy are displayed. Solar energy is typically used for preheating, whereas additional energy sources, or auxiliary heating, cover the remaining heat demand (back-up). Figure 19 illustrates typical ways of charging a heat storage with auxiliary heating.

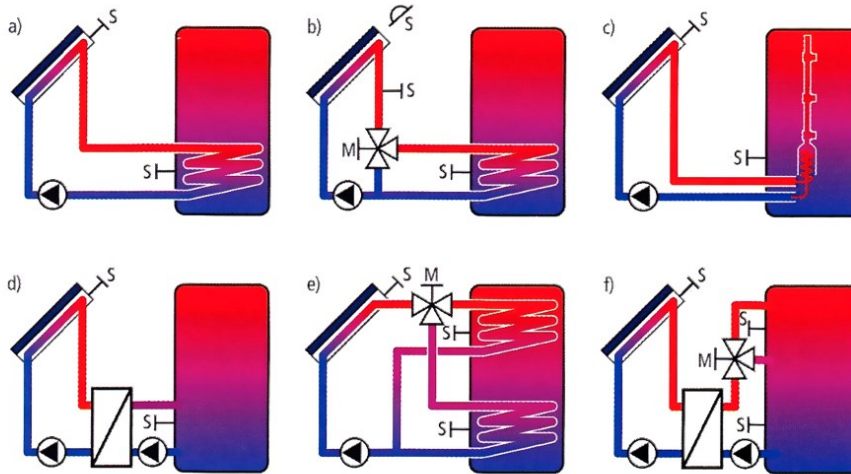


Figure 18: Common types of store charging with solar energy. S= temperature sensor (DGS, 2010)

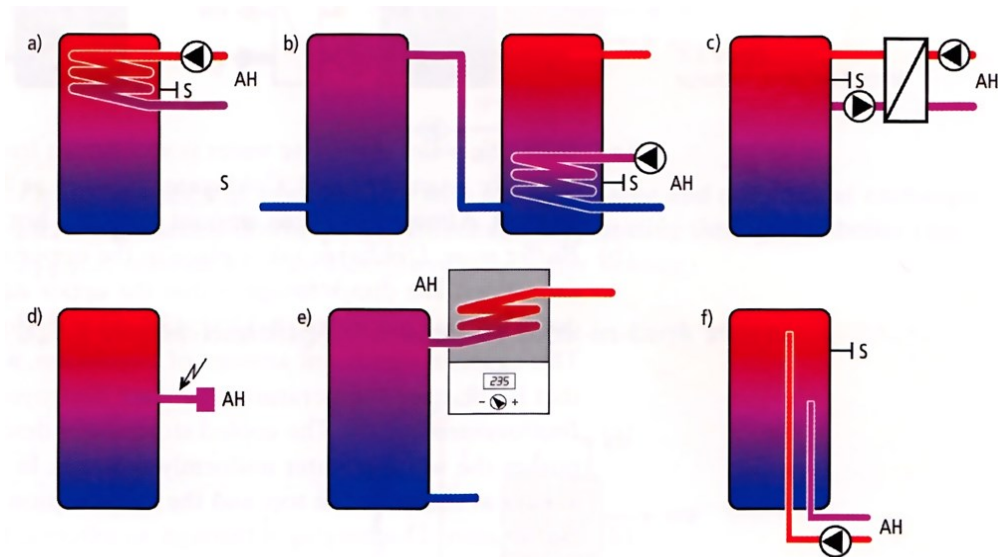


Figure 19: Types of store charging with auxiliary heating (AH) S= temperature sensor (DGS, 2010)

### 3.2.2 Thermal stratification and energy contents of a store

Thermal stratification is a phenomenon that occurs as a result of different densities, in which the water separates into “lighter” hot water at the top and “heavier” cold water at the bottom. This stratification effect has an especially positive influence on the efficiency of a solar thermal system. When hot water is extracted from the top, cold water flows in through the tank bottom. This prevents mixing of hot and cold water, which subsequently minimizes the need for auxiliary heating. A high level of stratification is attained when the storage tank is slim.

The energy contents of a store can be expressed through equation 4 (DGS, 2010).

$$Q = m \cdot c_{p,water} \cdot \Delta\theta \quad [Wh] \quad (4)$$

where

$Q$  is the heat quantity [Wh],

$m$  is the mass [kg],

$c_{p,water}$  is the specific heat capacity of water = 1,16 Wh/(kgK),

$\Delta\theta$  is the temperature difference [K],

If the same energy content is charged into a store that cannot form layers, i.e. no thermal stratification, a *uniform mixed temperature* occurs instead. Research has shown that a fully stratified water tank, in comparison with a fully mixed water tank, can increase the energy store efficiency and the whole system efficiency up to 6% and 20%, respectively (Han et al., 2008). The thermal stratification effect is illustrated in Figure 20.

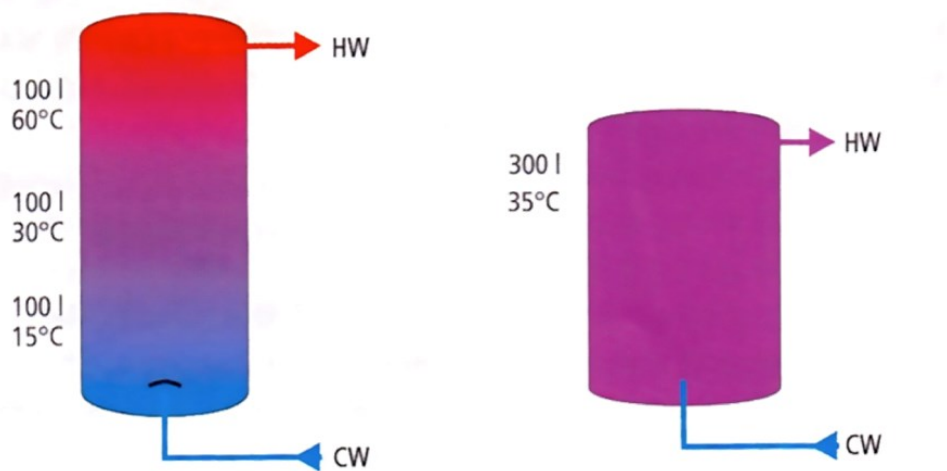


**Figure 20: Left: Stratification. Right: Uniform mixed temperature (additional heating needed) (DGS, 2010)**

In addition to tank dimensions, degradation of thermal stratification in the tank can also be caused by other factors. These include heat loss to the surroundings, thermal mixing at the inlet, forced convection flow through the tank, natural convection flow induced by conduction within the tank walls, and heat diffusion inside the tank due to vertical temperature gradients (Dehghan & Barzegar, 2010).

### 3.2.3 Design and dimensioning of the storage tank

In general, it is important that the heat store tank is large enough to cover (accumulate) the total hot water demand. If the tank is too small, an optimum utilization of the solar collectors is not possible, and an overproduction of solar energy may frequently occur during periods with high radiation. On the other hand, the storage tank should not be too large, as this will result in a long heating and cooling time (Zijdemans, 2012).

The design and size of the tank is mainly based on heat demand, choice of auxiliary heating, collector type and collector area. Other factors to consider are temperature stratification within the tank, as well as costs related to both investment and operation (Andresen, 2008). Zijdemans (2012) presents some simplifications with respect to the dimensioning of the storage tank in a solar thermal system, which is displayed in Table 5.

**Table 5: Simplified dimensioning of a storage tank volume in a solar thermal heating system for multi-family dwellings (Zijdemans, 2012)**

	Storage tank volume	
	DHW* heating	DHW heating + space heating
<b>Per dwelling in a multi-dwelling-building</b>	200 – 300 l	300 – 500 l
<b>Per 100 m<sup>2</sup> dwelling in a multi-dwelling-building</b>	300 – 500 l	600 – 800 l

For combination systems, the tank size normally increases in accordance with the solar collector area. The collector yield during periods of moderate radiation can be optimized by tilting the solar collectors at a steeper inclination angle. Consequently, the tank volume may be slightly reduced due to lower heat generation during summer (Zijdemans, 2012).

Heat loss from the storage tank can be calculated according to equation 5 (DGS, 2010).

$$\dot{Q}_{Store, loss} = kA\Delta\theta \quad [W] \quad (5)$$

where

k is the heat loss coefficient [W/m<sup>2</sup>K],

A is the heat transfer surface area of the tank [m<sup>2</sup>], and

$\Delta\theta$  is the temperature difference between the heat store and the surroundings [K].

kA is often provided by the manufacturer in W/K.

### 3.2.4 Temperature requirements in storage tanks

According to Zijdemans (2012), the temperature of a domestic tap water system is mainly influenced by three factors:

1. The temperature out of the mixing valve must be low enough to avoid scolding
2. The temperature must be high enough to meet the consumer demand
3. The temperature must be high enough to prevent Legionella growth in the water heater as well as in the pipelines

#### ***Scolding***

The risk of scolding occurs at temperatures as low as 40°C for adults, and at even lower temperatures for children and elderly. According to the Norwegian building regulations of 2010, TEK10, the recommended maximum tap water temperature out of the mixing valve is 55°C.

#### ***Consumer demand***

Domestic hot water has various areas of use in a household, such as showering, dishwashing, hand washing, cleaning, etc:

Bathing, showering and hand washing:	38 - 40°C
Dishwashing and rinsing:	40 - 50°C
Laundry and rinsing:	40 - 50°C
Floor cleaning:	45 - 55°C

These temperatures represent the minimum tap water temperatures out of the mixing valve. This means that the water temperature in the upper part of the tank must be equally high or higher in order to meet all the demands.

#### ***Legionella protection***

The Legionella bacteria naturally exists in moist areas, and normally it constitutes no significant health risk to healthy persons. However, should the bacteria multiply, the high concentration may be harmful to human beings. Its growth is also affected by other factors such as acidity, salinity and oxygen content. The bacteria multiplies at temperatures between 20-50°C, with an optimum range of 35-47°C. In the case of water heaters, sludge, which typically settles at the bottom of the tank, may provide especially good living conditions for the Legionella at temperatures lower than 60°C (Zijdemans, 2012).

### 3.3 Solar circuit

The solar circuit consists of all pipes and components that connect the solar collector to the heat store unit (Zijdemans, 2012). Figure 21 provides an overview of these. In this study, rapid air bleeders, flowmeters and safety devices will not be further discussed.

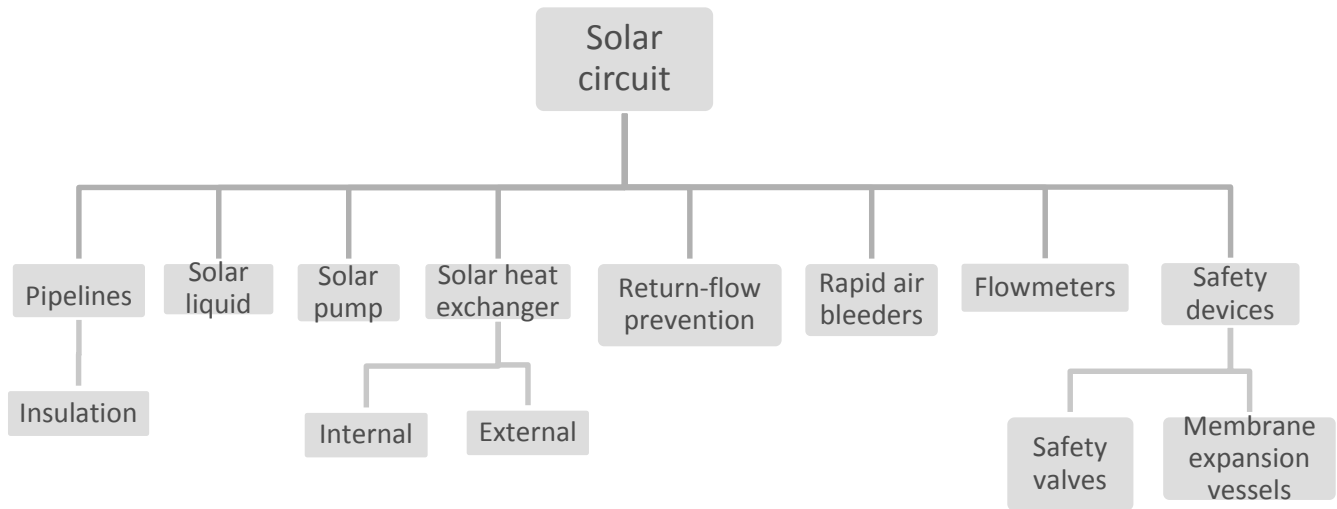


**Figure 21: An overview of the components of a solar circuit**

#### 3.3.1 Pipelines

The pipelines transfer the heat transfer fluid, or the solar liquid, between the solar collector and the heat store tank. The most frequently used material is copper. Long and poorly insulated pipelines may have a significant negative impact on the overall heat yield of a solar thermal system. Equation 6 can be used for calculating heat loss in insulated pipes (DGS, 2010).

$$Q_{pipe, loss} = \frac{2\pi\lambda\Delta\theta}{\ln\left(\frac{D_{ins}}{D_{pipe}}\right)} \quad \left[ \frac{W}{m} \right] \quad (6)$$

where

$\lambda$  is the thermal conductivity of the insulating material [W/mK]

$D_{ins}$  is the outside dimension of the insulated pipe [mm]

$D_{\text{pipe}}$  is the outside diameter of the pipe [mm]

$\Delta\theta$  is the temperature difference between the pipe and the ambient air [K]

### 3.3.2 Solar liquid

The task of the solar liquid is to transfer the generated heat from the collector to the heat store tank inside the solar circuit. Today, water and a mixture of water and propylene glycol are the most frequently used heat transfer fluids. Since the operating temperatures in a solar collector may range from  $-15^{\circ}\text{C}$  to  $+350^{\circ}\text{C}$ , the use of pure water as heat transfer fluid is challenging, as water freezes at  $0^{\circ}\text{C}$  and evaporates at  $100^{\circ}\text{C}$ . Therefore, the cold climate in northern countries like Norway increases the risk of freezing, and the addition of propylene glycol is necessary.

(Zijdemans, 2012). Table 6 displays different mixture ratios of propylene glycol and water, as well as the corresponding freezing points.

**Table 6: Freezing point of propylene glycol at different ratios water-glycol mix ratios [%]**  
(Zijdemans, 2012)

<b>Concentration of propylene glycol [%]</b>	<b>0</b>	<b>10</b>	<b>20</b>	<b>30</b>	<b>36</b>	<b>40</b>	<b>43</b>	<b>48</b>	<b>52</b>	<b>55</b>	<b>58</b>	<b>60</b>
<b>Freezing point [°C]</b>	0	-3	-7	-12	-18	-20	-23	-29	-34	-40	-46	-51

Although the addition of propylene glycol increases the frost- and evaporation protection, this measure is not exclusively beneficial. First of all, water is highly corrosive. This effect is further increased with the addition of propylene glycol. Secondly, a higher percentage of propylene glycol affects important heat transfer qualities of the liquid, such as reduced thermal capacity and thermal conductivity, and increased viscosity and creep capacity (DGS, 2010).

When using a freezing protective liquid as heat transfer fluid, the freezing point of the liquid should be checked every year. Additionally, a chemical analysis of the liquid should be performed between every third to fifth year in order to reveal changes of the liquid qualities (Zijdemans, 2012).

### 3.3.3 Solar pump

The solar pump is one of the most important components of a solar thermal system. The pump circulates the solar liquid through the system so that heat is transferred from the collector to the storage tank. The energy needed to run the pump itself is relatively small compared to the amount



of energy that it transfers. Nevertheless, it is important to choose a pump with high efficiency (Zijdemans, 2012). Furthermore, the temperature difference between the feed and return flow in the solar circuit is affected by the volumetric flow rate in the solar circuit. The achievable temperature difference between the feed and return flows can be calculated according to the following formula:

$$\Delta\theta = \frac{Q_{sol}}{Cp_{sl} \cdot \dot{V}} \quad (7)$$

where  $Q_{sol}$  is the usable thermal output converted by the collector (W),  $Cp_{sl}$  is the specific heat capacity of the solar liquid (Wh/kgK) and  $\dot{V}$  is the volumetric flow rate (l/h) (DGS, 2010).

### 3.3.4 Solar heat exchanger

In an indirect solar thermal system, a heat transfer unit, i.e. a solar heat exchanger, is required in order to transfer the collector yield to its final destination: the storage tank. It is common to distinguish between two types: *internal* and *external* heat exchangers. Internal heat exchangers are manufactured as either *finned tube* or *plain tube* coils, illustrated in Figure 22. The latter provides a better heat exchange capacity per square meter of exchanger face.

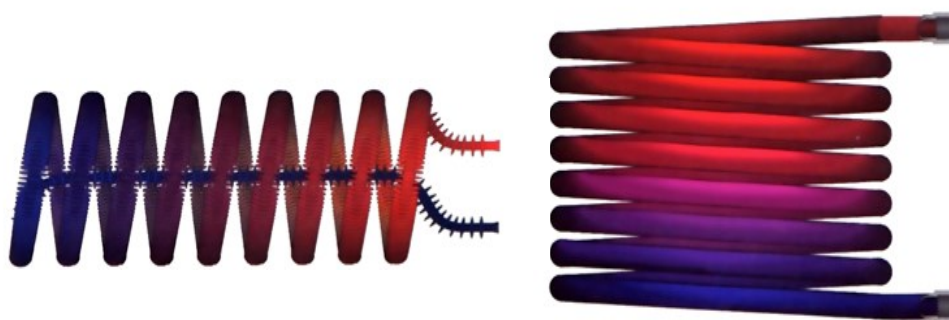
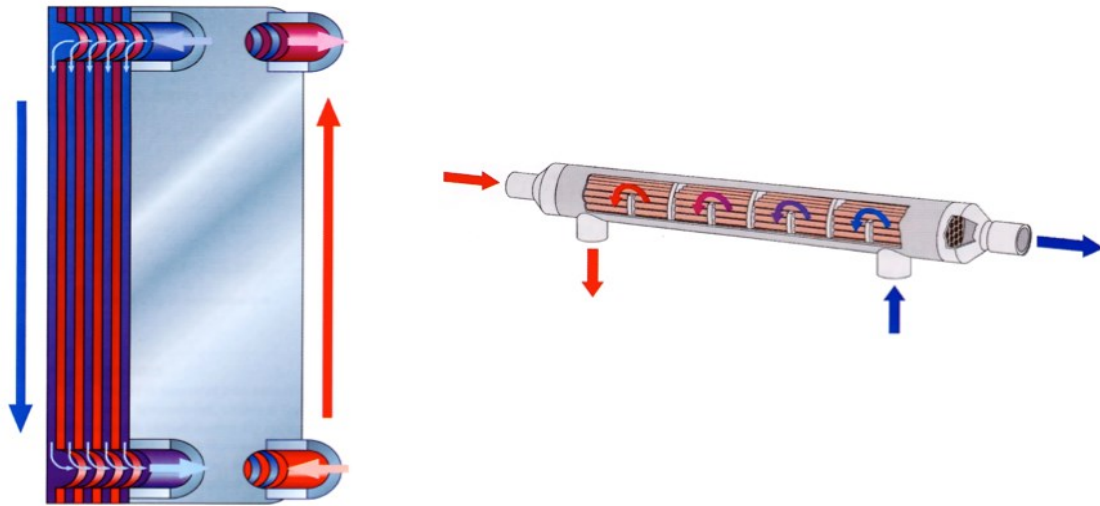


Figure 22: Left: Finned tube heat exchanger. Right: Plain tube heat exchanger (DGS, 2010)

External heat exchangers are available as either *plate* or *tubular* heat exchangers. Figure 23 shows the principal function of the two. The solar liquid and the tank water flow into the external heat exchanger in a separate counter-current flow.



**Figure 23: Left: Plate heat exchanger. Right: Tubular heat exchanger (DGS, 2010)**

There are both advantages and disadvantages for choosing an external heat exchanger over an internal heat exchanger. Most importantly, the external heat exchanger has a higher heat capacity than the internal, which allows for the use of only one single heat exchanger to charge several stores. On the other hand, external heat exchangers are more expensive since they in most cases require an additional circulation pump on the secondary side of the heat exchanger. Due to this economical aspect, external heat exchangers are more commonly used in larger systems, where one exchanger can replace several heat exchangers for charging several stores (DGS, 2010).

### 3.3.5 Return-flow prevention

During periods of limited solar radiation, the temperature within the storage tank may exceed the temperature of the liquid in the solar collector. As a consequence of this temperature difference, gravitational return-flow may occur. In other words, heat from the tank is undesirably withdrawn and released into the environment. This can easily be prevented by adding a check valve, which only opens while the solar pump is running (Zijdemans, 2012).

### 3.3.6 Overheating protection

According to the Norwegian Standard *NS-EN 12976-1: 2006 Thermal solar systems and components*, a system is to be designed “in such a way that prolonged high solar irradiation without heat consumption does not cause any situation in which special action by user is required to bring the system back to normal operation” (NS-EN 12976-1, 2006, page 8). Overheating is the effect that arises when the solar collectors supply more energy to the solar circuit than what is being removed. This typically occurs when the user is on holiday and hot water is not being

consumed, but it can also occur if the solar collectors are oversized, or if the storage tank is too small. This may lead to very high temperatures in the solar liquid and in the water within the storage tank. A potential consequence of overheating is boiling, which at worst may cause damage to the system. There are several ways of protecting the solar system against overheating. These include:

- Releasing excess heat by means of night cooling or automatic tapping of domestic hot water
- Reducing the collector efficiency by lowering the volumetric flow rate in the solar circuit so that the temperature in the solar collector increases, which increases the collector heat loss
- Controlled boiling
- Installing a temperature-controlled cooling fin in the solar circuit

It should be noted that efforts to reduce the collector efficiency by increasing collector heat loss is not very efficient in the case of evacuated tube collectors, since this type has especially good insulation properties (Zijdemans, 2012). In addition to those mentioned above, a few other measures can also be done to reduce or avoid high temperatures in the solar circuit (DGS, 2010). By installing the collectors at a steeper inclination angle, the amount of excess heat and the occurrence of collector stagnation during summer are reduced. Simultaneously, the yield is increased during winter. Another measure is to utilize the excess heat for heating of for instance swimming pool water.

### 3.4 Controller

The task of the controller is to start the circulation pump in the solar circuit (solar pump) when there is solar energy to harvest, i.e. when the temperature in the solar collector is higher than the temperature in the storage tank (Zijdemans, 2012). The most common control method is by means of *temperature difference control*.

In a standard temperature difference control, two temperature sensors are required: one that measures the temperature at the hottest part of the solar circuit, right before the collector outflow, and one that measures the tank temperature at the height of the solar coil. The signals from the two temperature sensors are compared in a control unit. When a preset temperature difference is reached, typically 5-8 K, the pump is switched on. This limit is called the *switch-on* temperature difference. Similarly, the pump is turned off when a given *switch-off* temperature difference is reached, typically 3K. Figure 24 illustrates the concept of this type of control.

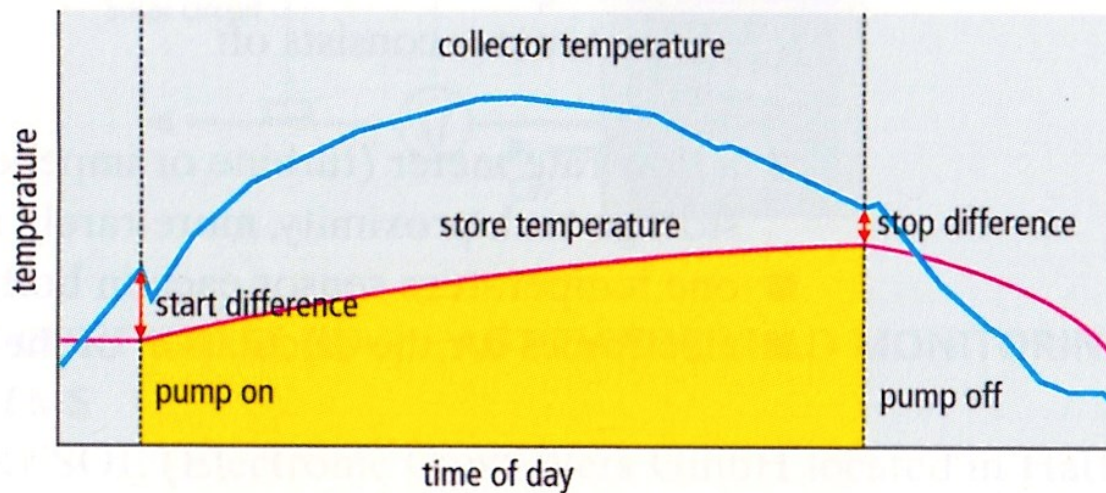


**Figure 24: A daily progression of a temperature difference controller with respect to collector temperature and heat store temperature (DGS, 2010)**

The chosen switch-on temperature difference depends on various factors, including the pipeline distance between the collector and the heat store (DGS, 2010). Furthermore, the effectiveness of the controller is highly dependent on correct installation and function of the two temperature sensors.

A third sensor that measures the upper section of the heat store can also be added. This makes it possible to read the draw-off temperature from the upper area of the tank. To protect against overheating, the system can then be set to switch itself off should the maximum heat store temperature be reached.

## 4 Function and yield control of small solar thermal systems

The most common sources of errors and faults in a solar thermal system are displayed in Figure 25. Other than during planning (45%), faults primarily occur during the installation itself (39%) or during production (16%). The most common faults are related to hydraulics (62%), as well as process, measuring and control (27%). In comparison, collectors and heat store constitute a relatively small share (DGS, 2010).

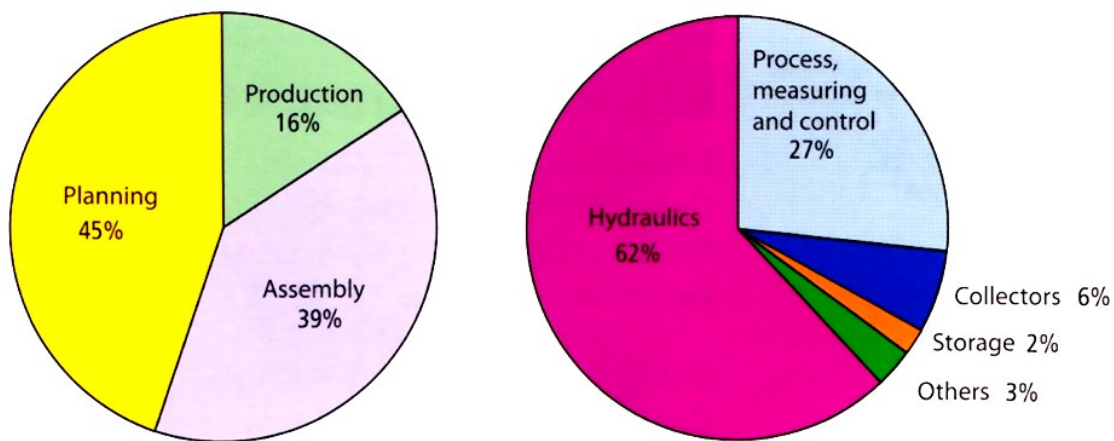


**Figure 25: Left: Distribution of the phases during which errors normally occur in a solar thermal heating system. Right: Distribution of common errors (DGS, 2010)**

Since the auxiliary heater in solar-plus-supplementary systems often automatically provides sufficient hot water temperatures in the storage tank by means of after heating, disturbances in the solar thermal system are often noticed too late, or in some cases not at all (DGS, 2010). Since a system's performance can be significantly reduced due to errors, identification and correction of these faults is crucial. This chapter targets methods to uncover these. Indicators that can be used to evaluate the performance of a solar thermal system are provided in *4.3 Evaluation of system performance*.

## 4.1 Function and yield control

Several approaches have been developed for monitoring and fault detection. Some methods that are currently available on the market for small solar thermal system are:

- *Automatic controller with error signals*: the controller automatically checks different state values. In the case of a disturbance, an error signal appears on the display
- *Remote display of system parameters*: allows for remote monitoring
- *Process monitoring by continuous analysis of system data*: logged data can be analysed over a PC interface with the help of appropriate software

The efficiency of a solar thermal system can be determined with the support of heat metering, where the solar yield is measured by using one or more separate heat meters over a given period of time. The main components of a heat meter are:

- A flow rate meter
- Two temperature sensors: one for the supply flow and one for the return flow
- Electronics for calculating heat yield

The thermal output of a circuit is estimated by measuring the temperature of the hot supply flow and the cold return flow, as well as the volumetric flow rate of the heat transfer medium. Figure 26 depicts the setup of a heat meter in a solar circuit (DGS, 2010).

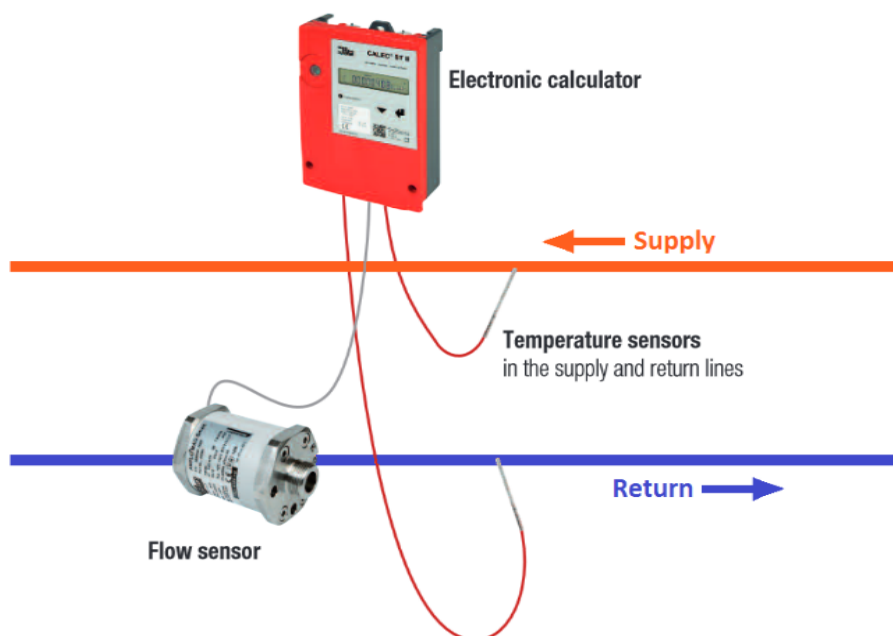


Figure 26: Function of a heat meter (Auquametro, 2015)

## 4.2 Fault detection

When there is reason to believe that the system is not functioning in a satisfactory manner, the main challenge is to identify the error. In this chapter, two methods of fault detection will be discussed: *troubleshooting* and *simulation-based fault detection*.

### 4.2.1 Troubleshooting

The most common approach for identifying errors in a solar thermal system is troubleshooting, which is fault detection based on measured data (temperature, heat and flow sensors), followed by a detailed manual fault analysis by an expert (Keizer, 2012). Examples of fault algorithms by means of troubleshooting is shown in Table 7.

**Table 7: Cause-effect assignment of errors in a solar thermal energy system (DGS, 2010)**

<b>Error description</b>	<b>Resulting effect</b>
Collector connection faulty	Pump cycles
Collector sensor incorrectly positioned	Pump cycles
Leakage in solar heat exchanger	System pressure too high
Initial pressure of expansion vessel too low	System pressure occasionally too high
Initial pressure of expansion vessel too high	System pressure occasionally too low
Shut-off valve in solar circuit closed	Temperature difference ( $\Delta\theta$ ) too high
Cable break between controller and pump	
Collector temperature sensor defective/inaccurate	Pump runs at wrong times
Store temperature sensor defective/inaccurate	
Inputs on the controller defective	Temperature difference ( $\Delta\theta$ ) too high;
Outputs on the controller defective	pump runs at night
Controller software defective	
False setting of volumetric flow	Temperature difference ( $\Delta\theta$ ) too high
Air bleeding incorrect	
Gravity brake open	Pump also runs at night
Gravity brake contaminated	
$\Delta\theta$ setting unfavourable	Temperature difference ( $\Delta\theta$ ) too high
Incorrectly programmed timer	Pump runs at night

Troubleshooting is a relatively cheap approach that relies on few sensors to check the functioning of several components in the solar loop. A significant challenge concerning this method, however, is that the data is not automatically analysed for faults, making it difficult to detect errors and faults. Moreover, this method requires the skills of a professional to perform the manual analysis (Keizer, 2012).

## 4.2.2 Simulation-based fault detection

Fault detection can be a complex procedure. Another way of determining faults is by comparing measured and simulated energy yields or other system characteristics. This can be done by creating a simulation model of the existing system. Kalogirou (2004) sums up the greatest advantages by using computer modelling of solar thermal systems:

- Eliminate the expense of building prototypes
- Complex systems are organised in an understandable format
- Provides thorough understanding of system operation and component interactions
- Possible to optimise the system components
- Possible to estimate the amount of energy delivery from the system
- Provides temperature variations of the system
- Estimate the design variable changes on system
- Performance by using the same weather conditions

In this thesis, detecting faults by means of measurements and simulations is the chosen procedure for improving system performance. This will be further explained in chapter 6. *Methodology*.

## 4.3 Evaluation of system performance

In order to evaluate the performance of a solar thermal system, it is necessary to define indicators that can be used to describe how well such a system is functioning. The most frequently used indicator is the *solar fraction*. According to *NS-EN ISO 9488:1999 Solar energy vocabulary* (Standard Norge, 1999), the solar fraction in its simplest form can be defined as follows:

$$\text{Solar fraction} = \frac{\text{Energy supplied by the solar part of a system}}{\text{Total system load}}$$

This definition can, however, be imprecise and misleading since it does not specify any losses that the system might have. Thus, an additional comment is provided together with the definition in NS-EN ISO 9488: 1999 that the solar part of a system and any associated losses must be specified in order to uniquely define the solar fraction.



A second indicator is the *fractional energy savings*, which can be used to calculate the reduction of purchased energy achieved when using a solar-plus-supplementary system (Standard Norge, 1999). In other words, it is a comparison of a system that only uses conventional heating with a system that uses both conventional heating and additional solar input. The fractional energy savings can be calculated according to the following formula:

$$f_{sav} = 1 - \frac{Q_{aux}}{Q_{conv}} \quad (8)$$

Where  $f_{sav}$  is the fractional solar savings,  $Q_{aux}$  is the auxiliary energy used by the solar heating system and  $Q_{conv}$  is the energy used by the conventional heating system. The formula assumes that both systems use the same kind of conventional energy (for instance electricity).

The Norwegian Standard NS-EN 12977-2: 2012 *Thermal solar systems and components – Custom built systems* illustrates the definition of fractional energy savings, which is displayed in Figure 27.

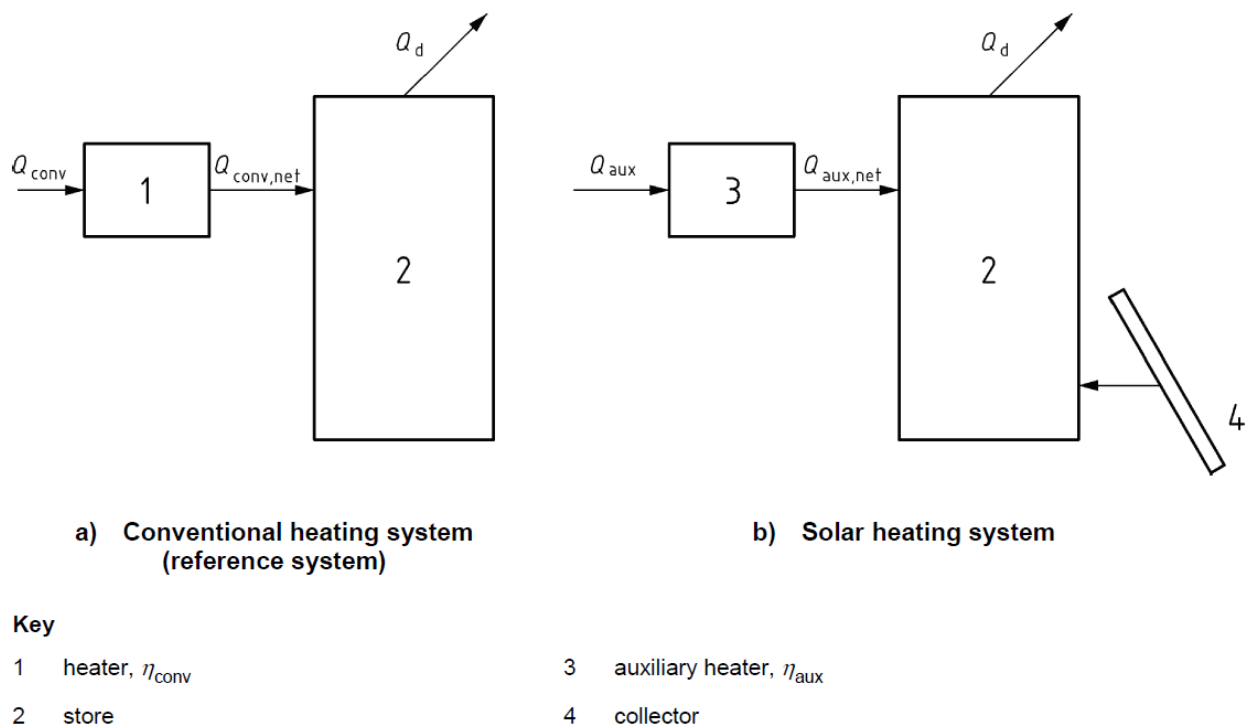


**Figure 27: Comparison of conventional heating system and a solar heating system (Standard Norge, 2012)**

## 5 Case description

---

### 5.1 Løvåshagen

Løvåshagen housing cooperative is located in Fyllingsdalen, 4 km outside the city centre of Bergen, Norway. It was finished in 2008 and consists of four buildings with a total of 80 dwellings, in which 52 dwellings (two buildings) are of low energy standard and 28 dwellings (2 buildings) are of passive house standard (Northpass, 2011). An overview of the entire housing cooperative is displayed in Figure 28.



**Figure 28: Overview of Løvåshagen housing cooperative (Northpass, 2011)**

Each of the passive house dwellings has its own solar thermal system with two solar collectors mounted on the roof. These are intended to cover some of the heat demand for both preparation of domestic hot water (DHW) and space heating. Løvåshagen has been regarded as a pilot project, of which one of the goals was to gain wanted experience with the use of solar energy as a heat source in Norway. Having been operating for several years, it is of great value for future reference to conduct a thorough assessment of this project, with the intention of revealing problems and faults, and thereby discovering the potential for improvement.

In this master thesis, the solar thermal heating system of one particular passive house dwelling will be investigated.

## 5.2 Heat demand and heat supply

There are two hydronic heating units in the dwelling: one small radiator in the hallway, and floor heating in the bathroom. The remaining space heating demand is covered by the mechanically balanced ventilation system with heat recovery. Table 8 shows the calculated specific heat demand for each passive house dwelling that was stipulated at the design stage.

**Table 8: Estimated net heat demand for the passive house dwellings (Northpass, 2011)**

	[kWh/(m <sup>2</sup> ·year)]
Space heating	12,8
Heating of ventilation air	2,2
Domestic hot water (DHW)	30,0
Net heat demand	45,0

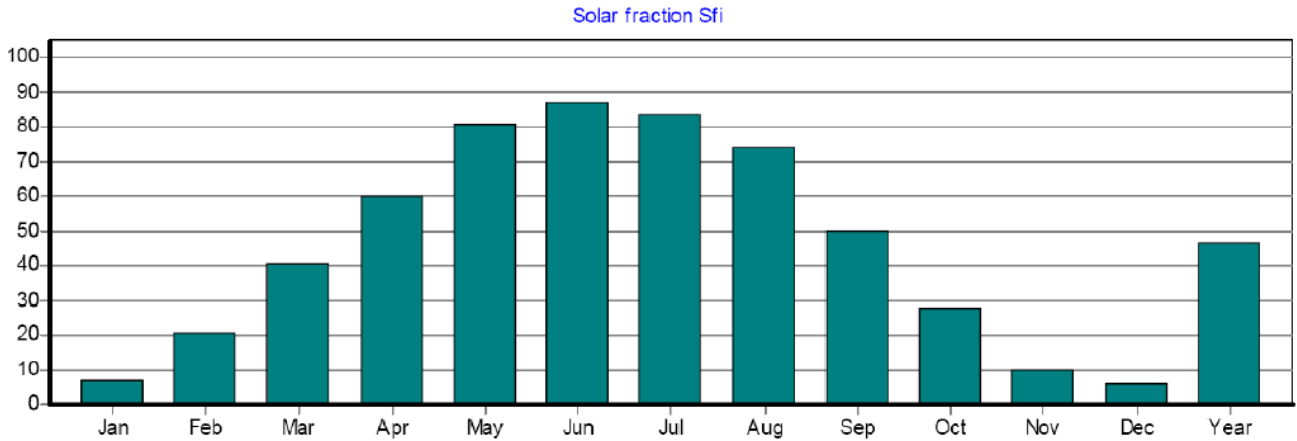
As presented in the table, the project strives to achieve a maximum energy demand for space heating of 15 kWh/m<sup>2</sup>. Since the objective of this case study is to further investigate the solar system, its main concern is the heat demand required for heating of DHW and hydronic space heating. When excluding heating of ventilation air from the net heat demand in Table 8, the remaining heat that should to be covered by the thermal system is 42,8 kWh/(m<sup>2</sup>·year). Table 9 below displays the estimated share of solar energy and electricity needed to satisfy these heating demands.

**Table 9: Solar fraction of total heat supply (Northpass, 2011)**

Energy type	Heat supply [kWh/(m <sup>2</sup> ·year)]	Fraction of total heat supply (solar fraction)
Solar energy	20,2	47%
Electricity	22,6	53%
Total	42,8	100%

As seen in Table 9, the solar heating systems installed in the passive house dwellings are each designed to cover approximately 47% of the total heat demand by means of solar energy. The remaining 53% is to be supplied by electricity.

Figure 29 below shows the stipulated monthly solar fraction during one year.



This system has been calculated on 18.09.2006 with the POLYSUN 3.3 simulation program.

Figure 29: Calculated monthly solar fraction (Andresen, 2008)

### 5.3 Description of the solar thermal system

Two evacuated tube collectors with heat pipe of the type Apricus AP-20 are used. Total collector area is 3,2 m<sup>2</sup> (effective absorber area). Figure 30 shows an illustration of this collector type, as well as the construction of each evacuated tube.

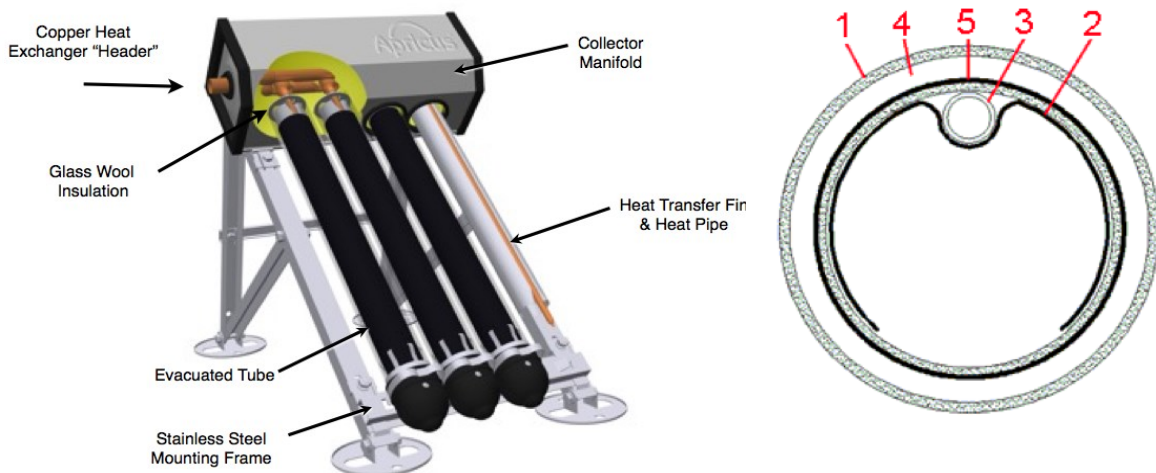


Figure 30: Left: A schematic illustration of the Apricus evacuated tube collector (Apricus, 2011). Right: Construction of an Apricus AP-20 tube: 1) Glazing 2) Heat-conduction metal sheet 3) Heat pipe 4) Vacuum 5) Absorber (SPF, 2004)

Institut für Solartechnik (SPF), an official accredited testing institute for thermal solar collector components and systems, published a test report in 2004 on the Apricus AP-20 collector. The optical efficiency ( $\eta_0$ ) and the two heat loss coefficients ( $a_1$  and  $a_2$ ) are displayed in Table 10. The full report can be found in *Appendix B.1 Collector*.

**Table 10: Optical collector efficiency ( $\eta_0$ ) and heat loss coefficients ( $a_1$  and  $a_2$ ) for the three reference areas (SPF, 2004)**

	Reference area		
	Gross (2,886 m <sup>2</sup> )	Aperture (1,876 m <sup>2</sup> )	Absorber (1,606 m <sup>2</sup> )
$\eta_0$ [-]	0,399	0,614	0,717
$a_1$ [W/m <sup>2</sup> K]	0,85	1,30	1,52
$a_2$ [W/m <sup>2</sup> K <sup>2</sup> ]	0,0047	0,0073	0,0085

*Test fluid: water-glycol 33,3%, Volume current: 120 l/h*

The two collectors are connected to a 290 l storage tank, which is located in the bathroom. The tank is a customized CTC 300 KEK 9/2/3 from CTC. On days when solar heat production is inadequate, necessary auxiliary heating is supplied to the tank through an immersed electrical heating element. In case of very high temperatures during summer, the solar circuit is cooled down by the activation of cooling radiators, which are positioned on the roof. A sketch of the storage tank and the location of the various coil- and port inputs are provided in Figure 31.

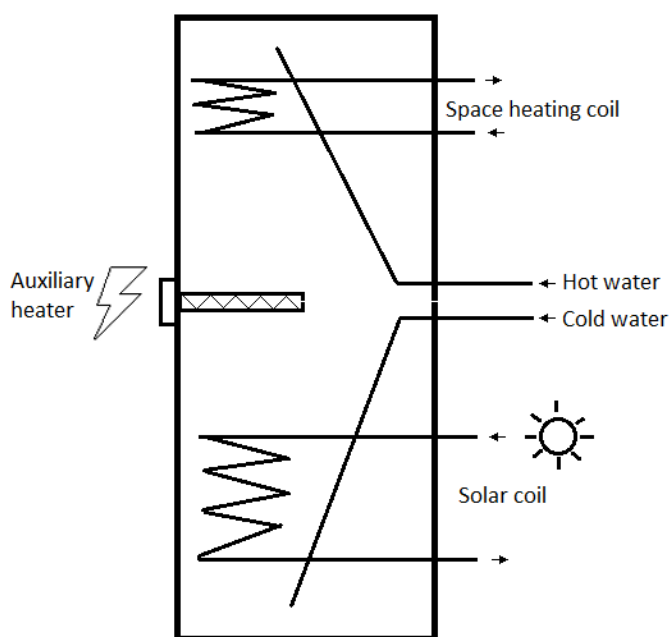


**Figure 31: Illustration of the customized CTC tank used in the solar thermal heating system**

Figure 32 shows a simplified schematic of the entire solar circuit. An overview of the system components and controller settings is provided in chapter 8. *Simulation inputs*. Moreover, detailed specifications of the main components can be found in *Appendix B*.

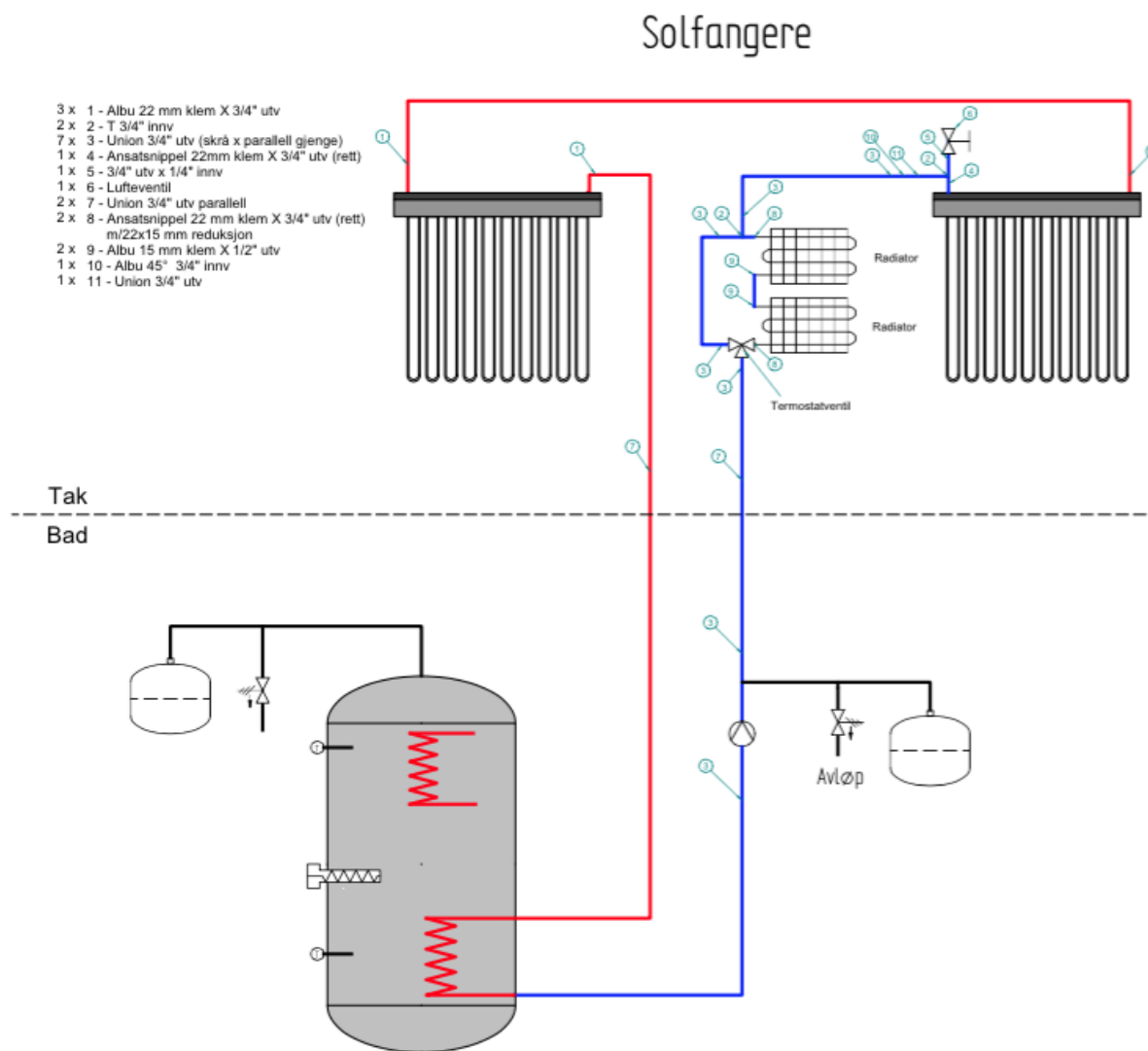


Figure 32: Hydraulic scheme of the solar circuit. *Source: Skjølberg Energiteknikk*

## 5.4 Relevant experiences and findings

Since its completion in 2008, certain experiences related to this case study has been gained.

In 2010, Nesland conducted a master thesis, in which energy consumption in both the passive house dwellings and the low-energy dwellings were investigated. The results revealed that the annual energy consumption varied greatly, and that these fluctuations appeared to be strongly related to the energy demand for domestic hot water preparation. Furthermore, the annual heat demand for space heating appears to be significantly influenced by the use of floor heating in the bathroom. In respect to the solar thermal system, Nesland concluded that the findings suggest that the solar contribution in the passive house dwellings is in fact lower than expected. Incorrect controller settings are pointed out as a plausible cause.

In a report published by SINTEF in 2012, *Prosjektrapport 90 – Systematisering av erfaringer med passivhus*, a systematic overview of experiences with passive houses in Norway is provided. The report includes some information related to the passive house dwellings in Løvåshagen. The study states that preliminary measurements conducted has revealed that the energy consumption varies strongly between the different dwellings. It comments on the fact that such scattering of measured values are not uncommon in large projects, but that the average level is slightly too high. Moreover, it is pointed out that the use of solar collectors - thus the expected reduction in delivered energy - is not reflected in the results. The report concludes that a reason for this may be of a technical nature, and not necessarily related to user habits. A suggested contributing factor is that the hydronic heating systems in the passive house dwellings are neither executed nor operated according to the plan. It is, however, emphasized that this statement requires energy measurements on a more detailed level.

The total delivered energy in 2011, 2012 and 2013 for the examined dwelling is displayed in Table 11. The data is provided by BKK. The table shows that on an average, the total delivered energy to the dwelling is 5570 kWh/year, which equals a specific value of 74,2 kWh/m<sup>2</sup>.

**Table 11: Annual delivered energy and annual specific delivered energy 2011, 2012 and 2013 (Obtained from BKK via Magnar Berge)**

	<b>kWh</b>	<b>kWh/m<sup>2</sup></b>
<b>2011</b>	5946	79,2
<b>2012</b>	5422	72,2
<b>2013</b>	5341	71,1

## 5.5 Ongoing study

Since May 2013, several sensors have been installed in 5 dwellings with the purpose of measuring various parameters. Among these are measurements of temperature, relative humidity, energy consumption and CO<sub>2</sub>-content. The study is coordinated by Magnar Berge, PhD fellow for the Research Centre on Zero Emission Buildings (ZEB) and co-supervisor for this master thesis.

During the execution of this master thesis, Berge has provided access to the database containing the measured results of the examined system. A more detailed elaboration of the method for collecting and processing this data, as well as a description of the measurements, are provided in chapter 6. *Methodology* and 7. *Description of measurements*.

## 5.6 Visual check

A visual check of the solar thermal systems at Løvåshagen revealed that the condition of these systems are not flawless. Figure 33 below shows some pictures taken by Magnar Berge on site. As can be seen from the pictures, some of the solar thermal systems in Løvåshagen are subject to poor insulation of pipes and connections, as well as broken collector tubes.



**Figure 33: Pictures taken of the solar thermal systems at Løvåshagen. Top and bottom left: Incomplete insulation of pipes and connections. Top and bottom right: Broken collector tubes. Photos: Magnar Berge**



An image of the storage tank, which was taken during a field trip made in relation with the project work during autumn 2014, is shown in Figure 34.



**Figure 34: Image of the customized storage tank and the hydraulic connections**

## 5.7 Modification 2015

In January 2015, the solar heat exchanger (solar coil) in the investigated system was replaced. One of the motivations for altering the system was the strong suspicion that the internal coil was one of the main performance-reducing factors. In addition to having a small surface area, it is made of stainless steel – which only has a fraction of the heat transfer qualities of copper, which is a common material used for this kind of application. The modification involved switching this internal coil with an external plate heat exchanger, thereby hoping to significantly increase the utilization of solar energy. Another measure that was taken was to replace the overheating protection (cooling radiators on the roof) with a different solution.

Figure 35 shows a system drawing of the modified system. During solar charging, a thermostatic valve ensures that the bottom of the tank is heated first. When the temperature of the water reaches 68°C, the valve starts to release hot water into the top of the tank instead. In the event of strong solar radiation, there is a risk that the temperatures in the solar circuit reach too high values. In the original system configuration, cooling radiators were used to prevent overheating. In the altered system, however, a special valve (located after the plate heat exchanger) will open in the case of very high temperatures. As a result, the pressure drops in the circuit due to the “missing water” and cold water is led through the heat exchanger, thereby cooling the solar circuit. The greatest benefit with this solution is that cooling of the tank is avoided.

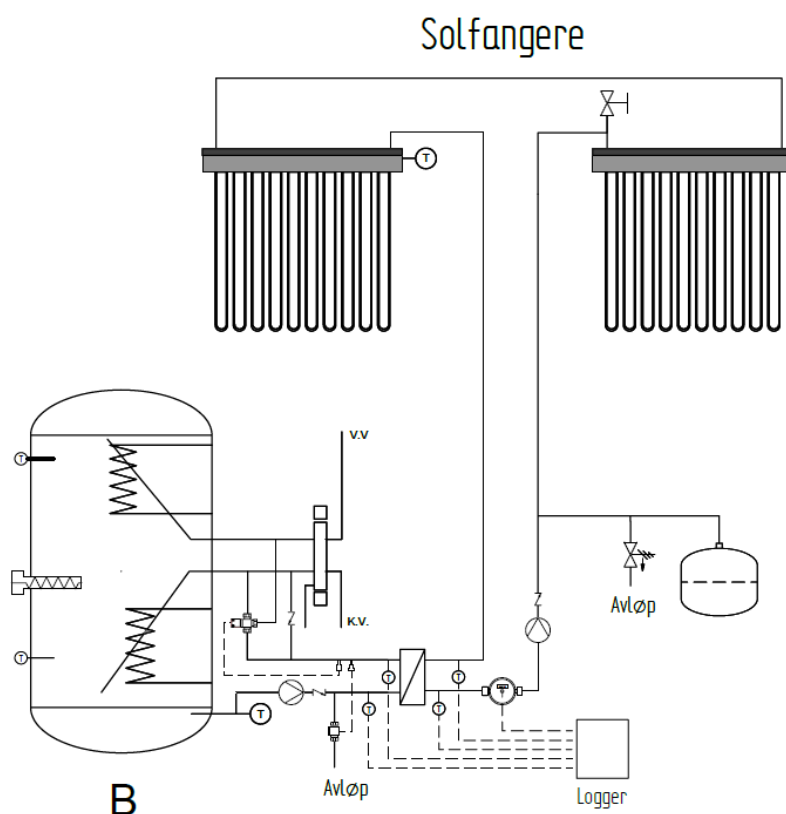


Figure 35: Modified system. Source: Skjølberg Energiteknikk

In addition to the physical modifications of the system, the controller setting of the immersed electrical heating element was slightly altered: instead of a switch-on temperature of 75°C, the heater was set to activate at 65°C. Moreover, the solar circuit pipes that were lacking insulation were sealed with 10 mm insulation. Finally, the temperature sensor at the collector outlet were fastened and its connection insulated.

## 6 Methodology

---

In this chapter, the chosen procedure for investigating the system performance, as well as for identifying potential improvements, will briefly be explained. The approach can be separated into the following main parts:

1. Identifying the performance of the investigated system by collecting and processing measured data, and then comparing these with results obtained from the simulation model
2. Performing a parametric analysis, in which the influence of different design-, operation- and user-related parameters are investigated
3. Creating new and improved scenarios based on the parametric study, and simulating the performance of these

### ***Measurements***

In the case description, an ongoing study was mentioned, in which measurement data was made available to be used in this thesis. Since this master thesis primarily targets the solar thermal heating system, only data that is relevant for the assessment of its performance will be considered. The measurement period 01.01.14 – 31.12.14 is the main period investigated. By then, the measuring equipment had already undergone some minor alterations that may have affected the results.

As explained in the previous chapter, the examined system was modified in January 2015. To assess whether this modification had a positive effect on system performance, measured data from the period 01.01.15 – 31.05.15 will also be collected and processed in this study.

A further elaboration of the measurement setup and the procedure for processing collected data is provided in chapter 7. *Description of measurements.*

### ***Simulations***

To provide a deeper understanding of how well the investigated system is functioning, and to be able to compare with the measured results, a simulation model of the system was created. The simulation software used was Polysun, for which a free Educational Base Programme licence (for the Polysun version 7.2.4) was provided by Vela Solaris to be used for this thesis. The programme was chosen because it was regarded as having high flexibility in terms of customizing the simulation model, as well as being user-friendly and quickly to learn. Furthermore, the integrated shading simulator was considered especially relevant for this particular case study. A brief description of this simulation tool is provided in chapter 8.1 *Description of Polysun.*

Even though the system in question was modified at the beginning of this study (January 2015), it was decided that a simulation model of only the original system was to be created. This was decided for the following reasons:

1. No measured values were available for the modified system at the commencement of this study. This made it impossible to incorporate annual heat consumption values into the model in order to make it as similar to the real system as possible
2. An examination of the pre-modified system was considered greatly valuable. This is due to the fact that the 27 other solar thermal heating systems of Løvåshagen housing cooperative resemble the system on which the measurements from 2014 are based on (the original system design). If this study reveals alterations that may potentially improve the solar contribution, then the same implementations may be conducted on the other systems as well, thereby also increasing *their* performance
3. It was desired to keep this study within reasonable limits

The input values for the simulation model created in Polysun, as well as comments regarding the creation of this, are presented in chapter 8. *Simulation inputs*.

### ***Evaluation of measured and simulated system performance***

As explained in the literature review, different performance indicators can be used to determine the performance of a solar thermal heating system. It was decided that the solar fraction is a satisfying indicator for this case study, as it establishes the overall performance of a system, and not just for one component. In this case study, the solar fraction will be calculated based on the amount of solar energy supplied to the tank and the amount of auxiliary energy consumed by the immersed electrical heating element. This results in the following equation:

$$\text{Solar fraction} = \frac{\text{Solar energy supplied to tank}}{\text{Solar energy supplied to tank} + \text{Auxiliary energy supplied to tank}}$$

In order to discuss the energy savings from having a heating system with solar input, the fractional energy savings will be calculated for the existing system by running simulations in Polysun. The method for estimating this is provided in chapter 9.3.2. *Fractional energy savings*.

To provide a better understanding of the system as a whole, more detailed results will be presented based on the simulation model in *chapter 9.4 Detailed simulated results*. In this regard, certain indicators will be used to describe the functioning and performance of the investigated system:

$E_{sol}$  is solar irradiation onto total collector area,

$Q_{sol}$  is the collector yield, i.e. useful thermal output of the collectors, and

$S_{sol}$  is the net amount of solar energy utilized in the storage tank.

The boundary layer for each of the three indicators are shown in Figure 36 below.

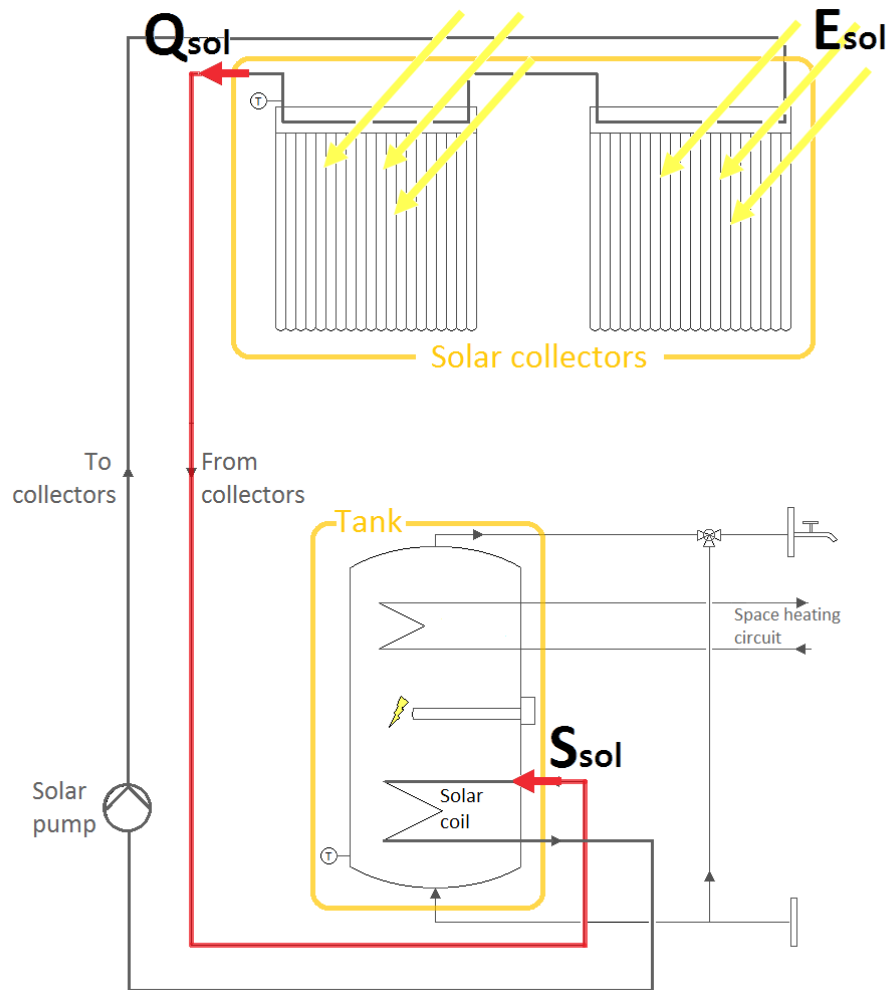


Figure 36: The different boundary layers for  $E_{sol}$ ,  $Q_{sol}$  and  $S_{sol}$

### ***Parametric study***

Once the measured and simulated performance is established, a parametric study of the main parameters will be conducted, based on the simulation model in Polysun. The intention is to investigate their effect on system performance, and thereby reveal the potential for improving both the design and the operation of the system. A more detailed description of the procedure and conditions for conducting this study is provided at the beginning of chapter 10. *Parametric study*.

## 7 Description of measurements

---

As mentioned in chapter 5.4 *Ongoing study*, measurements have been made of the investigated system since May 2013. In this subchapter, a brief description of devices, measurement setup and the procedure for processing the retrieved data is provided.

### 7.1 Devices

#### ***Energy meter and water meter***

In order to measure the thermal outputs (collectors, radiator, floor heating) and the DHW volume withdrawal, energy meters and a water meter were installed.

Energy meters (kWh meters) of the type Aquametro PMW20 Basic with Aquametro Calc ST calculator for net operation were used. The basic function and measuring principle of this meter was illustrated in Figure 26 in the literature review (chapter 4.1 *Function and yield control*). The energy meter is equipped with passive or active flow meters and a 2-wire or 4-wire Pt100 or Pt500 temperature sensor (Aquametro, 2015).

To measure the consumption of hot water, a mechanical water meter with remote reading output from SIEMENS (WFW) was used. The meter accumulates flow values as pulse variables, where one pulse equals a volume of 10 liters of water.

#### ***Sensors for remote readings***

WiSensys, a platform for wireless measurements developed by Wireless Value, was used to monitor the system online. It is useful for various purposes, such as quantifying energy consumption or measuring temperatures. Data is digitally sent to a base station by means of wireless technology, from which it is automatically forwarded to the web-based application, WebSensys ([www.websensys.no](http://www.websensys.no)). Here, the measured results can easily be downloaded and displayed in different formats and time intervals (WiSensys, 2014).

To monitor the solar yield online, as well as the heat consumption for DHW, radiator and floor heating, sensors were installed on the thermal heating system. Figure 37 shows the location of these. It should be noted that the sketch illustrates the setup *before* the modification was implemented in January 2015.

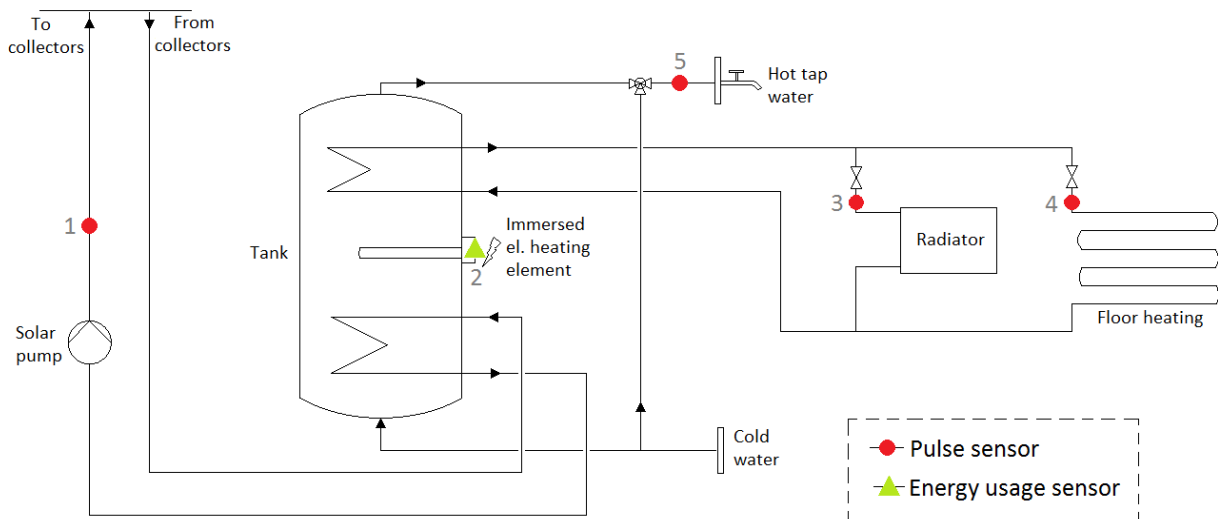


**Figure 37: A principal sketch of the instrument setup for remote monitoring**

Two sensor principals were used: *pulse* and *energy usage*. A pulse sensor detects and counts pulses. When connected to an energy meter, it can be used to measure energy consumption. For every kWh, one pulse is registered. The energy usage sensor is a sensor that measures energy usage directly (kWh). This is achieved by plugging the investigated energy meter into the power outlet of the sensor (WiSensys, 2015).

An overview of the sensor types and locations installed on the thermal system is presented in Table 12. Location 1-5 corresponds with the positions displayed in Figure 37.

**Table 12: Overview of each sensor type and its location on the solar thermal heating system**

Location	Sensor	
	Name	Type
1 Solar circuit	WS-DLX	Pulse
2 El.heating element (tank)	WS-DLR	Electrical energy usage
3 Radiator circuit	WS-DLX	Pulse
4 Floor heating circuit	WS-DLX	Pulse
5 DHW circuit	WS-DLX	Pulse

## 7.2 Reliability of devices and challenges during measurements

The reliability of the measured data that is collected is mainly determined by the devices. The energy meters and the water meter were assumed to provide precise measurements, given that they were correctly mounted and calibrated. As for the two sensor types used to accommodate remote

readings, i.e. the energy usage sensor and the pulse sensor, it was the pulse sensor that was the main source of problems when analysing and processing the measured data collected from Websensys.

### 7.2.1 Challenges during measurements

The primary focus of this study is the measured results from 2014. During the examined period, however, data from occasional time intervals during the year are lacking due to disconnections between the sensors and the WiSensys base station. There were three main challenges when retrieving the measured data:

1. *Missing intervals*: several minor intervals of data in WebSensys were lacking, everything from between a few days to several weeks
2. *Deviation between remote and direct readings*: at times, the remote readings of the solar yield differed considerably from the corresponding direct readings
3. *No available remote readings of the radiator consumption*

Consequently, it was necessary to make certain approximations and assumptions during the processing of the measured results. In general, the occasional lack of data only influenced the accuracy of the daily, weekly, and sometimes the monthly values. In other words, the annual values for the energy consumption and solar yield are unaffected in all cases, except in the case of radiator. Co-supervisor Magnar Berge made several visits within the measurement period, during which he manually read the thermal outputs displayed on the meters. These direct readings are attached in *Appendix A.2 Direct readings*. Due to the lower accuracy of the pulse sensor that was connected to the meters, the manual readings were used to control the accuracy of the digitally logged values. The electrical heating element, which was connected to an energy usage sensor, could not be read directly since it had no display. Since this sensor has a high accuracy ( $\pm 1\%$ ), it was assumed that the remote readings retrieved from this sensor were reliable.

In the following subchapter, the chosen procedure for stipulating the monthly heat consumption and solar yield generated by the collectors, as well as the approximation of the hourly domestic hot water draw-off curve, will be elaborated.

### 7.2.2 Correction of measured results and stipulation of missing values

#### **1. Complete the thermal output curves for auxiliary and solar heating of the tank**

In order to retrieve monthly data, interpolation was used to stipulate the missing intervals. The energy usage sensor, which was used to measure auxiliary energy consumption (electricity), automatically reset itself several times during the year, whenever a maximum value of 596,25 kWh was reached. This knowledge, combined with the different slopes of the curve (before each



peak), made it possible to stipulate the actual consumption curve over the course of the year, thereby estimating the monthly values.

The complete consumption curve for year 2014 of the electrical heating element and the solar yield curve of the collectors are presented in Figure 38 below. The solid lines represent the measured values that were retrieved from the base station. The dotted lines represent the interpolated values that were applied to replace the missing intervals. The corresponding DHW curve and the floor heating curve of 2014, as well as the measured values of the modified system of 2015, are displayed in *Appendix A*.

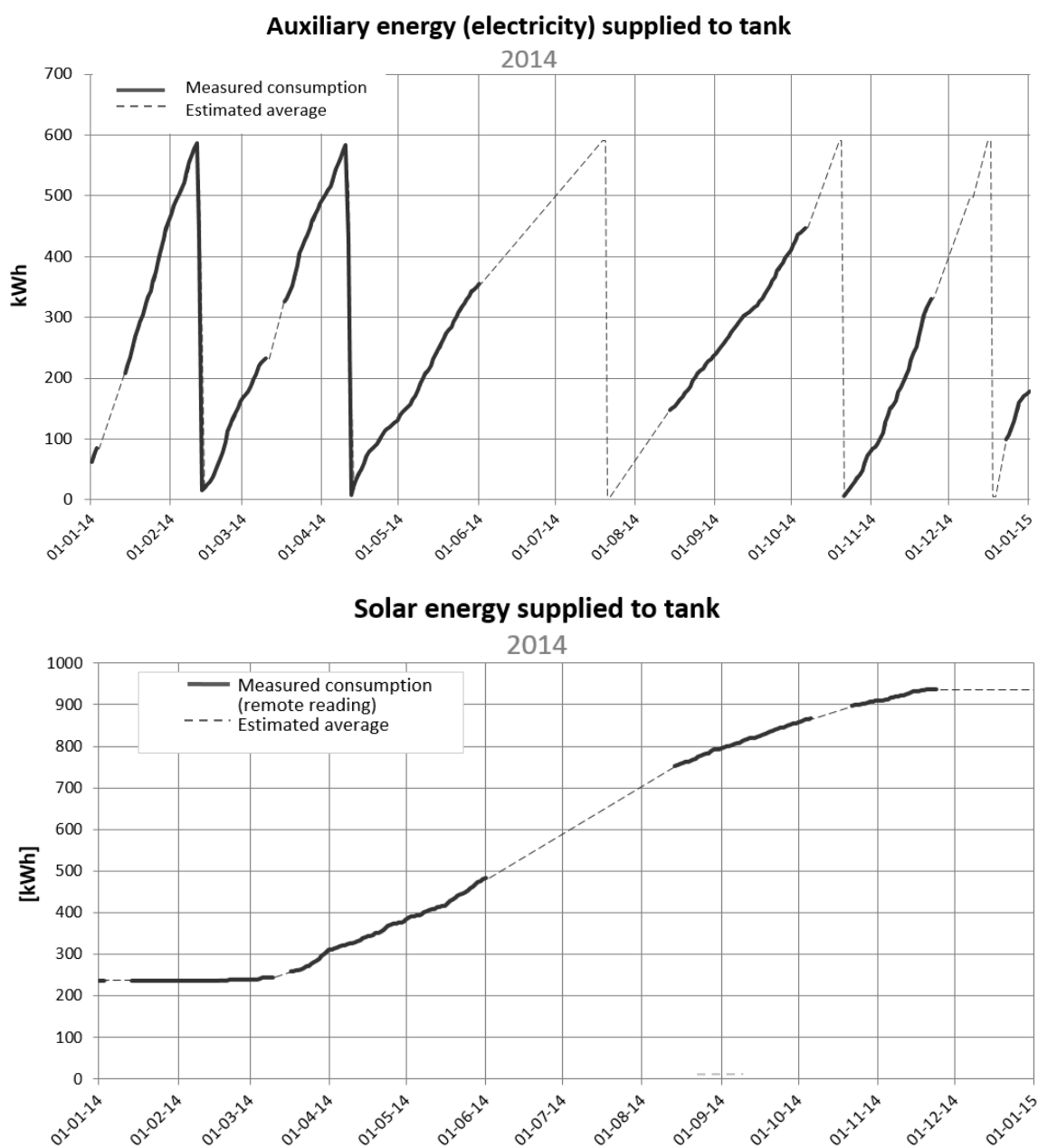


**Figure 38: Top: auxiliary energy consumption curve of the immersed electrical heating element. Bottom: Solar yield curve**

## 2. Control and correction of the remote readings according to the direct readings

As explained in the introduction, it was only necessary to correct the solar yield curve from Figure 38. On an annual basis, the value of the direct readings constituted only 54% of that of the remote readings retrieved from Websensys. The average daily curve of year 2014 was therefore obtained by multiplying with a factor of 0,54, as seen in Figure 39.

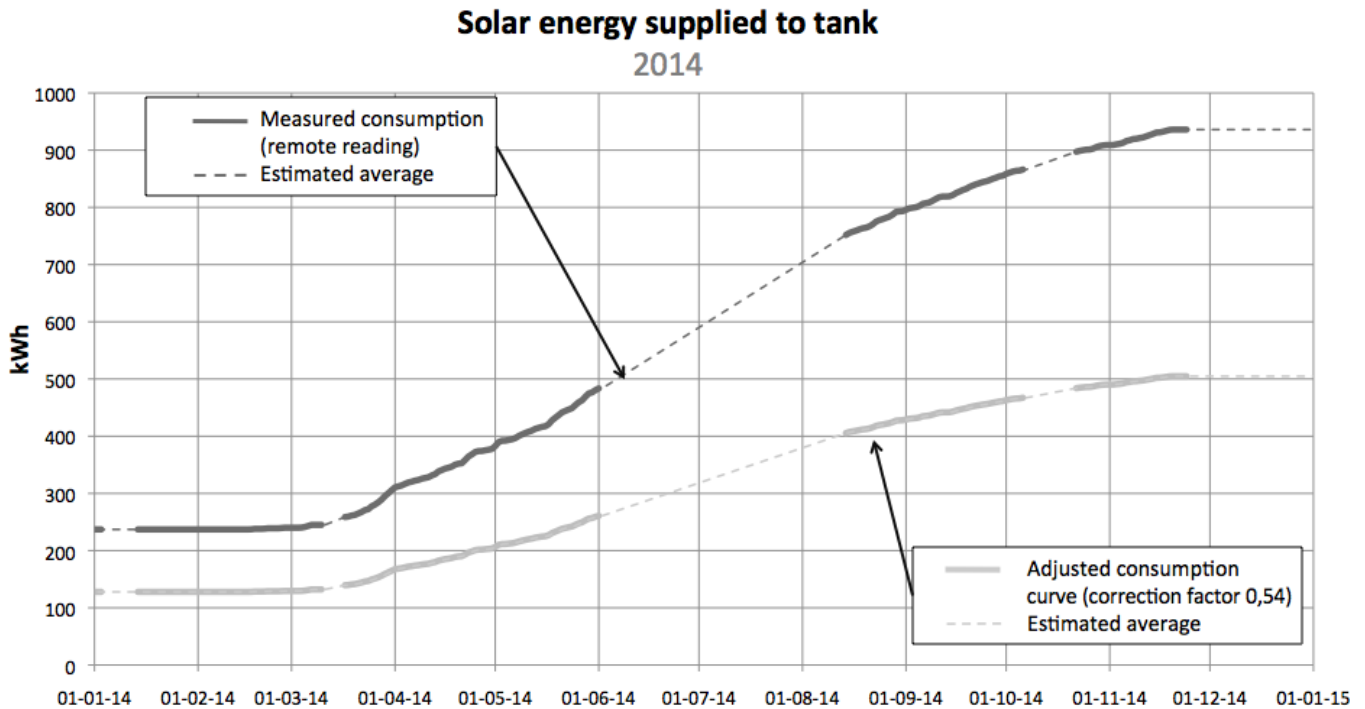


Figure 39: The solar yield curve of the collectors, both before and after correction

## 3. Stipulate the annual thermal output to radiator

The direct reading (*Appendix A.2*) showed that the thermal output that was delivered to the radiator during the time period 11.11.13 – 19.11.14 was 264,4 kWh. This period exceeds the duration of one year by 7 days. In the time period 19.11.2014-29.01.2015, the average thermal output of the radiator was 0,319 kWh/day. Based on the assumption that this was a typical daily heat demand, the annual radiator consumption between 11.11.13 – 11.11.15 (i.e. subtracting 7 days) was stipulated through the following calculation:

$$\text{Thermal output from radiator} = 264,6 - \left( 7 \text{ days} \cdot 0,319 \frac{\text{kWh}}{\text{day}} \right)$$

### 7.2.3 Estimation of annual DHW consumption curve

Since the variation in consumption of domestic hot water (DHW) depends on the needs and habits of the user, it was considered advantageous to create an approximated hourly consumption profile from 2014 that could be implemented into the simulation model. Since data was occasionally missing, interpolation was used to estimate the monthly values (as explained in the previous section). Moreover, data from 15.05.13 to 31.12.13 and from 01.01.15 to 01.03.15 were used to supplement the missing sections. For instance, where weekend data was missing, representative weekend consumption data from another date was inserted. Similarly, missing data from a weekday was supplemented with data from a corresponding weekday. The resulting DHW curve is displayed in chapter 8. *Simulation inputs* in Figure 47.

## 7.3 Volume to energy conversion

The pulse sensor that was connected to the water meter registered the hot water consumption in liters. Conversion of volume (l) to energy (kWh) was done according to equation 9.

$$E = \frac{V \cdot c_{p_{water}} \cdot \Delta t}{60 \cdot 60} \quad (9)$$

where

E is energy [kWh],

V is volume [l],  $c_{p_{water}}$  is the specific heat capacity of water (4,2 kJ/kg°C), and

$\Delta t$  is the temperature difference between hot and cold water [°C] |

(Wigenstad, 2009). In consultation with my supervisor, it was decided to assume a hot water temperature of 50°C in the calculations. The cold network water temperature that is supplied to the tank bottom was based on measured data provided by Bergen Vann KF. The measured temperature of the cold water, measured on an hourly basis, during 2014 is displayed in the next chapter 8. *Simulation inputs*. The average cold water temperature, as well as the minimum and maximum value, is summarized in Table 13 below.

**Table 13: Measured cold city water temperature in 2014**

<b>Max. temperature [°C]</b>	10,8
<b>Min. temperature [°C]</b>	5,4
<b>Average temperature [°C]</b>	7,9

For the volume to energy conversion in equation 9, the average measured cold water temperature of 7,9°C was used.

## 7.4 Suspicion of return-flow

For some period of time, it was suspected that return-flow was occurring in the solar loop. This phenomenon was explained in 3.3.5 *Return-flow prevention*. For this reason, ultra sound measurements was conducted on the solar loop in the time period of January to April 2014. However, the results revealed no data that could confirm this suspicion. Furthermore, the check valve, which is supposed to prevent return-flow, showed no particular defects during an examination.

## 8 Simulation inputs

---

### 8.1 Description of Polysun

Polysun is a simulation software developed and distributed by Vela Solaris, which is a useful tool for planning and designing solar thermal-, photovoltaic- and heat pump systems. Polysun is also suitable for optimizing and assessing both existing and new systems. The software is available on two user levels: a professional level and a designer level. The former is a simple, user-friendly sales- and design tool suitable for installers and salespersons, whereas the latter is more advanced, and is applicable for system designers, energy consultants and development engineers (Vela Solaris, 2014).

The design procedure of Polysun can roughly be separated into five simple steps (Vela Solaris, 2014):

1. Selecting worldwide weather data
2. Defining the hydronic scheme. In addition to having a comprehensive template selection, it is also possible for users to create their own hydronic template
3. Defining consumer demands. Even with limited information available, it is possible to obtain accurate simulations
4. System dimensioning. A database of commercially available products is provided, including collectors, tanks, heat generators and heat exchangers. It is also possible to modify the system components, e.g. the collector area and collector inclination angle
5. Results evaluation

#### ***Meteonorm weather database***

Polysun allows the user to select any location through an online map, the Open Street Map, from which a utility program, called Meteonorm, automatically generates the necessary weather data. Meteonorm is a software created by Meteotest, which consists of weather data that is retrieved from 8325 weather stations worldwide as well as five geostationary satellites. The software can provide accurate data for any place on Earth. Weather data for new locations is generated through the use of coordinates and state of the art interpolation models. Climatic data include weather parameters like diffuse- and direct radiation, temperatures, wind speed and air humidity (Meteotest, 2015).

#### ***Shading editor***

The newest releases of Polysun (5.8 or newer) include a shading editor, making it possible for the user to account for the surrounding topography and obstructions in the simulations. By stating the

distance and height of nearby objects, the dimensions are automatically reflected on the horizon line. This allows for more accurate site data entry, as well as better yield calculations, and helps assess the impact of shading (Pressbox, 2014). A screenshot of the horizon editor with the shading feature is illustrated in Figure 40.

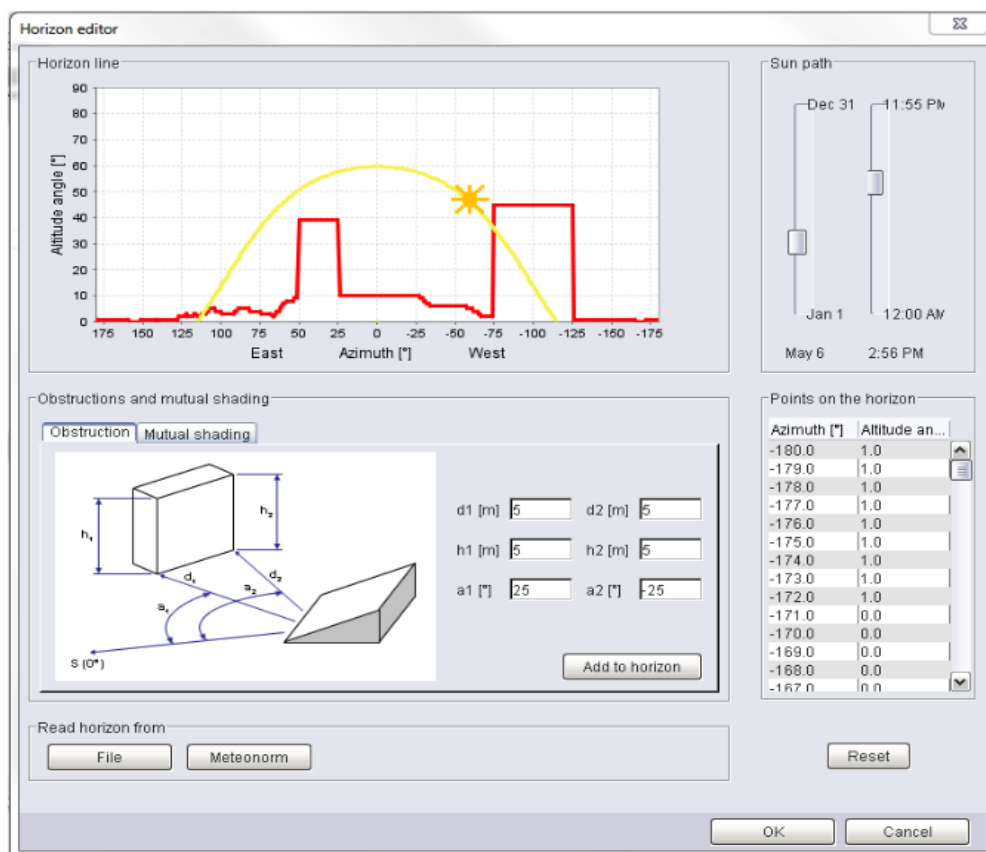


Figure 40: Polysun horizon editor (Pressbox, 2014)

In the remaining subchapters, the settings and input values used to create the simulation model of the investigated system will be reviewed. In cases where the model deviates from the physical system, or where additional explanations are considered necessary, comments are provided at the end of each subchapter.

## 8.2 Meteorological inputs

### 8.2.1 Location and climate settings

The exact location of the Løvåshagen housing cooperative was selected in Polysun through the Open Street Map, as shown in Figure 41. The location could then be matched with relevant climatic data from the Meteonorm weather database.

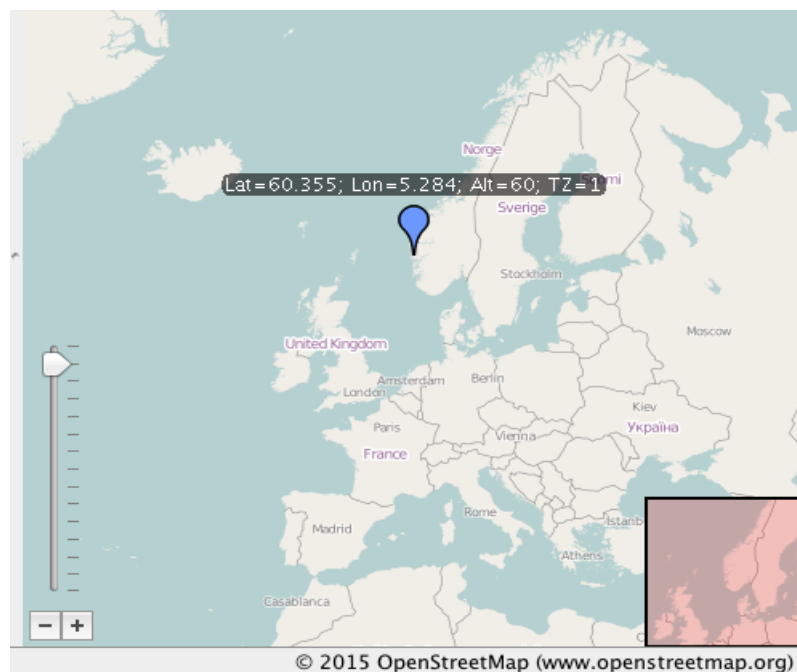


Figure 41: Open Street Map viewer in Polysun

The chosen location settings and the corresponding annual weather data for this particular location are displayed in Table 14. Additionally, the diffuse and direct irradiation on a horizontal surface (in  $W/m^2$ ) during one year are illustrated in Figure 42, and the variation in the average outdoor temperature is depicted in Figure 43.

Table 14: Coordinates and corresponding weather data for the location of Løvåshagen housing cooperative in Bergen, annual sums

<b>Fyllingsdalen, Bergen</b>	<b>Latitude: 60.355°</b>	<b>Longitude: 5.284°</b>	<b>Elevation: 60 m</b>
Average outdoor temperature	7,8		°C
Global irradiation*	760,2		kWh/m <sup>2</sup>
Direct irradiation	346,9		kWh/m <sup>2</sup>
Diffuse irradiation	437,3		kWh/m <sup>2</sup>

\*Irradiation on a horizontal surface

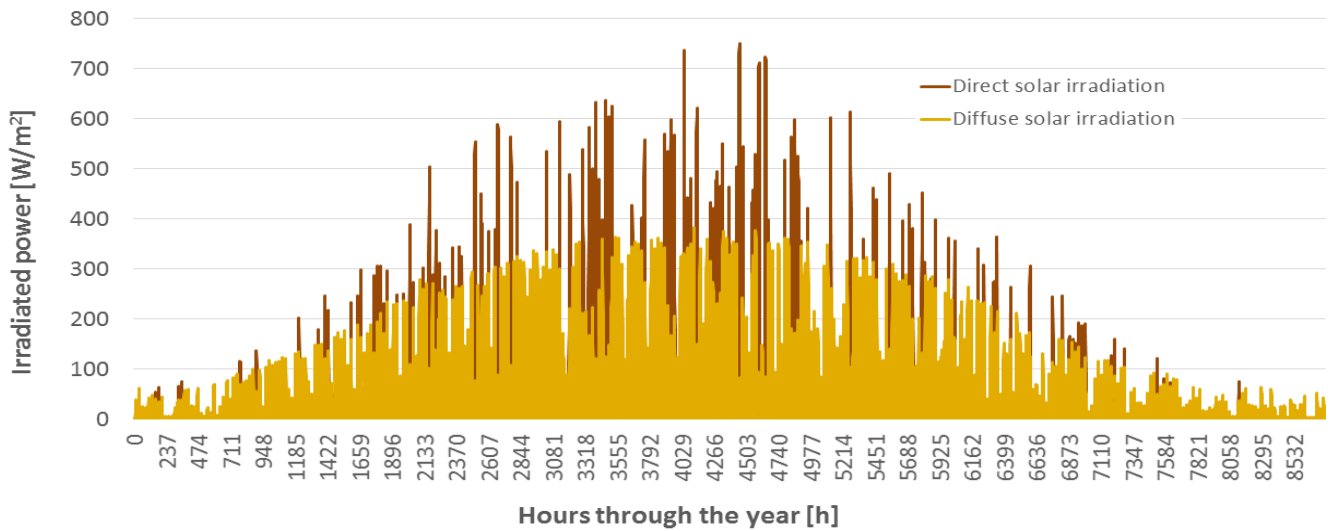


**Figure 42: Global irradiation (direct and diffuse) on a horizontal surface ( $\text{W}/\text{m}^2$ ) in Fyllingsdalen in Bergen**

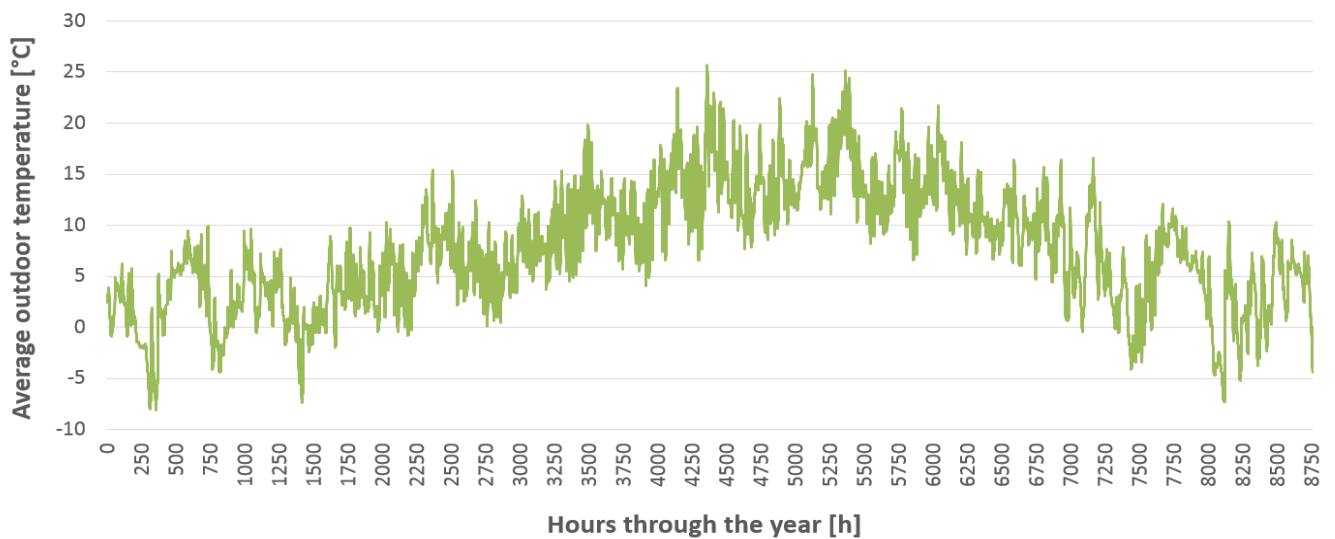


**Figure 43: Average outdoor temperature in Fyllingsdalen in Bergen**

The highest temperatures occur in July, with temperatures ranging from a minimum of  $7,7^{\circ}\text{C}$  to a maximum of  $25,7^{\circ}\text{C}$ . The coldest days appear in January, when the temperatures vary from  $-8,1^{\circ}\text{C}$  to  $9,9^{\circ}\text{C}$ .



## 8.2.2 Horizon profile and collector field settings

The horizon line from the chosen location was imported from Meteotest (online) into Polysun. To further incorporate shading of nearby objects, necessary dimensions were specified in the shading editor. The shading editor has two main features: obstructions and mutual shading. In this case, only row-to-row shading between the collectors was relevant, and therefore only mutual shading inputs were required. The input parameters are displayed in Table 15 below. Figure 44 shows the resulting horizon line along with the sun path line on June 1<sup>st</sup> at noon.

**Table 15: Shading editor inputs: Mutual shading**

<b>d</b>	Row distance	2,1 m
<b>w</b>	Collector length	1,9 m
<b><math>\alpha</math></b>	Collector inclination angle	51°
<b>a</b>	Orientation angle (azimuth)	-10°

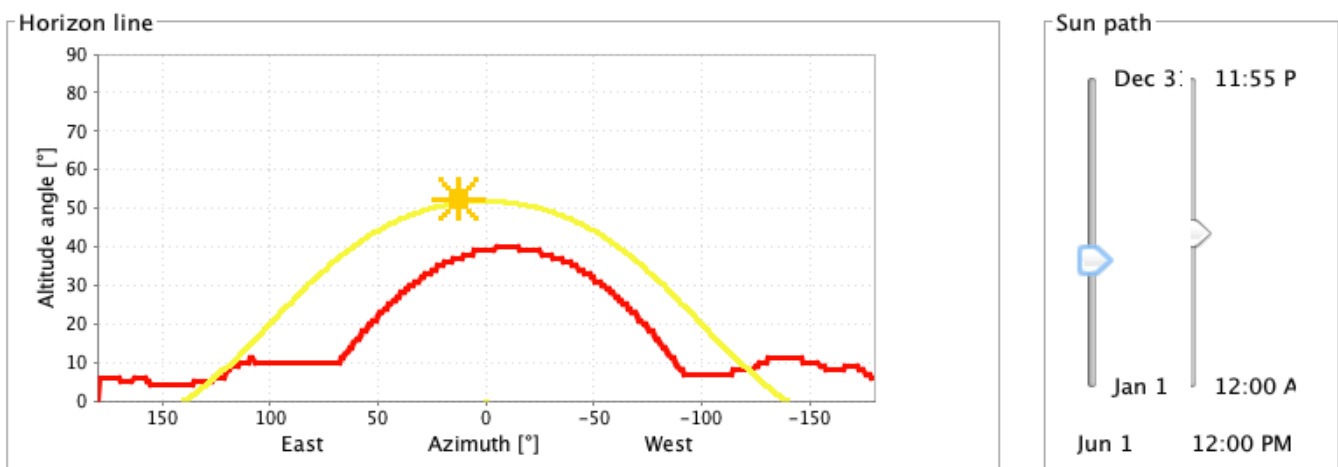
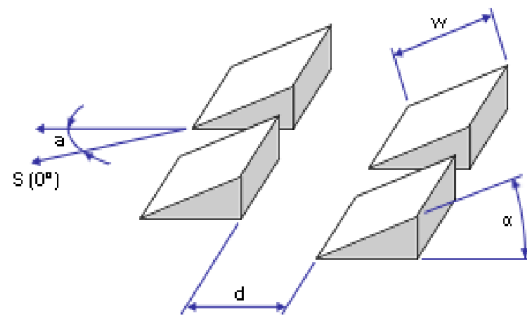


**Figure 44: Red line: The horizon for the chosen location. Yellow line: Altitude angle of the sun on June 1<sup>st</sup> at 12:00 PM**

The pronounced peak in the middle of the horizon line (red) represents the impact of mutual shading, whereas the variation of the horizon line in east and west indicates the contours of the surrounding topography, i.e. trees, bushes, hills etc.

## 8.3 Polysun model

### 8.3.1 Hydraulic scheme

Figure 45 shows the hydraulic scheme of the model that was created and simulated in Polysun.

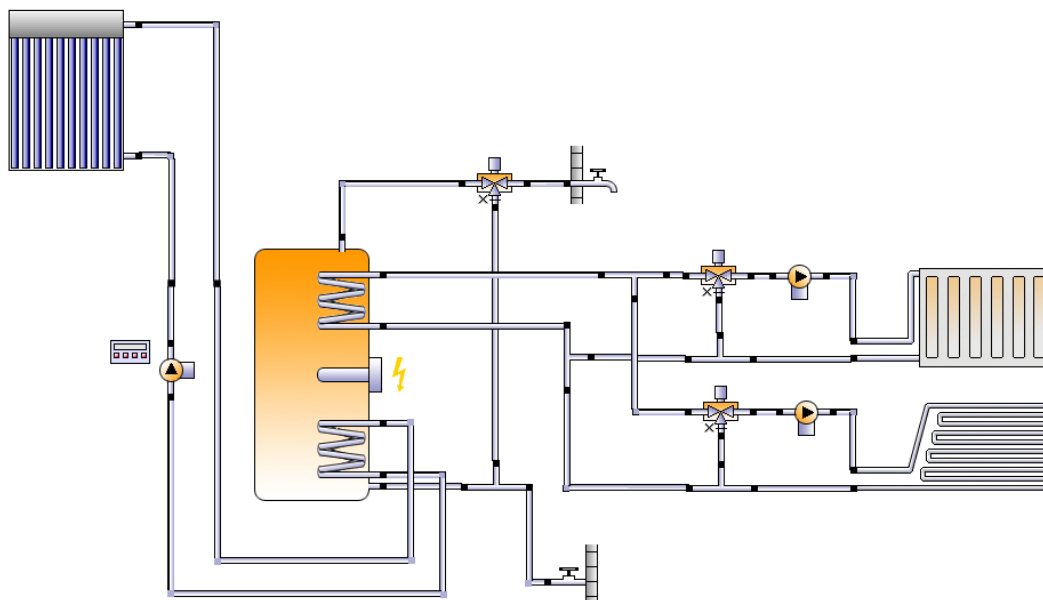


Figure 45: Hydraulic scheme of the simulation model created in Polysun

### 8.3.2 Component overview

In Table 16, an overview of the most important input parameters for the various components in the simulation model is displayed. At the end of this subchapter, a few comments regarding the gathering of necessary component data, as well as deviations between the Polysun inputs and the actual system, is provided.

Table 16: Overview of component inputs

COLLECTOR	AP-20	
Data source	SPF	
Number of collectors	2	
Number of arrays	1	
Total gross area	5,77	m <sup>2</sup>
Total aperture area	3,752	m <sup>2</sup>
Total absorber area	3,21	m <sup>2</sup>
Inclination angle (hor.=0°, vert.=90°)	51	°
Orientation (E=+90°, S=0°, W=-90°)	-10	°

<b>HEATING ELEMENT: FLOOR HEATING</b>		
Number of heating modules	1	
Power per heating element under standard conditions	1000	W
Nominal inlet temperature	60	°C
Nominal return temperature	40	°C
<b>HEATING ELEMENT: RADIATOR</b>		
Number of heating modules	1	
Power per heating element under standard conditions	1000	W
Nominal inlet temperature	60	°C
Nominal return temperature	40	°C
<b>PUMP: FLOOR HEATING</b>		
	Eco, small	
Average circuit pressure drop	0,001	bar
Flow rate	30	l/h
<b>PUMP: RADIATOR LOOP</b>		
	Eco, small	
Average circuit pressure drop	0,0005	bar
Flow rate	43	l/h
<b>PUMP: SOLAR LOOP</b>		
	Wilco-Star-ST 20/6	
Average circuit pressure drop	0,171	bar
Flow rate		
Minimum value	692	l/h
Maximum value	1041	l/h
<b>STORAGE TANK</b>		
Volume	290	l
Height	1,6	m
Material	Stainless steel 1.4521	
Insulation	Mineral wool	
Thickness of insulation	40	mm
<b>AUXILIARY HEATING</b>		
Immersed electric heating element		
Max. power	2	kW
Efficiency	100	%
<b>SOLAR LOOP</b>		
Fluid mixture	Propylene mixture	
Fluid concentration	40	%
Fluid domains volume	12	l
Pressure on top of the circuit	4	bar
Pipes		
Outer diameter	18	mm
Inner diameter	16	mm
Pipe insulation		
Conductivity at 0°C	0,038	W/(m·K)
Thickness	14	mm

### 8.3.3 Comments regarding Polysun inputs vs. actual conditions

The newer versions of Polysun allows for relatively detailed inputs of the different components of a solar thermal system. In the hope of achieving more accurate simulations, it was desirable to create a model that would resemble the real system as much as possible. However, to gather detailed information of an already installed system turned out to be a comprehensive and at times challenging process. In cases where necessary input data was lacking, default settings were used unless otherwise is explained. The deviations that are considered most significant will be explained briefly in the following paragraphs.

#### 8.3.3.1 Storage tank

It should be noted that the internal components of the tank that was illustrated in Figure 45 are not correctly scaled according to actual positions and inputs. In reality, the hot water port and the cold water port are located at the center of the tank wall (as shown in Figure 31 in chapter 5. *Case description*), from which the water is led to either the top or the bottom. In Polysun, however, it is not possible to replicate these side ports. In the simulation model, the hot and cold water therefore enters the tank from the top and the bottom, respectively. An illustration of the tank created in Polysun with the different inputs is illustrated in Figure 46 below. The positions of the coils and the ports are shown in relative dimensions, i.e. scaled in percentage from the tank bottom.

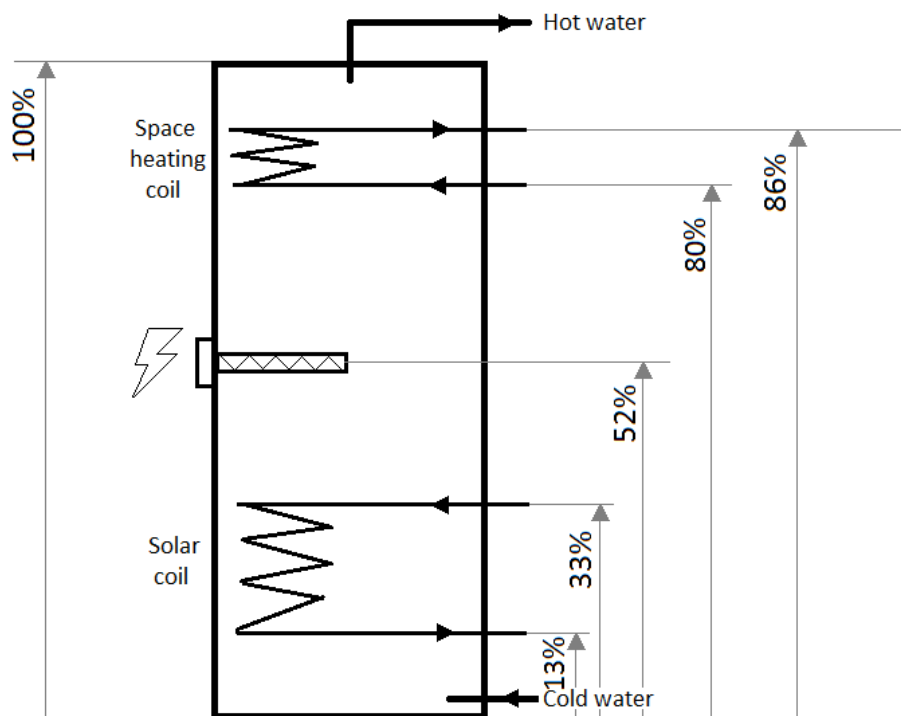


Figure 46: Simplified sketch of the various tank component inputs in Polysun

### 8.3.3.2 Circulation pumps

The circulation pump of the solar circuit (the solar pump) is a speed-stage switching pump that operates according to its characteristic pressure curves. It can be regulated at three different stages, each with its own pump characteristic. Moreover, the pump is fixed at one stage and must be regulated manually. The corresponding pump characteristic for the pump that is used in the investigated system, the Wilo-Star-ST 20/6, are attached in *Appendix B.3.1*. In the simulation model, the pump was set to operate at stage one.

In the space heating circuit, running a simulation was not possible when using only one circulation pump. As an alternative, the model was created with one pump for each heating element, i.e. one pump for the radiator circuit and one pump for the floor heating circuit.

### 8.3.3.3 Auxiliary heater

For the sake of simplicity, the efficiency of the immersed electrical heating element was set to 100%.

### 8.3.3.4 Space heating circuit

In reality, the effects of the radiator and the floor heating element are based on flow control, using thermostatic valves. In Polysun, however, there are no two-way valves available. Instead, the amount of water is regulated by using three-way-valves (shunt valves).

## 8.4 Heat demand input

### 8.4.1 Heating of domestic hot water and space heating

Table 17 lists the inputs for the annual heat demand.

**Table 17: Inputs for annual heat demand (DHW and space heating) in Polysun**

<b>Domestic hot water demand</b>		
Average daily volume withdrawal	57,7	l/d
Temperature setting	50	°C
<b>Space heating demand</b>		
Heated living area	75,1	m <sup>2</sup>
Heating setpoint temperature	20	°C

### 8.4.2 Annual DHW consumption profile

Based on measurements from 2014, the domestic hot water volume withdrawal was identified on an hourly basis and imported into Polysun, see Figure 47. Comments and approximations regarding the creation of this annual consumption profile was provided in chapter 7.2.3. It should be noted that the resolution of the graph makes it impossible to display the value for every hour during one year.

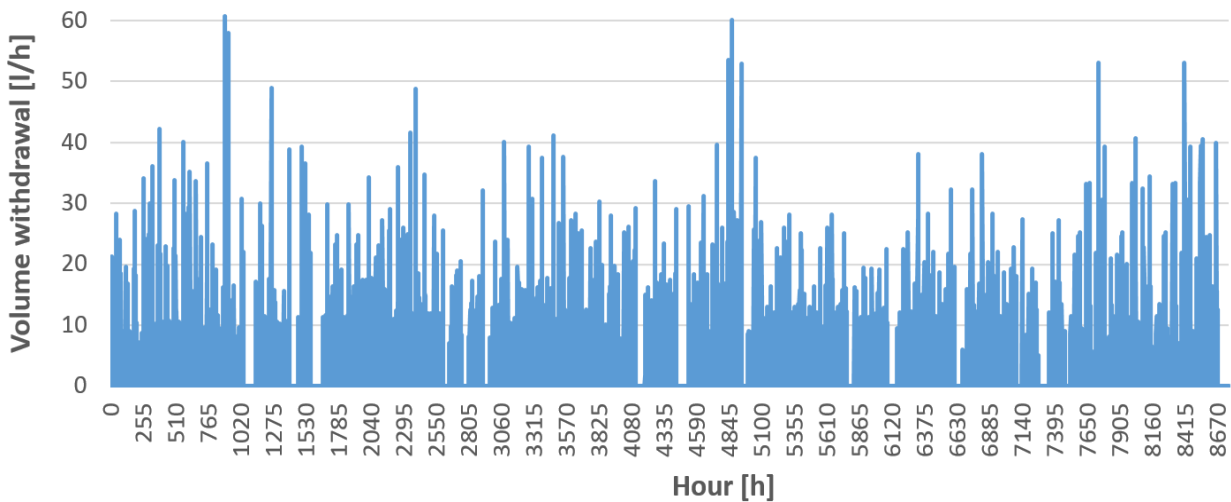


Figure 47: Measured DHW consumption curve from 2014, imported into Polysun

### 8.4.3 Hot and cold temperature setting

The temperature setting for the hot water in the mixing valve was set to 50°C. The temperature curve of the cold network water in 2014 was acquired from the municipality and imported into Polysun, see Figure 48. The cold water that flows into the tank has an annual average temperature of 7,9°C.

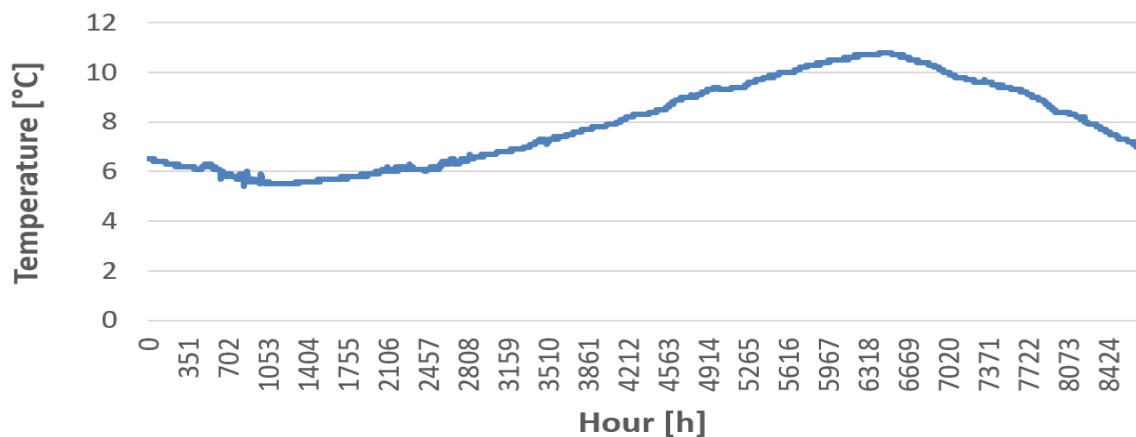


Figure 48: Cold city water temperature during 2014 on an hourly basis. Source: Bergen Vann KF

## 8.5 Controller inputs

### 8.5.1 Controller settings

The system controller is equipped with three temperature sensors:

T1: located at the collector outlet,

T2: located at the bottom of the tank, and

T3: located inside the tank at the electrical heating element

The locations of the different temperature sensors (T<sub>1</sub>, T<sub>2</sub> and T<sub>3</sub>) are illustrated in Figure 49 as red dots.

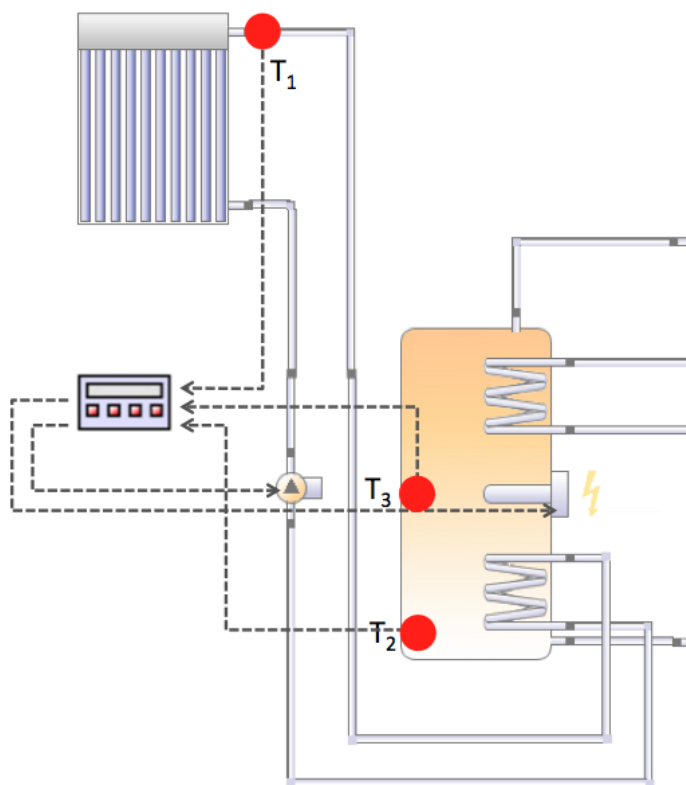


**Figure 49: Illustration of the controller inputs and outputs in Polysun**

An overview of the control of both the solar pump and the electrical heating element is provided in Table 18.

**Table 18: Controller inputs based on the actual controller settings in 2014**

<b>Solar pump controller</b>	
Switch-on temperature difference	$T_1 - T_2 \geq 6 \text{ K}$
Switch-off temperature difference	$T_1 - T_2 \leq 4 \text{ K}$
Emergency shutdown collector temperature	140°C
Maximum store temperature	90°C
<b>Auxiliary heating controller</b>	
Switch-on temperature	$T_3 < 75^\circ\text{C}$
Switch-off temperature	$T_3 > 77^\circ\text{C}$

As described in the table, the solar pump is switched on at a temperature difference  $T_1 - T_2$  equal to or larger than 6 K, and is accordingly switched off when the same temperature difference reaches a minimum of 4 K. As a precaution against very high temperatures, the overheating protection function is automatically activated at a collector outlet temperature above 140°C, which cools down the solar loop. The maximum tank storage temperature is set to 90°C. Above this limit, the storage tank will no longer be loaded with solar energy. The immersed electrical heating element, which feeds the tank with auxiliary heat at times when solar energy is limited, is turned on when the temperature of its surrounding water falls below 75°C ( $T_3$ ). To prevent it from switching on and off with at very short time intervals, the switch-off temperature is set at a couple degrees higher, at 77 °C.

#### *8.5.1.1 Comments regarding the location of the bottom tank sensor, $T_2$*

Polysun separates the tank into the 12 isothermal layers illustrated in Figure 50. The temperature sensor that measures the tank water temperature ( $T_2$ ) is, in reality, located inside the drain valve of the tank, approximately 3% from the tank bottom. Therefore, layer 1 (bottom layer) was chosen as input in Polysun, which is equal to 0–8,3% from tank bottom.



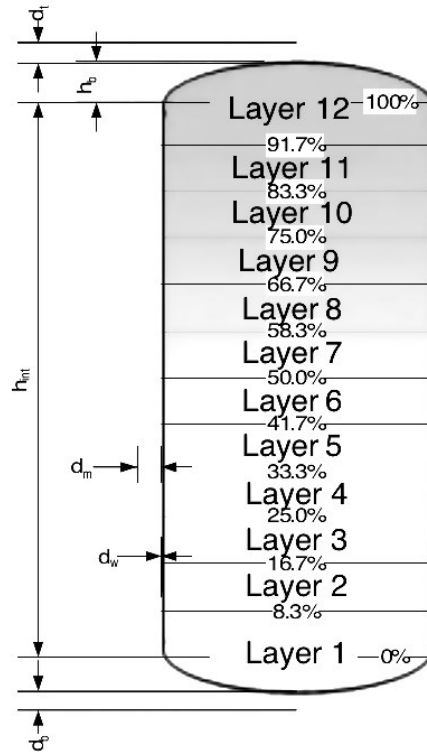


Figure 50: The twelve isothermal tank layers in Polysun (Vela Solaris, 2014)

### 8.5.1.2 Comments regarding the protection against overheating

The existing system has a cooling radiator installed on the solar circuit on the roof, just before the first solar collector (see Figure 32). This is activated when the collectors reach the emergency shutdown temperature of 140°C. This particular emergency cooling device is not available in Polysun. Consequently, its effect on the system can therefore not be accurately established. However, the simulation software does specify the maximum collector temperature, which was set to 140°C in the controller settings.

To further investigate the operating conditions of the system, and to get an impression of how frequent the cooling radiators would be activated in the model, the number of stagnation days was used as an indicator, as well as the collector temperature.

## 9 Results

As explained in chapter 6. *Methodology*, measured data from 01.01.2014 – 31.05.2015 was collected and assessed in order to get an indication of how well the system is performing, both before and after the modifications made in January 2015. In this chapter, the measured data will first be reviewed together with the simulated results based on the Polysun model that was presented in chapter 8. *Simulation inputs*. Then a more detailed presentation of the various simulated parameters is provided, including collector yields, temperatures, volumetric flow rates, heat losses, etc. At the end of this chapter, the results will briefly be discussed, and a preliminary evaluation of the current function and performance of the investigated solar thermal system will finally be made.

### 9.1 Heat demand

As explained in chapter 6. *Methodology*, the measured annual heat demand for year 2014 - for space heating by means of two heating units (radiator and floor heating) and heating of domestic hot water (DHW) - was used as input in the simulation model. In this subchapter, these results will be briefly presented.

Figure 51 and Figure 52 show the measured monthly heat demand for DHW and the measured monthly floor heat demand, respectively. In the two diagrams, the original system configuration represents values from 2014, whereas the modified system represents values from 2015. The latter are only available until May of the same year.

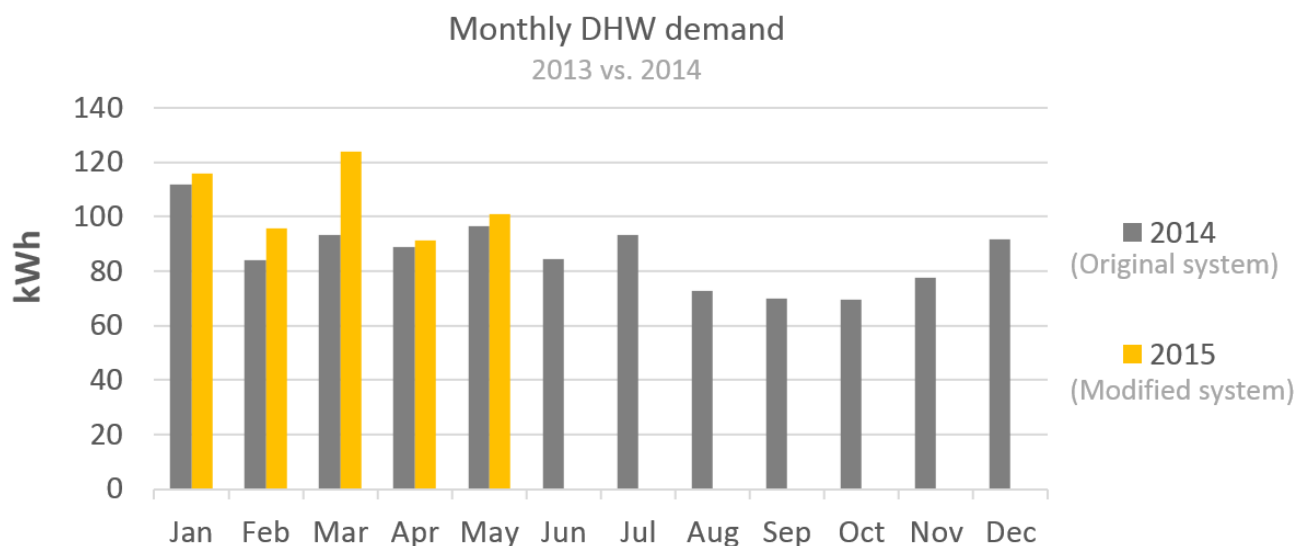
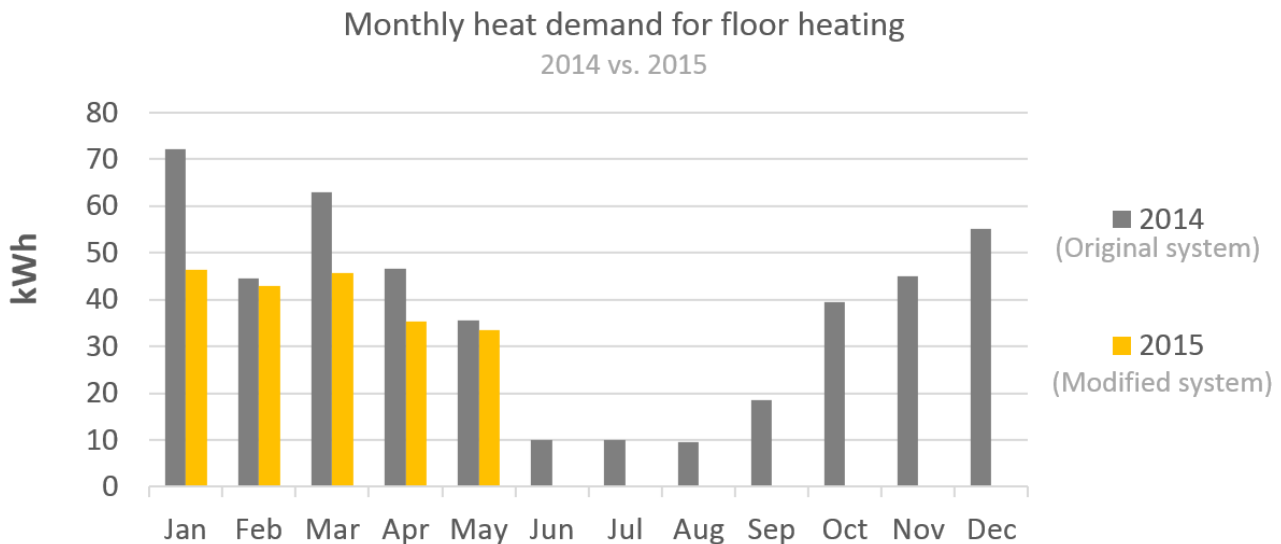


Figure 51: Monthly measured heat demand for DHW in 2014 and 2015



**Figure 52: Measured monthly heat demand for heating of bathroom floor in 2014 and 2015**

Due to reasons mentioned in 7.2.1 *Challenges during measurements*, the monthly thermal outputs from the radiator were not logged at all during the measurement period. Thus, only the annual heat consumption of this unit could be obtained through direct readings on site, which are presented in Table 19 below along with the annual values for DHW and floor heating consumption.

**Table 19: Measured heat demand in 2014 for the investigated dwelling**

	Energy demand [kWh/year]	Specific energy demand [kWh/m <sup>2</sup> /year]
Space heating (radiator + floor heating)	712	9,5
Domestic hot water (DHW)	1034	13,8
<b>Total heat demand</b>	<b>1746</b>	<b>23,3</b>

As displayed table, the annual heat demand in 2014 for space heating and DHW preparation was 712 kWh and 1034 kWh, respectively. This equals a total heat demand of 1746 kWh/year. With a floor area of 75,1 m<sup>2</sup>, this corresponds to a specific annual heat demand of 23,3 kWh/(m<sup>2</sup>·year).

## 9.2 Energy supply

Figure 53 depicts the simulated solar yield in kWh for each month during one year with the corresponding measured results, both before and after the modification.

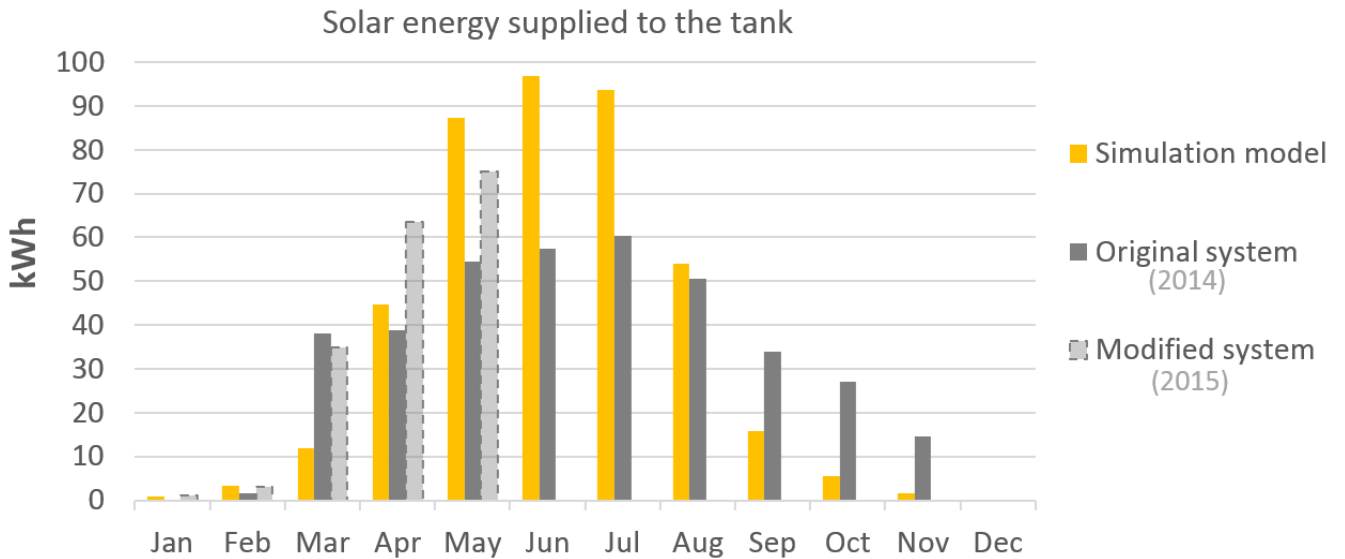


Figure 53: Measured and simulated monthly solar yield

The results show that the *measured* solar yield is higher in 2015, with the modified system, compared to the yield of 2014, before any alterations were made. The exception occurs in March, when the results of 2014 appear to have been slightly better than in the following year.

The *simulated* monthly solar yields are consistently higher than the corresponding measured results from April to August. During the months with moderate to low radiation, however, the measured solar yield exceeds that of the simulated results, with the exception of January and February. Both measured cases experience a large “jump” in solar yield from February to March, whereas the simulation model has a similar effect from March to April.

The corresponding monthly auxiliary energy (electricity) consumed by the immersed electrical heating element for the three cases are provided in Figure 54.

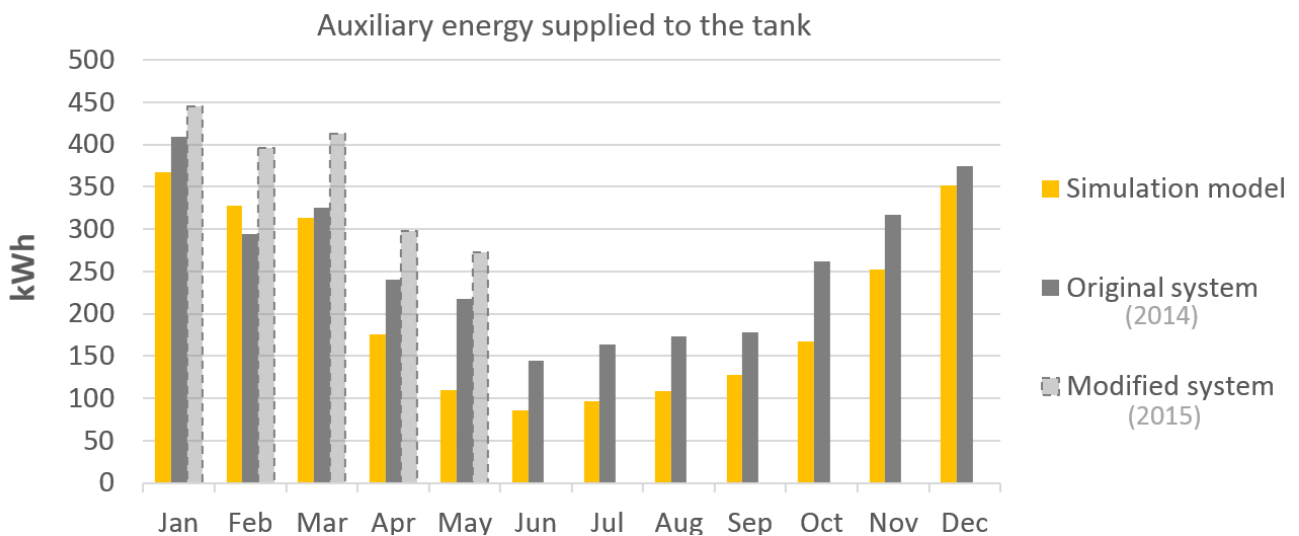
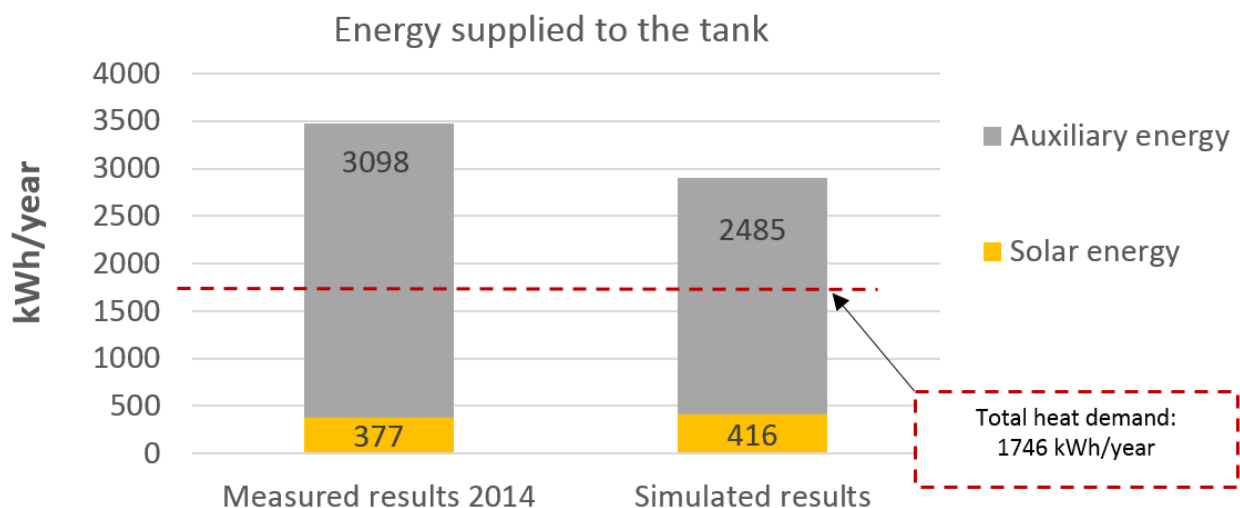


Figure 54: Measured and simulated monthly auxiliary energy supplied to the tank (immersed electrical heating element)

Similar to the solar yields presented in Figure 53, the measured auxiliary energy consumption is higher in 2015 compared to in 2014. Moreover, the simulated auxiliary energy is lower than the two measured cases throughout the whole year.

Figure 55 summarizes the annual energy supplied to the tank by type (auxiliary energy and solar energy), for both the simulated case and for the measured case on which the simulation model is based (2014). For comparison, the measured annual heat demand for space heating and heating of DHW, which is 1746 kWh/year, is included in the diagram as a red, dotted line.



**Figure 55: Measured and simulated energy supplied to the tank in 2014. The measured total heat demand for heating of DHW and space heating in 2014 is included with a dotted line**

The results in Figure 55 show that for both the measured and the simulated case, the amount of energy supplied to the storage tank was excessive, compared to the actual heat demand. Moreover, this tendency was less prominent for the simulated model.

## 9.3 System performance

### 9.3.1 Solar fraction

Based on the solar yields and the energy consumed by the auxiliary heater, which was presented in the previous subchapter in Figure 53 and Figure 54, the monthly solar fractions can be calculated for each of the three cases (simulation model, original system and modified system) according to the definition of solar fraction (presented in chapter 6. *Methodology*). The results are plotted in Figure 56 below.

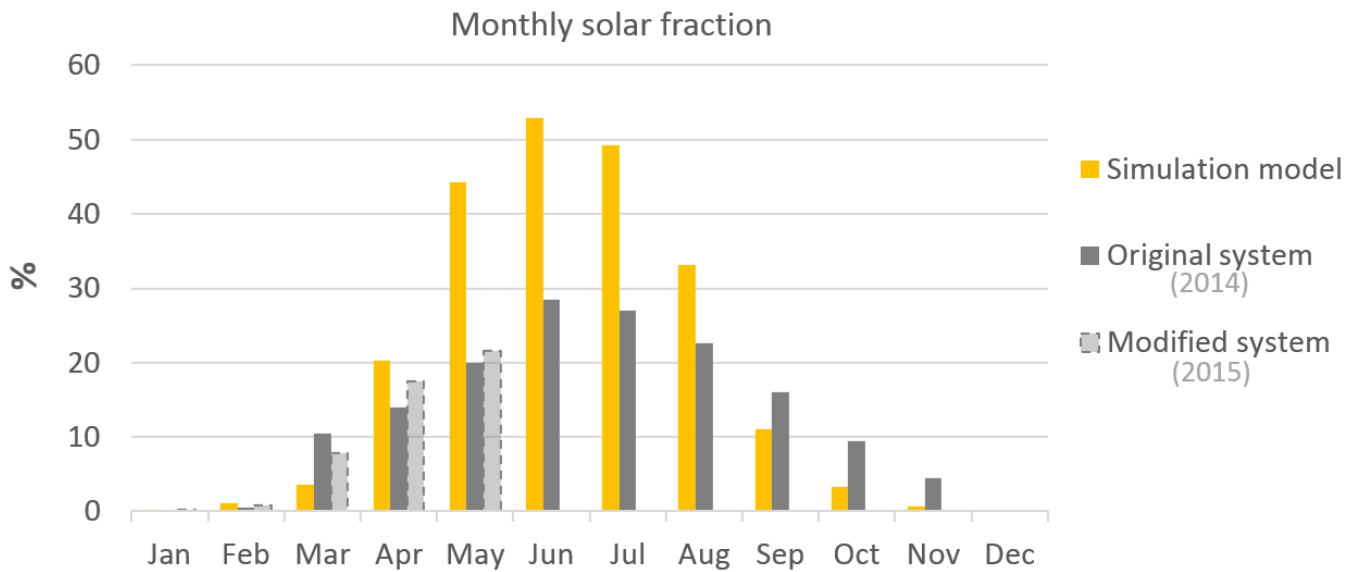


**Figure 56: Measured and simulated monthly solar fraction**

As can be seen from graph, the simulated monthly solar fractions are significantly higher during periods of high solar radiation. Furthermore, the measured monthly solar fraction that was obtained in June and July 2014, with the original system configuration, were only 28,5% and 27,0%, respectively. The corresponding simulated values were 52,9% and 49,2%. In January, no solar energy was utilized in neither the simulated case nor in the measured, pre-modified system. In December, all three cases have a solar fraction of 0%.

The average annual solar fraction for the original system design (2014) and the simulated model are summarized in Table 20. For the sake of comparison, the initial design goal of this project is included.

**Table 20: Measured (2014) and simulated annual solar fraction**

Annual solar fraction		
Measured 2014	Simulated in Polysun	Initial design goal
10,8 %	14,3 %	47,0%

### 9.3.2 Fractional energy savings

Seeing that both the measured and the simulated results reveal that the system is not performing as well as intended, and that the difference between the amount of heat supplied to the tank deviates strongly from that of the actual heat demand, it is highly relevant to ask the following question: *would the results in fact have been better with the sole use of conventional heating, that is, without any solar input?*

A first step in answering this question was to calculate the monthly and annual fractional energy savings according to NS-EN ISO 9488:1999 *Solar energy vocabulary*. This term was defined in chapter 4.3 *Evaluation of system performance*. To calculate how much energy the system would consume if only using conventional heating, the simulation model was simulated without solar input in Polysun. To achieve this, the model was altered so that the solar pump was not operating during the simulation. This version could then be set as reference system, thereby representing the case when only electricity is used (immersed electrical heating element). The monthly fractional energy savings during one year is plotted in Figure 57 together with specific delivered energy to the heating system for both cases.

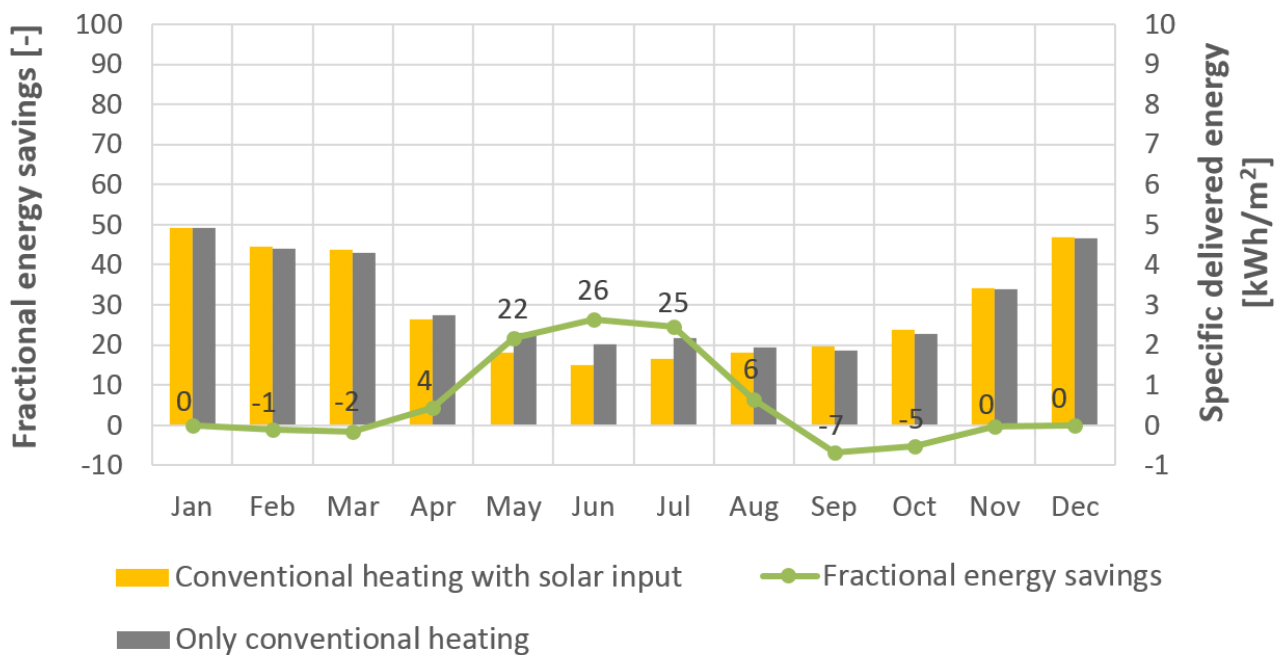


**Figure 57: Comparison between the investigated solar thermal system (reference system) and the use of only conventional heating (electricity)**

As can be seen from the graph, the energy savings with the current system design and operation are not very high compared to the energy consumed when only using electricity as energy source. The savings mainly occur from April to August, during which the highest fractional energy saving appears in June, with 26%. Moreover, the energy savings of February, March, September and October are negative. During these periods, the conventional heating system has a lower energy consumption than that of the system with solar input (reference system). As a result, the energy savings are only 3,8 % on an annual basis, as seen in Table 21.

**Table 21: Fractional energy savings for the investigated system, annual sums**

Annual specific delivered energy to heating system [kWh/m <sup>2</sup> ]		Annual fractional energy savings [%]
Solar heating system	Conventional heating system	
35,6	37,0	3,8

### 9.3.3 Original system vs. modified system

To get a better indication of whether or not the measured results presented in the previous chapter reveal that the modified system is performing better than the original system, a comparison of the first five months of years 2014 and 2015 is depicted in Figure 58 below. Both heat supply, by type (solar energy and auxiliary energy), as well as the different heat demands (DHW, floor heating and radiator) are shown to the left and to the right in the figure, respectively.

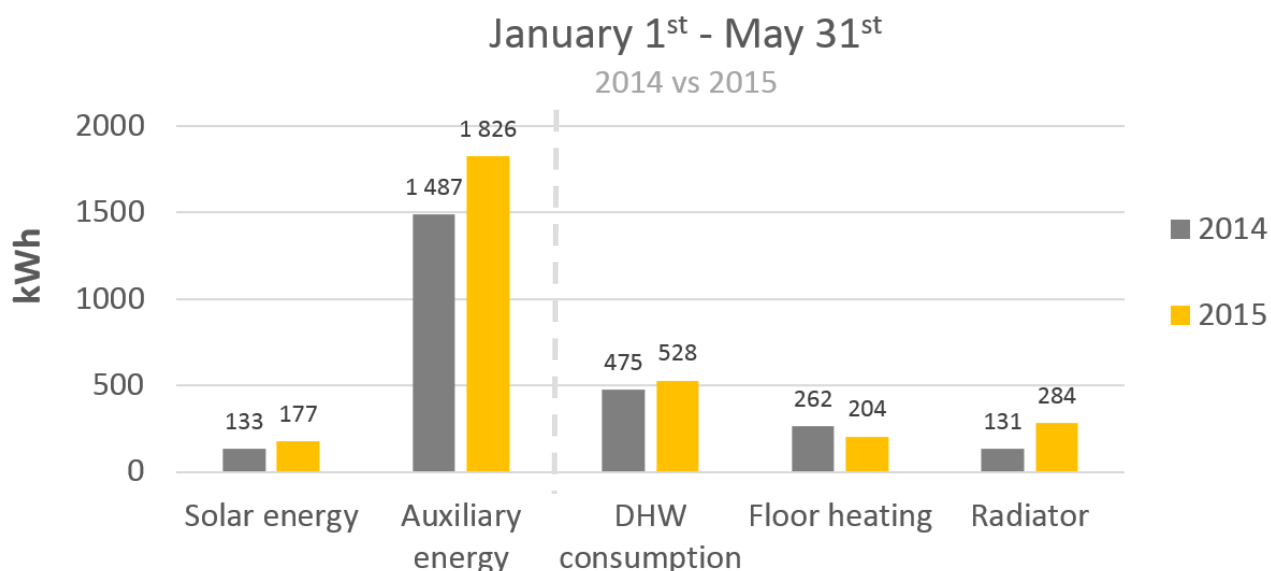


**Figure 58: Measured heat supplied to the tank, heat demand for space heating, and heating of DHW from January 1<sup>st</sup> to May 31<sup>st</sup>**



During the period 01.01.14 to 31.05.14, the solar collectors supplied 133 kWh to the storage tank. Simultaneously, 1487 kWh of auxiliary energy was consumed by the immersed electrical heating element. Within the same period in 2015 (01.01.15 to 31.05.15) with the modified system, the corresponding values were 177 kWh and 1826 kWh respectively. This equals an increase in both solar energy, by 33,4%, and auxiliary energy, by 22,8%, compared to the previous year.

The heat demands for heating of DHW and space heating in 2014 were 475 kWh and 393 kWh, respectively. Within the same period in 2015, the corresponding values were 528 and 488 kWh. This is equivalent to an increase in DHW demand by 11,2 %, and an increase in space heating demand by 24,2 % from 2014 to 2015.

The total heat demand and heat supply from January to May for the two periods are summarized in Table 22, as are also the calculated solar fraction for the given periods.

**Table 22: Heat supply vs. heat demand Jan-May 2014 and Jan-May 2015**

		<b>01.01.14 – 31.05.14 (Original system)</b>	<b>01.01.15 – 31.05.15 (Modified system)</b>
<b>Total heat supply (solar energy + auxiliary energy)</b>	kWh	1620	2003
<b>Total heat demand (DHW + space heating)</b>	kWh	868	1016
<b>Solar fraction</b>	%	8,2	8,8

As is displayed in the table, the total heat supply to the tank had a slightly higher than the total heat demand from 2014 to 2015; the total heat supply increased with 383 kWh, and the total heat demand increased with 148 kWh. This equals an increase by 23,6% and 17,1%, respectively. The solar fraction for the given periods in 2014 and 2015 were 8,2 % and 8,8 %, respectively.

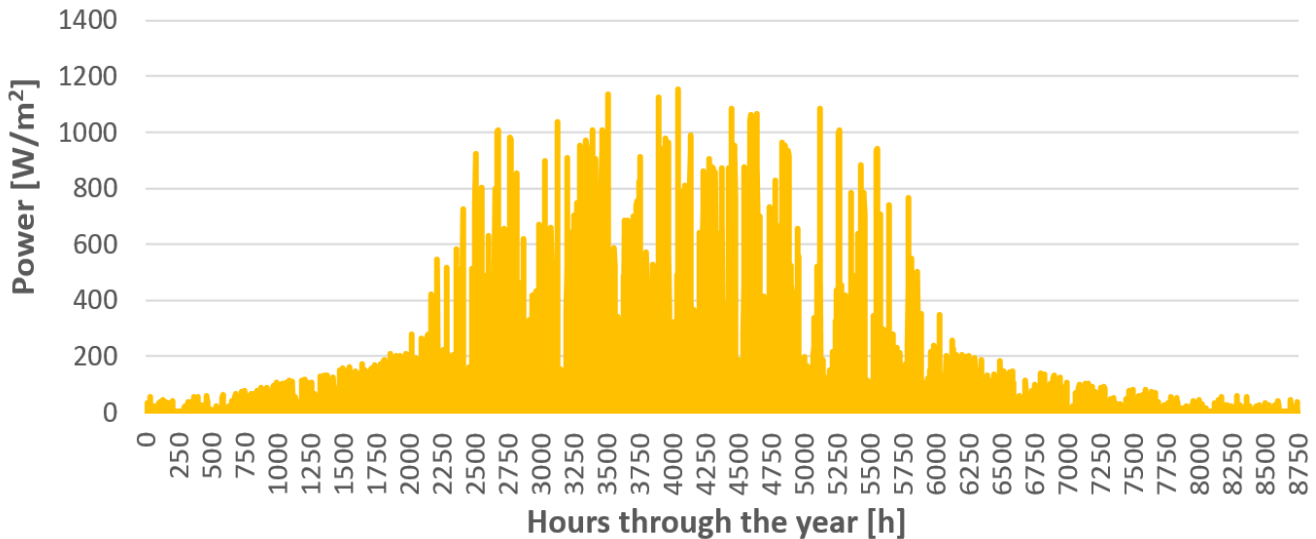
## 9.4 Detailed simulated results

In order to study the system more closely, as well as getting a better understanding of the system as a whole, this section considers the different parameters related to the main components of the investigated solar thermal system. Since the available measured data is limited, only data based on the simulation model (which represents the original system configuration in 2014) is included. Furthermore, the results presented here will be used as reference values in the parametric study in chapter 10. The terms used to describe the yields based on different boundary layers – Esol, Qsol and Ssol (gross, net- and input level) - were explained in chapter 6. *Methodology* (Figure 36).

## 9.4.1 Collector

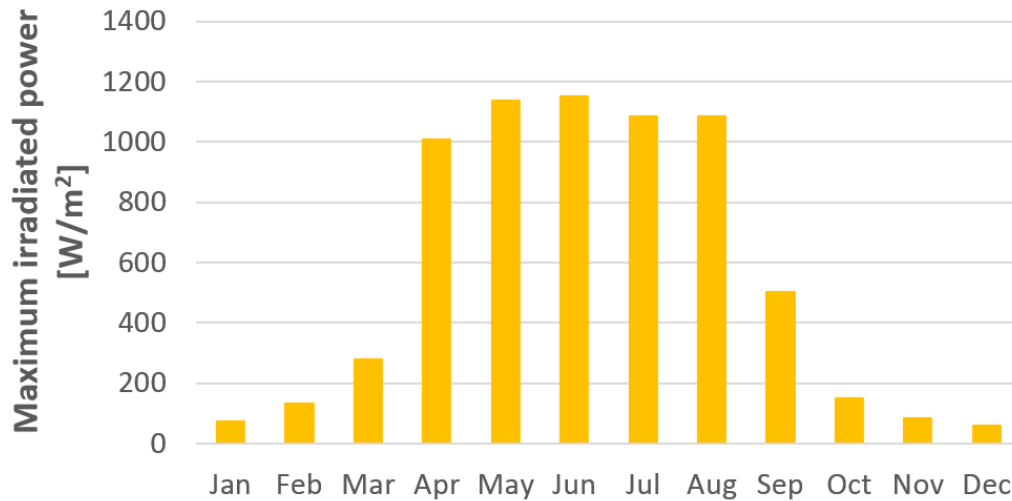
### 9.4.1.1 Solar irradiation per collector area

Figure 59 shows the irradiated power per collector area ( $\text{W}/\text{m}^2$ ) during one year.



**Figure 59: Irradiated power per  $\text{m}^2$  collector aperture area throughout the year. Total aperture area is  $3,8 \text{ m}^2$**

As explained in chapter 2.1 *Variation in solar irradiation*, the amount of radiation that hits a surface is influenced by several factors, of which local weather conditions is the main factor. On a clear summer day, the irradiated power may reach well above  $1000 \text{ W}/\text{m}^2$ , whereas on a cloudy day it can be as low as  $300 \text{ W}/\text{m}^2$ . During winter, this value may be even lower. This seems to correspond well with the simulated results presented in Figure 59. However, what is curious is that the amount of irradiation seems to undergo a sudden climb during March-April and then a large drop during August-September. This reduction differs from the global irradiation curve presented in Figure 42 in chapter 8. *Simulation inputs*, where a more even radiation curve was displayed. In fact, when further examining the maximum irradiated power per collector area for each month in Figure 60 below, these sudden gaps are made even clearer.



**Figure 60: Monthly maximum irradiated power per square meter collector aperture area [W/m<sup>2</sup>].**

The maximum irradiance during the simulated year occurs in June with a power of approximately 1150 W per square meter aperture area. Furthermore, it takes a considerable leap from March to April, from merely 280 W/m<sup>2</sup> to over 1000 W/m<sup>2</sup>, and correspondingly a large drop from August to September. Though a lower maximum irradiated power is to be expected as winter approaches and temperatures drop, these sudden pronounced leaps are suspicious, and should be investigated more closely.

The total solar irradiation during one year is summarized in Table 23 below.

**Table 23: Irradiation onto the two collectors, annual sums**

<b>Irradiation onto collector</b>	678,3	kWh/(m <sup>2</sup> ·year)
<b>Irradiation onto total collector area, Esol</b>	2437,6	kWh/year

On an annual basis, the specific irradiation onto the collectors are 678,3 kWh per square meter collector aperture area. With an aperture area of 3,8 m<sup>2</sup>, this corresponds to a total irradiation, Esol, of 2437,6 kWh/year. By comparison, the annual specific irradiation on a horizontal surface for the chosen location presented in Table 14 was 760,2 kWh/m<sup>2</sup>. Since the two collectors are tilted at an angle, which normally increases the amount of perpendicular solar beams that hit the receiving surface, the results presented in the table are lower than expected.

### 9.4.1.2 Collector yield and collector efficiency

Figure 61 shows the monthly collector yield,  $Q_{sol}$ , during one year. The collector yield represents the useful energy that is transferred from the collectors to the heat transfer fluid in the solar circuit. For the sake of comparison, the monthly irradiation curve,  $E_{sol}$ , is included in the graph with a dotted line.

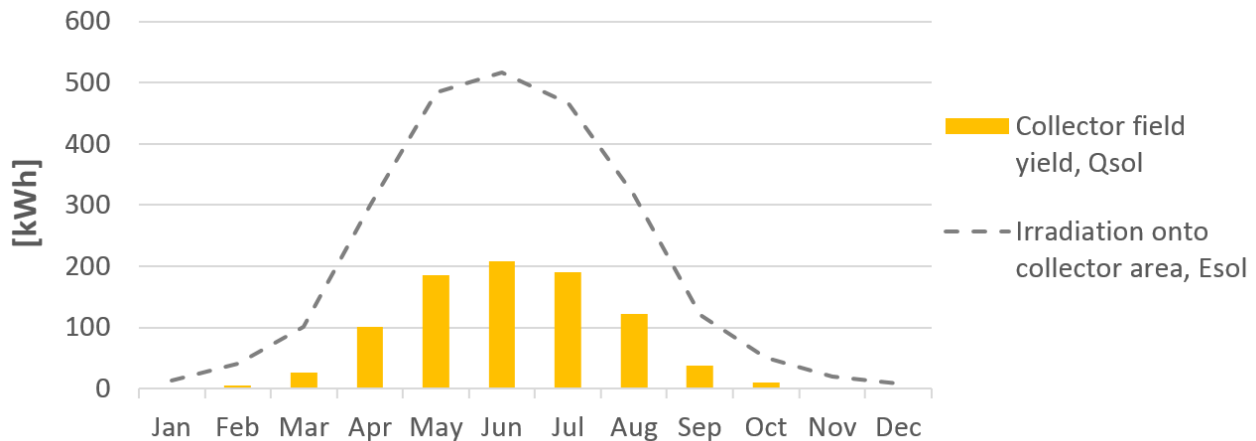


**Figure 61: Simulated monthly energy transferred from the collectors to the solar circuit (collector yield), together with the corresponding irradiation onto collector (aperture) area**

The graph shows that a large share of the solar radiation that reaches the collectors is lost to the surroundings. As discussed in chapter 3.1.2 *Collector performance and collector efficiency*, the collector yield, i.e. the useful thermal output, is strongly dependent on the efficiency of the collectors. The efficiency of a solar collector was defined as the ratio between the collected, useful energy,  $Q_{sol}$ , and the solar irradiation onto total collector area,  $E_{sol}$ . Thus, the following definition of collector efficiency can be applied:

$$\text{Collector efficiency} = 100 \cdot \frac{Q_{sol}}{E_{sol}} \quad [\%] \quad (10)$$

where  $Q_{sol}$  and  $E_{sol}$  are defined as explained above.

Figure 62 depicts the monthly average values for collector efficiency (%) during one year. As is displayed in the graph, the efficiency of the collectors are very low during periods of little to moderate radiation.

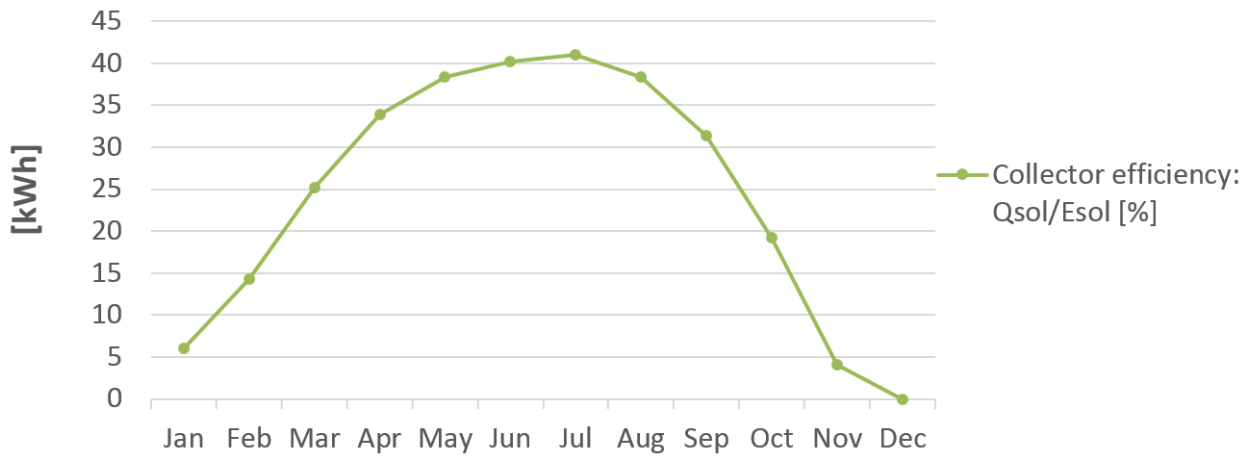


Figure 62: Monthly simulated collector efficiency [%].

Table 24 summarizes the annual performance of the collectors. The total irradiance onto the collector area,  $E_{sol}$ , was presented in the previous subchapter.

Table 24: Collector performance, annual sums

Collector yield	$Q_{sol}$	888,2	kWh
Annual collector efficiency	$Q_{sol}/E_{sol}$	36,4	%

As can be seen from the results in the table, the annual efficiency of the collectors is 36,4%. As previously explained, the collector efficiency is determined by the efficiency curve for the particular collector type, and can be calculated according to equation 1 in chapter 3.1.2. Figure 63 depicts the efficiency curve for various irradiation levels for the two Apricus AP-20 collectors, based on the optical efficiency and the heat loss coefficients stated in Table 10 in 5.3 Description of the solar thermal system.  $T_L$  is the temperature of the solar liquid in the collector manifold, and  $T_A$  is the ambient temperature.

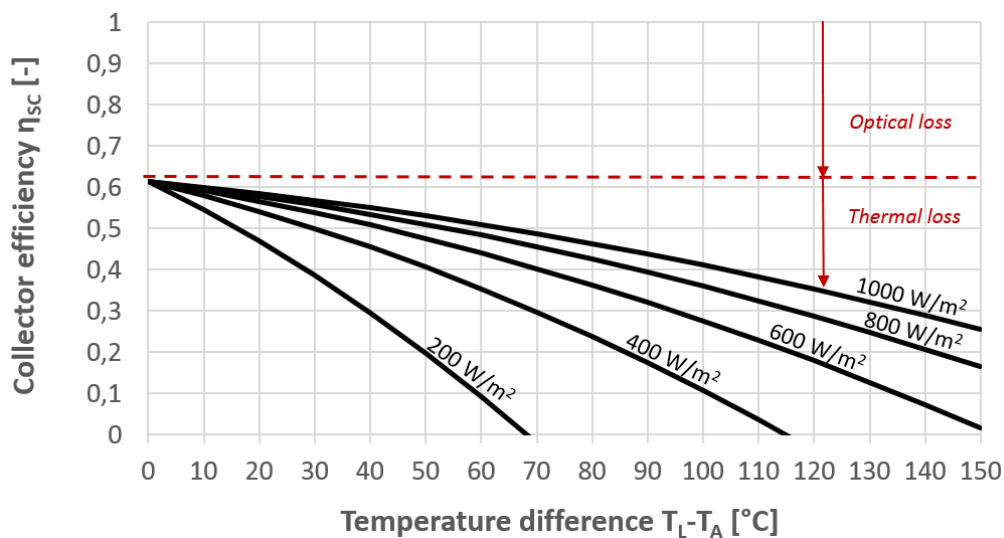


Figure 63: The efficiency curve for Apricus AP-20 for different irradiated powers ( $W/m^2$ )

As is illustrated by the efficiency curves in Figure 63, the temperature dependent losses (thermal losses) become more dominating when the irradiated power decreases. This suggests that shading, for instance from nearby collectors, may not only reduce the amount of solar irradiation that hits the collectors, it may also significantly reduce the collector efficiency.

## 9.4.2 Solar circuit

### 9.4.2.1 Flow rate in the solar circuit

The solar pump circulates the heat transfer fluid in the solar circuit between the collectors and the solar heat exchanger, which in this case study is a coil. As discussed in chapter 8. *Simulation inputs*, the pump is a speed-stage switching circulation pump that operates according to characteristic pressure curves. Figure 64 displays the maximum and minimum monthly volumetric flow rate in l/h during operating hours.

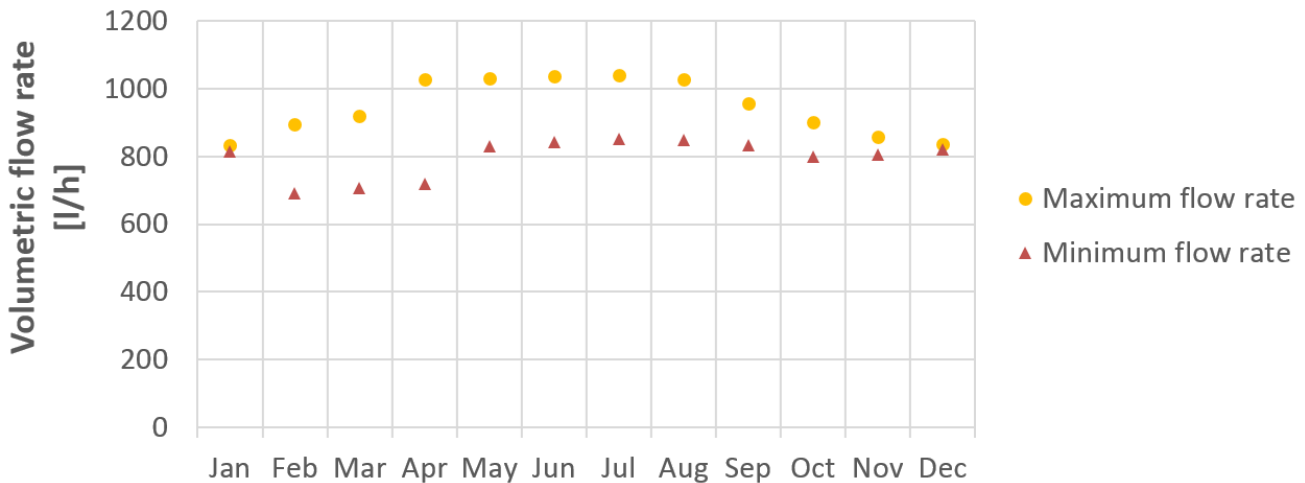


**Figure 64: Monthly maximum and minimum volumetric flow rate during one year**

The simulations show that the flow rate varies from approximately 690-900 l/h during periods of low to moderate radiation, until approximately 830-1040 l/h during periods of high radiation. Furthermore, the difference between the maximum flow rate and the minimum flow rate is very small from November to January. The impact of volumetric flow rates on system performance will be further discussed in the parametric study in chapter 10.

Figure 65 below depicts the volumetric flow rate on an hourly basis (l/h) during one year. When analysing the graph, one immediately notices an irregularity: the pump appears to be running continuously during the summer months without being switched off. This is a clear first sign that the pump control is not functioning satisfactory, and will thus be further explored in chapter 9.4.4 *Controller*.

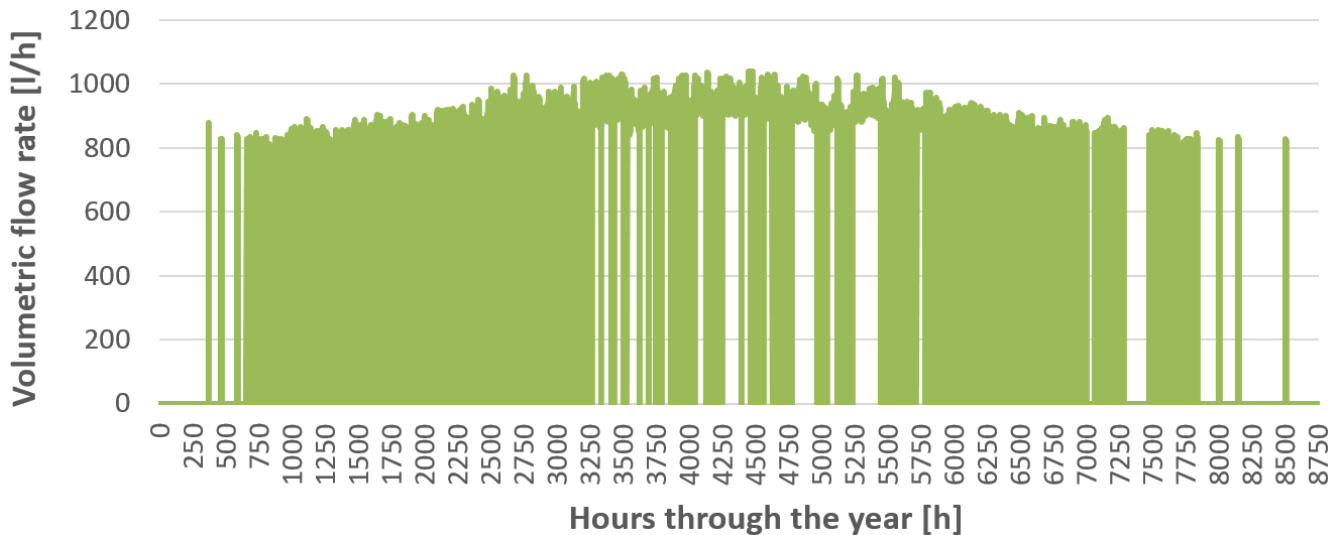


Figure 65: Flow rate through the collectors on an hourly basis throughout the year

#### 9.4.2.2 Temperature conditions in the solar circuit

As mentioned in chapter 8. *Simulation inputs*, the need for protection against overheating within the solar loop will be evaluated based on the number of stagnation days and the temperatures of the collector. As discussed in chapter 3, a solar thermal system can reach the so-called stagnation temperature during periods with high solar radiation when there is a large difference between the temperature of the solar liquid in the collector manifold and the temperature of the ambient air. At this point, energy is no longer transmitted from the collector to the solar loop since the amount of heat lost to the surroundings is just as large as the solar gains.

The maximum absorber temperature, or stagnation temperature, is strongly dependent on the collector type. For the two Apricus AP-20 collectors used in this study, the stagnation temperature is 245°C ( $G = 1000 \text{ W/m}^2$ ,  $T_A = 30^\circ\text{C}$ ) (SPF, 2004). To examine if stagnation occurs, the daily maximum collector temperature during one year is shown in Figure 66.

#### Collector

##### Daily maximum temperature [ °C]

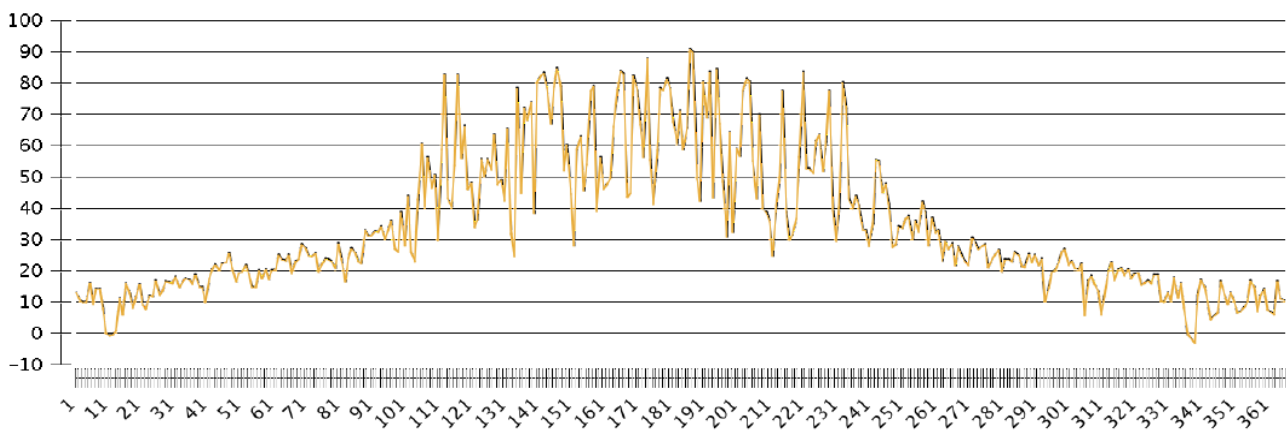


Figure 66: Daily maximum collector temperature during one year

The simulations reveal that there are no stagnation days at all during the simulated year – not even during summer. Moreover, the maximum temperature of the heat transfer fluid at collector outlet varies from over 90°C during summer to just below 20°C during winter. Similar to the solar radiation graphs presented earlier in this chapter, the maximum monthly collector outflow temperature takes a noticeable leap from March to April, and a noticeable drop from August to September.

As explained in chapter 3.1 *Solar collector*, evacuated tube collectors have the ability to generate relatively high temperatures even on colder days with moderate irradiation. This is because of the excellent insulation properties that this collector type holds. For this same reason, the collector temperature could be expected to reach even higher temperatures than 90°C during summer (higher than the temperatures displayed in Figure 66). Nevertheless, other factors would reduce the excess heat production during the high-radiation months, such as the fact that the collectors are tilted at a rather steep inclination angle.

#### 9.4.2.3 Heat loss in the solar circuit

Figure 67 illustrates the annual heat loss of the solar circuit in kWh. Furthermore, a distinction is made between heat loss to indoor room and heat loss to outdoor surroundings.

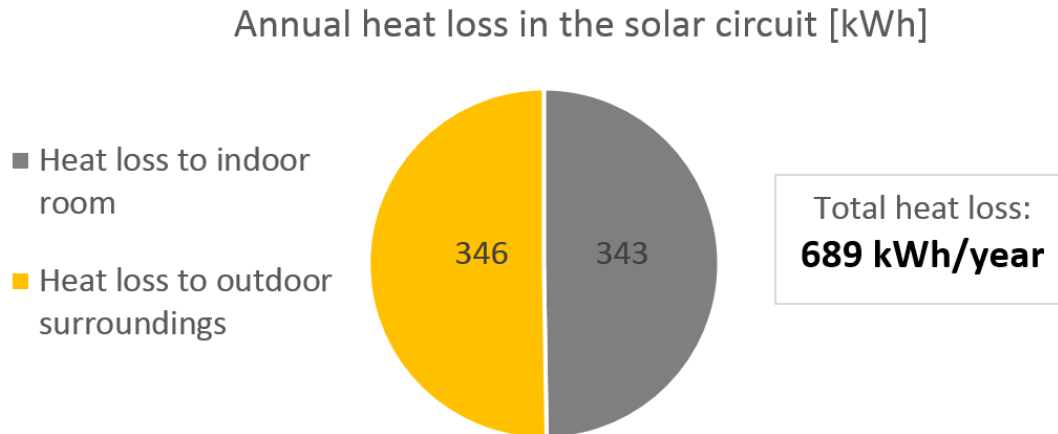


**Figure 67: Annual heat loss in the solar circuit in kWh**

As can be seen from the diagram, heat losses to indoor room are just as dominant as heat losses to outdoor surroundings. This is due to the long pipelines that run through the three floors of the building between the collectors and the tank. By comparison, the simulated annual solar energy that was supplied to the tank in chapter 9.2 *Energy supply* was 415,9 kWh/year, which is less than the total heat loss in the solar circuit.



### 9.4.3 Storage tank

#### 9.4.3.1 Solar energy supplied to the tank

Figure 68 depicts the monthly amount of solar energy supplied to the tank,  $S_{sol}$ , together with the monthly collector yield,  $Q_{sol}$ , that was presented in chapter 9.4.1.2.

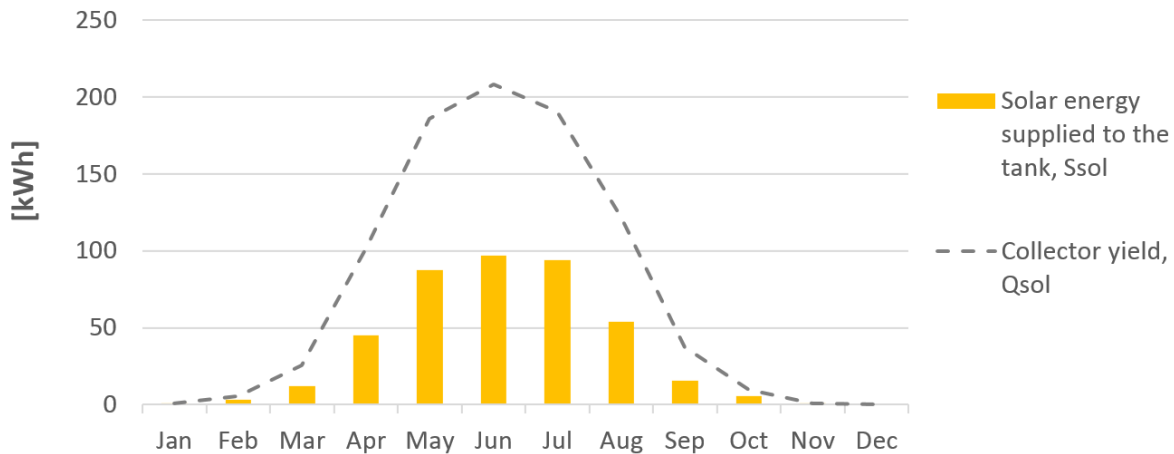


**Figure 68: Monthly amount of solar energy supplied to the tank,  $S_{sol}$ , together with the corresponding collector yield,  $Q_{sol}$**

As is shown in the graph in Figure 68, the amount of solar energy supplied to the tank is considerably lower than the useful thermal energy converted in the collectors. This difference is especially evident from April to August, when the solar radiation is at its highest.

The annual solar yield was presented in chapter 9.2 *Energy supply*. In Polysun, this value is a *net* value, which means that it is the sum of heat supplied to and removed from the solar heat exchanger (solar coil). Figure 69 shows the hourly amount of energy that flows through the solar coil during one year. Positive values indicate that the coil is supplying heat to the storage tank, whereas negative values indicate that the coil is withdrawing heat from the tank.

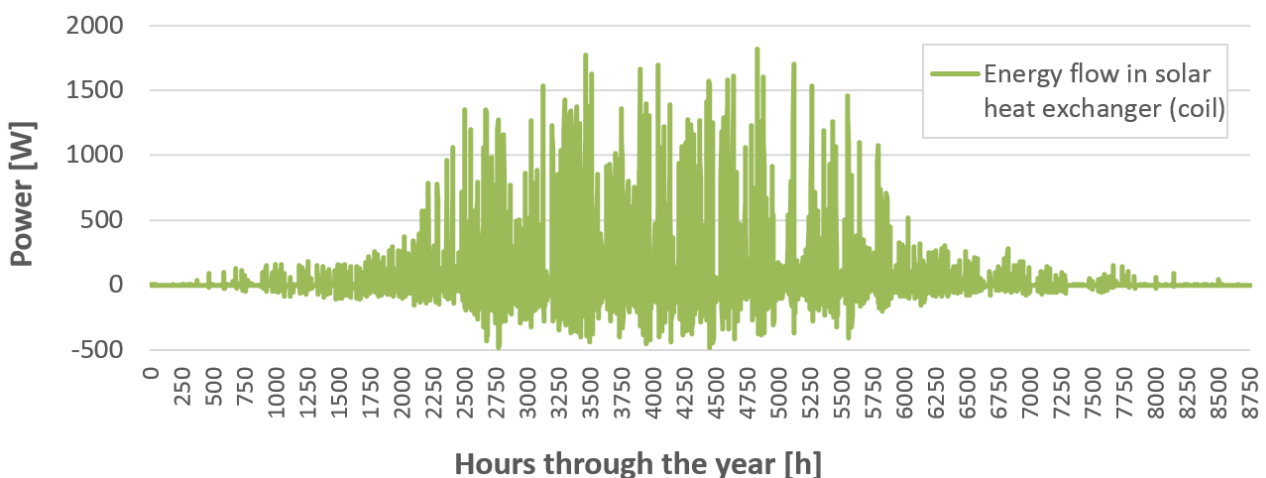


**Figure 69: Energy flow per hour in the internal solar heat exchanger (solar coil)**

The graph shows that the solar heat exchanger too often receives heat from, rather than supplies heat to, the storage tank during the high-radiation periods. This is highly disadvantageous, as it means that a large amount of heat is removed from the tank and released to the ambient.

### 9.4.3.2 Tank layer temperatures

The mean temperature for each of the twelve thermal layers in the storage tank is depicted in Figure 70, where the bottom layer (layer 1) is blue, and the top layer (layer 12) is red.

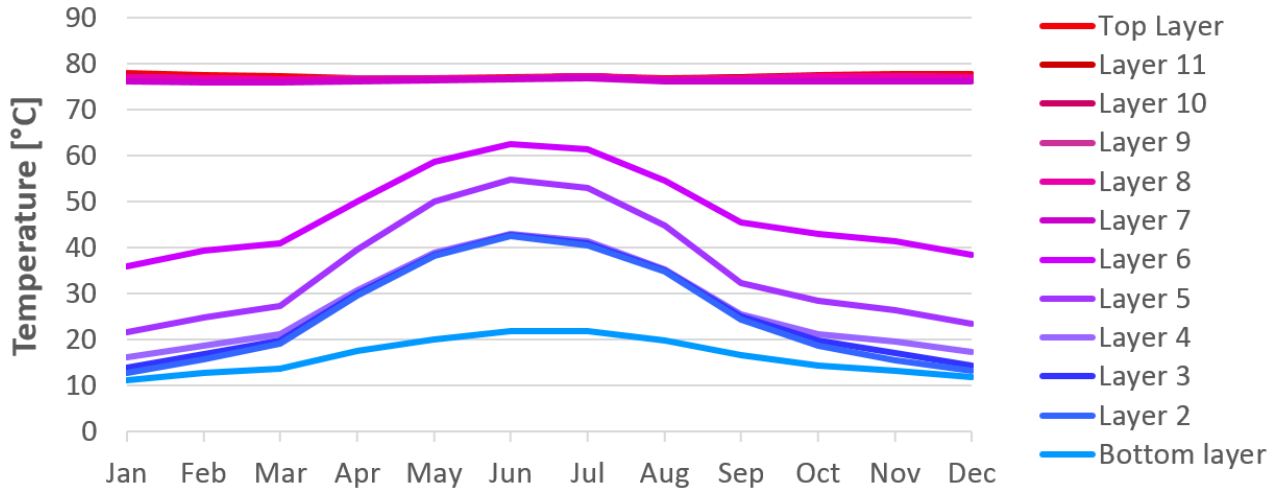


Figure 70: Monthly mean tank layer temperatures

The graph shows that the thermal stratification is to some extent present in the storage tank, but that layers 2, 3 and 4 have almost the same average temperature from April to September. Moreover, layer 7 to 12, i.e. the upper half of the tank, consistently hold high average temperatures above 75°C. Figure 71 displays the same layers on an hourly rate during one year.

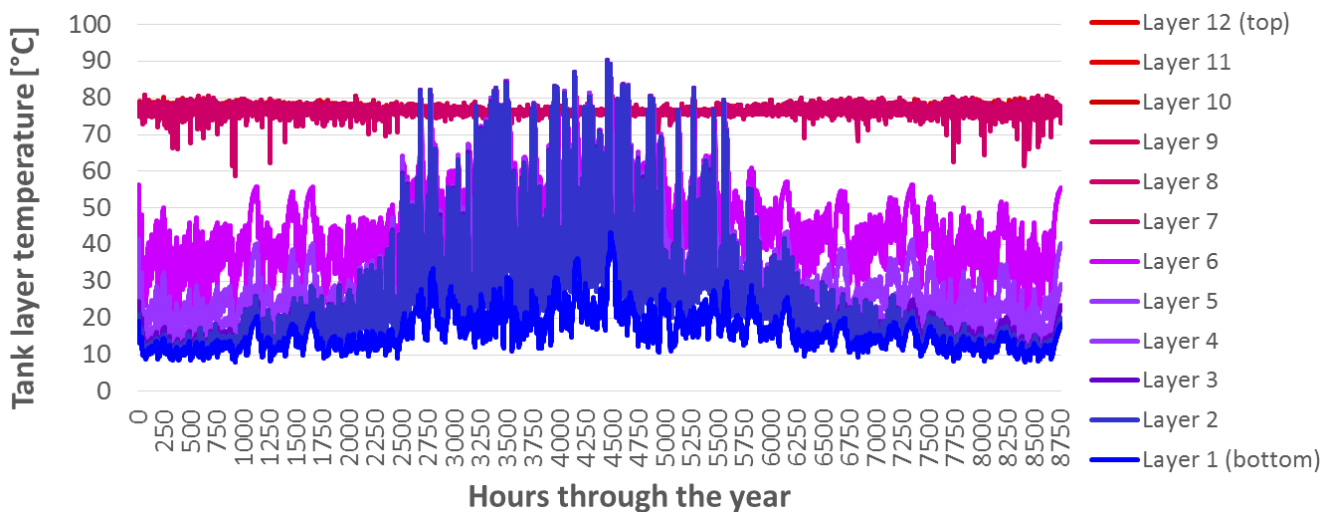


Figure 71: Tank layer temperatures from bottom layer (blue) to top layer (red).

The graph shows that the temperatures in the lower tank layers occasionally exceed the temperatures in the upper part of the tank: they can reach temperatures as high as 90°C. As shown in Figure 46 in chapter 8. *Simulation inputs*, the immersed electrical heating element is located within Layer 7 (52% from the bottom of the tank). It is turned on when the surrounding water temperature falls below 75°C, which explains the high water temperatures in the layers mentioned. During high radiation periods, the solar heat exchanger coil supplies solar energy to the tank starting from Layer 4 down to Layer 2.

The results presented in this subchapter suggests that the thermal stratification within the tank is not always sustained, and that a mixing of hot and cold water takes place. As explained in chapter 3.2.2. *Thermal stratification and energy contents of a store*, this leads to an increased need for auxiliary heating, and has a negative effect on the efficiency of a solar thermal system.

#### 9.4.3.3 Heat loss from the storage tank

The storage tank is located in the bathroom, which is a heated area. As described in chapter 3.2, heat loss from the tank increases in proportion with area and the temperature difference between the store and the surroundings. The annual heat loss from the storage tank in the examined system is shown in Table 25, including the specific heat loss in kWh per m<sup>2</sup> floor area (75,1 m<sup>2</sup>).

**Table 25: Tank heat loss**

<b>Annual heat loss from the storage tank</b>	<b>564 kWh</b>	<b>7,5 kWh/m<sup>2</sup></b>
---	----------------	------------------------------

The annual heat loss of the storage tank is 564 kWh. In this case, this is more than the annual solar energy supplied that is supplied to the tank.

#### 9.4.4 Controller

##### 9.4.4.1 Control of solar pump

The controller settings used to control the circulation pump in the solar circuit were elaborated in section 8.5.1 *Controller settings*. As previously discussed in this chapter, an evaluation of the volumetric flow rate revealed that the solar pump appears to remain turned on for several days during periods of high solar irradiation. In this subchapter, the operation of the pump will be further investigated.

Figure 72 below depicts the monthly electricity consumption of the pump together with the monthly operating time, which is scaled in percentage on/off. Additionally, the corresponding net solar energy supplied to the tank is included for comparison.

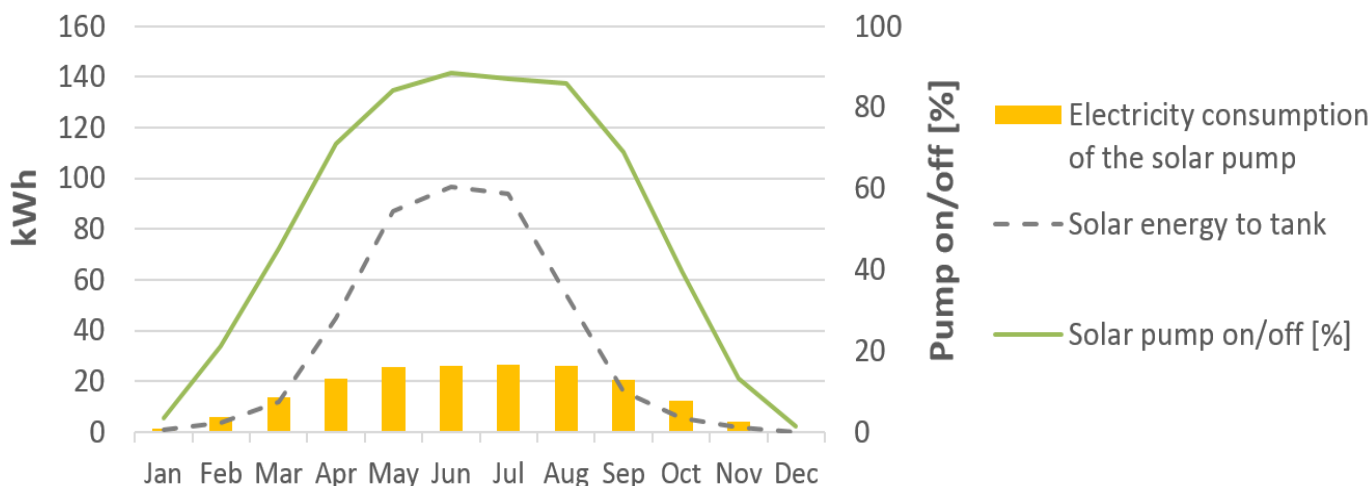


**Figure 72: Operation of solar pump vs. solar energy supplied to tank**

The graph shows that from April to September, the pump is turned on during 70 to almost 90 percent of the time. Furthermore, the pump actually consumes more energy than the amount of solar energy that it supplies to the tank from September to March. Although this effect is reversed during sunnier periods, the pump consumption is still very high. The annual values are summarized in Table 26 below.

**Table 26: Operation of the solar pump, annual sums**

<b>Total electricity consumption of the solar pump</b>	182,9	kWh
<b>Annual time ON</b>	50,9	%

During one year, the pump is turned on for over 50% of the time. Moreover, the total annual electricity consumption of the pump is 182,9 kWh, which corresponds to 2,4 kWh per m<sup>2</sup> floor area each year. This equals a share of 44% of the annual solar yield.

To give a better understanding of why the pump rarely switches off during high-radiation periods, a typical day in June is considered in Figure 73. The graph depicts the volumetric flow rate of the solar pump (l/h) together with the two solar pump controller inputs, the bottom tank layer temperature (°C) and the collector outflow temperature (°C), on a typical summer day.

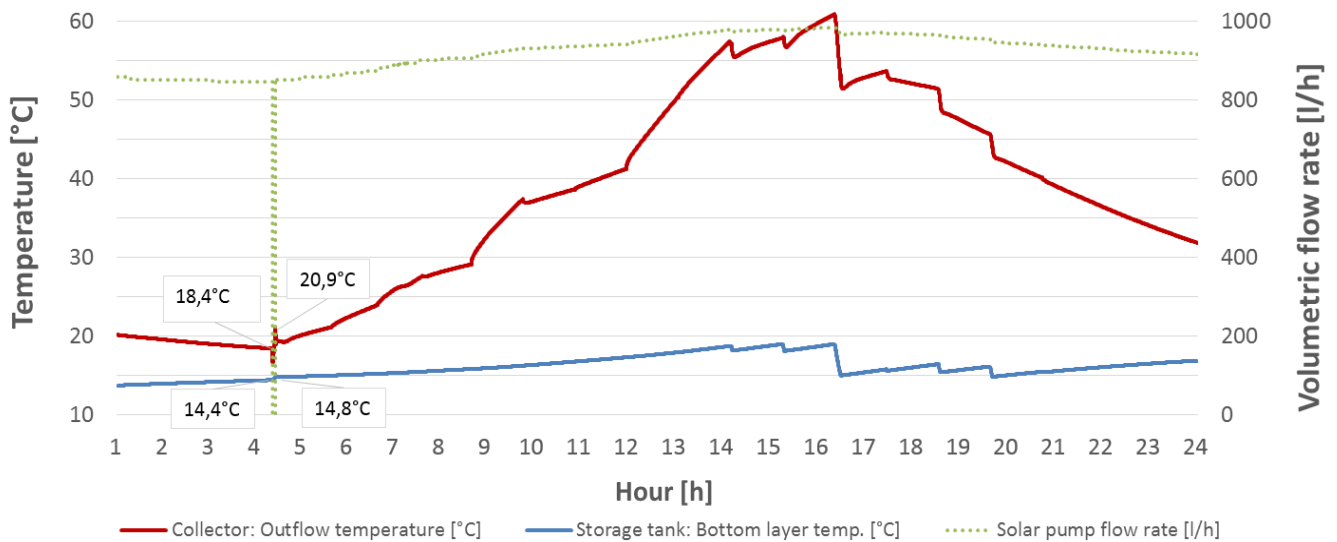


**Figure 73: Daily operation (June 1<sup>st</sup>) of the solar pump (l/h) based on bottom tank temperature and collector outflow temperature (°C)**

As illustrated in the graph, the pump runs throughout the entire day, except for during a very brief moment between 04:00 and 05:00 AM, where it is rapidly switched off and on. The switch-on temperature difference is 6 K between the collector outflow temperature and the tank temperature. Similarly, it is switched off at a temperature difference of 4 K.

According to the troubleshooting list in chapter 4.2, these are some suggestions related to the controller for possible causes for unwanted pump operation:

1. Unfavourable  $\Delta T$  settings
2. Incorrect placing of the tank temperature sensor
3. Incorrect placing of the collector temperature sensor

One immediate observation that can be made from Figure 73 is that the temperature at the bottom of the tank is constantly much lower than the collector outflow temperature. When the temperature at the collector outlet rises with increased radiation, but the temperature at the bottom of the tank remains unaffected, the switch-off temperature difference of 4 K is consequently seldom reached.

The consequence of incorrect controller settings are illustrated in Figure 74 below. The graph shows the temperature at (thermal) layer 4 together with the collector outflow temperature, as well as the energy flow in the solar coil on an hourly basis.

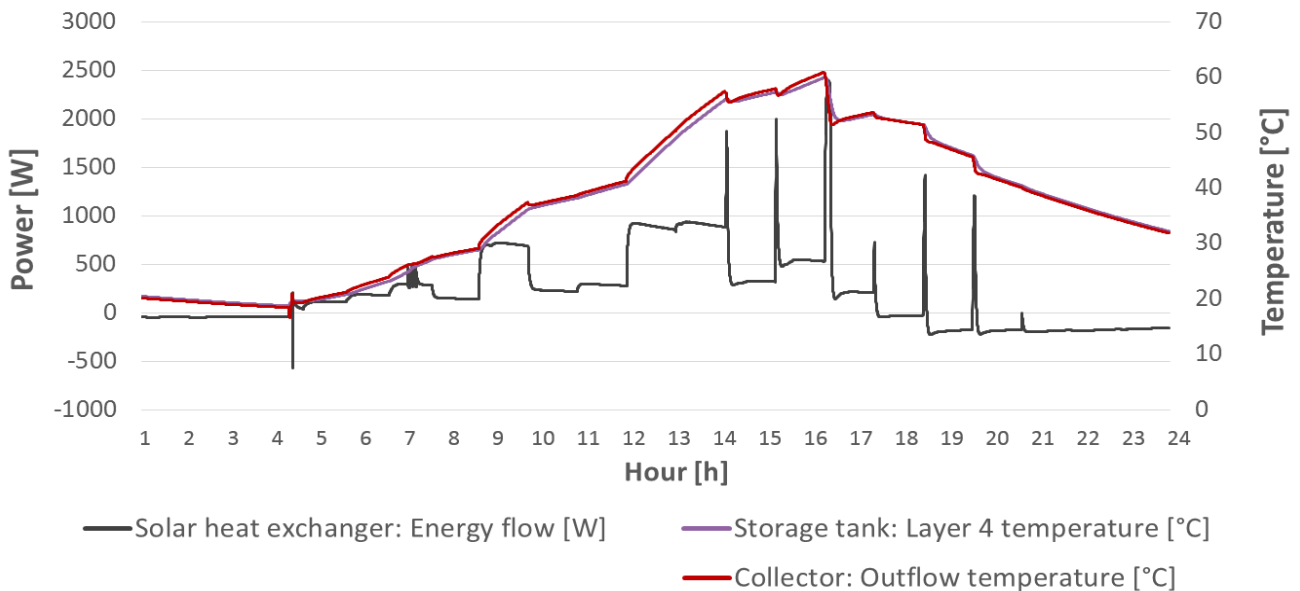


**Figure 74: The effect of incorrect controller settings (June 1<sup>st</sup>)**

As shown in the graph, the solar heat exchanger extracts heat from the tank during the night (negative power values, W). This is because the temperature in layer 4, where the solar energy enters the tank, is higher than the collector outflow temperature. Around 4:00-5:00 AM, the collector outflow temperature finally exceeds the temperature of the water that surrounds the upper coil connection, which results in energy being supplied to the tank (positive power values, W). During the day that is depicted, the positive energy flow lasts from approximately 5:00 AM until 5:30 PM, when the temperature at the storage tank once again exceeds the collector temperature. As a result, the pump circulates the heat transfer fluid in the solar circuit during the night and releases heat to the surroundings.

#### 9.4.4.2 Control of auxiliary heater

To see whether or not the auxiliary controller is working as desired, the same day that was considered in the previous subchapter is further examined for the electrical heating element. As is displayed in Figure 75, the electrical heater is frequently turned on and off at 75°C and 77°C, respectively, especially in the morning and in the afternoon, when hot water is typically consumed by the user. Moreover, the graph shows that the temperature in layer 7, i.e. in the middle of the tank, never falls below 72-73°C.

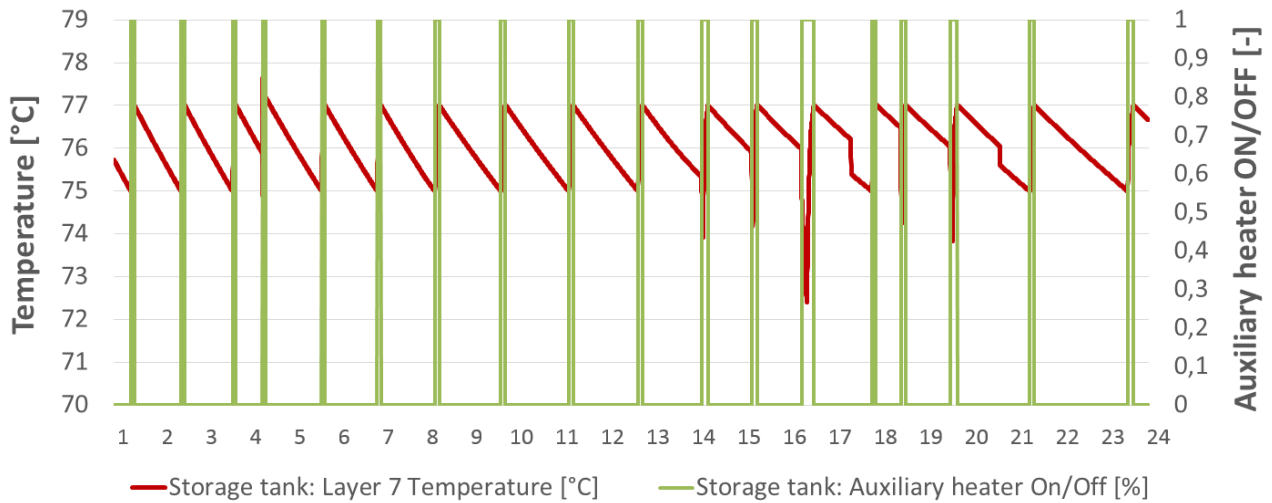


Figure 75: Operation of the auxiliary heater on June 1<sup>st</sup>

## 9.5 Discussion of measured and simulated results

Both the simulated results and the measured results presented in this chapter reveal that the utilization of solar energy is much lower than intended, and that the system is not functioning quite as it should be. Before a parametric study is conducted in chapter 10, some brief comments regarding the findings of this chapter is provided below.

The detailed simulations suggest that not only are the collectors exposed to less irradiation than expected; the energy flow between various system boundaries also reveals great heat losses from one part of the system to the next. In fact, of the total amount of irradiation that hits the total collector surface, only 36,4% is converted into useful heat by the collectors. Further 46,8% of this amount is supplied to the tank. This means that only 17,1 % of the initial solar energy available is utilized for heating of the tank water. Presumably, this number is even lower in real life. The energy flow from the collectors to the tank is illustrated in Figure 76 below.

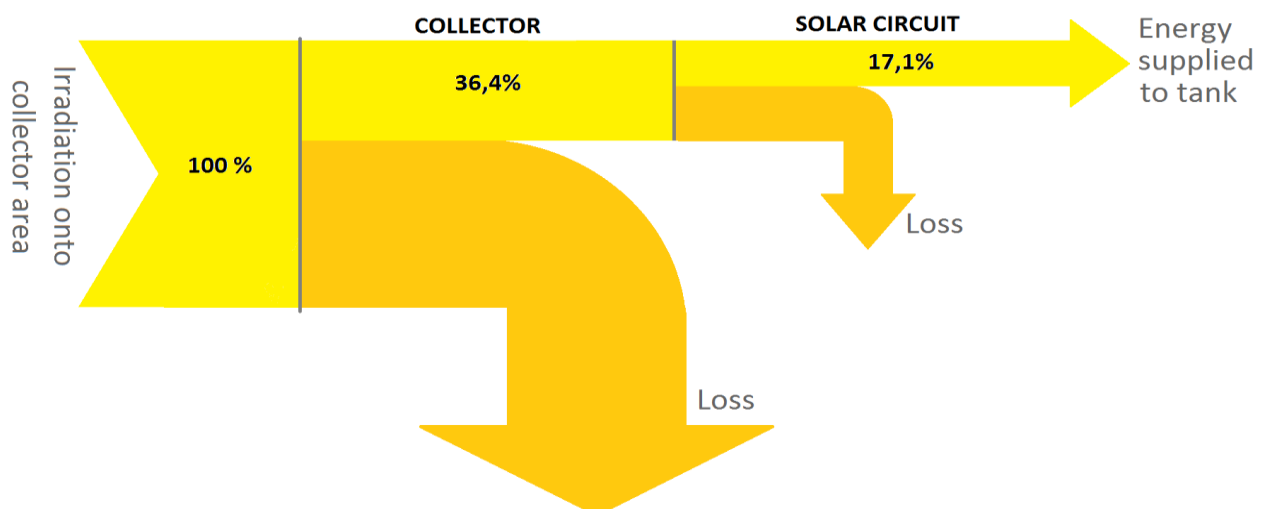


Figure 76: Illustration of solar energy flow from the collectors to the storage tank

With its current design and operation, it should be questioned whether or not the additional costs of installing and maintaining a solar-plus-supplementary system pays off, seeing that the energy savings were as low as 3,8 % on an annual basis. Even during summer, the savings are remarkably low. During periods of low to moderate solar radiation, the existing system actually consumes more energy than it would if one had been using a conventional heating system instead (immersed electrical heater only). This was shown in Figure 57 in section 9.3.2 *Fractional energy savings*. This is because during these periods, the solar pump runs during without sufficiently supplying the tank with solar energy, which was revealed in the detailed simulations in chapter 9.4.

### ***Original system design vs. modified system design***

A comparison of measurements within a given time period in 2014 and 2015 revealed that despite the increase in solar yield, the solar fraction has not noticeably been improved with the modified system. One reason for this could be that the total heat demand and the supply of auxiliary energy increased accordingly. The weather data for Bergen provided in *Appendix A.3* shows that January to May in 2015 was generally colder than the same period in 2014. Similarly, the relative humidity and the daily precipitation was higher. These are all factors that could explain the increased heat demand for space heating, which may further result in a higher auxiliary energy demand, as well as a slightly increased solar yield from the collectors. However, based on the results in this chapter, no conclusion can be made that the modified system is functioning better than the original system.

### ***Return-flow, controller settings and heat loss in solar circuit***

Detailed simulations of the Polysun model revealed that the control of the circulation pump in the solar circuit is not functioning as desired. As mentioned in chapter 5. *Case description*, it has been suspected that so-called return-flow is occurring at night, but that the ultra sound measurement conducted from January to April 2014 did not successfully prove this. In this chapter, the results indicate that during periods with higher radiation, for instance during June and July, the pump constantly circulates the heat transfer fluid in the solar circuit for longer periods of time without stopping. At times, this may occur on several days in a row. Moreover, this may be the very reason why suspicions of night-time return flow were never confirmed: the unwanted flow in the solar circuit is not caused by differences in densities (return-flow), but is instead a result of incorrect pump controller settings that only seems to be an issue during high-radiation periods. The ultra sound measurements, however, were conducted during low-radiation periods, when the control of the solar pump has better functioning. Whatever reason, the effect is equally unfavourable: heat is withdrawn from the tank and released to the surroundings. Since evacuated tube collectors have excellent insulation properties, one can assume that most of this heat is lost in the long solar circuit pipelines, both to indoor and outdoor surroundings. This would explain why more heat is lost in the solar circuit than the amount of heat that is actually utilized in the tank. It should be noted that



no measurements have been conducted to monitor the electricity consumption of the solar pump. The unfavourable pump operation can thus not be cross-checked with the real system. However, the simulated results suggest that the electricity consumption would be very high compared to the energy that is saved by solar energy. The effect of incorrect controller settings will be further studied in the next chapter.

### ***Shading and collector inclination angle***

There are several findings in this chapter that point towards shading as a potential performance-reducing factor. First of all, the total annual solar radiation onto collector area is lower than expected. Secondly, the maximum irradiated power curve that was displayed in the detailed simulations reveal a sudden increase from March to April, and a corresponding drop from August to April. A similar effect could be recognized in both the simulated and the measured solar yields presented in Figure 53 in chapter 9.2 *Energy supply*. Moreover, the two collectors are tilted at an inclination angle of  $51^\circ$ , which is steeper than the optimum inclination angle of  $34^\circ$  in Bergen. As explained in the literature review, a steeper angle normally reduces the amount of excess heat and the number of stagnation days during summer, as well as increasing the solar yield during the transitional periods. This corresponds well with the results presented in this chapter, since no stagnation days occur, and since the temperatures in the solar circuit are lower than expected during summer. The second argument, however, does not apply to this case study; if the collector inclination angle is optimized for heat generation during the transitional periods, the irradiation onto collector area should have been higher than what was revealed in the results. Thus, there must be another factor that is reducing the incoming radiation, such as shading of surrounding topography, or shading from nearby collectors (mutual shading).

### ***Excess auxiliary heat supply***

Not only is the contribution of solar energy much lower than intended; the “energy budget” is also not in balance. This means that the system is supplying far more energy, i.e. auxiliary energy, than what is being consumed by the user. Even though some of this excess heat may be necessary in order to compensate for heat losses from tank or pipes, the amount is still very high, and reduces the performance (solar fraction) of the solar thermal system significantly. One potential reason is the high switch-on temperature setting of the immersed electrical heating element to ensure adequate protection against the growth of *Legionella*. Additionally, this heater is located at the middle of the tank, which means that the auxiliary volume constitutes half the tank. This will be further investigated in the parametric study.

### ***Deviation between measured and simulated results***

The measured auxiliary energy consumption was slightly higher than the corresponding simulated consumption. One explanation for this is that more solar energy is utilized in the simulation model. Another aspect is that in the simulation model, it is assumed an efficiency of the immersed electrical heating element of 100%, i.e. no heat loss. Despite the attempt to create a simulation model that resembles the investigated system as much as possible, both in terms of design and heat demand inputs, it will always deviate some from the real, full-scale system.

Finally, the measured heat demand for heating of DHW and space heating is relatively low compared to the initial estimations from the design stage presented in chapter 5. *Case description*. To examine if the lower heat demand is a contributing factor to the unsatisfying performance, this aspect will be further investigated in the parametric study in chapter 10.

## 10 Parametric study

---

### 10.1 Introduction

The behaviour of a solar thermal system depends on a large number of parameters related to its main components, such as collector inclination angle, collector area, pipe length, tank volume and controller settings. In this chapter, a parametric study will be conducted on the Polysun model, which from now on will be referred to as the *reference system*, in which the effect of various design- and operation parameters on system performance will be examined. Once the system is installed, the design parameters are in general more difficult and expensive to change, whereas the operation parameters are often considered easier to adjust. In addition, selected user-related parameters, like DHW demand and space heating demand, will be assessed to see how they influence the overall performance. In doing so, a more holistic approach is achieved, which will make it easier to make general assumptions of the solar thermal systems of Løvåshagen as a whole.

To find the improved value of each parameter, or, if possible, the optimum value, only one parameter was changed at a time while the other parameters were kept at their initial settings. The input values of the different parameters used in this parametric study are mainly based on recommendations and information from the literature review in chapter 3. If necessary, additional explanations are provided continuously throughout the chapter. The results will be presented according to the categorization illustrated in Figure 77 below. Moreover, each category is subdivided into its main components.

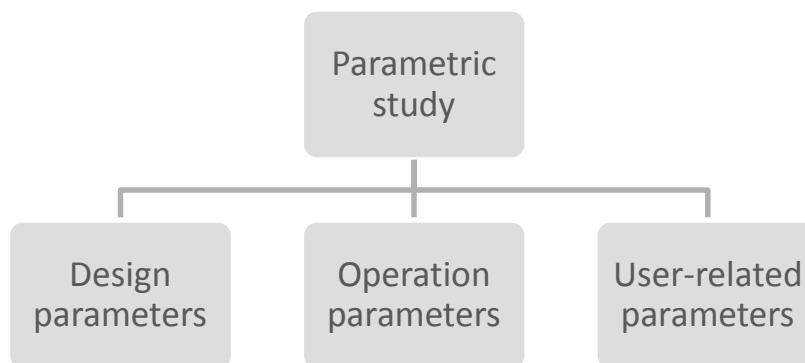


Figure 77: Overview of the main categorization in the parametric study.

In this parametric study, two main indicators will be used to study the influence of a parameter:

1. Solar fraction
2. Specific delivered energy

The chosen boundary limit for the solar fraction is the storage tank, and includes the immersed electrical heating element, as described in chapter 6. *Methodology*. Hence, heat losses in the solar circuit has already been taken into account. Since previous studies conducted on the Løvåshagen project suggest that the energy consumption of the passive house dwellings are higher than expected, the specific delivered energy (kWh/m<sup>2</sup>) is also included in the parametric study in this chapter to see if the energy consumed by the solar thermal heating systems may be a contributing factor. This performance indicator has a slightly wider boundary limit than that of the solar fraction: in addition to the energy required by the immersed electrical heating element, it also considers the parasitic energy needed for the operation of all the circulation pumps in the heating system, including the solar pump.

Since the goal of this study is not only to “optimize” each parameter, but also to attempt to understand *why* the system is not functioning as desired with the current design and operation, the results presented in this chapter will occasionally be explained beyond the solar fraction and specific delivered energy to the solar heating system. For instance, when the collectors are studied in *10.2.1 Collector*, it is occasionally also relevant to look at other indicators, such as the collector yield and the collector efficiency. Similarly, it is sometimes relevant to make further study of the amount of heat loss when considering insulation properties, or include the net utilized amount of solar energy when investigating parameters related to the storage tank. Seeing that shading affects the total irradiation onto the collectors, and that mutual shading is dependent on parameters like collector inclination angle and distance between collector rows, the impact of shading will also be studied in combination with each parameter investigated in *10.2.1 Collector*.

The results that showed insignificant impact on system performance will not be presented with tables or figures. Instead, a comment is provided, and the corresponding figures and tables can be found in *Appendix C*.

A summary of the parametric study is provided in chapter *10.5*, before various improved scenarios are suggested in chapter *10.6*. Finally, the scenario with the highest performance is simulated and analysed at the end of this chapter, in *10.7* and *10.8*.

## 10.2 Design parameters

### 10.2.1 Collector

#### 10.2.1.1 Effect of shading

The results presented in the previous chapter showed that shading is a potential performance-reducing factor for the solar thermal systems installed in the Løvåshagen housing cooperative. In this chapter, the extent of shading will be further investigated. As mentioned in chapter 8.

*Simulation inputs*, it is only mutual shading that is relevant for the investigated system, in addition to surrounding topography.

Mutual shading was described in 3.1.4 *Shading* in the literature review as the shading effect that arises when several collectors are installed in rows within the same collector field. Parameters like solar altitude angle, collector inclination angle and row-to-row distance influence the impact of mutual shading. Figure 78 shows the solar altitude diagram (yellow) for the chosen location for the first six months of the year along with the horizon line (red), which includes mutual shading caused by other collectors (distinct peak in the middle) and shading from surrounding topography. The position of the sun at 12:00 PM on each date is marked with a symbolic sun.

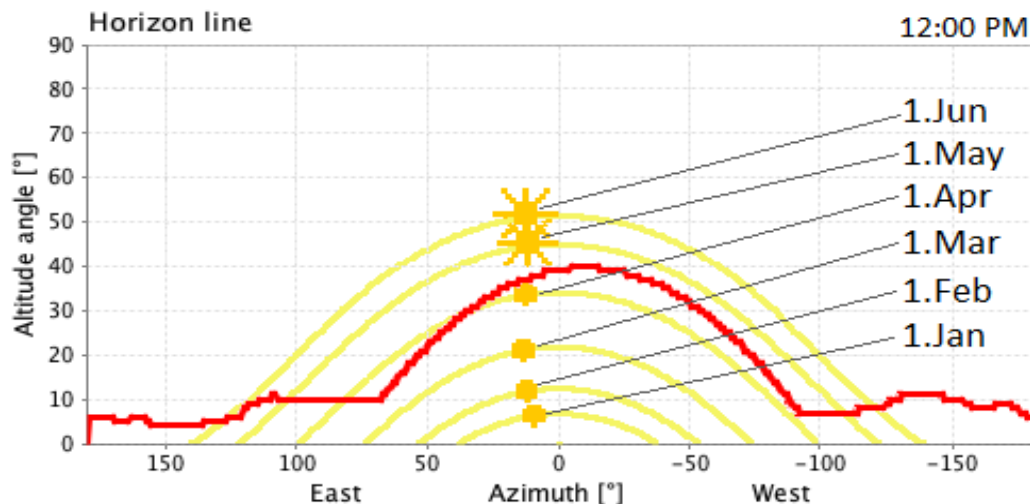
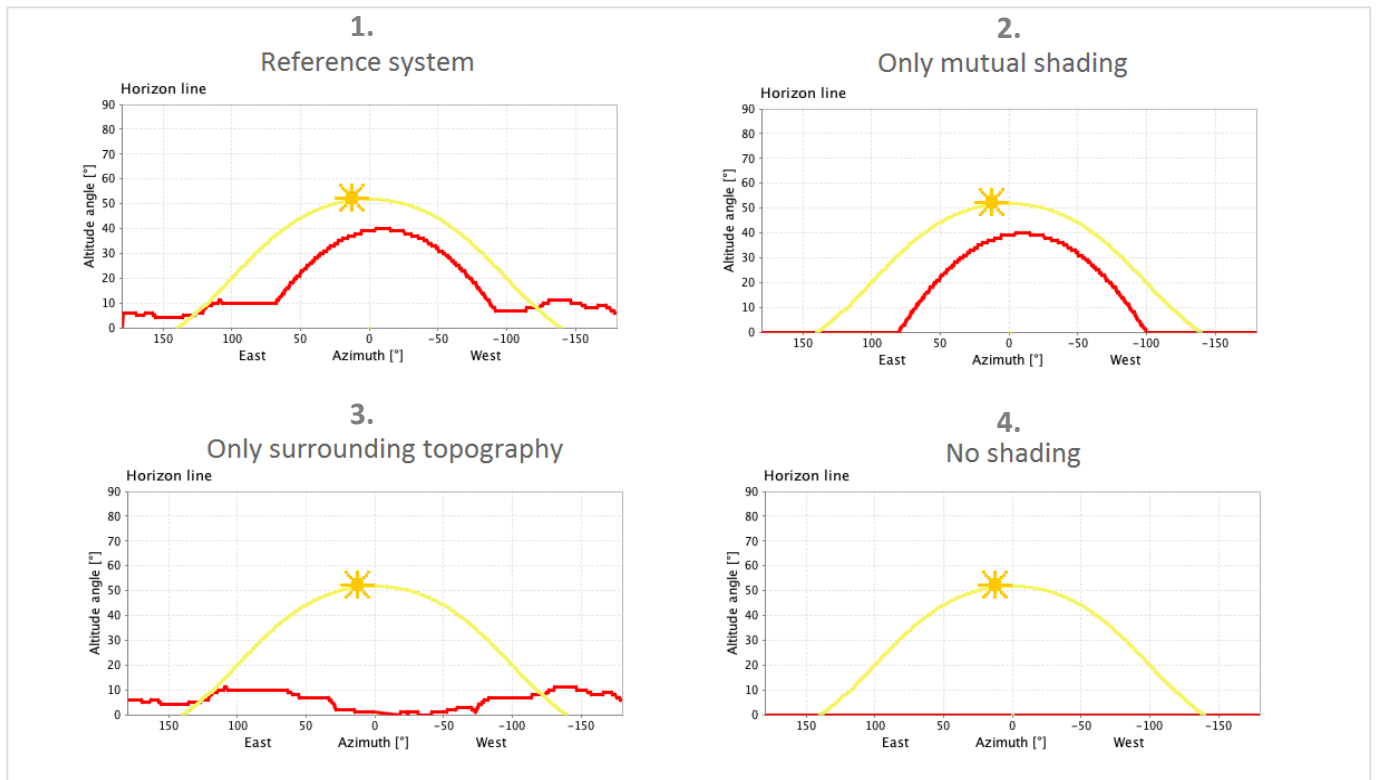


Figure 78: Solar altitude diagram (yellow) for the six first months together with the horizon line (red). The pronounced peak in the middle of the horizon profile represents the impact of row-to-row shading.

The figure indicates that shading caused by other collector rows may potentially be blocking the solar irradiation considerably, if not completely, during the first three to four months of the year. In fact, it is not until the end of April that mutual shading appears to have no significant influence. Moreover, the impact of mutual shading is slightly more dominating towards southwest. This is because of the  $-10^\circ$  southwest orientation of the collectors. To study the effect of both mutual shading and the surrounding topography on system performance, the model was simulated for four different cases:

1. *Reference system*
2. *Only mutual shading*, i.e. no surrounding topography
3. *Only surrounding topography*, i.e. no mutual shading from other collectors
4. *No shading*, i.e. no shading from neither surrounding topography nor other collectors

The aggregated horizons for each case is depicted in Figure 79, whereas the monthly solar fractions are shown in Figure 80.



**Figure 79: The four horizons simulated in Polysun to study the effect of shading**

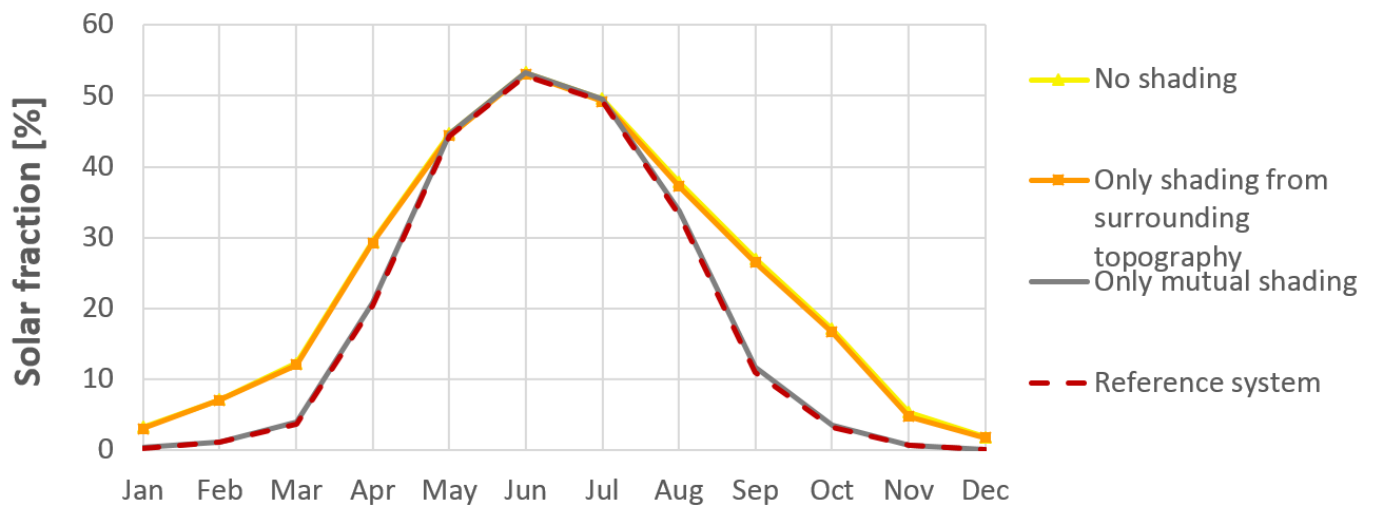


**Figure 80: The effect of shading on monthly solar fraction for different shading conditions**

The annual solar fraction and the annual specific delivered energy for each of the four cases are summarized in Table 27.

**Table 27: Effect of shading on system performance**

	1. Reference system	2. Only mutual shading	3. Only shading from surrounding topography	4. No shading
Annual solar fraction [%]	14,3	14,6	19,3	19,6
Annual specific delivered energy [kWh/m <sup>2</sup> ]	35,6	35,5	34,5	34,4

Based on the results presented above, the following can be observed:

- Shading due to surrounding topography (no mutual shading, case 2) has no particular impact on neither monthly nor annual solar fraction.
- Mutual shading caused by nearby collectors reduces the performance significantly. This effect, however, is mainly present from August to April, and is less prominent during the high-radiation periods.

Finally, the annual irradiation onto collector area, the annual collector yield and the annual solar energy supplied to the tank for the case of shading (case 1, reference system) and for the case with no shading (case 4) are illustrated in Figure 81.

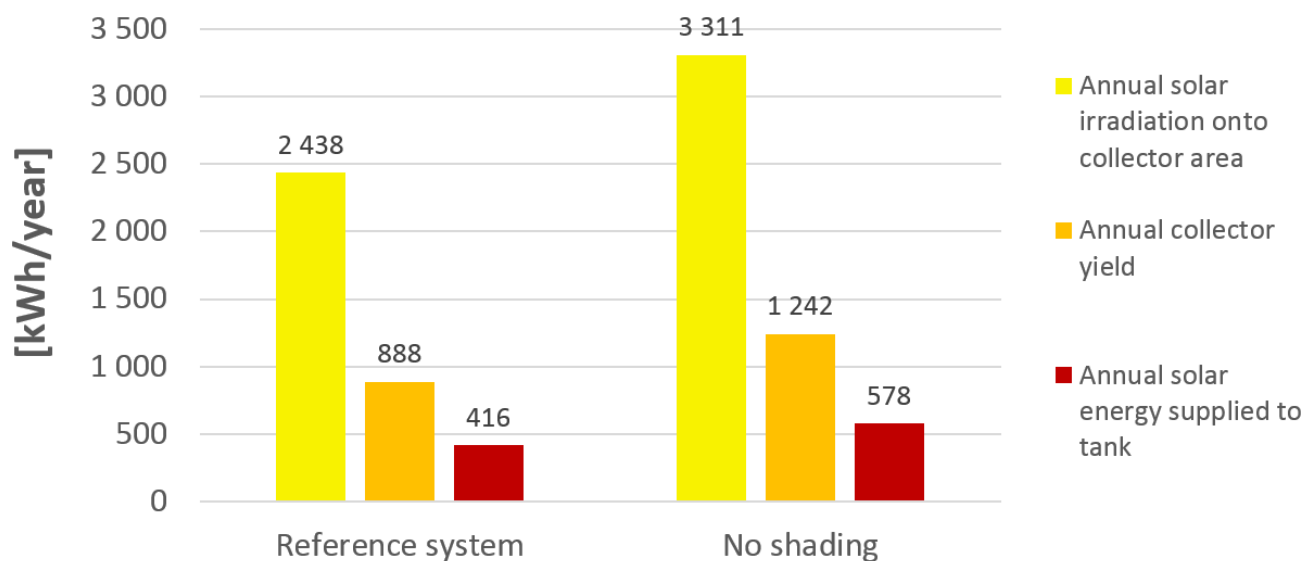


**Figure 81: The difference between solar irradiation, collector yield and solar energy supplied to the tank in kWh/year, both *with* and *without* shading.**

The results in Figure 81 reveal that by eliminating shading, the annual solar irradiation onto collector area ( $E_{sol}$ ) increases by 35,8% - from 2438 kWh to 3311 kWh. Similarly, the collector yield ( $Q_{sol}$ ) jumps from 888 kWh/year to 1242 kWh/year, which constitutes an increase of 39,9%. Despite this increase, the collector yield and the amount of solar energy supplied to the tank are still not adequate to achieve the initially planned solar fraction of 47%. With shading or no shading; less than half of the thermal output from the collectors is supplied to the tank ( $S_{sol}$ ). Thus, it is evident that the elimination of shading will not solve the problem in itself, and that additional measures must be considered in order to increase the solar yield and reduce the massive heat loss.

### 10.2.1.2 Effect of collector row-to-row distance

In the previous subchapter, different sun altitude angles were shown in Figure 78. With an altitude angle of the sun,  $\gamma_s$ , of roughly  $50^\circ$  in June in the middle of the day, the minimum row distance for the reference system according to equation 3 (chapter 3.1.4 *Shading*) is approximately 2,4 m. This is slightly larger than the current row distance of 2,1 m. On April 1<sup>st</sup>, however, the maximum altitude angle of the sun drops to approximately  $35^\circ$ , and the required row distance increases to 3,3 m, accordingly. In the calculations, an inclination angle ( $\beta$ ) of  $51^\circ$  is assumed, along with an azimuth angle (orientation angle) of  $-10^\circ$ , and a collector length ( $L$ ) of 1,9 m. These constitute the initial values of the reference system.

To study the influence of row distance between the collectors, distances spanning from 1-10 meters were simulated in Polysun. The generated horizons and their impact is illustrated for each row distance in Figure 82. The corresponding performances are displayed in Figure 83.

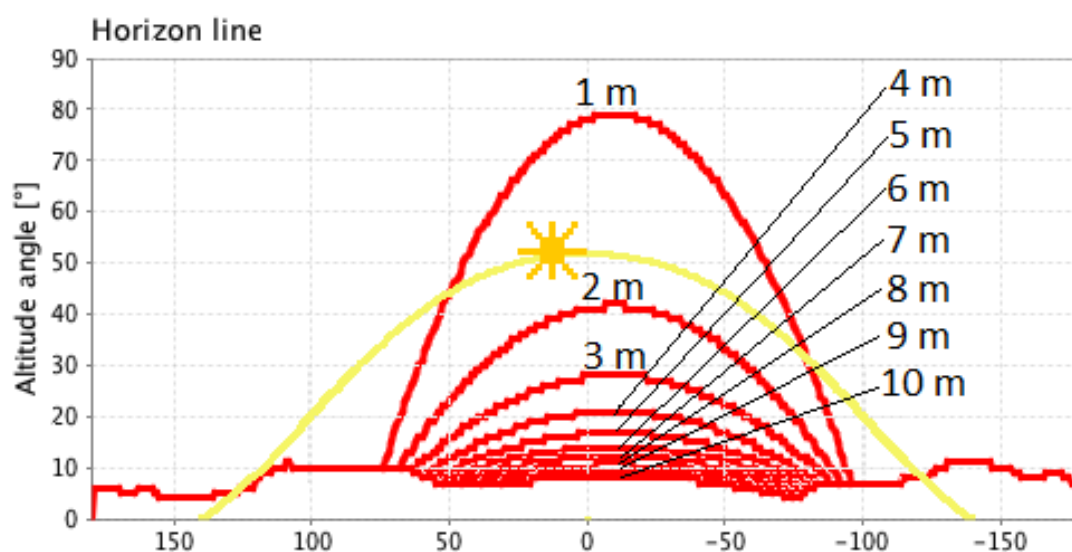


Figure 82: The effect of row distances 1-10 m on the horizon line (red). The yellow line represents the sun path on June 1<sup>st</sup>



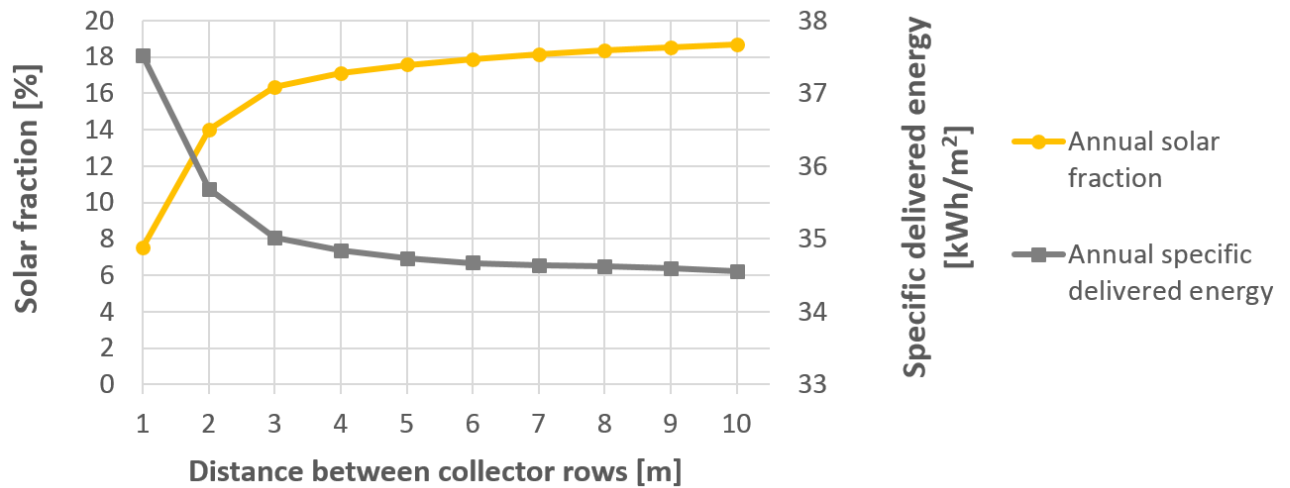


Figure 83: The effect of row-to-row distance on system performance.

The results show that the closer the collector rows are installed with respect to each other, the higher the impact of mutual shading on the horizon line, and the lower the annual solar fraction. The annual specific delivered energy increases accordingly. It is, however, mainly the first few meters that are the most crucial. If the row distance is increased from one to three meters, the solar fraction more than doubles from 7,6 % to 16,3 %. The corresponding reduction in annual specific delivered energy is from 37,5 kWh/m<sup>2</sup> to 35,0 kWh/m<sup>2</sup>.

The row distance that is needed to minimize shading is also dependent on the inclination angle of the collectors. Collectors with small inclination angles will have shorter shade patterns, which allows for a reduced distance between the rows. Similarly, collectors with large inclination angles will cast larger shade patterns, and thereby increase the necessary row distance to avoid shading. (AEE Intec, 2004). Figure 84 shows the annual useful thermal output from the collectors (left) and the annual solar fraction (right) for inclination angles of 20°, 40° and 60°.

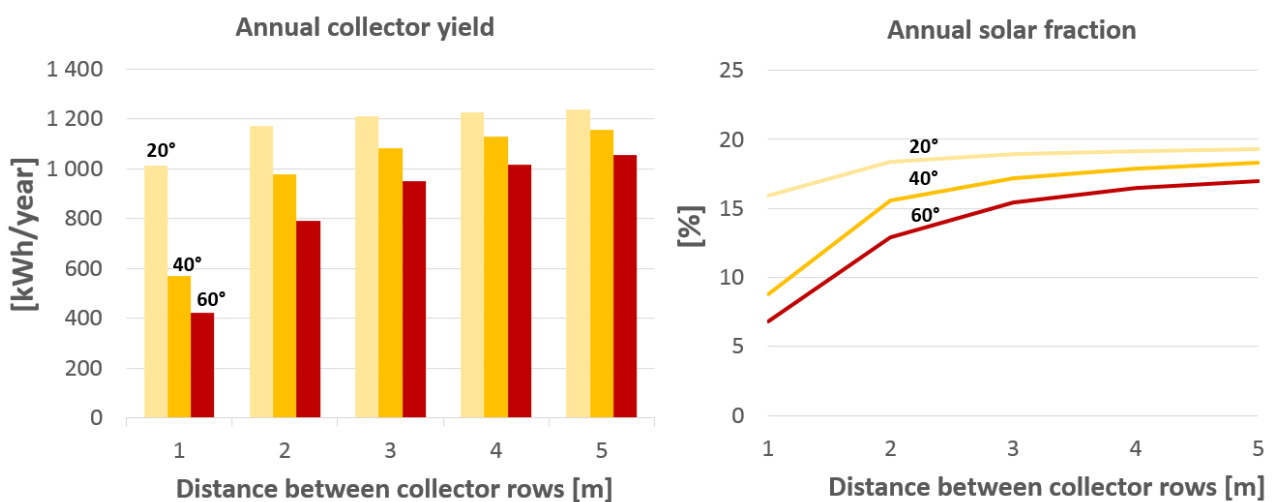


Figure 84: The effect of row-to-row distance on annual collector yield (left) and solar fraction (right) for collector inclination angles of 20°, 40° and 60°

To summarize the previous paragraph: the lower the inclination angle, the shorter the required row distance. As was displayed in the two graphs, a collector with a steeper inclination angle is more sensitive to the chosen row distance than a collector with a low inclination angle. The influence of the collector inclination angle will be further discussed in the next subchapter.

### 10.2.1.3 Effect of orientation angle and inclination angle of the collectors

According to the *Apricus Solar Collector Installation and Operation Manual* (Apricus Solar, 2013), the evacuated tube collectors should be installed within the range 20°-80° in order to ensure an optimal operation of the heat pipes. At first, only the angles of the two investigated collectors were altered, and their corresponding performance plotted. However, since the inclination angle of the collectors that were positioned in the front remained unchanged and mutual shading was still present, the results showed no significant difference. The results are attached in *Appendix C.1.1*. One of the goals of this study is to consider the solar thermal systems at Løvåshagen housing cooperative as a whole. Hence, the effect of simultaneously altering the orientation angle and the inclination angle of nearby collectors was regarded as more useful than only altering and studying them individually.

The collectors are installed at an azimuth angle of -10° (10° southwest) and an inclination angle of 51°. The simulated annual solar fraction and the corresponding specific delivered energy for inclination angles 20°-80° (the recommended operating range) and orientation angles -30° to 30° (W=-90°, E=+90°, S=0°) are presented in Figure 85.

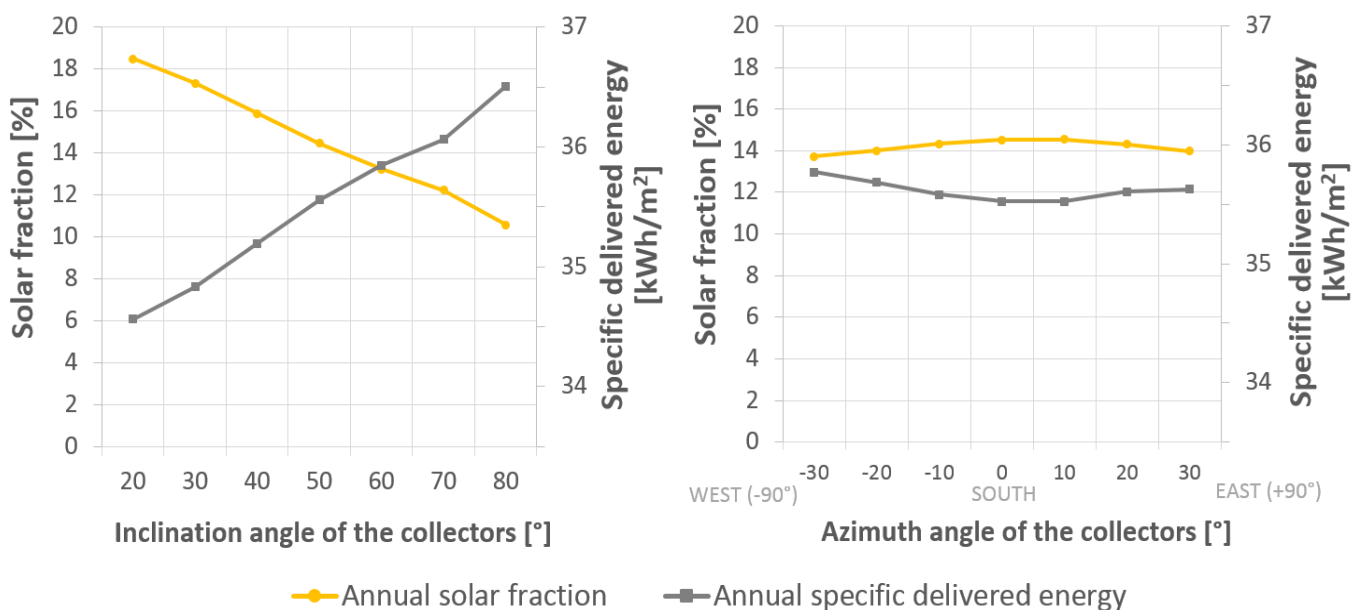
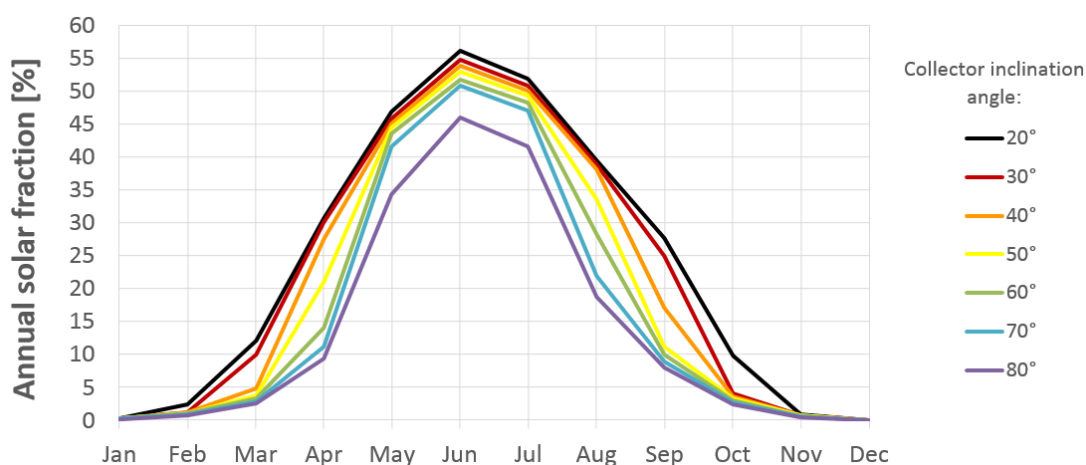


Figure 85: Effect of orientation (left) and the inclination angle (right) on system performance

The results show that an alteration in inclination angle has a greater influence on system performance than a corresponding change in the azimuth angle. As discussed in chapter 2.1.3, it is normally ideal to have the collectors facing directly south, i.e. 0°. Furthermore, a southwest orientation is normally preferred over a southeast orientation. In this case, however, an orientation of 10° towards east actually leads to a slightly, though hardly significantly, higher annual solar fraction and smaller annual specific delivered energy. This is because the impact of the surrounding topography is more significant in the west than in the east, which could be seen in the horizon line in Figure 44 (chapter 8.2.2).

The inclination angle, on the other hand, has a considerably higher impact on the annual performance. With the current row distance, the optimum inclination angle is 20°. When tilting all the collectors to 20°, the annual solar fraction and the annual specific delivered energy is 18,5% and 34,6 kWh/m<sup>2</sup> respectively. By comparison, the corresponding values are 10,6% and 36,5 kWh/m<sup>2</sup> if the collectors are tilted at 80°.

The simulated monthly solar fraction during one year at various inclination angles from 20°-80° are shown in Figure 86.



**Figure 86: The impact on annual solar fraction when tilting all the collectors at Løvåshagen housing cooperative at different inclination angles within the recommended range of 20°-80°**

The results in this chapter imply that by simply lowering the inclination angles of all the collectors that are mounted on the roof of the housing cooperative, the impact of mutual shading can to a large extent be reduced. As illustrated in Figure 86, a lower angle results in higher solar fraction during summer, as well as greatly increasing the solar share during the transitional periods. The performance increase achieved through changing the inclination angle from 51° (reference system) to 20° is summarized in Table 28 below.

**Table 28: Potential improvement of system performance when altering the inclination angle**

Inclination angle [°]	Annual specific delivered energy	Solar fraction
	[kWh/m <sup>2</sup> ]	[%]
20	34,6	18,5
51 (Reference system)	35,6	14,3
Change in performance	2,8% reduction	29,4% increase

Though the optimum inclination angle for the current system design and shading conditions is 20°, it is also necessary to consider other factors mentioned in the literature review regarding the recommended inclination angle. A lower angle will indeed result in higher collector yield, both on an annual basis and during summer. On the other hand, snow and dirt may form more easily on top of the collector tubes.

***Comments regarding the optimum inclination angle without shading***

It is important to point out that the results of changing the inclination angle are slightly different when the shading factor is eliminated from the simulation model, which is illustrated in Figure 87 below. The two performance curves show that the impact of altering the inclination angle is much smaller compared to when mutual shading was included in the simulations. Moreover, the results show that without shading, the optimum inclination angle is obtained within the range of 30-40°, i.e. the angle with lowest specific delivered energy and highest solar fraction. This fits well with the optimum inclination angle of Bergen, which was stated as 34° in the literature review.

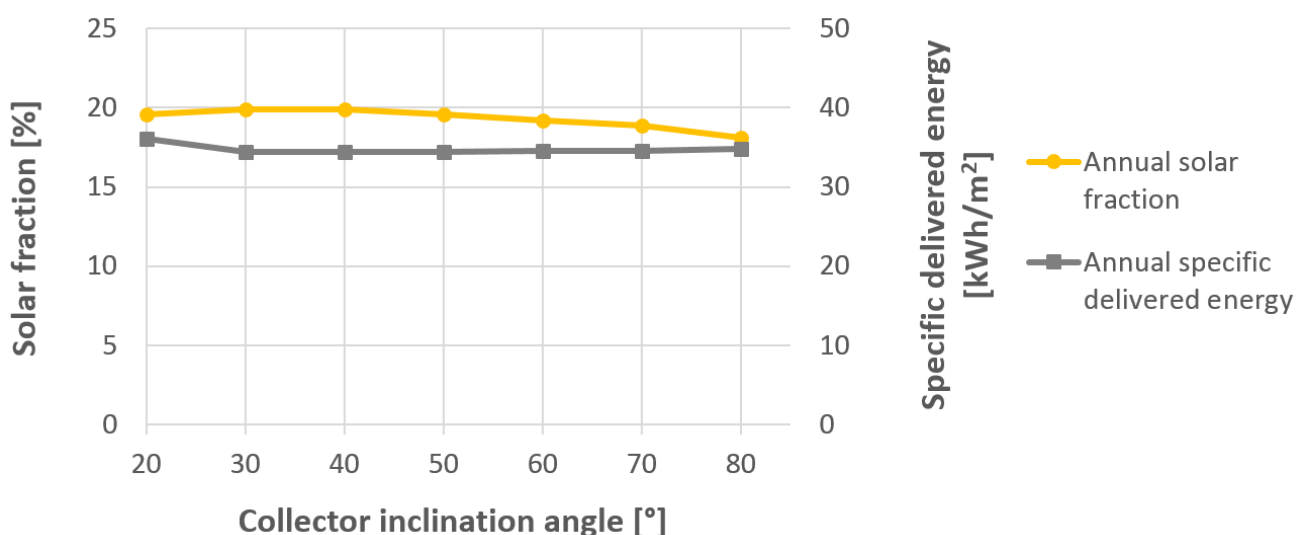


**Figure 87: Effect of different inclination angles on system performance when shading is eliminated**

#### 10.2.1.4 Effect of solar collector area

The two Apricus AP-20 collectors used in the reference system have a total collector absorber area of 3,2 m<sup>2</sup>. To investigate how the system performance is affected by the collector area, the Polysun model was simulated for various absorber areas ranging from 1 to 10 m<sup>2</sup>. The results are plotted in Figure 88 below.

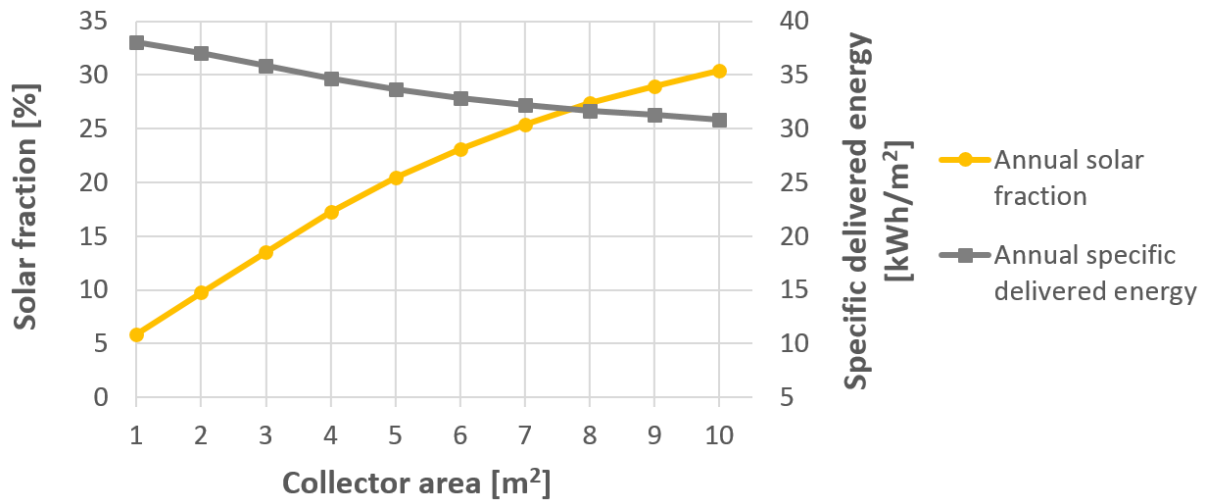


Figure 88: Effect of collector area on system performance

From the results, it is evident that the solar fraction increases significantly with a larger collector area. Accordingly, the annual specific delivered energy to the heating system decreases. If the collector area is doubled from 3,2 m<sup>2</sup> to 6,4 m<sup>2</sup>, the annual solar fraction and the annual specific delivered energy increases and decreases by 67,8% and 8,1 %, respectively.

To achieve an annual solar fraction of 47% (initial design goal), the solar fraction during the high-radiation months must be higher in order to compensate for limited radiation during winter.

According to *Apricus Solar Collector Installation and Operation Manual* (Apricus Solar, 2013), the solar collectors should normally be sized so that a solar fraction of 90°-95% is attained during summer. As stated in Figure 56 in chapter 9. *Results*, a simulated solar fraction of approximately 53% and 50% was obtained with the reference system in June and July, respectively. Moreover, similarly to the other parameters related to the collector presented in the preceding subchapters, also the influence of solar collector area is strongly affected by shading.

The left graph of Figure 90 below depicts the monthly solar fraction throughout the year for a collector area of 2, 4, 6 and 8 m<sup>2</sup>. For comparison, the corresponding simulated results for the case *without* shading are shown to the right.

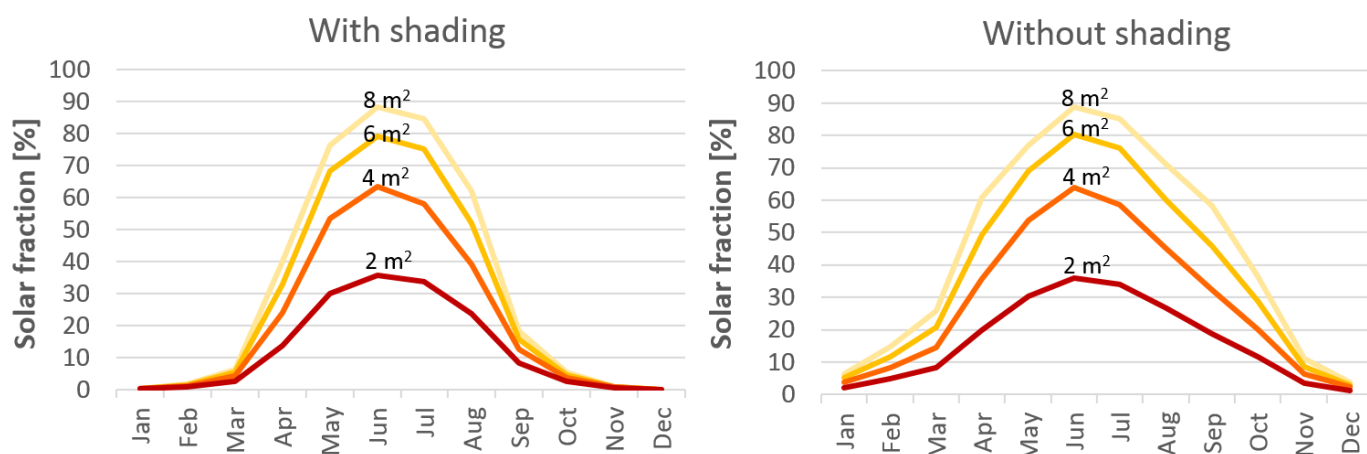


Figure 90: Monthly solar fraction for different collector absorber areas, both *with* shading (left) and *without* shading (right)

As can be seen from the two graphs, a larger collector area results in a substantial increase in the solar fraction during summer. As suggested earlier in chapter 10.2.1.1 *Effect of shading*, mutual shading appears to have no considerable impact on system performance during summer. This theory is confirmed in the results in Figure 90 above, where the solar fraction of June and July for both with shading and without shading are practically the same. It is in the remaining ten months of the year, however, that the two cases differ. With no shading, the solar utilization can be extended into the transitional periods – and even more so with a larger collector area. Moreover, the results show that although shading is eliminated, the current absorber area of 3,2 m<sup>2</sup> is still not adequate to achieve the desired solar fraction of 90-95% during the high-radiation periods.

The annual performance for three selected collector areas are summarized in Table 29. The chosen values correspond to the total area of one, two and three collectors of the collector type that is currently used in the reference system (Apricus AP-20).

Table 29: Effect of one, two or three collectors on annual performance, both *with* and *without* shading

Number of collectors (absorber area)	Annual solar fraction [%]		Annual specific delivered energy [kWh/m <sup>2</sup> ]	
	<i>Shading</i>	<i>No shading</i>	<i>Shading</i>	<i>No shading</i>
1 collector (1,6 m <sup>2</sup> )	8,2	11,1	37,5	37,1
2 collectors (3,2 m <sup>2</sup> ), <i>reference system</i>	14,3	19,5	35,6	34,5
3 collectors (4,8 m <sup>2</sup> )	19,8	27,3	33,9	31,9

### 10.2.1.5 Effect of collector heat loss

As previously discussed in chapter 3. *Design and operation of a solar thermal system*, the efficiency of a collector is determined by the efficiency curve of the particular collector type. Notably, the thermal heat loss in a collector increases with both reduced irradiated power ( $\text{W}/\text{m}^2$ ) and a higher temperature difference between the solar liquid in the collector manifold,  $T_L$ , and the ambient air,  $T_A$ . In chapter 9. *Results*, the efficiency of the investigated collectors was established to an annual average of 36,4%. To illustrate how the efficiency is affected by solar irradiation, the simulation model was simulated both *with* and *without* shading. Figure 91 depicts the average monthly collector efficiency during the course of one year for the two cases. As seen in the graph, the collector efficiency is significantly improved during the colder months with low to moderate radiation when shading is eliminated.

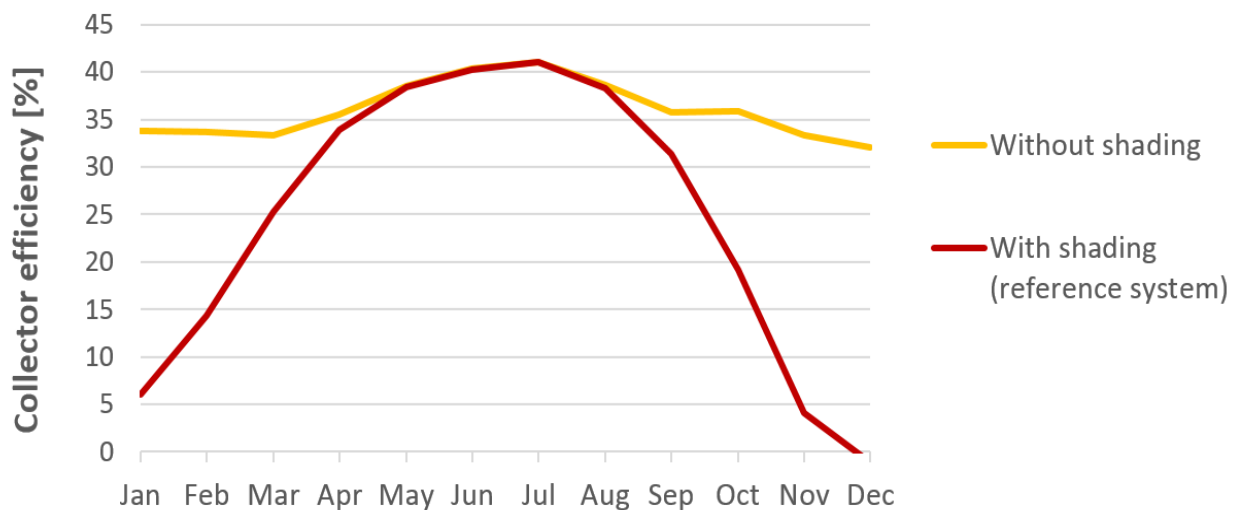


Figure 91: Monthly average collector efficiency *with* and *without* shading of the collectors

In order to investigate the influence of heat loss from the collector on system performance, the Polysun model was simulated for five different collector types with the characteristics presented in Table 30 below, including the reference collector (Apricus AP-20). The collectors were simulated with the same absorber area. In addition to other evacuated tube collectors, two flat-plate collectors were included for comparison.

**Table 30: Characteristics of the different solar collectors simulated in Polysun**

Name	Type	$\eta_0$ [-]	$a_1$ [W/m <sup>2</sup> /K]	$a_2$ [W/m <sup>2</sup> /K <sup>2</sup> ]
Apricus AP-20 (reference system)	Evacuated tubes with heat pipe	0,614	1,30	0,0073
Thermomax HP400 20	Evacuated tubes with heat pipe	0,750	1,18	0,0100
VitoSol 200 D20	Evacuated tubes with double-pipe connection	0,809	2,22	0,0021
VitoSol 200-F 5DI	Flat-plate collector	0,785	3,76	0,0224
FPC-A32	Flat-plate collector	0,750	2,77	0,0230

The efficiency curve of each of the collector types are displayed in Figure 92 for two different irradiance levels in W/m<sup>2</sup>: clear and sunny (1000 W/m<sup>2</sup>) to the left, and cloudy (300 W/m<sup>2</sup>) to the right. As mentioned in chapter 3.1.2 *Collector performance and collector efficiency*, the typical operating areas for water heating and space heating is temperature differences ( $T_L - T_A$ ) ranging from approximately 20°C - 100°C.

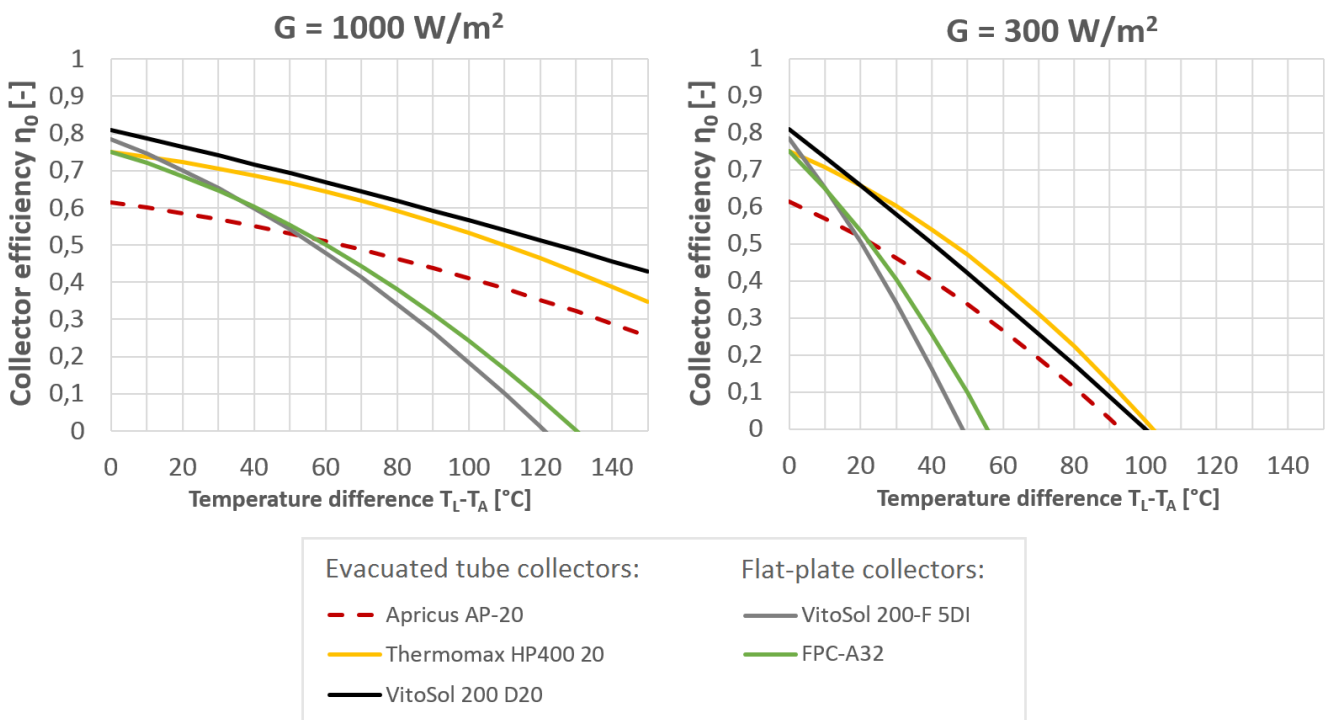


**Figure 92: Efficiency curves of the collectors. Left: clear, sunny day (1000 W/m<sup>2</sup>). Right: cloudy day (300 W/m<sup>2</sup>)**

The results in Figure 92 show that when the irradiated power is high (1000 W/m<sup>2</sup>), the reference collector, Apricus AP-20, has a lower efficiency, and thus higher thermal losses, than the two other evacuated tube collectors. At temperature differences  $T_L - T_A$  lower than 50-60°C, even the



flat-plate collectors have higher efficiency. For the entire temperature range, the VitoSol 200 D20 has the best performance, followed by the Thermomax HP400 20.

On cloudy days with lower irradiation ( $300 \text{ W/m}^2$ ), the two flat-plate collectors quickly reach stagnation. Their efficiency exceeds that of the reference collector, Apricus AP-20, for temperature differences lower than approximately  $20^\circ\text{C}$ . Moreover, the Apricus AP-20 is still performing worse than the two other tube collectors, though the difference in performance is smaller at higher temperatures. Unlike for high radiation levels, the efficiency of the Thermomax HP400 20 on cloudy days is higher than that of the VitoSol 200 D20 for all temperature differences greater than approximately  $20^\circ\text{C}$ . The annual solar fraction and the annual specific delivered energy for each of the collector types are summarized in Figure 93.

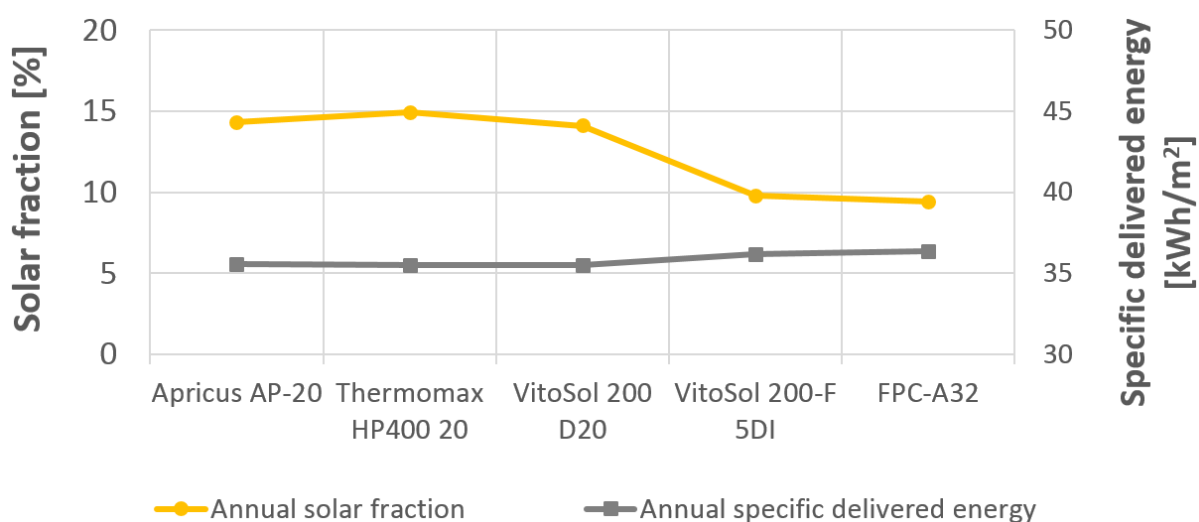


**Figure 93: System performance for each collector type**

The results show that the evacuated tube collectors have significantly better annual solar fractions than the two flat plate collectors, whereas the annual specific delivered energy differs only slightly. This is because of the great insulation properties that these collectors hold. The collector that holds the highest annual solar fraction is the second evacuated tube collector with heat pipe, the Thermomax HP400 20.

It should, however, be kept in mind that the collectors were simulated with the same absorber area. If the model was instead simulated based on the number of collectors (i.e. two collectors), the difference between the collector types would have been much larger. For instance, the Thermomax HP400 20 has approximately the same length and width (outside dimensions) as the reference collector, Apricus AP-20, but the absorber area is almost twice as large. The positive effect of having a larger collector area has already been discussed in the previous subchapter.

## 10.2.2 Tank

### 10.2.2.1 Effect of tank insulation thickness

As discussed in chapter 9. *Results*, the annual heat loss from the storage tank is 564 kWh, or 7,5 kWh per m<sup>2</sup> floor area. This amount is equally large as the simulated amount of solar energy that is supplied to the tank during the course of one year. The storage tank used in the reference system is insulated with 40 mm mineral wool, which has a thermal conductivity of 0,033 – 0,040 W/(m·K) (Zijdemans, 2012). To study the impact of tank heat loss on the annual performance, the model was simulated with insulation thicknesses ranging from 0 mm to 100 mm. The results are shown in Figure 94 below, together with the annual specific tank loss in kWh per m<sup>2</sup> floor area.

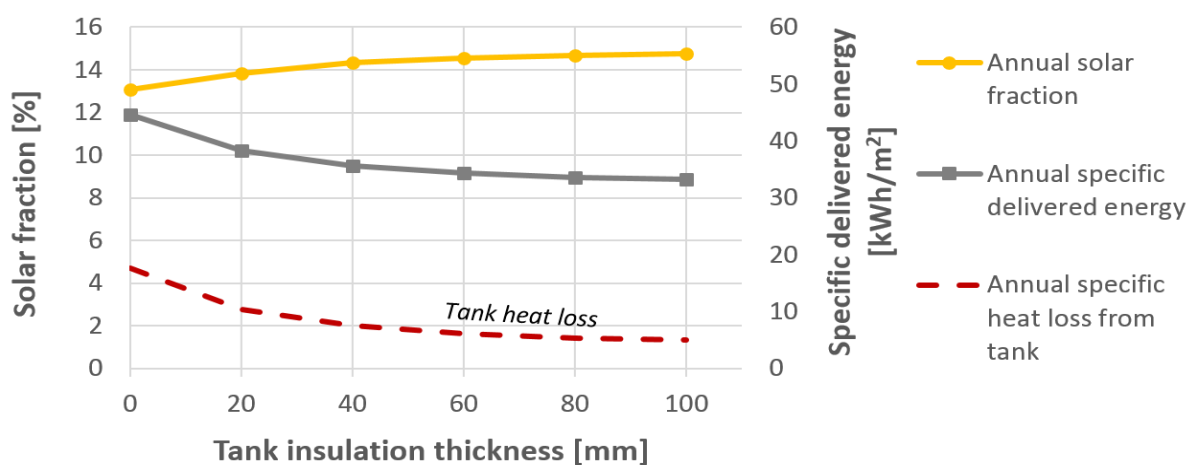


Figure 94: Effect of tank insulation thickness on annual performance

The annual solar fraction increases with a thicker insulation. The annual specific delivered energy decreases accordingly, along with a reduced tank heat loss. This effect is particularly evident when the insulation is very thin. A typical tank insulation thickness found in the Polysun database was 80 mm, which constitutes twice the thickness of the insulation used in the reference system. The impact on performance, as well as on the specific tank loss, of having no insulation, 40 mm insulation (reference system) and 80 mm insulation are summarized in Table 31 below.

Table 31: Effect of tank insulation thickness on annual performance for three cases

	Tank insulation thickness		
	0 mm	40 mm (reference system)	80 mm
Annual solar fraction [%]	13,1	14,3	14,7
Annual specific delivered energy [kWh/m <sup>2</sup> ]	44,6	35,6	33,6
Annual specific tank loss [kWh/m <sup>2</sup> ]	17,5	7,5	5,4

### 10.2.2.2 Effect of tank volume

The initial tank size used in the reference system is 290 liter. To study the effect of tank size on system performance, the model was simulated for tank volumes spanning from 50 l to 600 l. The simulated annual solar fraction and the annual specific delivered energy are presented in Figure 95 below. In addition, the annual specific heat loss from the storage tank, i.e. the annual heat loss per m<sup>2</sup> floor area, is included in the tank with a red, dotted line.

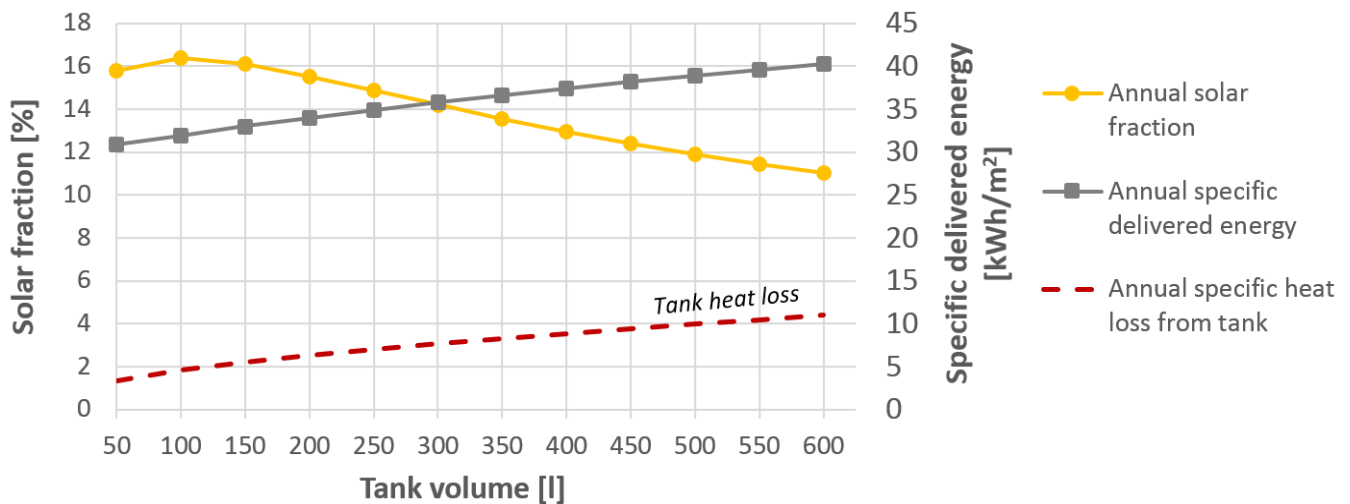


Figure 95: Effect of tank volume on system performance

The results show that the annual specific delivered energy increases significantly with a larger tank size. As discussed in chapter 3.2.3 *Design and dimensioning of the storage tank*, the heat loss from the storage tank is proportional with the heat transfer surface area of the tank. Hence, a larger tank will lead to more heat loss, resulting in higher auxiliary energy demand. This corresponds well with the results presented in Figure 95 above. From 50 l to 600 l, the annual specific heat loss from the tank is more than tripled: from 3,3 kWh/m<sup>2</sup> to 11,0 kWh/m<sup>2</sup>. Within the same range, the annual specific delivered energy increases from 30,8 kWh/m<sup>2</sup> to 40,3 kWh/m<sup>2</sup>, which equals a 30,8% increase.

The behaviour of the solar fraction curve differs slightly: the annual solar fraction increases along with a smaller tank size until a turning point of approximately 100 l, under which the solar fraction decreases. This may be related to the DHW demand of the user of the examined system. In general, a tank volume that is 1-2 times the amount of daily hot water consumption is recommended to get through a few sunless days without significant support from auxiliary heating (DGS, 2010). This coincides well with the results presented here, where the average daily hot water consumption is less than 60 l per day, and where a higher solar fraction is obtained when the tank size is close to 100 l.

It should be noted that the DHW demand for the user in this case study is significantly lower than the estimations made in the design phase, as was described in chapter 5. *Case description*.

Therefore, the current tank size of 290 l may be suitable for one of the other dwellings in Løvåshagen, where the DHW demand is higher. The effects of both DHW demand and space heating demand will be further investigated in chapter 10.4 *Parameters related to the user*.

Another influencing factor in this case study is the low amount of solar energy supplied to the tank throughout the year, as discussed in chapter 9. *Results*. If the system is not functioning properly and is failing to generate enough heat, inserting a large tank will not in itself increase the system performance. With this in mind, the system may benefit from having a larger tank volume than 100 l with an improved system design and operation.

### 10.2.2.3 Effect of tank height

The benefits of having a slim tank were discussed in chapter 3.2.2 *Thermal stratification and energy contents of a store*. It is not possible to change the tank diameter in Polysun. However, with a constant tank volume, a change in tank height can be used to study how the narrowness of the tank affects the system performance. The model was therefore simulated for different tank heights ranging from 1,4 m to 2,2 m. The results are plotted in Figure 96.

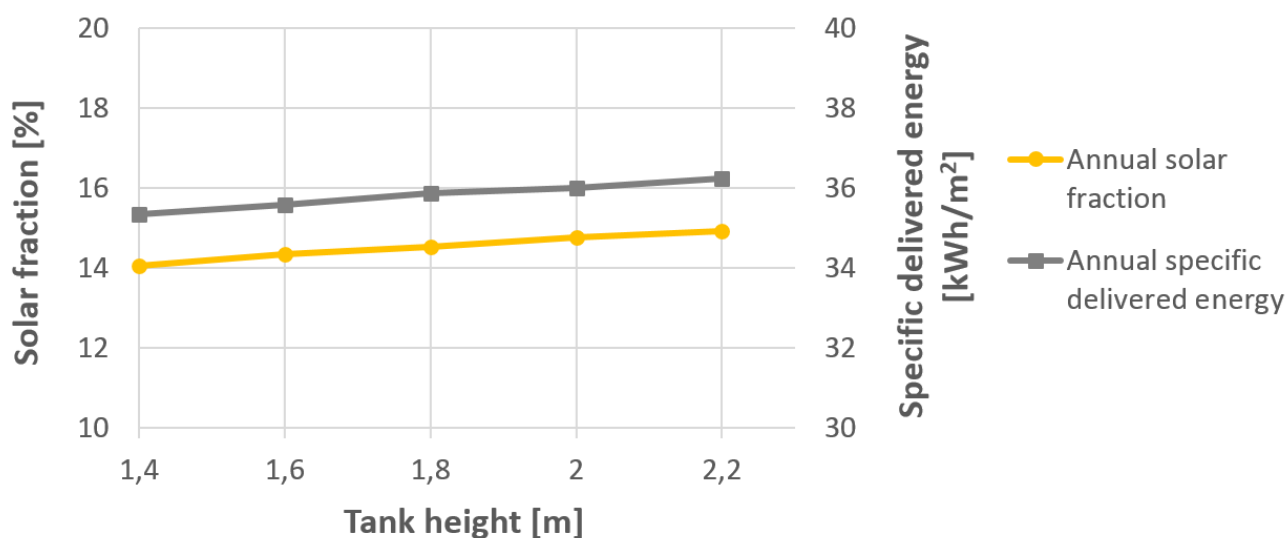


Figure 96: Effect of tank height on system performance

As mentioned in chapter 8. *Simulation inputs*, the initial tank height used in the reference system is 1,6 m. The tank layer temperatures presented in Figure 70 and Figure 71 in chapter 9.4 *Detailed simulations* revealed that the thermal stratification is not always maintained during the high-radiation periods. This could be one of the reasons why the annual solar fraction is somewhat enhanced with a slimmer tank in Figure 96. The annual specific delivered energy, however, increases accordingly.

#### 10.2.2.4 Effect of tank coil- and heating element positions

In Polysun, the positions of all the tank elements are scaled in percentage from the tank bottom. For the two coils (the space heating coil and the solar coil), the position of the upper connection must be stated along with the respective coil heights, as illustrated in Figure 97.

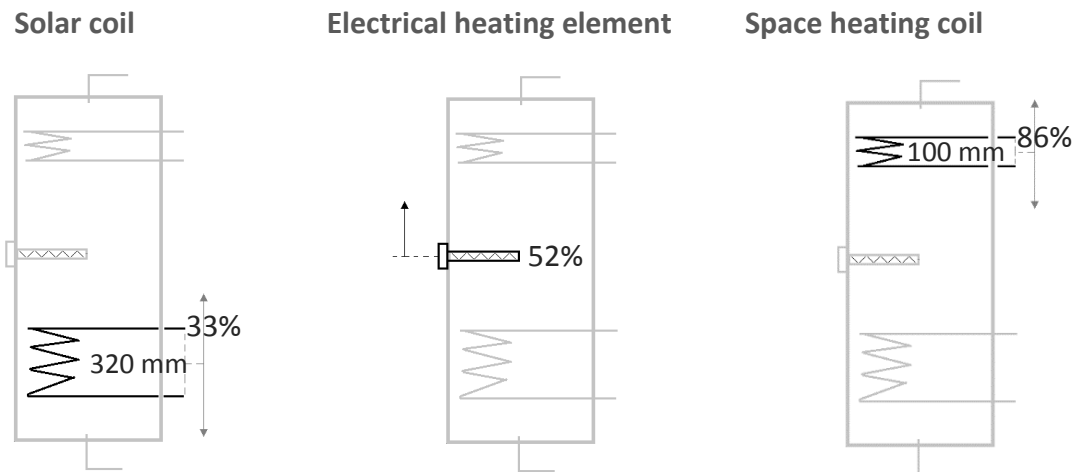


Figure 97: The input positions of coils and electrical heating element in the tank in Polysun.

To study the impact of the tank component locations, the three positions were altered one at a time; the solar coil from 25% to 40%, the electrical heating element from 40% to 65%, and the space heating coil from 55% to 90%. The two coil heights were kept fixed during the simulations. The annual solar fraction and annual specific delivered energy for the three cases are illustrated in Figure 98 and Figure 99, respectively. The initial settings are included in the graph with dotted lines.

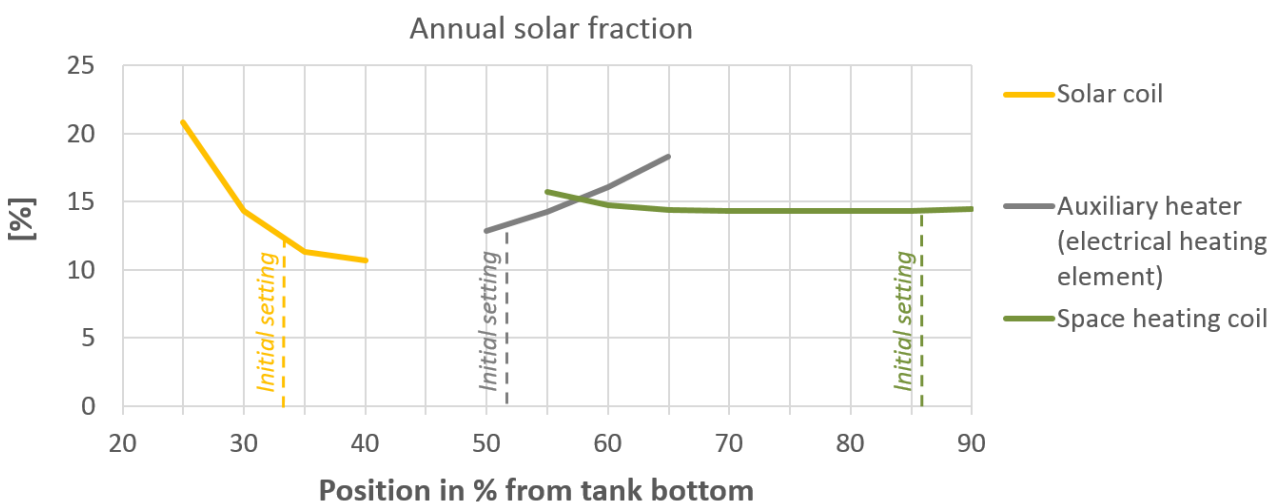
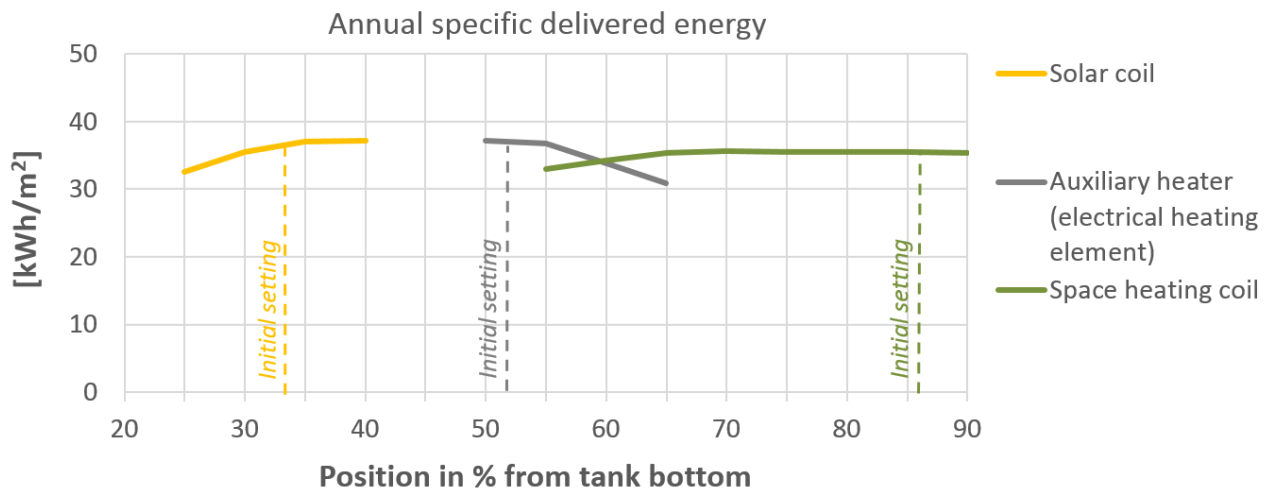


Figure 98: Effect of tank coils- and heating element position on annual solar fraction



**Figure 99: Effect of tank coils- and heating element position on annual specific delivered energy**

The upper solar coil connection is located at 33% from the tank bottom in the reference system. By lowering the coil down to 25%, the annual solar fraction increases from 14,3% to 20,9%, and the annual specific delivered energy decreases from 35,6 kWh/m<sup>2</sup> to 32,5 kWh/m<sup>2</sup>. Moreover, further investigations of the solar pump operation revealed that this positive effect on system performance is strongly related to the temperature at the tank bottom. By lowering the solar coil, the bottom tank temperature rises, which has a positive influence on the pump operation: it no longer operates constantly during night, and the annual pump consumption decreases from 182 kWh to 17,2 kWh. This affects the required total specific delivered energy to the solar heating system, as seen in Figure 99. As a result, less heat is removed from the tank, which reduces the need for auxiliary heating. The effectiveness of the solar pump controller will be further investigated in chapter 12.3 *Operation parameters*.

In this case study, the auxiliary heater is located approximately at the middle of the tank (52% from tank bottom), which means that the auxiliary volume, i.e. the volume above the heater, constitutes almost half the tank. As seen in the detailed simulations in chapter 9.4, the temperatures above this level rarely falls below 75°C. Moving the position of the electrical heater further up is equivalent to reducing the effective auxiliary volume. As a result, the annual specific delivered energy curve depicted in Figure 99 decreases. Furthermore, this significantly increases the utilization of solar energy and has a positive impact on the annual solar fraction in Figure 98. It should, however, be noted that the position of the heater cannot be moved too far up, as this may lead to inadequate heat coverage during the winter.

A change in the space heating coil position had only a minor impact on both annual solar fraction and on annual specific delivered energy. These were, however, slightly improved with a lower

tank position. This is presumably because more solar energy is utilized for space heating if the coil is located closer to the solar coil. There is, however, a limitation to how low this coil could be positioned within the tank, since it must be placed above the auxiliary heater (52%) in order to satisfy the heat demand when there is little or no solar radiation.

### 10.2.2.5 Effect of solar coil height

The solar coil height was simulated from 300 mm to 500 mm (reference system: 320 mm). The results are shown in Figure 100.

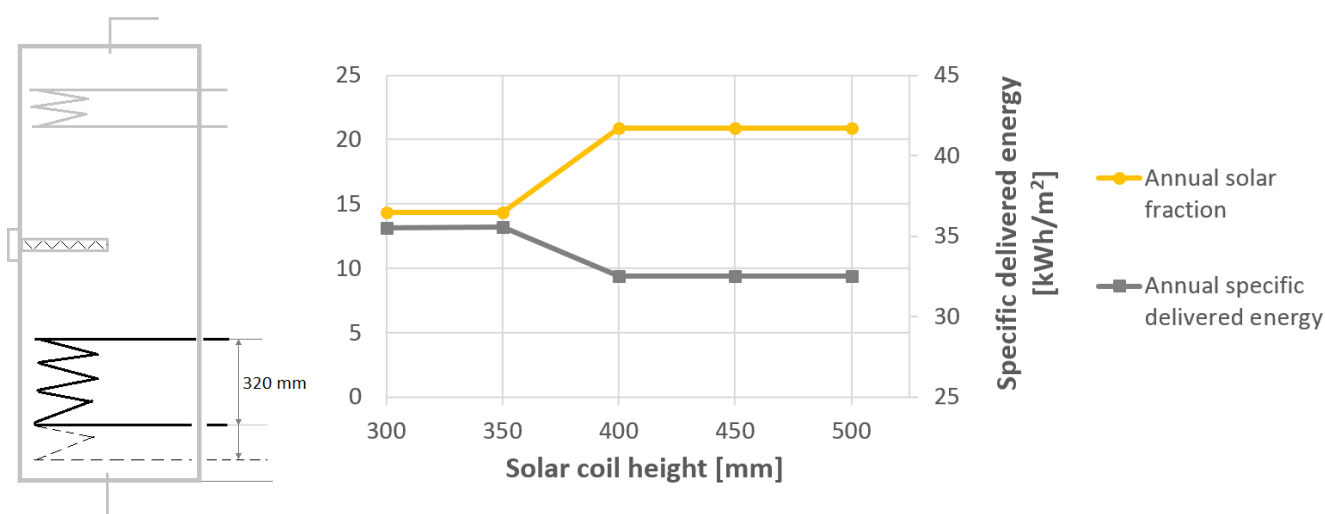


Figure 100: Effect of solar coil height on system performance

The solar fraction increases considerably with a larger solar coil height. The position of the upper coil connection is fixed at 33%, which means that a larger coil height leads to improved heating of the bottom tank water. For the same reasons that were explained in the previous subchapter regarding the solar coil position and the pump operation, this has a strong influence on both annual solar fraction and annual specific delivered energy. This positive effect, however, is only effective until a height of approximately 400 mm. A larger coil height have no further impact; at this point, the temperature at the bottom of the tank is just high enough for the current controller settings to function properly.

### 10.2.2.6 Effect of solar heat exchanger properties

The solar heat exchanger, or the solar coil, is made of stainless steel with a surface area of 0,8 m<sup>2</sup>. As explained in chapter 5. *Case description*, the solar coil was one of the main motivations for implementing the modification in January 2015. In addition to being small of size, it was argued that the material it is made of (stainless steel) has much worse heat transfer properties than for instance copper, which is a common material used for this kind of application. In this subchapter, an attempt will be made to reveal whether or not the solar heat exchanger reduces the performance of the system.

#### **Effect of solar coil surface area**

According to DGS (2010), this type of heat exchanger can be sized according to the following rule: *0,2 m<sup>2</sup> exchanger surface area per m<sup>2</sup> collector surface area*. With a collector area of 3,2 m<sup>2</sup> (absorber area), this corresponds to a required solar heat exchanger area of 0,64 m<sup>2</sup>. It is important, however, to emphasize that this rule applies for the sizing of coils in DHW systems. In combination systems, like in this case study, additional heat exchanger area should be added. With this in mind, the surface area of 0,8 m<sup>2</sup> used in the reference system seems relatively suitable for the current collector size. To investigate the influence of the solar heat exchanger area, the model was simulated for different coil areas ranging from 0,2 m<sup>2</sup> to 2 m<sup>2</sup>. The results are presented in Figure 101.

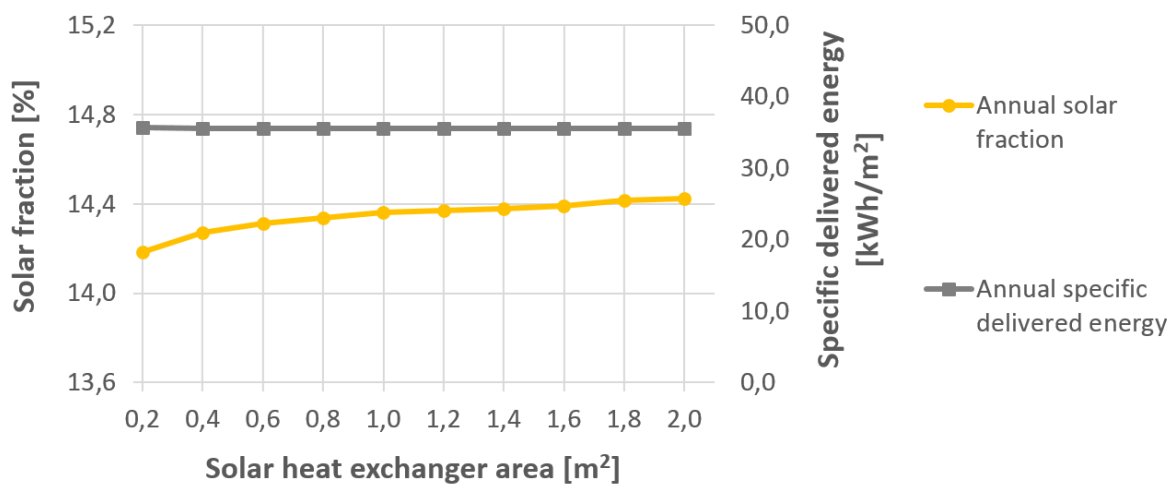


Figure 101: Effect of solar heat exchanger area on system performance

As seen in the graph, a larger solar heat exchanger area leads to slightly higher annual solar fraction, but appears to have no noticeable impact on the annual specific delivered energy.



### ***Effect of solar coil material***

The simulation model was also simulated for different heat exchanger materials with the thermal properties displayed in Table 32. As shown in the table, the current material of stainless steel has significantly lower thermal conductivity than copper and aluminium.

**Table 32: Thermal conductivity of selected materials**

<b>Material</b>	<b>Thermal conductivity [W/(m·K)]</b>
Copper	394
Aluminium	239
Stainless steel ( <i>reference system</i> )	15

The resulting performance diagram is attached in *Appendix C.1.2*. Despite the significant difference between the thermal conductivity, the simulations revealed no noticeable impact when changing the material.

The results presented in this chapter regarding the solar heat exchanger (solar coil) are not significant enough to confirm the suspicion that the solar heat exchanger is an important contributing factor for why the system is not performing as desired. Notably, there are other parameters investigated in this study that appears to have much more significant impact. It should, however, be kept in mind that the solar coil's small effect on system performance could be related to the previously mentioned pump operation, in which heat is removed from the tank during night: If a larger surface area results in more heat being supplied *to* the tank, then more heat can potentially be withdrawn *from* the tank.

### 10.2.3 Solar circuit pipelines

The results presented in chapter *9.4 Detailed results* revealed that the amount of heat that is lost in the solar circuit pipeline during the course of one year is larger than the annual amount of solar energy supplied to the tank. Moreover, heat loss to indoor room is just as dominant as heat loss to outdoor surroundings. As seen in equation 6 in chapter *3.3.1 Pipelines*, the total heat loss from pipes is a function of pipe diameter, insulation thickness, thermal conductivity of the insulation, pipe length and temperature difference between the hot liquid and the colder surrounding air. In this subchapter, some of these parameters will be further investigated.

### 10.2.3.1 Effect of pipe insulation thickness

The solar circuit pipes in the reference system consist of pre-insulated HT Armaflex pipes, which have a thermal conductivity of 0,038 W/(m·K) at 0°C. The insulation thickness is 14 mm. To investigate the influence of pipe insulation thickness on system performance, the model was simulated with thicknesses ranging from 10 to 40 mm. The results are displayed in Figure 102.

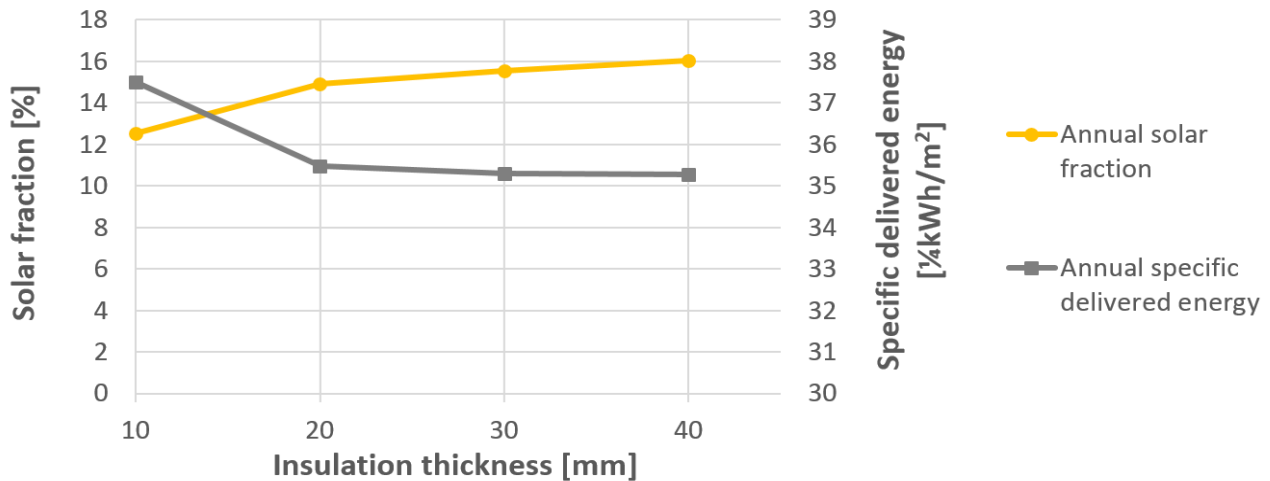


Figure 102: The effect of pipe insulation thickness on system performance

The results show that a thicker insulation has a positive impact on both performance indicators. This coincides well with the pipe heat loss equation, which shows that an improved insulation thickness results in less heat loss from the solar circuit pipes. Moreover, thicker insulation increases the solar energy contribution to the tank, and thereby reduces the need for auxiliary heating. Figure 103 below depicts the annual heat loss from the solar circuit together with the annual solar energy supplied to the tank. The influence is especially present when the insulation is thin.

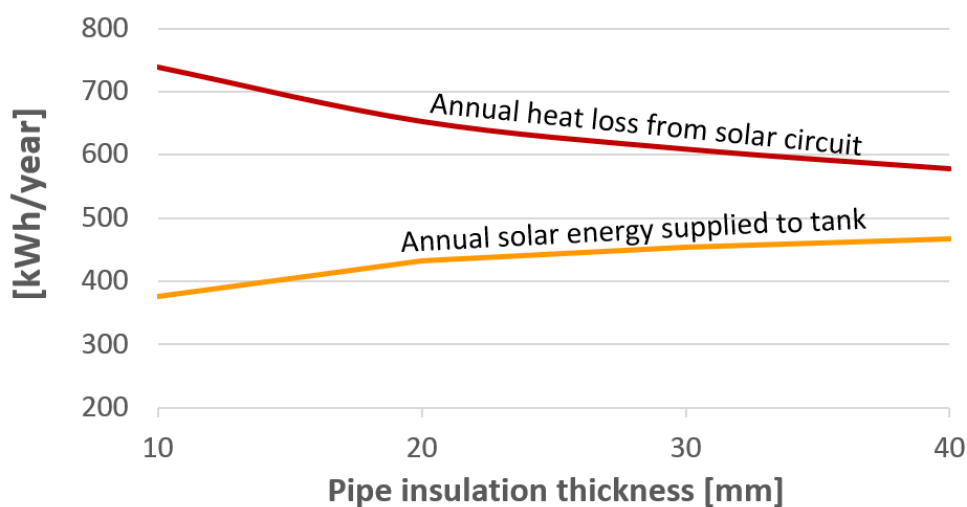


Figure 103: The impact of pipe insulation thickness on annual heat loss in the solar circuit and on annual solar energy supplied to the storage tank.

According to the European standard *EN 12977-2: 2012 Thermal solar systems and components – Custom built systems*, pipes with external diameters up to  $22\pm 1$  mm should have an insulation thickness of  $22\pm 2$  mm. This value assumes a thermal conductivity of  $0,04 \pm 0,01$  W/(m·K) at  $10^{\circ}\text{C}$ . This fact, in combination with the results presented above, suggests that the current pipe insulation thickness of only 14 mm that is found in the reference system is inadequate.

### 10.2.3.2 Effect of pipe diameter

The solar circuit pipes in the reference system have an inner and outer diameter of 16 mm and 18 mm respectively. To study the effect of pipe diameter on system performance, different external diameters spanning from 12 mm to 22 mm were simulated. The wall thickness remained unchanged at 1 mm during the simulations. The results are shown in Figure 104 below.

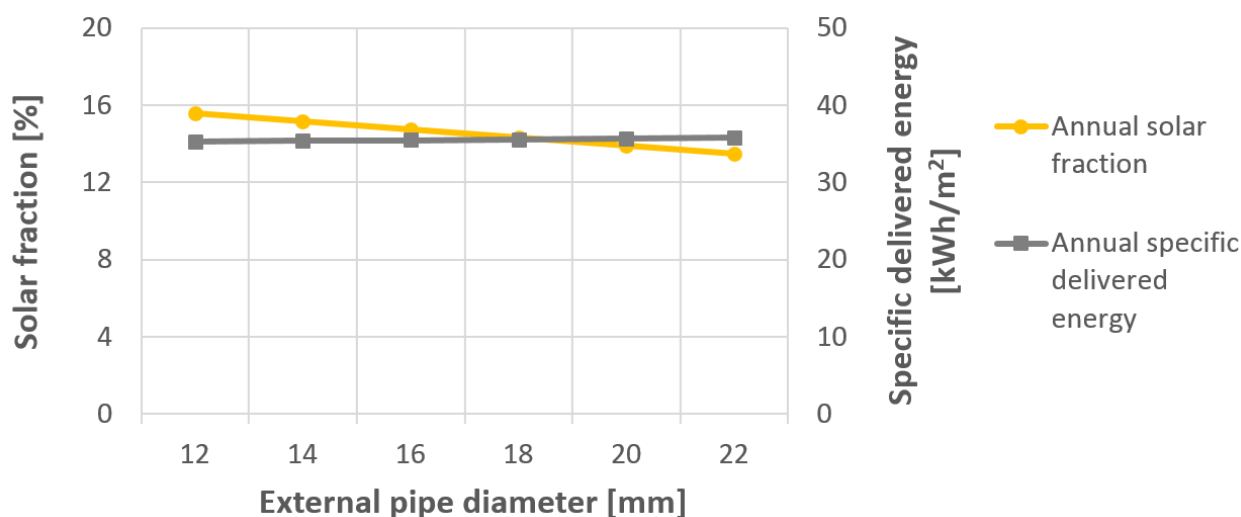
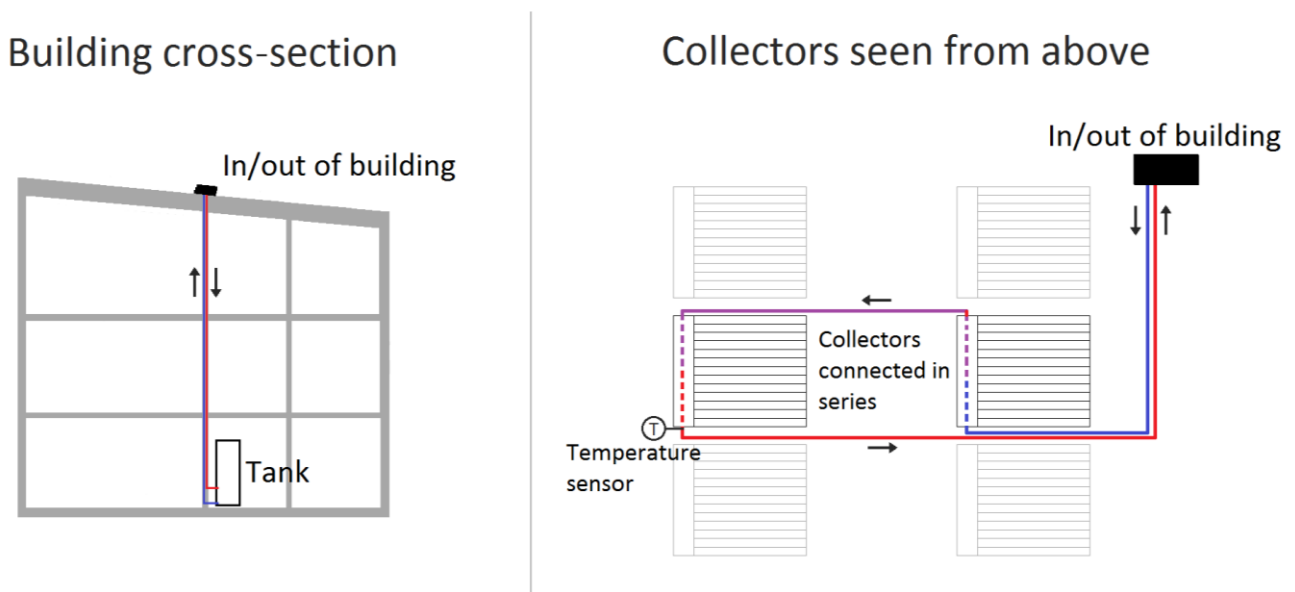


Figure 104: Effect of external pipe diameter on annual performance. Wall thickness is 1 mm

As illustrated in the diagram, an increase in pipe diameter results in a slightly lower annual solar fraction. This is because a larger pipe diameter increases the total pipe heat loss due to a larger surface area. A smaller diameter would normally result in slightly higher energy consumption of the solar pump, which would increase the delivered energy. This effect is, however, minimized since less auxiliary energy is required when the total heat loss is smaller. As a result, the total delivered energy remains relatively unaffected by a change in diameter.

### 10.2.3.3 Effect of distance between collector and tank

The investigated system belongs to a dwelling located on the ground floor level in a 3-storey building, which results in relatively long pipelines between the two collectors on the roof and the storage tank located in the bathroom. In this subchapter, the consequence of long pipelines will be studied more closely. To get an idea of how far the useful thermal output of the collectors must travel before finally entering its final destination in the storage tank, a simplified sketch of the building cross-section (left), as well as the collector layout on the roof seen from above (right), is provided in Figure 105.



**Figure 105:** Left: Cross-section of the building. Right: overview of how the two collectors are installed with respect to each other on the roof

The current solar circuit supply pipe length (red) and return pipe length (blue) for the investigated system were approximated to 18,5 m and 15 m, respectively, based on the architect drawings and on measurements conducted on site.

The model was simulated for various pipeline lengths, distinguishing between pipe lengths exposed to the ambient and pipe lengths exposed to indoor room. The simulations were performed systematically: first, the indoor pipe length was altered (both supply and return line) while the outdoor pipes remained unchanged; next, the opposite was conducted. All other parameters, such as pipe diameter and insulation properties, were kept at their initial settings. In this case study, the total indoor and total outdoor pipe length is approximately 17,5 m and 16 m, respectively. The simulated effect of indoor and outdoor pipes on annual solar fraction and on annual specific delivered energy, are depicted to the left and to the right, respectively, in Figure 106. The third graph depicts the corresponding heat loss to indoor and outdoor surroundings.

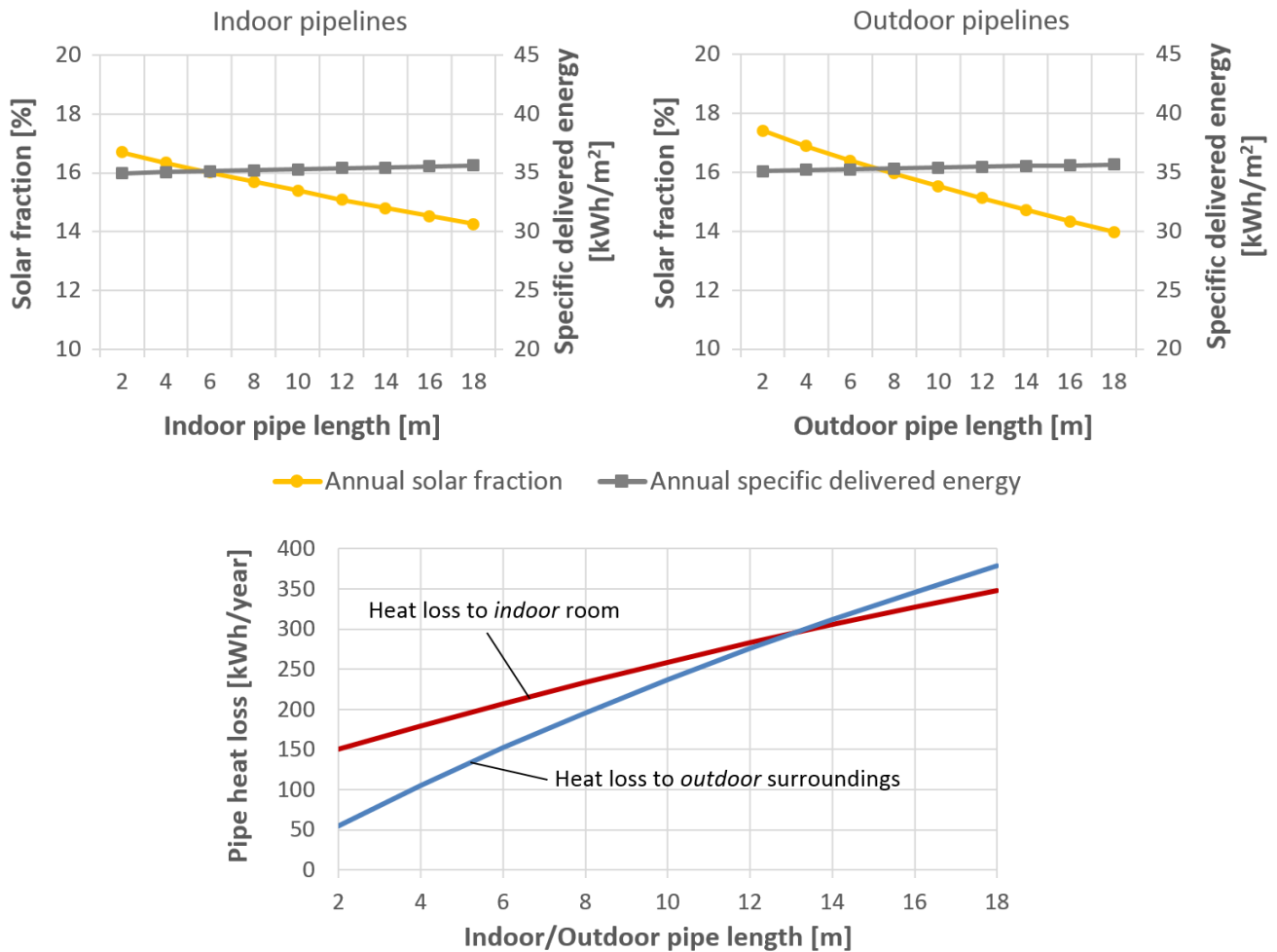


**Figure 106: Top: Effect of indoor (left) and outdoor (right) pipe length on system performance. Bottom: Heat loss to indoor or outdoor room as a function of indoor or outdoor pipe lengths**

As seen in Figure 106, the annual solar fraction decreases significantly with an increase in both indoor and outdoor pipe length, whereas the annual specific delivered energy increases only slightly. When increasing the indoor pipe length from 2 to 18 meters, the annual heat loss is more than doubled from approximately 150 kWh to 350 kWh, with a corresponding reduction in the annual solar fraction by 14,4 %. On the other hand, the same increase in outdoor pipe length causes a multiplication in annual heat loss by a factor of 7,5, from approximately 50 kWh to 375 kWh, and reduces the solar fraction by 19,5%. Thus, it is evident that heat loss to outdoor surroundings has a greater impact on the solar fraction than heat loss to indoor room. This makes sense, as the pipes located outside of the building are exposed to a higher temperature difference between the solar liquid and the ambient, than the pipes located inside the building. Therefore, it is particularly important to keep outdoor pipe lengths at a minimum, and to ensure that they are adequately insulated.

To examine if all the solar thermal systems in Løvåshagen are subject to great heat loss, the model was simulated for three cases with different indoor pipe lengths presented in Table 33.

**Table 33: Simulated cases**

<b>Tank location</b>	<b>Total indoor pipe length (both supply and return pipe)</b>
Ground floor (reference system)	17,5 m
1 <sup>st</sup> floor (top floor)	12 m
2 <sup>nd</sup> floor (top floor)	6,5 m

In addition to the long indoor pipelines, an immediate observation that can be made from the sketch of the collector layout in Figure 105 is that the solar liquid does not only have to travel through several floors before reaching the tank; the distance between the second collector and the opening to the building seems unnecessarily long. As a result, approximately 16 m of the pipeline is exposed to ambient air. Even with well-insulated pipes, this layout will cause unfavourable heat loss. Thus, an improved layout is suggested in Figure 107 below, in which the collectors are instead placed next to each other. As a result, the pipelines on the roof can be much shorter – and the accompanying heat loss will be reduced.

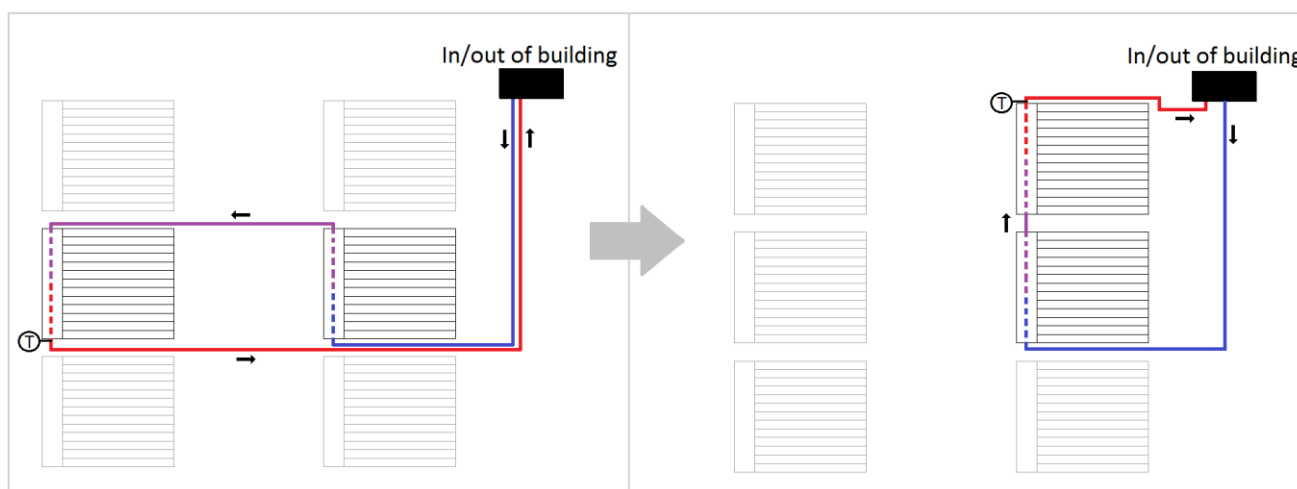


**Figure 107: Current collector layout (left) and suggested improved collector layout (right)**

The total heat loss for each of the three cases that were presented in Table 33, is displayed in Table 34 below, for both the existing and the suggested improved layout.

**Table 34: Annual heat loss for each case, both with and without improved collector layout**

	Total heat loss in solar circuit [kWh/year]	
	<i>Current roof layout</i>	<i>Improved roof layout</i>
<b>Ground floor</b>	689,0	599,8
<b>1<sup>st</sup> floor</b>	643,5	544,5
<b>2<sup>nd</sup> floor</b>	591,8	480,0

The corresponding annual solar fraction and annual specific delivered energy are shown in Figure 108. The benefits of shorter external pipes are represented in the graph, with corresponding dotted lines, and represent the suggested improved collector layout.

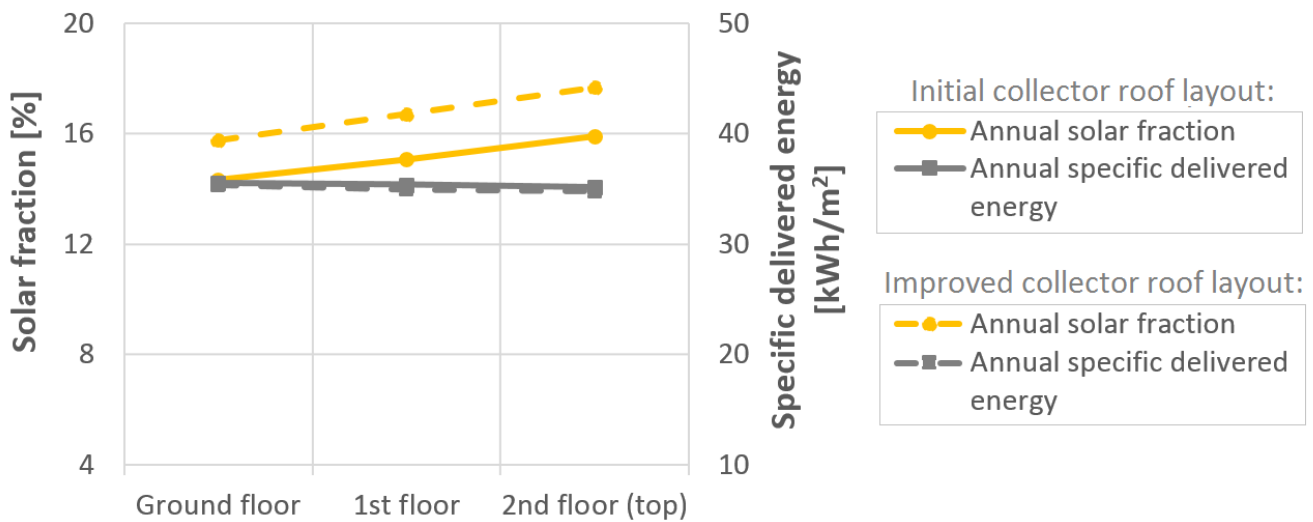


**Figure 108: Effect of solar circuit pipe length on system performance**

As can be seen from the diagram, the annual solar fraction increases as the tank location draws nearer to the two collectors. The solar contribution is further enhanced by altering how the solar collectors are placed on the roof, both according to each other and to the building opening. The annual specific delivered energy decreases only slightly with a higher floor level and an improved collector layout. Moreover, the results suggest that an identical solar thermal system located on the 2<sup>nd</sup> floor will have an annual solar fraction that is 11,2% higher than that of the reference system, which is located on ground floor level. When also improving the collector roof layout, the total increase is 23,8%.

## 10.3 Operation parameters

This chapter targets the parameters that are relevant for the operation of the solar system.

### 10.3.1 Solar pump controller

The solar pump controller regulates the on/off operation of the pump within the solar circuit. As previously mentioned, this is done by measuring the temperature difference between the hot collector outlet and the colder tank temperature.

On several occasions in the previous chapters, the control of the solar pump has already been highlighted as a potential performance reducing factor. Since Polysun does not allow for an altering of the position the collector outlet temperature sensor, only the effect of unfavourable placing of the tank temperature sensor and the impact of  $\Delta T$  settings will be further investigated in this subchapter.

#### 10.3.1.1 Effect of tank temperature sensor location

In chapter 3. *Design and operation of a solar thermal system*, it was mentioned that a correct placing and functioning of the tank temperature sensor strongly affects the effectiveness of the controller. To further study the influence of changing the position of the tank sensor, simulations were made for the five different locations shown in Figure 109. Layer 1 is the bottom layer, which represents the initial setting used in the reference system. As previously stated, the solar energy from the collectors enters the tank through the solar coil at a tank height of 33% (upper section of layer 4), whereas the cooled heat transfer fluid exits the tank through the lower solar coil connection at approximately a tank height of 13% (layer 2). The electrical heating element is located at 52% (layer 7).

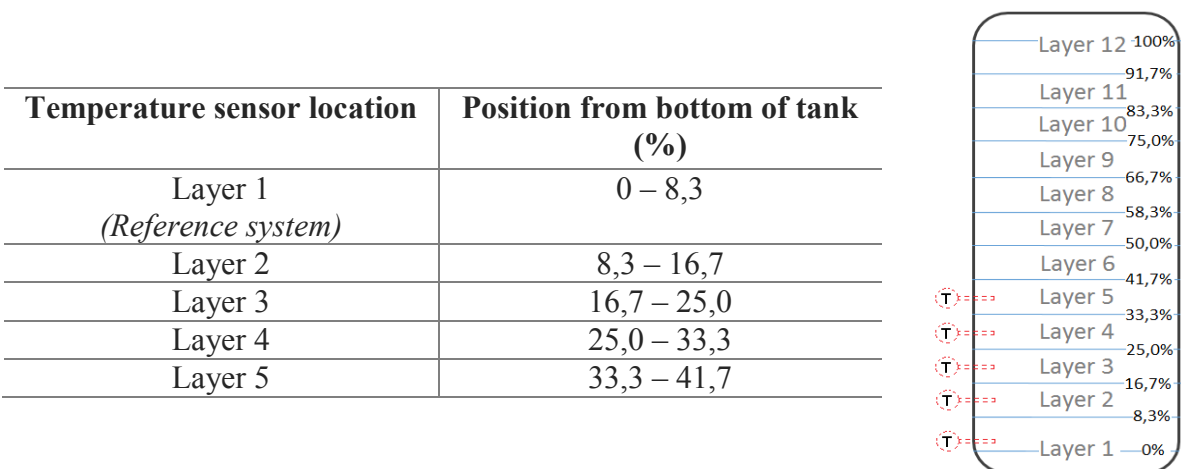


Figure 109: The various tank sensor locations that were simulated in Polysun



Figure 110 illustrates the simulated monthly solar fraction during one year for each of the five cases.

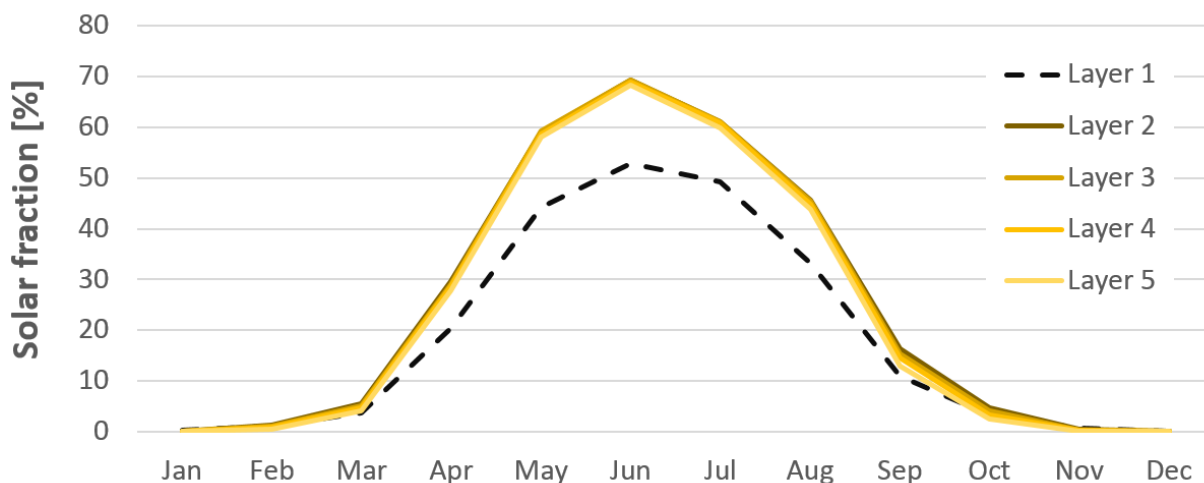


Figure 110: Effect of different locations of the tank sensor on monthly solar fraction.

As can be seen from the graph, layer 2 results in the highest solar fraction throughout the year, closely followed by layer 3, 4 and 5. This is because the lower solar coil connection is located within this layer. Layer 1 (reference system), on the other hand, causes a significantly smaller solar fraction during the summer months, compared to the other cases. The resulting annual solar fraction and the annual specific delivered energy are summarized in Table 35.

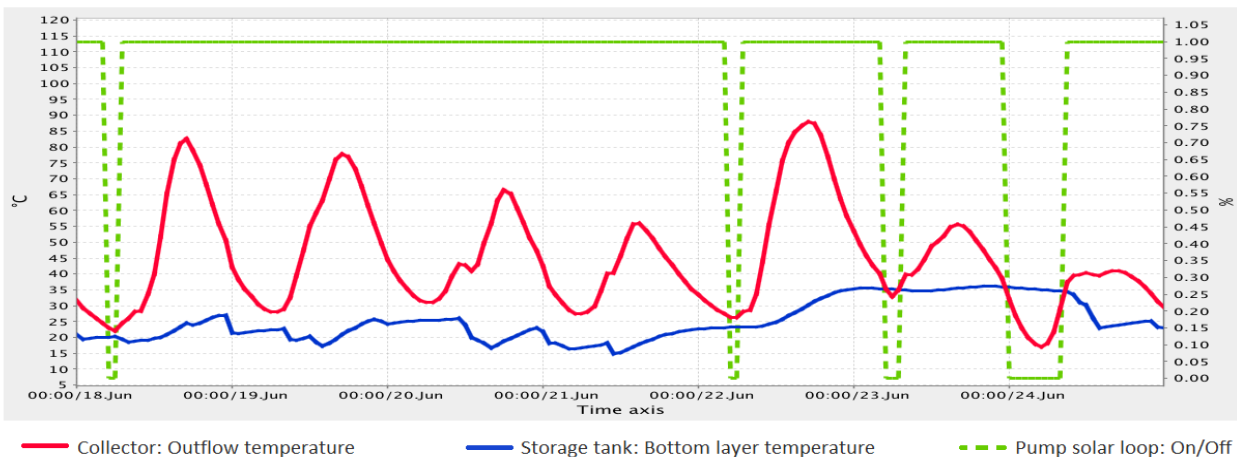
Table 35: Annual performance for five different tank sensor locations

	Layer 1	Layer 2	Layer 3	Layer 4	Layer 5
Annual solar fraction [%]	14,3	20,0	19,7	19,3	18,8
Annual specific delivered energy [kWh/m <sup>2</sup> ]	35,6	32,0	32,0	32,0	32,2

As discussed in chapter 9.4.4 *Controller*, the reduced performance of placing the temperature sensor within layer 1 is a result of incorrect temperature readings. When the temperature sensor is located too low in the tank, its readings are strongly influenced by the cold network water temperature, which enters the tank through the tank bottom. This water is consistently much colder than the temperature of the water that surrounds the solar coil. As a result, the  $\Delta T$  between the tank temperature sensor and the temperature sensor at the collector outlet is very often higher than the switch-off  $\Delta T$  of 4 K during periods with high radiation. Consequently, the pump is not always switched off during night. This effect is illustrated in Figure 111 below, which depicts a typical week in June for both a tank sensor location at layer 1 (top) and at layer 2 (bottom). The graphs show the collector outflow temperature of the solar liquid (red line), the temperature of the tank at

the chosen sensor location (blue line) and the pump operation (dotted, green line). A pump value of 1 equals ON, and 0 equals OFF.

### Tank sensor location: Layer 1



### Tank sensor location: Layer 2

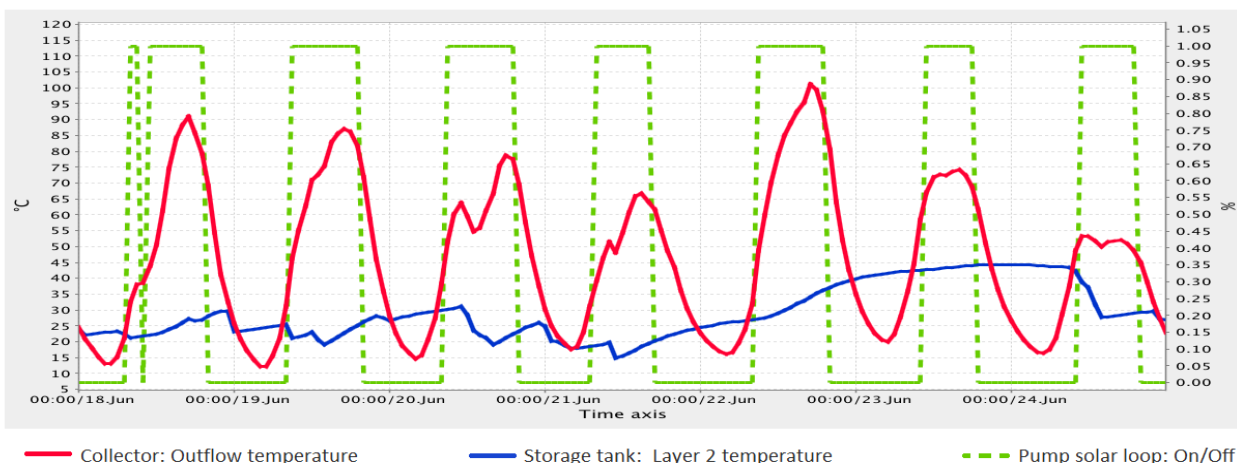


**Figure 111: Solar pump control (1=ON, 0=OFF) during one week in June for the two different sensor locations**

With the initial settings of the reference system, the solar pump consumes 182,9 kWh each year, which equals a specific consumption of 2,4 kWh per square meter floor area. This constitutes 44% of the annual solar energy that it supplies the tank, which is very high. By simply moving the sensor up to layer 2, the pump consumption drops to 11,5 kWh/year, that is, 0,2 kWh per square meter floor area, and the annual solar fraction increases from 14,3% to 20,0%.

The moving of the sensor does not only significantly reduce the pump consumption; also, the total heat loss in the solar circuit declines by almost 50%, as shown in Table 36 below.

**Table 36: Heat loss in the solar circuit with different tank sensor locations**

Tank sensor location	Heat loss to indoor room [kWh/year]	Heat loss to outdoor surroundings [kWh/year]	Total heat loss [kWh/year]
Layer 1 (ref)	342,8	346,2	689
Layer 2	193,6	155,4	349
<b>Reduction in heat loss by moving the tank sensor from layer 1 to layer 2</b>	<b>-43,5%</b>	<b>-55,1%</b>	<b>-49,3%</b>

To illustrate why the heat loss in the solar coil is significantly reduced when changing the tank sensor location from layer 1 to layer 2, the hourly energy flow in the solar coil is depicted in Figure 112. The graph shows the energy that is supplied to (positive values) and removed from (negative values) the tank during the course of one year in W. As can be seen from the graph, an evident reduction in heat removal from the tank is achieved by relocating the tank temperature sensor.

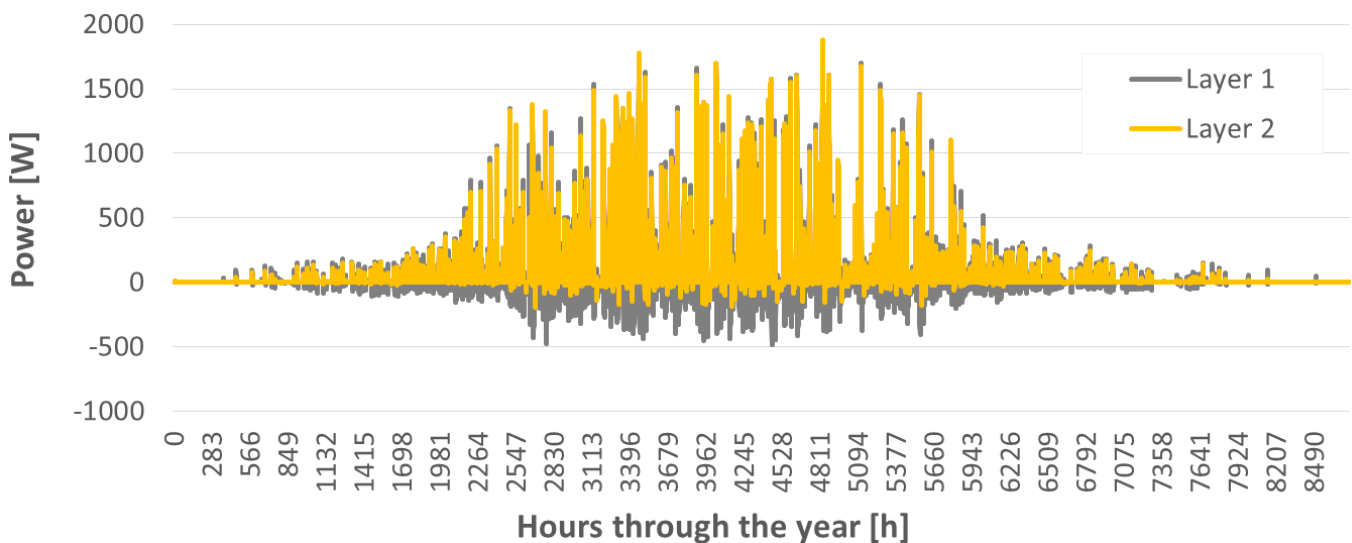


**Figure 112: Energy flow in the solar coil for two different tank locations. Positive values represent energy that is supplied to the tank, whereas negative values represent energy withdrawal**

### 10.3.1.2 Effect of $\Delta T$ settings of the solar pump controller

The Apricus’ installation and operation manual (Apricus Solar, 2013) states that a switch-on  $\Delta T$  of 8 K and a switch-off  $\Delta T$  of 2 K are usually appropriate, but that the settings may need to be altered according to the particular system design and location. The model was simulated with selected switch-on and switch-off  $\Delta T$  settings, and the two annual performance indicators are shown in Figure 113 below.

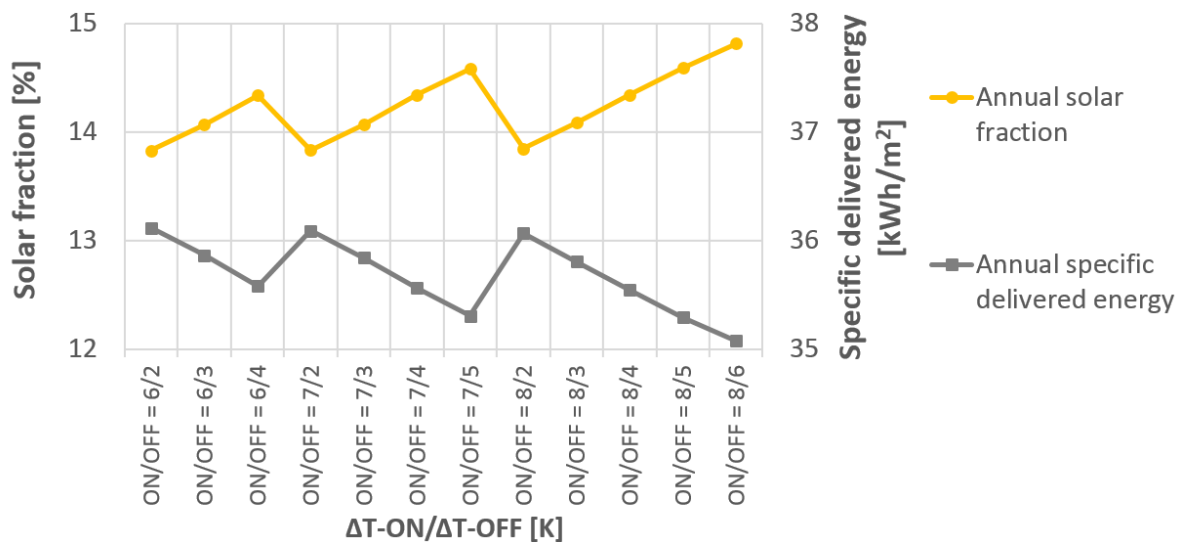


Figure 113: The effect of  $\Delta T$  switch-on and  $\Delta T$  switch-off settings on annual system performance

As displayed in the graph, the current switch-on/switch-off  $\Delta T$  of 6K/4K is not the optimum control setting for the investigated system. With the current design and operation, the system would benefit from having both a higher switch-on  $\Delta T$  and a larger switch-off  $\Delta T$ . It is, however, important to emphasize that the optimum temperature setting is highly dependent on the chosen tank sensor location, which was elaborated in the previous subchapter. If the on/off setting is increased to 8K/6K, the annual specific delivered energy decreases from 35,6 kWh/m<sup>2</sup> to 35,1 kWh/m<sup>2</sup>. This is a slightly bigger reduction than the reduction that was obtained when moving the tank sensor from layer 1 to layer 2 in the previous chapter. The annual solar fraction, on the other hand, only increases from 14,3% to 14,8%. As recalled in the previous subchapter, a relocation of the tank temperature sensor from layer 1 to layer 2 resulted in an annual solar fraction of 20,0%. Hence, these two aspects regarding control of the solar pump are strongly correlated, and should be adjusted with respect to each other, as well as to the particular system design.

### 10.3.2 Control of the auxiliary heater

The switch-on temperature for the immersed electrical heating element (layer 7) is set to 75°C in the reference system, which is much higher than the draw-off temperature setting of 50°C. Zijdemans (2012) lists the pros and cons of having a high water temperature in the tank. The benefits include a reduction in necessary tank size and increased safety against formation of the Legionella bacteria, which was discussed in the literature review in chapter 3. On the downside, a higher temperature results in a greater tank heat loss and reduces the utilization of low-temperature energy sources for preheating of hot water, due to the higher need for after-heating.

To study the impact of different switch-on settings for the immersed electrical heater, the model was simulated for selected switch-on temperatures ranging from 50°C to 75°C. The switch-off

temperature was constantly set to be 2°C higher than the switch-on temperature. The simulated annual solar fraction and the corresponding specific delivered energy are presented in Figure 114.

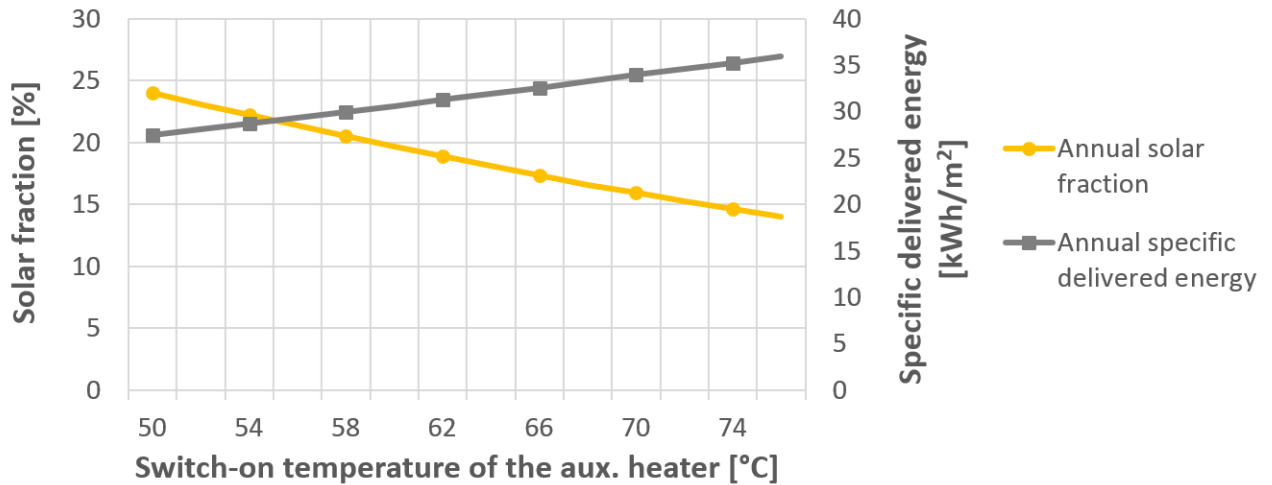


**Figure 114:** The effect on system performance when changing the switch-on temperature of the auxiliary heater. The switch-off temperature is 2°C higher than the switch-on temperature.

As depicted in the graph, a higher switch-on temperature results in a higher annual specific delivered energy, as well as a considerably lower annual solar fraction. This is because of the significant increase in necessary auxiliary energy that is required to compensate for the increased energy demand for after-heating. Furthermore, a higher temperature setting reduces the utilization of solar energy. The distribution of solar energy and auxiliary energy supplied to the tank for the different switch-on temperatures are illustrated in Figure 115 below.

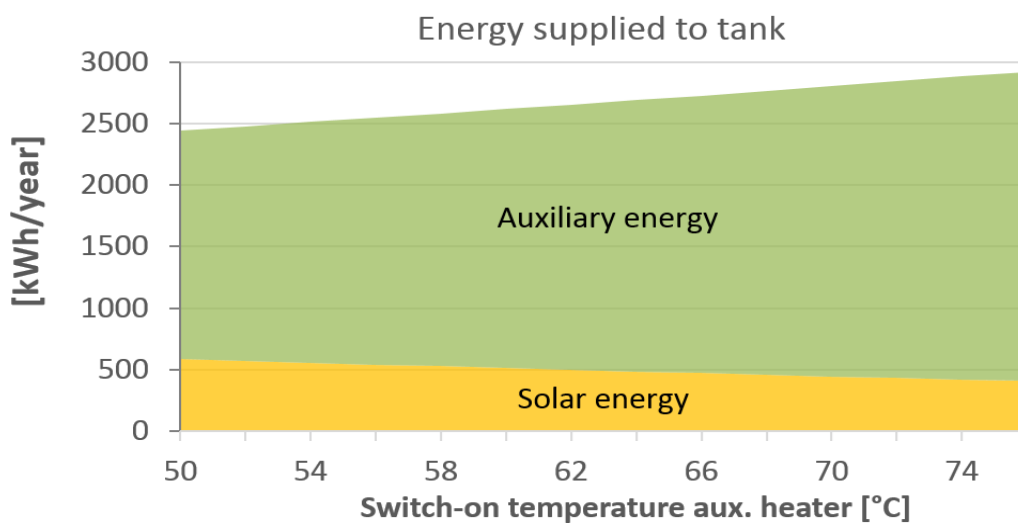


**Figure 115:** The impact of various switch-on temperatures on the amount of solar- and auxiliary energy supplied to the tank

### ***Comments regarding the impact of Legionella protection***

As discussed in the literature review in chapter 3.2.4 *Temperature requirements in storage tanks*, the growth of Legionella bacteria stagnates at temperatures below 20°C and above 50°C. Above 55-60°C, the bacteria will eventually die. This effect can significantly be enhanced by raising the temperatures to 65-70°C (Folkehelseinstituttet, 2009).

The consequence of setting the switch-on temperature of the auxiliary controller to 75°C in the reference system instead of the 50°C, which is the same as the draw-off temperature setting, is illustrated in Table 37.

**Table 37: Impact of measures for Legionella protection on annual system performance**

<b>Auxiliary controller SWITCH-ON temperature setting [°C]</b>	<b>Annual specific delivered energy [kWh/m<sup>2</sup>]</b>	<b>Annual solar fraction [%]</b>
50°C	27,4	24,1
75°C (Reference system)	35,6	14,3
Impact on performance when increasing the switch-on temperature from 50°C to 75°C	+29,9%	-40,7%

In this case study, the Legionella protection increases the auxiliary energy consumption by almost 30%. Correspondingly, the annual solar fraction is reduced by almost 41%. As a general rule, it is recommended that in dwellings and other private households for which the user controls the temperature conditions in the storage tank, the temperature should hold at least 70°C (assuming that a mixing valve is installed). An alternative measure is to set the tank temperature to hold a minimum of 60°C, and then manually (or otherwise) raise the temperature above 70°C on a regular basis. In this way, an adequate protection is maintained, and unnecessary heating is avoided (Folkehelseinstituttet, 2009). However, in order for this strategy to work, well-established routines, as well as a certain level of knowledge on Legionella among the users, would be required.

### **10.3.3 Effect of volumetric flow rate in the solar circuit**

As presented in equation 7 in chapter 3.3.3, the flow rate through the collectors affect the amount of heat that is absorbed by the solar liquid in the collector manifold. The volumetric flow rate in the solar circuit is controlled by means of characteristic pressure curves of the solar pump. As seen in the simulated results in chapter 9. *Results*, the volumetric flow rate varies between approximately 690 l/h and 1040 l/h, depending on season and time of day. In order to investigate the impact on system performance, the model was simulated for the three speed stages of the particular pump, as seen in Figure 116. As previously mentioned, the three stages and their

corresponding pressure curves are attached in *Appendix B.3.1*. Stage 1 has the lowest volumetric flow rates, whereas stage 3 has the highest.

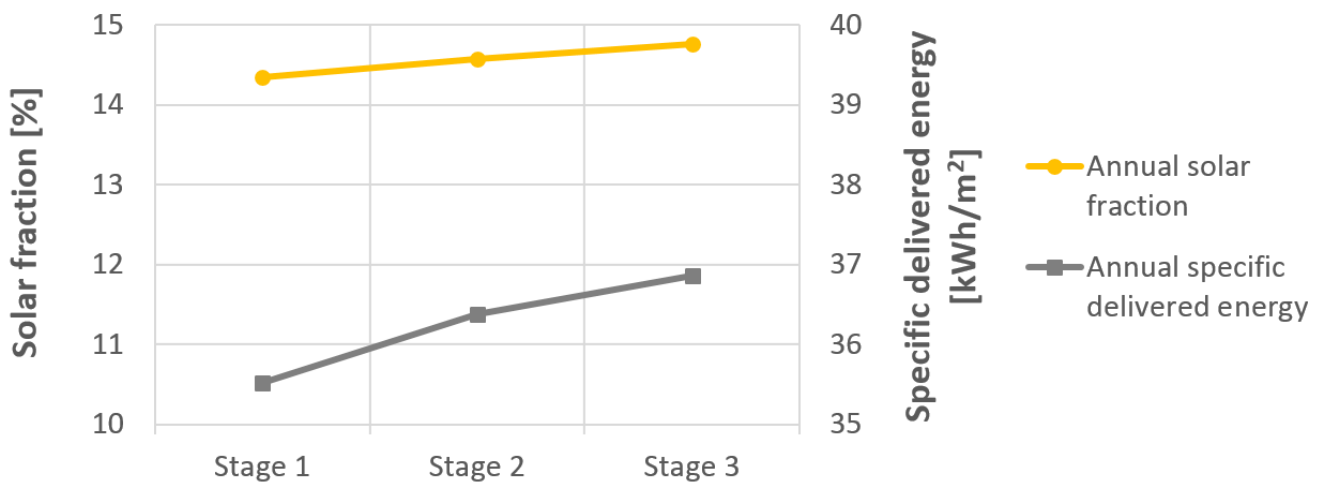


**Figure 116: Effect of volumetric flow rate (l/h) on annual system performance**

The results presented in the graph show that the annual solar fraction increases slightly with a higher volumetric flow rate. The annual specific delivered energy increases accordingly, due to the increased pump consumption.

It should also be kept in mind that very high flow rates through the collectors could result in insufficient temperature generation in the solar liquid, which may reduce the amount of solar energy transferred to the storage tank. Furthermore, if not enough heat is removed from the collectors, the temperature difference between the solar liquid in the collector and the ambient air increases, thereby reducing the efficiency of the collectors.

Since the amount of solar energy varies according to the season and the time of day, the current pump operation based on pressure curves provides a good solution for solar thermal heating systems. During winter and in the morning/evening hours, the radiation from the sun is weaker and the pump should operate slower in order to generate usable flow temperatures. As the sun gets stronger during summer and in the mid-day hours, the flow rate should be faster. This can to a certain extent be recognized in the monthly solar fraction curve displayed in Figure 117 below, which depicts the monthly solar fraction in May, June and July, for each of the three pump speed stages. As can be seen from the graphs, a higher speed slightly increases the solar fraction during summer.

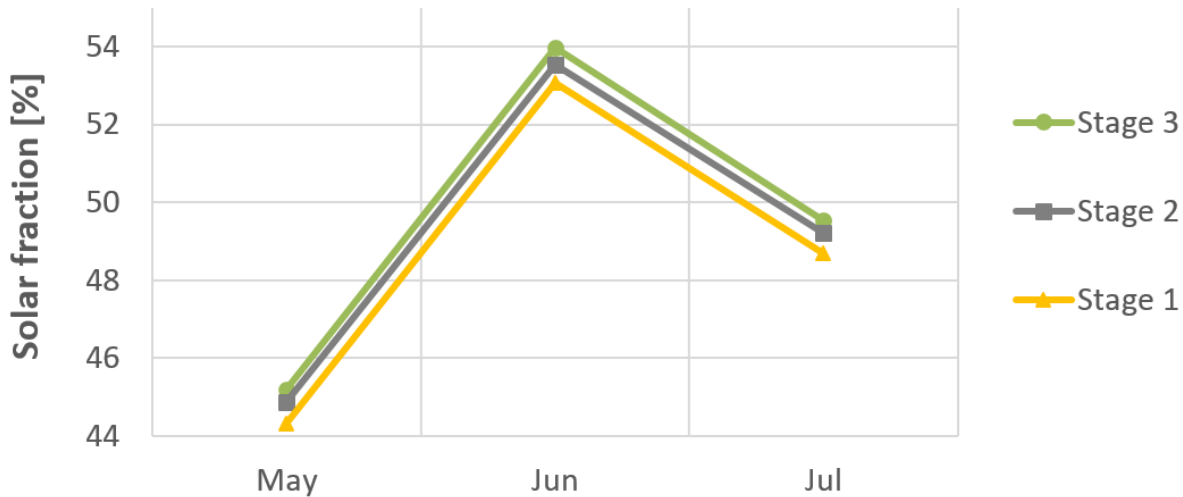


Figure 117: Monthly solar fraction in May, June and July for pump speed stage 1, 2 and 3

#### 10.3.4 Effect of propylene glycol concentration of the solar liquid

The heat transfer fluid in the solar circuit is a mixture of water and propylene glycol, called Tyfocor L. The manufacturer recommends a propylene glycol concentration of 40-75% (Tyforop, 2009). The initial concentration used in the reference system was unknown. Therefore, the system was simulated using a vol-% of 40%. In this parametric study, the influence on performance was investigated for glycol proportions ranging from 25-75%. The corresponding annual solar fraction and annual specific delivered energy can be found in *Appendix C.2.3*.

The results revealed that a change in the concentration of propylene glycol had minor impact on the two performance indicators, though an increase in vol-% appears to result in a slight increase in both the annual solar fraction and the annual specific delivered energy. Nevertheless, this effect is not as significant as that of the other parameters investigated in this study.

The minimum average outdoor temperature registered in the simulation model was  $-8,1^{\circ}\text{C}$  (Meteonorm). This is relatively high compared to many other locations in Norway. This is due to the mild, coastal climate that is found in Bergen. As stated in *Appendix B.3.3*, the freeze protection of a propylene glycol concentration of 40% is  $-20^{\circ}\text{C}$ . This indicates that the freeze protection within the solar thermal system is more than adequate.

Based on the literature review conducted in this study, the glycol concentration was expected to have a larger impact on system performance than what appears to actually be the case. As discussed in chapter 3.3.2 *Solar liquid*, an increased concentration is not very beneficial in terms of for instance thermal capacity and conductivity. It should, however, be kept in mind that other factors may affect the results, for instance the efficiency of the frequently discussed pump operation.



## 10.4 Parameters related to the user

In this subchapter, the impact of selected user-related parameters will be studied. Doing so may make it easier to reveal important design features that can contribute to the evaluation of other solar systems, located in the other passive house dwellings of the Løvåshagen housing cooperative. These solar systems are similar to that of the reference system, but may be subject to other heat demands and consumption habits.

### 12.4.1 Effect of DHW demand

According to DGS (2010), the following categorization of daily hot water consumption may be applied:

Low consumption:	20-30 l/day per person
Normal consumption:	30-50 l/day per person
High consumption:	50-70 l/day per person

In a dwelling of 75 m<sup>2</sup>, it is reasonable to assume that the number of inhabitants may vary from only one person up to a family of four, which causes significant variations in the total hot water consumption. Based on the three consumption groups above, the approximated DHW consumption (l/day) of a dwelling is roughly estimated according to the number of inhabitants in Table 38.

**Table 38: Daily DHW demand according to different consumption levels and number of persons in the household**

	<b>Low consumption</b>	<b>Normal consumption</b>	<b>High consumption</b>
	<b>[l/day]</b>	<b>[l/day]</b>	<b>[l/day]</b>
<b>1 person</b>	20-30	30-50	50-70
<b>2 persons</b>	40-60	60-100	100-140
<b>3 persons</b>	60-90	90-150	150-210
<b>4 persons</b>	80-120	120-200	200-280

In 2014, the average daily DHW consumption for the investigated dwelling was only 57,7 l/day. To investigate how the annual domestic hot water consumption affects the performance of a solar thermal system, the model was simulated for average daily consumptions ranging from as little as 30 l/day (1 person, low consumption) to 200 l/day (3 persons, high consumption). The results are presented in Figure 118.

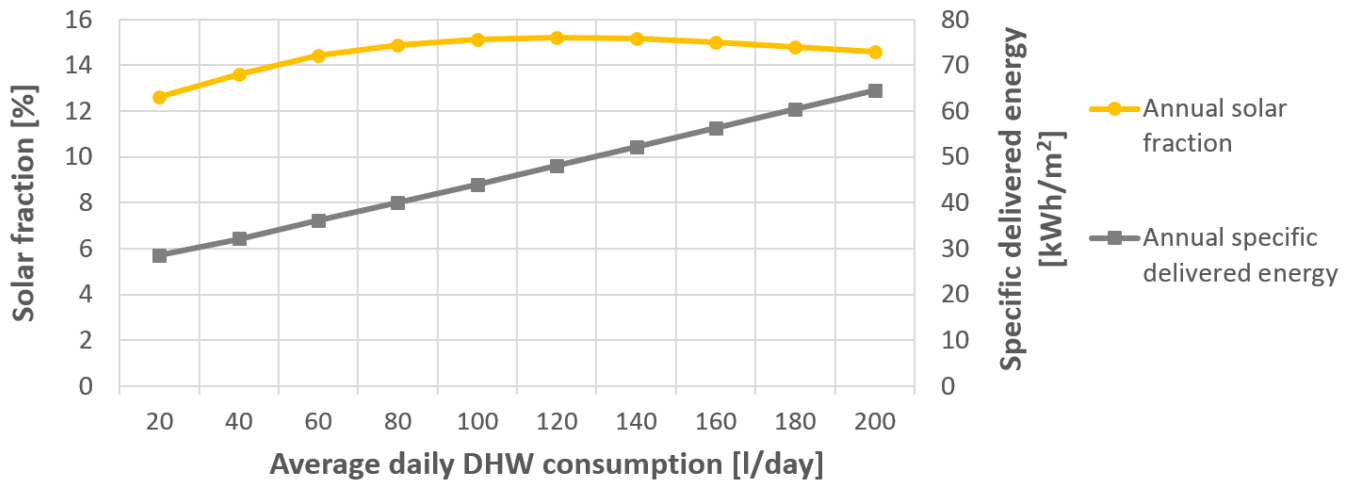


Figure 118: The effect of average daily DHW consumption on annual performance

The results in Figure 118 suggest that an identical solar thermal heating system in one of the other dwellings in Løvåshagen may achieve a higher solar fraction if the DHW consumption is higher than that of the reference system. However, this is not in itself a guarantee of higher performance; the solar fraction increases along with a higher consumption only up to an average daily consumption of approximately 120 l/day, where it reaches a maximum and starts decreasing. This is because the auxiliary energy consumption becomes more dominating, as seen in Figure 119.

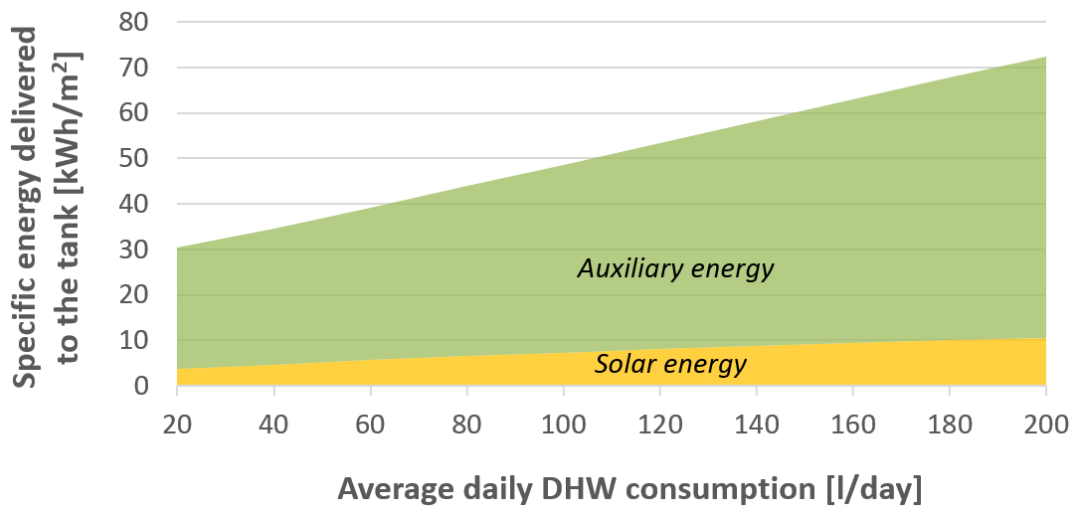


Figure 119: The distribution of solar- and auxiliary energy supplied to the tank for different average daily DHW consumptions

Though to suggest that the user consumes the same amount of DHW every day throughout the year is not realistic, the results still provide an indication of how a change in DHW consumption affects the system performance. An average daily consumption of 120 l/day corresponds to an annual consumption of 43,8 m<sup>3</sup>/year, and falls within the range of a household of three people with

normal consumption habits (based on the values in Table 38). If assuming a temperature difference between hot and cold water of 42,1°C as explained in 7. *Measurement descriptions*, this equals an annual heat demand of approximately 2150 kWh/year, or a specific heat demand of 28,6 kWh per floor area. This is very similar to the annual DHW heat demand that was estimated in the design phase of the Løvåshagen project (explained in chapter 5. *Case description*), which was 30,0 kWh/m<sup>2</sup>.

### 10.4.2 Effect of daily DHW consumption profiles

As explained in chapter 8. *Simulation inputs*, the annual DHW consumption curve was measured for every hour and imported into Polysun. To study the impact of user habits on the system’s performance, the model was simulated for different daily DHW draw-off profiles. Polysun provides several different draw-off profiles to choose from, some of which are included in Figure 120. Among these, the *multi-family dwelling* profile resembles the daily consumption of the user in the reference system the most.

The DHW load is scaled according to a chosen daily consumption, which is set to 57,7 l/day (reference system). Moreover, the amount of hot water consumed every month was specified to match the measured values. In doing so, only the hourly loads differed from that of the reference system, thus the effect of various daily profiles could be studied. The results are shown in Figure 121.

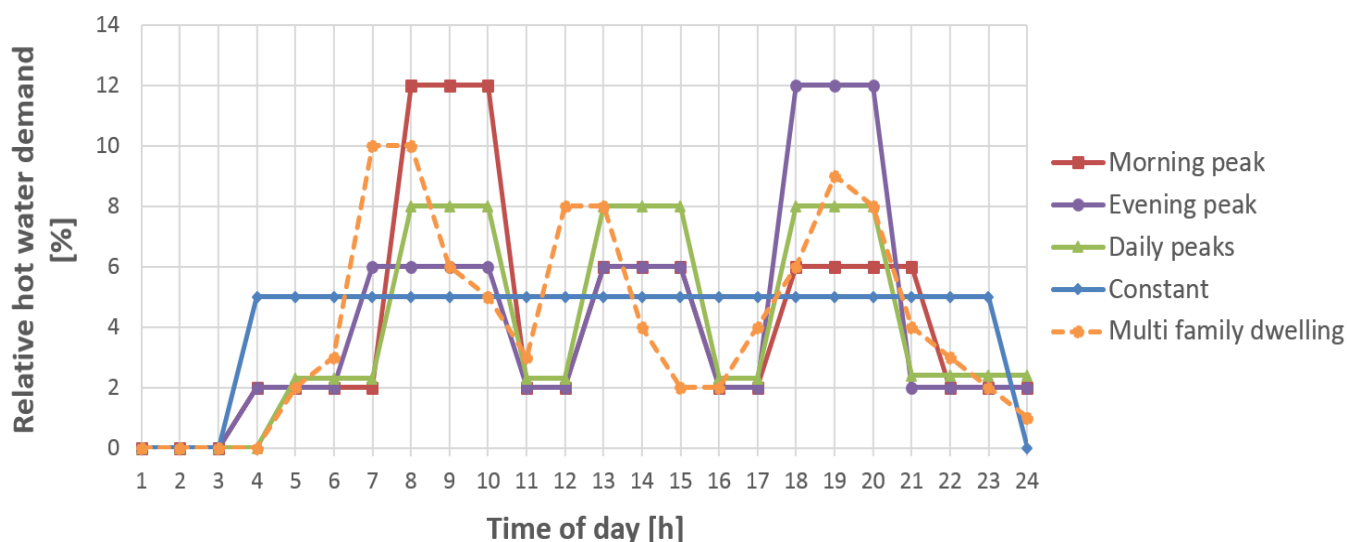


Figure 120: Selected draw-off profiles available in Polysun

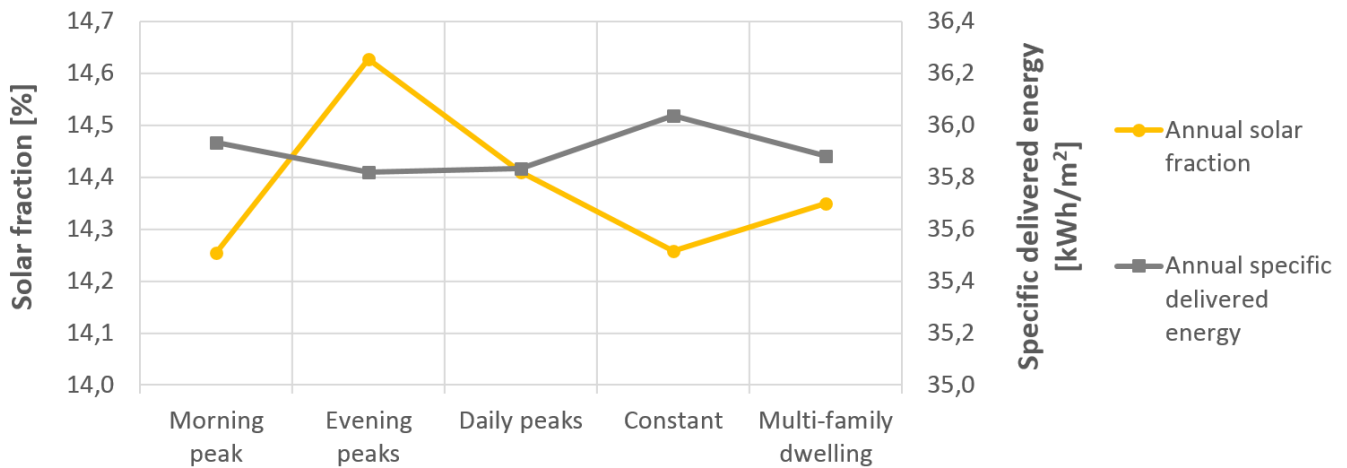


Figure 121: Effect of different draw-off profiles on annual system performance

The graph shows that *evening peaks* resulted in the highest annual solar fraction and the lowest specific delivered energy. This makes sense, as the storage tank has been charged with solar energy during the daytime, which is then ready to be used in the evening. Morning peaks and constant consumption resulted in the lowest performance.

#### 10.4.3 Effect of space heating demand

The space heating demand of the user of the reference system is much lower than the estimated demand from the project design phase. To see if an increase in the annual heating demand may affect the overall collector yield and system performance, the model was simulated for values from 600-2200 kWh/year, which equals a specific heat demand of 8–29,3 kWh/(m<sup>2</sup>·year).

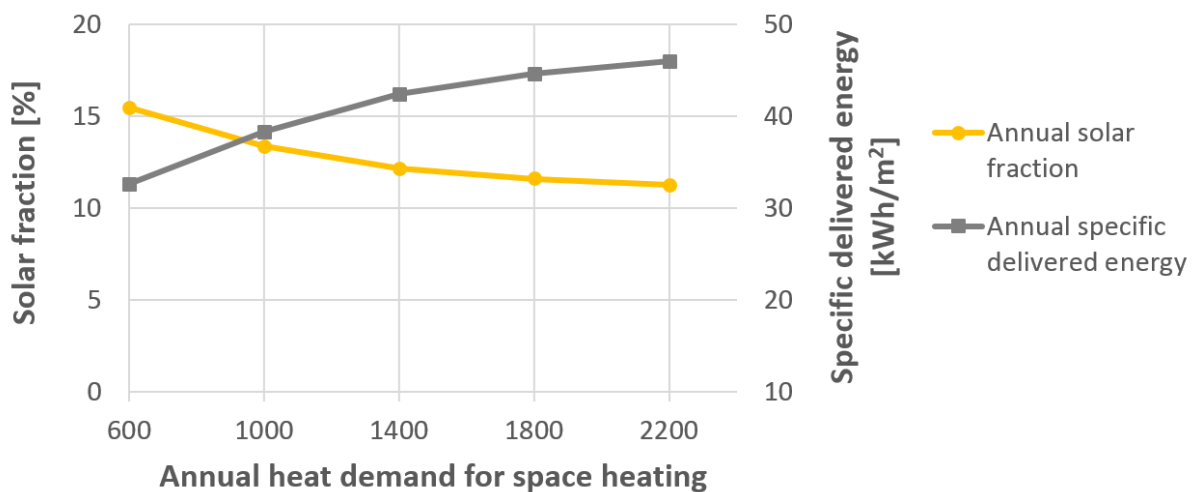
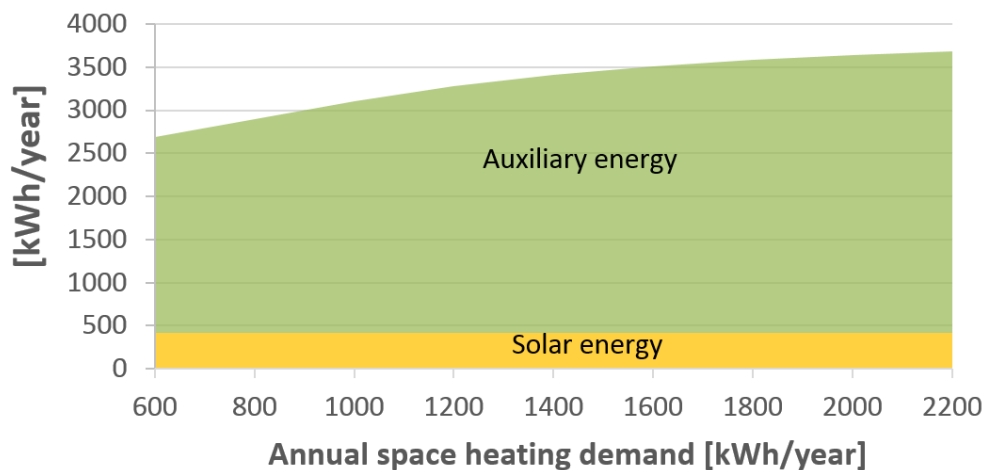


Figure 122: Effect of annual heat demand for space heating on annual system performance

Unlike in the case of higher DHW consumption, an increase in space heating demand does not lead to a higher annual solar fraction. With a greater heat demand and no change in the amount of solar energy supplied to the tank, the auxiliary energy demand increases correspondingly – which results in a lower solar fraction. The distribution of annual auxiliary- and solar energy supplied to the tank is illustrated in Figure 123 below.



**Figure 123: Distribution of auxiliary- and solar energy supplied to the tank for various annual space heating demands**

It should be noted that the poor effect on annual performance could be related to the location of the space heating coil in the tank. In the reference system, the space heating circuit gathers heat at a height of 80-86% from the tank bottom (layer 11). Furthermore, the space heating coil is located above the immersed electrical heater. Thus, when heat is removed from the tank to be used for space heating, the auxiliary heater is activated as soon as the temperature in layer 7 falls below 75°C. Unless the solar collectors manages to supply the tank with temperatures above 75°C, all space heating is covered by auxiliary energy.

## 10.5 Summary of parametric study

In this subchapter, the design- and operation parameters from the parametric study are summarized.

Figure 124 shows the *reduction* in specific delivered energy with respect to the reference model and its initial settings,  $\Delta E$ , when choosing an optimized or improved design- or operation parameter. Similarly, the corresponding *increase* in annual solar fraction,  $\Delta SF$ , is also depicted. Both values are given in %. The purpose of Figure 124 is to identify which of the parameters that have the greatest influence on system performance. Moreover, the results will be used as basis for suggesting improved solutions in the next subchapter.

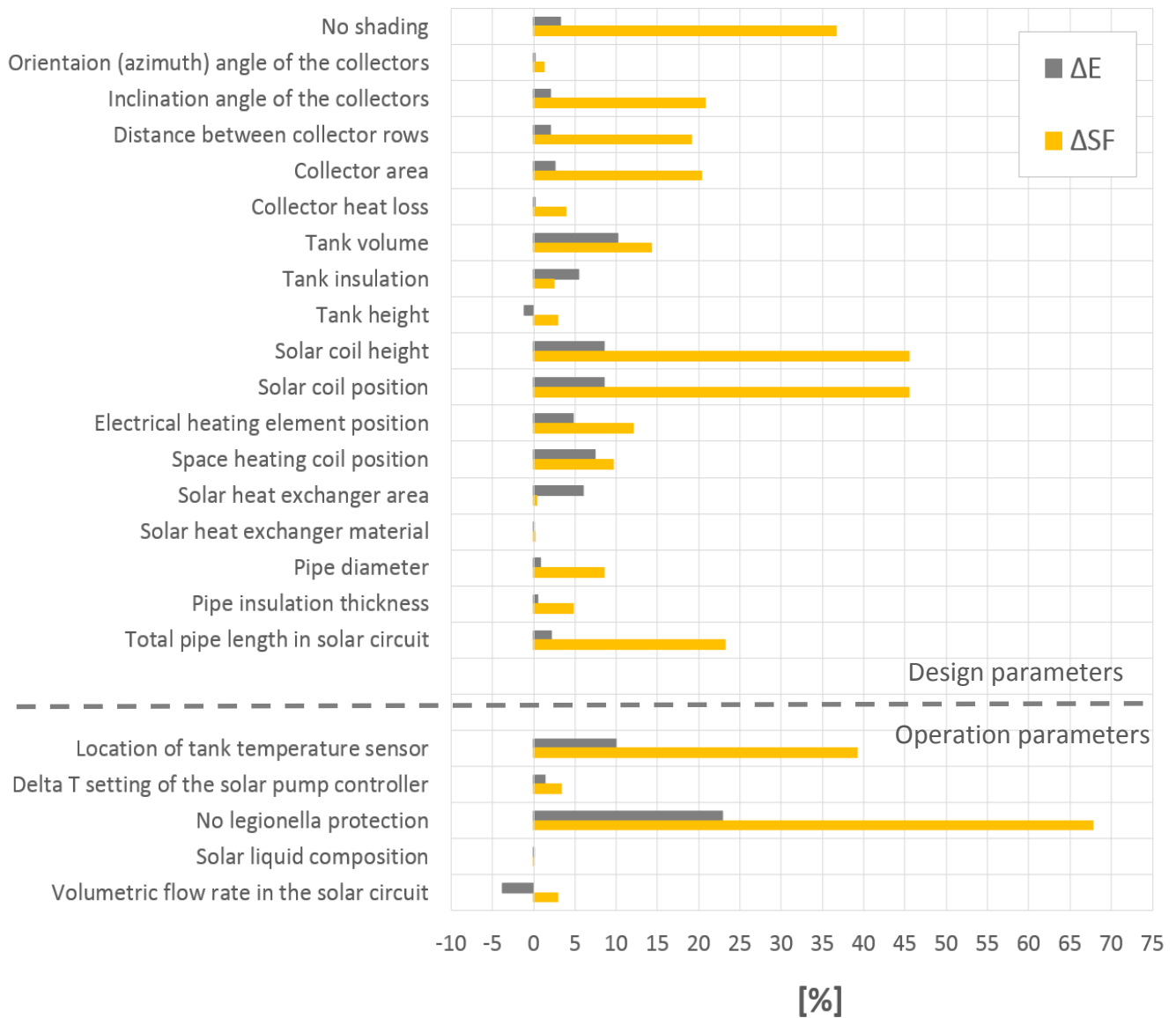


**Figure 124: Summary of the parametric study conducted on various design- and operation parameters**

In the parametric study, the optimized value could not always be obtained for every parameter. In such instances, the chosen parameter value in Figure 124 was based on discussions made in each subchapter throughout the parametric study. For instance, a continuing increase in solar collector area results in higher solar fraction and reduced delivered energy to the heating system. However, an unlimited collector size is not realistic, and the size of the building roof would obviously have its limits. Thus, a collector absorber area of 4,8 m<sup>2</sup> was chosen, as this size equals three Apricus AP-20 collectors (reference collector type), or 2 Apricus AP-30 collectors with the same properties. Similar decisions were made regarding minimum distance between the collectors rows, insulation thickness of the pipes and storage tank, pipe diameters, etc. Despite the lower performance, a collector inclination angle of 30° was chosen over 20°, with the intention of minimizing the risk of dirt or snow settling on top of the evacuated tubes.

As for the design parameter, it is clear from Figure 124 that the amount of solar irradiation that hits the collectors (represented in the diagram by shading, collector orientation angle, collector inclination angle, row distance and collector area) strongly affects the annual solar fraction. Other important design features relate to the tank configuration (such as the tank volume and the positions of tank elements), or to the solar circuit (pipe length). Among the operation parameters, the switch-off temperature of the immersed electrical heating element and the location of the tank temperature sensor are by far the most influential.

It should be noted that some of the parameters investigated in this study had a similar effect on system performance. For instance, the moving of the solar coil closer to the tank bottom had an equally positive effect on the annual solar fraction, as the extension of the solar coil height towards the bottom (but with fixed position of the upper coil connection). However, in both cases, the increased performance is strongly related to the control of the solar pump, which is switched on and off based on temperature readings from sensors located at the very bottom of the tank and at the collector outlet. One of the main issues discussed in this study is that the bottom tank temperature is consistently low due to the input of cold network water in this area. This results in problems with the pump operation, since the switch-off temperature difference is seldom reached. The simulations showed that each implementation of the two cases mentioned (solar coil position and solar coil height) resulted in an increased temperature of the water that surrounds this temperature sensor, which subsequently improved the function of the solar pump controller. Notably, a similar effect could also be achieved by moving the temperature sensor further up in the tank. Thus, it is important to be aware of the fact that though a change in parameters may make a significant impact individually, a combination of these may not necessarily lead to the same increase in the overall system performance.

As seen in the diagram, a change in a parameter may also lead to contradicting results. Where a change leads to an increase in one performance indicator, it may have a negative impact on another. This is the case when increasing either the tank height or the volumetric flow rate in the solar circuit: the solar fraction increases ( $\Delta SF = \text{positive}$ ), but at the same time the total specific delivered energy to the heating system increases ( $\Delta E = \text{negative}$ ). It should also be kept in mind that when altering a parameter, the amount of energy that is saved and the increase in solar contribution must be considered in context with costs. For instance, the increasing of the solar collector area will also result in higher investment costs. Furthermore, many of the investigated parameters in this study are both difficult and expensive to alter once the system is installed.

## 10.6 Suggested improved scenarios

In this subchapter, several suggested improved scenarios described in Table 39 will be evaluated. In Scenario 1 to Scenario 5, the main components of the investigated system are improved and, if

possible, optimized. Scenario 6 and 7 targets shading and tank location, respectively, thereby hoping to get an indication of how the other solar thermal systems might be performing compared to the examined system. Scenario 8 to 19 consists of different combinations of Scenario 1-7. In this way, it is possible to investigate the effect of improving only a few or several components in the solar thermal system.

Since an external plate heat exchanger has replaced the internal solar coil in the modified system, an improved scenario of the solar coil is included in Scenario 3, even though the parametric study revealed no significant impact on system performance. This is to examine whether or not the effect of other coil properties changes when other parameters are improved simultaneously.

In order to include both reduced heat loss from the collectors and larger collector absorber area in Scenario 1, the two Apricus AP-20 collectors were replaced with another evacuated tube collector with heat pipe, called Thermomax HP400 20. This collector type has approximately the same width and height as the two reference collectors. The properties of this collector were elaborated in chapter 10.2.1.5 *Collector heat loss* in the parametric study.

As previously discussed, some parameters had the same effect on system performance. It was decided only to alter the height of the solar coil in Scenario 2, and to leave the position of the upper solar coil connection unchanged, at 33%. The argument for this is that when several parameters are improved simultaneously, more solar energy will be supplied to the tank, thus a lowering of the solar coil position would minimize the solar storage volume. For the same reason, it was decided not to reduce the tank volume in this scenario to match the low heat demand of the user.

The temperature sensor that controls the auxiliary energy supply to the tank is located on the same level as the immersed electrical heater, which is within thermal layer 7 in the reference system. Whenever the controller (Scenario 5) was altered together with the storage tank (Scenario 2), this temperature sensor was moved according to the location of the electrical heater, which is in layer 8.

**Table 39: Suggested improved scenarios**

	<b>Components</b>	<b>Parameters</b>
<b>Scenario 1</b>	Solar collectors	Inclination angle of all collectors: 30° Orientation angle of all collectors: South (0°) Row distance between collectors: 3 m Increased area and reduced collector losses by replacing collectors with: 2 x Thermomax HP400 20
<b>Scenario 2</b>	Storage tank	Tank insulation thickness: 80 mm Position of auxiliary heater: 65% (layer 8) Position of space heating coil: 80% Solar coil height: 400 mm



<b>Scenario 3</b>	Solar heat exchanger (coil)	Solar coil material: Copper Solar coil surface area: 1,6 m <sup>2</sup>
<b>Scenario 4</b>	Solar circuit pipelines	External pipe diameter: 14 mm Insulation of solar circuit pipelines: 22 mm Improved collector layout on roof
<b>Scenario 5</b>	Controller	<u>Solar pump controller:</u> Temperature sensor at Layer 2 $\Delta T$ switch-ON/switch-OFF : 7K/3K <u>Auxiliary heater controller:</u> Temperature sensor located at same level as el. heating element Switch-on temperature: 70°C Switch-off temperature: 72°C
<b>Scenario 6</b>	Shading	No shading from surrounding topography No mutual shading (row-to-row shading)
<b>Scenario 7</b>	Tank location	2 <sup>nd</sup> floor (top floor)
<b>Scenario 8</b>	Solar collectors and storage tank	Scenario 1 + 2
<b>Scenario 9</b>	Solar collectors and controller	Scenario 1 + 5
<b>Scenario 10</b>	Solar collectors, storage tank and controller	Scenario 1 + 2 + 5
<b>Scenario 11</b>	Storage tank and solar circuit pipelines	Scenario 2 + 4
<b>Scenario 12</b>	Storage tank and controller	Scenario 2 + 5
<b>Scenario 13</b>	Storage tank, solar circuit pipelines and controller	Scenario 2 + 4 + 5
<b>Scenario 14</b>	Solar collectors, storage tank, solar circuit pipelines and controller	Scenario 1 + 2 + 4 + 5
<b>Scenario 15</b>	Solar collectors, storage tank, solar circuit pipelines, controller and shading	Scenario 1 + 2 + 4 + 5 + 6
<b>Scenario 16</b>	Solar collectors, storage tank, solar circuit pipelines, controller and tank location	Scenario 1 + 2 + 4 + 5 + 7
<b>Scenario 17</b>	Solar collectors, storage tank, solar circuit pipelines, controller, shading and tank location	Scenario 1 + 2 + 4 + 5 + 6 + 7
<b>Scenario 18</b>	Solar collectors, storage tank, solar circuit pipelines, controller, shading, tank location and solar heat exchanger	Scenario 1 + 2 + 3 + 4 + 5 + 6 + 7
<b>Scenario 19</b>	Limited modifications, storage tank	Scenario 0 + 2

As previously mentioned, a system can be both expensive and difficult to alter once it is installed and up and running. This is the case in this master thesis. To investigate how well the current system could potentially perform without taking drastic measures, a final scenario, Scenario 0, was created. In this scenario, parameters that are assumed to be less radical and relatively easy to change are included. This scenario is presented in Table 40 below.

**Table 40: Scenario 0: Limited modifications**

<b>Collector orientation</b>	Inclination angle of <i>all</i> collectors: 30°
<b>Solar loop controller input</b>	Temperature sensor at Layer 2 ΔT switch-ON/switch-OFF : 6K/4K
<b>Auxiliary heating controller</b>	Temperature sensor located at same level as el. heating element Switch-on temperature: 70°C Switch-off temperature: 72°C
<b>Pipelines</b>	Improved insulation of outdoor pipes: 22 mm

All the scenarios in Table 39 and Table 40 were simulated, and the resulting annual solar fraction and annual specific delivered energy for each scenario is presented in Figure 125. The initial value of the reference system is included for both performance indicators with a dotted line.

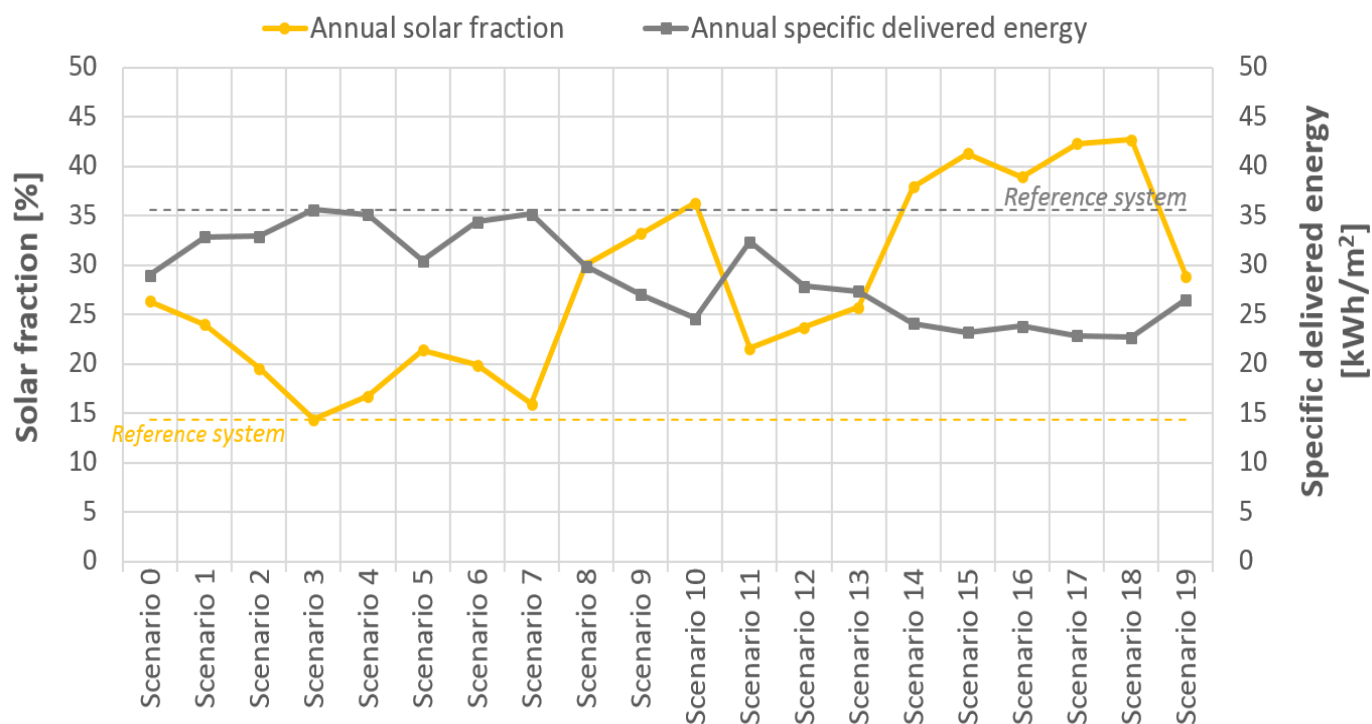


**Figure 125: Annual solar fraction and specific delivered energy for improved scenarios**

The simulations showed that an improvement of the solar collectors (Scenario 1) resulted in an increased annual solar fraction by as much as 67,8% compared to the reference system, and correspondingly a reduction in annual specific delivered energy by 7,7%. An alteration of the tank design (Scenario 2) had a similar reduction in annual specific delivered energy (reduction by 7,6%), whereas the annual solar fraction increased by 36,8%. It should be noted that this was without optimizing the tank size so that it would be more suitable for the low heat demand for the user in the reference system, as explained in chapter 10.2.2.2 *Effect of tank volume*. On its own, an improvement of the controller (Scenario 5) had a very satisfying effect, with an increase in annual solar fraction by 49,7% and a reduction in annual specific delivered energy by 14,6%. Scenario 6 and 7 each resulted in an increase in annual solar fraction by 16,9% and 11,3%, respectively. The same scenarios had a smaller impact on annual specific delivered energy than the scenarios mentioned above, with corresponding reduction values of only 1,3%, and 1,2%. A complete elimination of shading of the collectors in Scenario 6 led to a 39,2% higher solar fraction, but only a decrease in delivered energy by 3,4%.

The best performance that was achieved without the complete elimination of shading was in Scenario 16, in which an annual solar fraction of 38,9% and a specific delivered energy of 23,8 kWh/(m<sup>2</sup>·year) were obtained. This equals an increase and decrease by 172% and 33,1%, respectively, compared to the reference system.

After improving several components in Scenario 15, the addition of Scenario 7, i.e. tank location, in Scenario 17 resulted in an increase in solar fraction from 41,3% to 42,3%, and a corresponding reduction in annual specific delivered energy from 23,2 kWh/m<sup>2</sup> to 22,9 kWh/m<sup>2</sup>. This shows that, with a well-functioning solar thermal heating system, the significance of having the storage tank located on ground floor instead of on second (top) floor is detectable on the system performance, but not crucial.

The highest annual solar fraction and the lowest specific delivered energy were obtained with Scenario 18, closely followed by Scenario 17. The difference between the two is the properties of the solar coil. The effect of improvement of the solar coil had little effect by its own in Scenario 3, in which the solar fraction increased by only 0,6%. The specific delivered energy remained the same as for the reference system. When the solar coil alterations were introduced after having implemented all the other modifications, the two performance indicators both increased and decreased by 0,01% and 0,01 %, respectively from Scenario 17 to Scenario 18 (with and without Scenario 3). Thus, the impact of the solar coil is yet again confirmed to be not very crucial in terms of reducing the performance of the investigated system. In Scenario 18, the parameters shading, location of storage tank, collectors, storage tank, solar heat exchanger, solar circuit pipelines, and the controller, were improved. The annual solar fraction of this scenario is 42,7%, which is almost three times the annual solar fraction of the reference system. Notably, this is rather

close to the intended solar fraction of 47%. The corresponding annual specific delivered energy is 22,7 kWh/m<sup>2</sup>, which constitutes a reduction of 36,3%.

In Scenario 0, where only a few selected parameters which were considered relatively easy to change were altered, the solar fraction and specific delivered energy obtained was 26,3% and 29,0 kWh/m<sup>2</sup>, respectively. To study the effect of further changing the storage tank design, Scenario 0 was combined with Scenario 2 in Scenario 19. This resulted in an annual solar fraction of 28,9% and a specific delivered energy of 26,5 kWh/(m<sup>2</sup>·year).

## 10.7 Sensitivity analysis of the best scenario

Since all the scenarios presented in this chapter are suggested solutions for improving system performance, and not necessarily the optimized solutions, a sensitivity analysis was conducted on Scenario 18. This makes it possible to study the potential influence of making further changes in parameter values. Selected parameters from the scenario were further modified by  $\pm 10\%$ . Additionally, two user-related parameters (DHW demand and space heating demand), as well as tank volume, were included in the sensitivity analysis, to see if the impact of these had changed now that the system was functioning better.

The two diagrams in Figure 126 show the variations in both annual solar fraction and annual specific delivered energy.

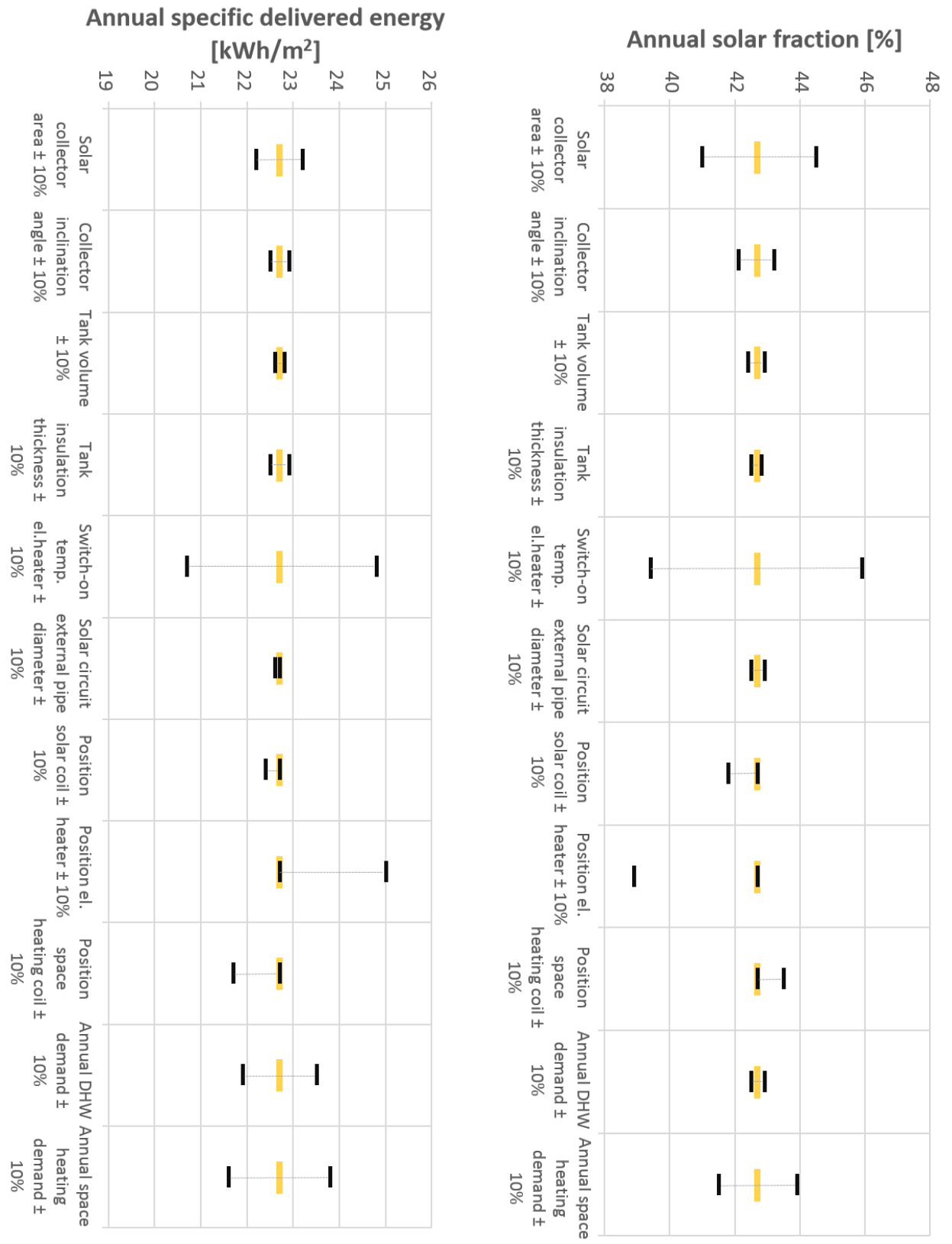


Figure 126: Sensitivity analysis of Scenario 18, annual solar fraction (right) and annual specific delivered energy (left)

The total collector absorber area in Scenario 18 is 4,3 m<sup>2</sup>. A 10% increase in collector area would have resulted in an annual solar fraction and a specific delivered energy of 44,5% and 22,2 kWh/(m<sup>2</sup>·year), respectively. If the switch-on temperature of the electrical heater was lowered slightly further, the annual solar fraction would have been 45,9%, which is 7,5% higher than the initial solar fraction in Scenario 18, and 221,0% higher than the reference system. As previously discussed, the reference system has a simulated solar fraction of 14,3% and an annual specific delivered energy of 35,6 kWh/m<sup>2</sup>. The results in the sensitivity analysis indicate that with a further increase in for instance the collector area or a further lowering of the switch-on temperature of the auxiliary heater, the initial goal of an annual solar fraction 47% could be within reach.

Moreover, it is evident from the sensitivity analysis that some parameters affect the system performance differently than in the simulations made earlier in the parametric study. For instance, a 10% increase in tank volume in Scenario 18 increases the annual solar fraction slightly, whereas the same change in tank volume in the reference system in chapter 10.2.2.2 *Effect of Tank volume* ended up reducing the performance. This positive effect suggests that the current tank size of 290 liters is more suitable if the system is functioning better. One reason for this could be the reduced temperature setting of the auxiliary heater, and thus the reduced tank temperature. As discussed in the parametric study in 10.3.2 *Control of auxiliary heater*, a lower tank temperature results in a higher required tank volume. Another explanation could be related to the fact that the solar energy supply to the tank has increased considerably with a better functioning of the system. As a result, the tank must be large enough to be able to store this energy.

As for the two user-related parameters, the change in DHW resulted in slightly surprising results. In the parametric study, an increase in annual DHW consumption had a positive impact on annual solar fraction, whereas the specific delivered energy increased. In the sensitivity analysis in Figure 126, on the other hand, a higher heat demand resulted in reduced annual solar fraction, which is the opposite effect. This may be related to the discussion in the previous paragraph regarding sufficient tank size; if the system has reached a point of “saturation”, a higher heat demand will only reduce the performance unless other measures are taken, like installing a larger tank.

## 10.8 System performance with improved design and operation

In this chapter, a brief comparison of the solar fraction, the delivered energy and the fractional energy savings between the reference system and Scenario 18 will be presented. Scenario 18 is the scenario that achieved the highest annual performance in chapter 10.6 *Suggested improved scenarios*.

Figure 127 below depicts the simulated monthly solar fraction for a system configuration equal to Scenario 18. The monthly amount of solar energy and auxiliary energy supplied to the storage tank are displayed to the left in the diagram in kWh. For comparison, the annual solar fraction curve of the reference system is included in the graph with a dotted line.

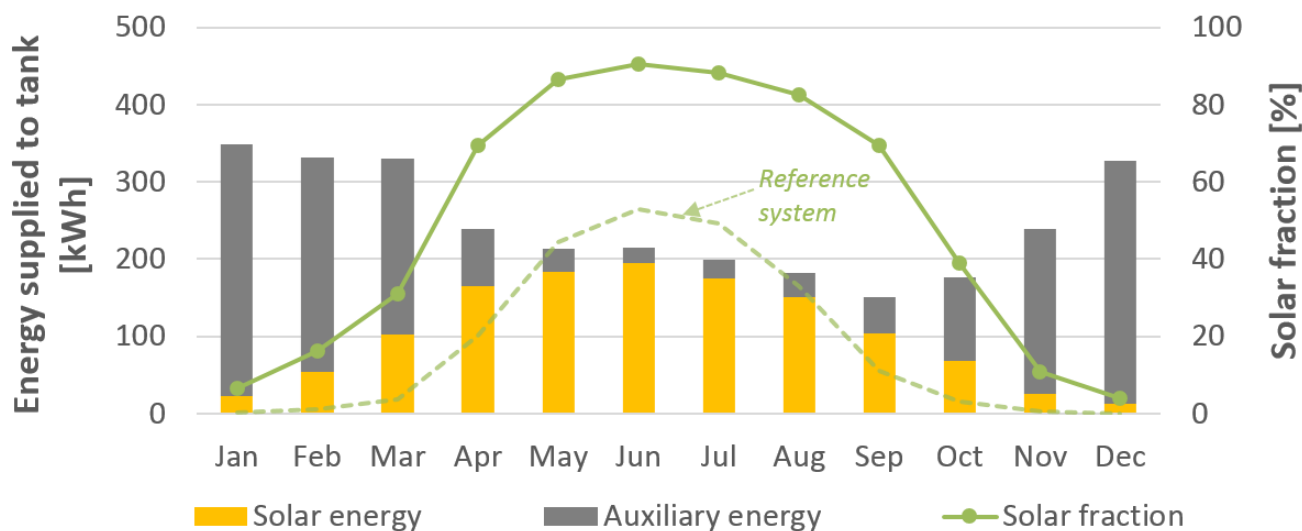


**Figure 127: Monthly share of solar- and auxiliary energy with the corresponding solar fraction (Scenario 18)**

As is illustrated by the Figure 127, the solar contribution in Scenario 18 is significantly higher throughout the whole year compared to that of the reference system, with its initial settings. The positive increase in solar fraction during the transitional periods is especially beneficial in terms of utilizing solar energy for space heating. In the case of Scenario 18, the system is able to achieve a solar fraction of 90,6% and 88,2 % for June and July, respectively. This equals a corresponding increase from the simulated reference system by 71,3% and 79,3%.

Figure 128 depicts the monthly specific delivered energy for Scenario 18 with respect to the reference system. The solar thermal heating system in Scenario 18 requires significantly less delivered energy compared to the reference system. On an annual basis, the specific delivered energy is 36,2% lower than the initial 35,6 kWh/m<sup>2</sup> of the reference system.

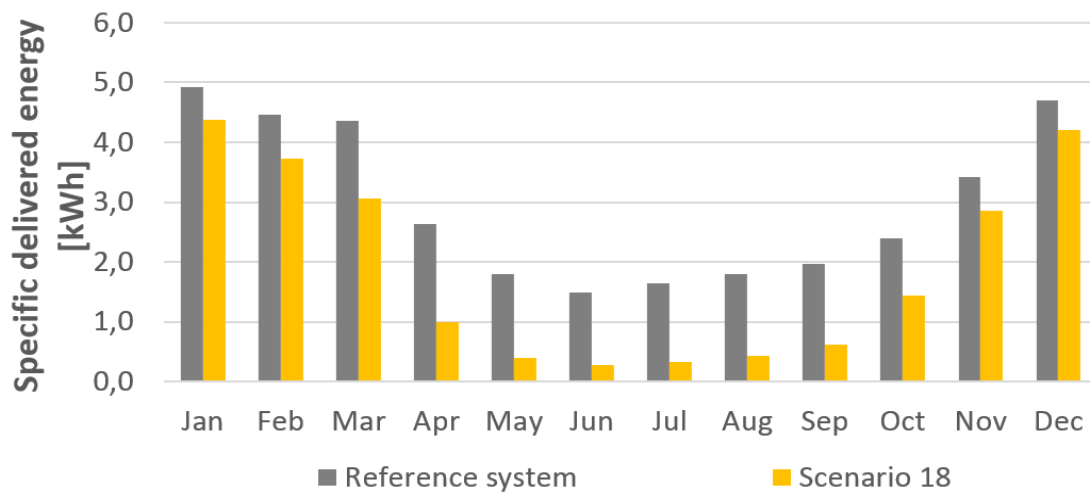


Figure 128: Specific delivered energy, Reference system vs. Scenario 18

The fractional energy savings indicator also can be used to compare two solar thermal heating systems. The corresponding monthly fractional energy savings when choosing Scenario 18 over the reference system are shown in Table 41.

Table 41: Fractional energy savings compared to reference system

	Fractional energy savings [%]											
	Jan	Feb	Mar	Apr	May	Jun	Jul	Aug	Sep	Oct	Nov	Dec
<b>Scenario 18</b>	11,1	16,4	30,0	62,4	77,9	81,2	80,4	76,1	68,8	39,7	16,3	10,5

As seen in Table 41, the energy savings are more than 60% every month from April to September. On an annual basis, the average fractional energy savings compared to the reference system are 36,2%. Table 42 summarizes the annual values presented in this chapter. Additionally, the number of stagnation is included. With this system design and operation, Scenario 18 has 29 days stagnation days each year, mainly during the hottest summer months. The reference system, on the other hand, had zero stagnation days.

Table 42: Summary annual values, Scenario 18

<b>Solar energy supplied to the tank</b>	1261,1	kWh/year
<b>Auxiliary energy supplied to the tank</b>	1693,0	kWh/year
<b>Annual solar fraction</b>	42,7	%
<b>Delivered energy to heating system</b>	1704,0	kWh/year
<b>Specific delivered energy to heating system</b>	22,7	kWh/(m <sup>2</sup> ·year)
<b>Fractional energy savings compared to reference system</b>	36,2	%
<b>Number of stagnation days throughout the year</b>	29	days



## 11 Discussion

---

In this chapter, some of the findings of this thesis is discussed and compared, including comments regarding relevant previous experiences from this case study, presented in chapter 5. *Case description*. A discussion of the investigated system is provided, and the results are also considered on a more holistic approach, by the providing of comments relevant to the solar systems in Løvåshagen as a whole.

It is important to keep in mind that a solar thermal heating system is very complex, and that the results simulated in Polysun may differ considerably from the real, full-size system. For the same reason, it is possible to imagine that the parametric study could have reveal different results than the ones presented in this thesis, had the system design and operation of the reference system been only slightly different. This was for instance indicated in the sensitivity analysis made of the best scenario (Scenario 18) in chapter 10.7, in which some of the parameters that had positive effects on system performance in the parametric study, suddenly showed either a negative or no noticeable influence after the system was improved. Moreover, some of the parameters, such as the location of the tank temperature sensor, had significant impact on the results, and might have influenced the impact of several of the other investigated parameters.

### 11.1 Original system

#### ***Heating system with solar input vs. conventional heating system***

According to Siren M. Dahl, the chairman of Løvåshagen housing cooperative, the user of the investigated system pays approximately 170 NOK each month for maintenance of the solar thermal collectors. On an annual basis, this equals 2040 NOK. Considering that the measured solar production in 2014 was only 377 kWh, the financial profitability of the investigated system is rendered questionable. Nevertheless, several faults and errors revealed in this report related to both the design and the operation of the system, suggest that the general use of solar thermal heating in passive house dwellings should not be rejected based on the performance of this particular system.

#### ***Delivered energy to the heating system***

Previous findings and experiences relevant for this this case study implied that the total delivered energy to the passive house dwellings in Løvåshagen generally appears to be slightly too high, and that having solar collectors on the roof is not reflected specifically in the measured energy consumptions. The fractional energy savings that were calculated in chapter 9. *Results* confirmed the latter: with the current design and operation, the energy saved by having a solar thermal system in the investigated dwelling was a modest 3,8 %. In fact, the results revealed that from September to March, the use of the examined system actually leads to a greater energy consumption than

would have been consumed with the use of the immersed electrical heating element as the only energy source.

As for the generally high energy consumption in the passive house dwellings, the following observations can be made based on the findings in chapter 9 and 10:

- Both the measured and the simulated results reveal that there is significant disagreement between the actual heat demand of the user and the amount of energy that is supplied to the storage tank
- The parametric study revealed that the switch-on temperature setting of the immersed electrical heating element not only considerably reduced the utilization of solar energy; it also significantly increased the amount of delivered energy to the heating system
- The incorrect control of the circulation pump in the solar circuit results in a very high pump consumption, and causes a significant amount of heat loss from the storage tank - which increases the need for auxiliary energy
- An important factor to consider is the heat demand of the users of each passive house dwelling. The results in chapter 10.4 *Parameters related to the user* revealed that an increase in annual DHW consumption and/or space heating had a very negative impact on the energy consumed by the auxiliary heater

Based on the measurements provided by BKK via Magnar Berge (see Table 11 in chapter 5.4), the total specific delivered energy to the investigated dwelling can be estimated to an average of 5570 kWh/year, or 74,2 kWh/(m<sup>2</sup>·year). Moreover, the measured energy consumed by the auxiliary heater in 2014 was measured to 3098 kWh/year (41,3 kWh/ (m<sup>2</sup>·year)). This means that over 50% of the total average delivered energy is used by the immersed electrical heating element to heat the storage tank. With additional energy required for the circulation pumps - especially for the solar pump, which appears to operate continuously during summer -, this share can be assumed to be even larger. This result is not completely surprising, as the heat demand for DHW and space heating in residential buildings of passive house standard constitutes a significantly larger share than that of existing buildings. It should, however, be kept in mind that the results might differ for dwellings with other heat demands.

### ***Planning, assembly and operation***

As mentioned in the introduction of chapter 4, faults are typically made in the planning process, during assembly, or during the operation of the system. In this case study it appears as though the system performance is subject to faults made in all three phases.

It is important to keep in mind that this system was planned long before its completion in 2008. The simulation tools for planning and dimensioning solar thermal heating systems have significantly improved since the commencement of the Løvåshagen project. The newest versions of the simulation tools available on the market allows the user to account for important design

issues, such as heat loss, distinction between indoor and outdoor room, shading, etc. Shading is a particularly important feature, and is highly relevant for this case study, as the performance of the reference system has most likely suffered from the lack of adequate simulation tools that would be able to consider shading from nearby collectors.

Regarding assembly, it was mentioned in chapter 5. *Case description* that a visual check of the system revealed pipes and connections with lacking insulation, as well as inadequate fastening of the collector temperature sensor. In the publication *Suksessfaktorer for økt bruk av solvarme* by SINTEF in 2014 (Fredriken et al., 2014), interviews of private solar thermal system owners in Norway revealed a general lack of necessary solar thermal skills among plumbers, and that errors are often made as a consequence of this. This may also be a contributing factor for the investigated system.

The findings in this case study is not only a reminder of how important it is to consider every thinkable aspect already at the design stage, it also illustrates the importance of correct control and monitoring once the system is installed. The latter is essential for the maximization of utilization of solar energy, and to realize the full potential of the system. Along with important design features such as the collector inclination angle, the location of the temperature sensor that measures the cold tank water appears to be one of the key issues for reduced performance during the high-radiation months. It is very unfortunate that a system like the one in this case study has operated for so many years without the detection and correction of even the simple faults, such as incorrect controller settings. In SINTEF's report (mentioned above), it is stated that in order for a solar thermal system to function properly, it is crucial that the users themselves control the system and that they possess adequate knowledge of it (Fredriken et al., 2014). This is without doubt a statement that applies for this case study. If each solar thermal system was more easily monitored by the user, faults might have been discovered sooner. Moreover, this would perhaps encourage the users to get more involved with the function of their own system, and thereby to contribute to an increased utilization of solar energy.

### ***Broken evacuated tubes***

In chapter 5.3 *Relevant experiences and findings*, it was mentioned that some of the evacuated tubes were broken. When a tube breaks, the collector can still operate normally, though with reduced collector yield (Apricus Solar, 2013). Since the results in this chapter showed that the collector area has a considerable impact on system performance, broken tubes may be one reason for why the measured performance is even lower than the corresponding simulated performance presented in chapter 9. *Results*.

### ***Inclination angle and shading***

The solar collectors in this case study were most likely tilted at an inclination angle of 51° with the intention of maximizing the solar energy utilization for space heating during the transitional

periods. However, due to shading from nearby collectors, the effect turns out to have been the very opposite: the parametric study revealed that a steeper inclination angle leads to a higher row-to-row shading (mutual shading), and that this effect is especially dominant in the periods Spring-Summer and Summer-Autumn, i.e. when the solar altitude angles are lower.

The best solar fraction that was obtained without the complete elimination of shading in chapter *10.6 Suggested improved scenarios* was 38,9% (Scenario 16). To minimize shading when installing solar collectors in several rows behind one another, it is important to ensure a sufficiently large distance between the collector rows, as well as a sufficiently low collector tilt. Since some of the shading appears to be inevitable in this case study, and because roof space is limited, it would be beneficial to use collectors that have less thermal losses and a larger absorber area than the collector type that is currently installed.

### ***Protection against overheating***

The simulated results revealed that the cooling radiators have so far been redundant. However, if the solar radiation onto the collectors should increase after making improvements, protection against high temperatures in the solar circuit and in the storage tank is crucial. Although the improved scenarios revealed significant increases in system performance, the number of stagnation days increased accordingly. During summer, when the solar collectors supply more hot water than what is being consumed, excess heat is generated, and the temperatures in the solar circuit rises. To avoid damage to the system, it is important with adequate protection against overheating. Excess heat can also be reduced by installing a larger storage tank.

It should also be noted that even though the temperature sensor at the collector outlet was not examined in this study, a false positioning of this sensor may lead to incorrect temperature readings. Equally important is the presence of adequate insulation and proper fastening of this temperature sensor. At worst, the performance of the solar thermal system may be significantly reduced. As mentioned above, this sensor was improperly attached and that its connection to the collector were lacking insulation. This may be a contributing factor as to why the measured performance was worse than the one that was simulated.

## 11.2 Modified system

### ***Effect of modification***

When evaluating the performance of the modified system, it is important to consider the fact that additional improvements other than the introduction of a plate heat exchanger were conducted on the system. First of all, the insulation of the solar circuit pipelines were sealed where insulation was lacking. Secondly, the temperature sensor at the collector outlet was fastened, and the connections were insulated. As for the controller settings, the temperature sensor remained in layer

one like in the original system configuration, but the switch-on temperature of the immersed electrical heating element was changed from 75°C to 65°C.

The parametric study revealed no noticeable impact, neither when altering the thermal properties of the solar coil, nor when increasing its surface area. Therefore, a replacement in the modified system of the solar coil with an external plate heat exchanger will not necessarily lead to higher performance in itself. It may very well be the lower switch-on temperature of the auxiliary heater, along with the improved insulation of pipes and connections, that caused the increase in solar fraction. Finally, the increased heat demand in 2015 compared to 2014 might also have played a role.

### ***Thermal stratification***

The detailed simulations of the reference system showed that the thermal stratification is not always maintained within the tank, as the water in the lower layers may reach temperatures above 90°C. This is not uncommon when using evacuated tube collectors. Zijdemans (2012) recommends directing solar heat into the tank at two different temperature zones in order to improve the thermal stratification. This also increases the response time, and improves the utilization of solar energy. In the modified system configuration, this specific alteration has been made: water is heated in the external plate heat exchanger, before it is led into either the bottom or the upper part of the tank, depending on the water temperature. This seems like a good solution for avoiding uniform temperature mixing of the tank water, and for preventing the immersed electrical heating element from supplying more energy than what is necessary. However, since shading is a big issue in this study, being especially influential in the periods with low to moderate solar radiation, the positive impact of making this modification is not yet evident in the measured results (this thesis ended in the beginning of June 2015). Thus, it still remains to determine from the measured results from June, July and August if the introduction of solar energy at two different temperature zones does in fact further enhance the utilization of solar energy. Moreover, the full potential of the modified system will not be revealed unless some further alterations are made on the existing system, such as moving the tank temperature sensor and lowering the inclination angle of the collectors.

It should also be noted that a plate heat exchanger is quite expensive, and that this kind of heat exchanger is normally used for larger solar thermal systems. Furthermore, this solution requires an additional circulation pump, which increases the total energy consumption. Thus, a better solution for the Løvåshagen system would probably be to replace the tank with a better configuration than the current system.

## 11.3 General comments

### ***Variation in total heat demand***

The measured results revealed that the heat consumption of the user of the examined system is much lower than what was implied in the initial calculations for which the system is designed, which was presented in chapter 5.2 *Heat demand and heat supply*. In 2014, the measured specific space heating demand for this dwelling was 9,5 kWh/(m<sup>2</sup>·year). Space heating by means of heating of ventilation air was not monitored during the investigated periods, but during the design phase it was stipulated to 2,2 kWh/(m<sup>2</sup>·year) in the design phase. Thus, the maximum space heating demand for passive house buildings of 15 kWh/( m<sup>2</sup>·year) according to NS3700 is presumably achieved for the investigated dwelling. As for the heat demand required to cover the DHW consumption, it was estimated to be 1034 kWh/year, which equals a specific heat demand of 13,8 kWh/(m<sup>2</sup>·year). The latter constitutes less than half of the initially stipulated values.

It is important to keep in mind that the total heat demand may differ greatly for the various passive house dwellings, depending on numerous factors such as the number of inhabitants, the composition of users (adults/children, age), as well as the user's consciousness regarding own consumption and habits. An examination of selected user-related parameters in chapter 10.4 suggests that the performance of an identical solar thermal heating system in one of the other dwellings of Løvåshagen might either be suffering or benefitting from having a different heat demand than that of the investigated system.

Simulations revealed that a doubling in DHW consumption compared to the reference value resulted in an increase in annual specific delivered energy by as much as 35,1%. The corresponding increase in annual solar fraction was only 6,1%. Moreover, the annual solar fraction was much more sensitive towards a variation in annual space heating demand. This is presumably because the current space heating coil within the storage tank is located *above* the immersed electrical heating element. This means that unless the solar collectors supply the tank with temperatures above 75°C, only auxiliary energy is used for space heating. In other words, the solar thermal system installed in the passive house dwellings of Løvåshagen housing cooperative are not being used for the kind of system that this type of energy source is normally best suited for: preheating of DHW and low-temperature space heating.

### ***Variation in shading conditions***

It should be kept in mind that the other solar collectors installed on the roofs of the two passive house buildings may have different horizon profiles than the examined system, especially the ones located at the very south of the building. These are located on a slightly lower roof level than the investigated collectors, and are presumably more exposed to shading of nearby trees and hills. For them, the impact of shading from surrounding topography and potential obstructions might play an

even bigger role, and consequently the performance might be even lower. It may be worth considering the possibility of removing some of the nearby growth.

***Comments regarding measurements of another dwelling in the same housing cooperative***

In this master thesis, the main object of examination was the solar thermal heating system in one of the passive house dwellings. However, limited data from a second dwelling was obtained through Magnar Berge (co-supervisor). The floor area of this dwelling resembles that of the investigated dwelling (75 m<sup>2</sup>), and it is assumed that the two systems are identical both with respect to system design and to their operation. Despite this fact, direct readings from the second dwelling (attached in *Appendix A.2*) revealed the solar yield to be approximately 1080 kWh/year, which is 186% higher than that of the investigated system.

The main difference between the two dwellings is that the second dwelling is located on the 2<sup>nd</sup> floor (as opposed to on ground floor), and that the attached collectors are positioned at the front of the collector rows, i.e. mutual shading is eliminated. Compared to the investigated dwelling (reference system), measurements conducted on this second dwelling within the time period 28.05.13 – 18.06.14 revealed the following:

1. Heat demand for space heating: 160 % higher than that of the reference system
2. Heat demand for heating of DHW: 212 % higher than that of the reference system

The auxiliary energy consumption of the immersed electrical heater was not measured for the second dwelling, and the solar fraction could thus not be calculated. However, based on the already discussed findings in this report, it can be concluded that the higher solar yield in this dwellings is most likely caused by a combination of higher DHW demand, as well as reduced shading and a shorter pipe distance between the collectors and the storage tank. Moreover, it can be expected that the higher space heating demand significantly increases the auxiliary energy consumption.

Therefore, despite the higher solar yield for the second dwelling - and thus the seemingly better performance - an assumption should not yet be made that the solar fraction of this particular system is better than the system that was investigated in this master thesis.

## 12. Conclusion

---

The results revealed that the solar fraction measured in 2014 for the examined system was only 10,8%, whereas the corresponding simulated solar fraction was 14,3%. With the system's current design and operation, the benefits from having solar collectors compared to when only using a conventional heating system, are mainly present, though hardly significant, in May, June and July. On an annual basis, the energy savings constitute only 3,8%.

There are several contributing factors as to why neither the measured nor the simulated performance live up to the initial goals. Results from the parametric study of the various design- and operation parameters revealed that the performance of the system suffers from a combination of numerous factors, of which some are more influential than others. The parameters that had the greatest impact on system performance were: the switch-on temperature of the immersed electrical heating element, the position of the solar coil within the tank, the height of the solar coil, shading, and the location of the tank temperature sensor (used to control the solar pump). Regarding shading, particularly mutual shading caused by nearby collectors was crucial. Mutual shading is furthermore significantly affected by the collector inclination angle and the distance between the collector rows.

Several improved scenarios were suggested and simulated, until the scenario with the highest annual solar fraction and the lowest specific delivered energy to the heating system was obtained. The results revealed that the best outcome was attained when all of the main components were altered. These include: larger collector area, lower collector inclination angle, improved insulation of tank and pipes, changed locations of tank ports and coil positions, changed position of the tank temperature sensor used to control the solar pump, lower switch-on temperature setting of the auxiliary heater, and reduced pipe length of the solar circuit. Without the complete elimination of shading, the highest annual solar fraction and the lowest annual specific delivered energy to the heating system obtained were 38,9% and 23,8 kWh/m<sup>2</sup>, respectively. When including the elimination of shading, the corresponding values were 42,7% and 22,7 kWh/m<sup>2</sup>. This equals almost three times the solar fraction attained by the reference system. Moreover, a sensitivity analysis of the best scenario showed that an additional optimization of the various parameters is possible, which may increase the performance even further.

A limited scenario was created for the sake of studying the effect of changing only a few parameters that were assumed to be inexpensive and relatively easy to alter. This scenario involved lowering the inclination angle of the collectors from 51° to 30°, moving the tank temperature sensor further up in the tank, reducing the switch-on temperature of the electrical heating element from 75°C to 70°C, and, finally, insulating all the outdoor pipes with minimum 22 mm. The resulting solar fraction obtained in the simulations were 28,9%, which is more than twice



the solar fraction achieved in the initial system. Furthermore, these alterations reduced the specific delivered energy from 35,6 kWh/(m<sup>2</sup>·year) to 26,5 kWh/(m<sup>2</sup>·year).

A study of selected user-related parameters revealed that the total heat demand for space heating and heating of DHW strongly affects the auxiliary energy consumption, and that it may have negative impact on the annual solar fraction.

To conclude, the findings in this report suggest the presence of one or several faults in the design, the installation, and the operation of the investigated system. As a result, the performance of the system is significantly reduced, and is far from achieving the initially intended solar fraction of 47%. Furthermore, the results indicate a large potential for improvements, and that making alterations on the system is likely to help increase the solar contribution. It should be noted, however, that the fact that the system is already installed, makes an unlimited amount of changes neither physically possible, nor financially. Nevertheless, simulations reveal that by making only a few alterations, an increase in the utilization of solar energy may be achieved, both during summer and during the transitional periods.

## 13 Future work

---

If some of the suggested alterations are attempted implemented on the solar thermal heating systems of Løvåshagen housing cooperative (such as moving the tank temperature sensor and lowering the inclination angles of all the solar collectors on the roof) a continuation of measurements and monitoring would be advantageous for the sake of verifying their effect on system performance. Moreover, an evaluation of measurements from June and July 2015 should be conducted in order to determine whether or not the introduction of solar energy into the tank at two temperature zones in the modified system further improves the utilization of solar energy.

In this work, several aspects had to be considered, thus the process of understanding and analyzing the investigated solar thermal system turned out to be a comprehensive process. For this reason, certain elements remain to be considered for future reference:

The results of this report imply that through making improvements on all the main design- and operation parameters of the examined solar thermal heating system, the best annual solar fraction obtained was 42,7%. Simultaneously, a sensitivity analysis indicated that further improvements were possible. Due to the complexity of this kind of system, the development of an optimized system can be achieved by using more complicated mathematical models or more advanced simulation tools.

Seeing that this thesis focused mainly on the impact of various parameters on system performance, and not so much on costs and expenses, it would be of great value to conduct an economic analysis for the implementation of one or several of the suggested alterations in this study. A weighing of the benefits of higher solar energy utilization against increased costs should be done. One particular aspect is the possibility of replacing the existing storage tank as opposed to introducing a plate heat exchanger. An analysis of tanks available on the market could be made - both in terms of cost and performance -, followed by a suggestion of what is the tank most suitable for the solar thermal systems of Løvåshagen. Among the tanks that can be considered are mantled tanks, tanks with stratifier lances, tanks that are charged with solar energy at two temperature zones, separate tanks for DHW and for space heating, and, alternatively, a shared storage tank for all of the 28 dwellings.

It would be of interest if a study that focused on identifying the potential for using solar thermal heating in multi-storey residential buildings in Norway was conducted, according to Norwegian weather conditions, building regulations, building mass, esthetics, combination with other energy sources, the potential of shading, positioning of the collectors, etc. Moreover, a review of available surveillance systems on the market to be used for small solar thermal heating systems would be valuable, as well as an economical comparison of these.

## 14 References

---

- AEE Intec. (2004). *A planning handbook with a holistic approach*. Retrieved December 04, 2014, from <http://www.aee-intec.at/0uploads/dateien540.pdf>
- Andresen, I. (2008). *Planlegging av solvarmeanlegg for lavenergiboliger og passivhus. En introduksjon*. Oslo: Sintef Byggforsk
- Apricus. (2011). *Apricus OG-300 Solar Water Heating System Installation and Operation Manual*. USA: Apricus Inc
- Apricus Solar (2013). *Apricus Solar Collector Installation and Operation Manual - International Edition*. Apricus Solar Co., Ltd.
- Aquametro. (2015). *Selection guide for thermal energy measuring*. Retrieved June 01, 2015, from [www.aquametro.com/.../3850e\\_auswahlhilfe.pdf](http://www.aquametro.com/.../3850e_auswahlhilfe.pdf)
- Aquametro. (2015). *CALEC ST II. Multi-protocol heating and cooling energy calculator*. Retrieved May 28, 2015, from [http://www.aquametro.com/downloads/docs/3120e\\_calec-st-II.pdf](http://www.aquametro.com/downloads/docs/3120e_calec-st-II.pdf)
- Armacell Enterprise GmbH (n.d.) *Armaflex DuoSolar*. Retrieved on November 25, 2014, from [www.armacell.cn/%2FWWW%2Farmacell%2FAC](http://www.armacell.cn/%2FWWW%2Farmacell%2FAC)
- Dehghan, A., & Barzegar, A. (2010). *Thermal performance behavior of a domestic hot water solar storage tank during consumption operation*. Elsevier Ltd.
- Deutsche Gesellschaft für Sonnenenergie (DGS). (2010). *Planning and Installing Solar Thermal Systems. A guide for installers, architects and engineers*. London: Earthscan Ltd.
- Dokka, T.H., & Hermstad, K. (2006). *Energieeffektive boliger for fremtiden*. Trondheim: Skipnes Trykkeri.
- European Commission, J.R.C. (2015). *Photovoltaic Geographical Information System – Interactive Maps PVGIS*. Retrieved January 27, 2015, from <http://re.jrc.ec.europa.eu/pvgis/apps4/pvest.php>
- Folkehelseinstituttet. (2009). *Forebygging av legionellasmitte – en veiledning*. Retrieved June 04, 2015, from <http://www.fhi.no/dav/f7f3771daf.pdf>

- Fredriken, E., Godbolt, Å. L., Hauge, Å. L., Kristjansdottir, T., Lekang, Å. S., & Sørnes, K. (2014). *Suksessfaktorer for økt bruk av solvarme*. Oslo: SINTEF akademisk forlag.
- Halvorsen, U. M., Bernhard, P., Salvesen, F., Bugge, L., Andresen, I., & Simonsen, I. (2011). *Mulighetsstudie Solenergi i Norge*, Oslo: SINTEF Byggforsk, KanEnergi.
- Han, Y. M., Wang, R. Z., & Dai, Y.J. (2008). *Thermal stratification within the water tank*. Shanghai: Shanghai Jiao Tong University.
- Institut für Solartechnik (SPF). (2004). *Solar Collector Factsheet: SPF-Nr. C632*. Retrieved December 12, 2014, from <http://cieplozziemi.pl/LinkClick.aspx?fileticket=8VBOGDILaT4%3D&tabid=230>
- Kalogirou, S. A. (2004). *Solar thermal collectors and applications*. Elsevier Ltd.
- Keizer, C., (2012). *Simulation-based long-term fault detection of solar thermal systems*. Kassel: Kassel University press GmbH.
- Klinski, M., Thomsen, J., Hauge, Å. L., Jerkø, S., & Dokka, T. H. (2012). *Prosjektrapport 90 – 2012. Systematisering av erfaringer med passivhus*. Oslo: SINTEF akademisk forlag
- Lavenergiprogrammet. (2013). *Prosjektering av passivhus. 3. Utgave*. Oslo: Lavenergiprogrammet
- Meteorologisk Institutt. (2009). *MetLex: Soltimer*. Retrieved November 14, 2014, from <https://metlex.met.no/wiki/Soltid>
- Meteotest (2015). *Meteonorm Features*. Retrieved on April 04, 2015, from <http://meteonorm.com/>
- Nesland, O. (2010). *Energibruk og inn klima i passiv- og lavenergihus* (Master thesis, NTNU). Trondheim: NTNU
- Northpass (2011). *Løvåshagen Borettslag, Bergen*. Retrieved on October 05, 2014, from <http://northpass.ivl.se/search.4.7df4c4e812d2da6a416800033125.html?query=l%C3%B8v%C3%A5shagen&submit=Search>
- Quaschnig, V. (2004). *Solar thermal water heating*. Retrieved November 20, 2014, from [http://www.volker-quaschnig.de/articles/fundamentals4/index\\_e.php](http://www.volker-quaschnig.de/articles/fundamentals4/index_e.php)

- Quaschnig, V., (2005). *Understanding Renewable Energy Systems*. London: Earthscan
- Rindal, L.B., & Salvesen, F. (2008). *Solenergi for varmeformål – snart lønnsomt?*. Oslo: KanEnergi, NVE
- Standard Norge. (1999). *NS-EN ISO 9488:1999 Solar energy vocabulary*. Oslo: Standard Norge
- Standard Norge. (2006). *NS-EN 12976-1: 2006 - Thermal solar systems and components. Factory made system. Part 1: General requirements*. Oslo: Standard Norge
- Standard Norge. (2012). *NS-EN 12977-2: 2012 - Thermal solar systems and components – Custom built systems. Part 2: Test methods for solar water heaters and combisystems*. Oslo: Standard Norge
- Standard Norge. (2014). *NS 3031: 2014 - Calculation of energy performance of buildings. Method and data*. Oslo: Standard Norge
- Standard Norge. (2013). *NS3700: 2013 - Criteria for passive houses and low-energy buildings. Residential buildings*. Oslo: Standard Norge
- Tyforop Chemie GmbH. (2009). *Tyfocor L – Technical information*. Retrieved January 16, 2014, from <http://www.resol.de/Produkt dokumente/TYFOCOR-L.daten.pdf>
- Vela Solaris. (2014). *Photovoltaics, Solar Thermal and Geothermal – with Polysun you get everything in one tool!* Retrieved on November 05, 2014, from <http://www.velasolaris.com/english/product/overview.html>
- Vela Solaris. (2014). *Design and enhance your system with Polysun, the leading simulation software for solar thermal systems*. Retrieved October 14, 2014, from [http://www.velasolaris.com/files/solarthermal\\_e\\_digital.pdf&ei=3jqQVdzkAYHusgGmsYuICg&usg=AFQjCNH66tUX1F8C76BJfNr6uSW9FyO1KA&sig2=MEATx6WfuN4V3tUp3J4SOQ&bvm=bv.96783405,d.bGg](http://www.velasolaris.com/files/solarthermal_e_digital.pdf&ei=3jqQVdzkAYHusgGmsYuICg&usg=AFQjCNH66tUX1F8C76BJfNr6uSW9FyO1KA&sig2=MEATx6WfuN4V3tUp3J4SOQ&bvm=bv.96783405,d.bGg)
- Vela Solaris. (2014). *Polysun simulation software. User manual*. Retrieved on January 18, 2015, from [http://www.velasolaris.com/files/tutorial\\_en.pdf](http://www.velasolaris.com/files/tutorial_en.pdf)
- Pressebox. (2014). *New Polysun 5.8: nearby shading and visualization of controller connections*. Retrieved on December 18, 2014, from <http://www.pressebox.com/pressrelease/vela-solaris-ag/New-Polysun-58-nearby-shading-and-visualization-of-controller-connections/boxid/471796>

Wigenstad, T. (2009). *Prosjektrapport 39: Prosjektveileder. Forenklet anlegg for vannbåren oppvarming av boliger*. Oslo: SINTEF Byggforsk

Wilo. (2004). *Wilo Standard Pumps – Product Overview*. Retrieved on February 23, 2015, from [www.apper-solaire.org/%2FPages%2FGroupement%2FWiloStarST20-6.pdf&ei=plCdVdT-POHfywP1hIHYCg&usg=AFQjCNELJQZzdQOAaEyTJ5PVzNSTFATxfw&sig2=lhmySLydkQvk61zPnQ7nJA&bvm=bv.96952980,d.bGg](http://www.apper-solaire.org/%2FPages%2FGroupement%2FWiloStarST20-6.pdf&ei=plCdVdT-POHfywP1hIHYCg&usg=AFQjCNELJQZzdQOAaEyTJ5PVzNSTFATxfw&sig2=lhmySLydkQvk61zPnQ7nJA&bvm=bv.96952980,d.bGg)

WiSensys. (n.d.). *Products*. Retrieved October 25, 2014, from <http://www.wisensys.com/products>

WiSensys. (n.d.). *Wireless Measurement Platform*. Retrieved April 04, 2015, from <http://www.eurias.nl/pdf/WiSensys.pdf>

Zijdemans, D. (2012). *Vannbaserte oppvarmings- og kjølesystemer*. Oslo: SkarlandPress.

## Appendix A – Measured data

### A.1 Remote readings

Table A. 1: Measured results from 2014 (annual sums) - Remote readings 01.01.14 – 31.12.14

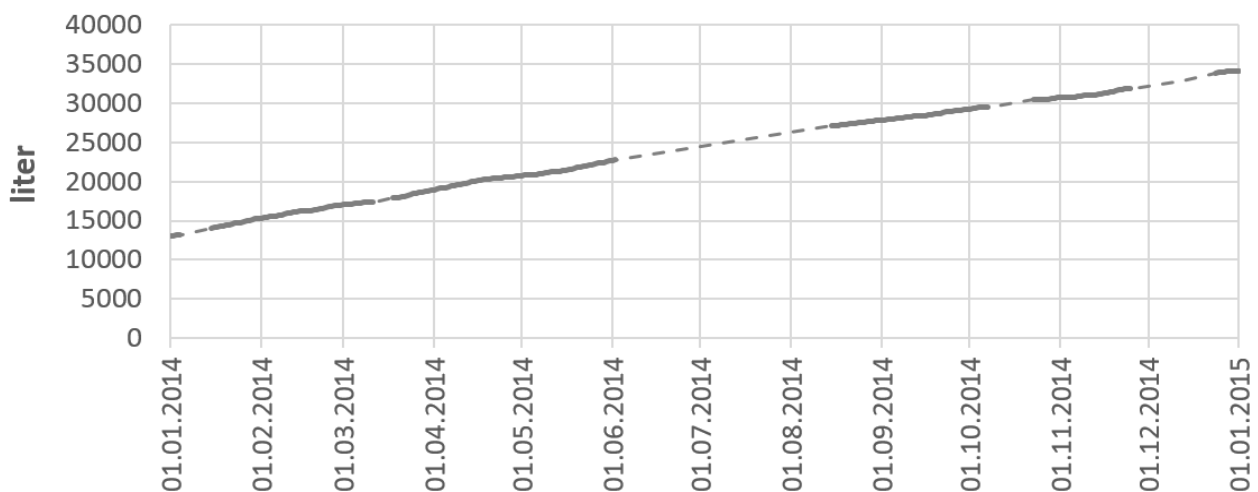
Radiator	Floor heating	DHW consumption	Electrical heating element (tank)	Solar energy supplied to tank
[kWh]	[kWh]	[l]	[kWh]	[kWh]
-	449,3	21052	3098	699

Table A. 2: Measured results from 2015 – Remote readings 01.01.15 – 31.05.15

Radiator	Floor heating	DHW consumption	Electrical heating element (tank)	Solar energy supplied to tank
[kWh]	[kWh]	[l]	[kWh]	[kWh]
-	204	10747,2	1825,8	177,4

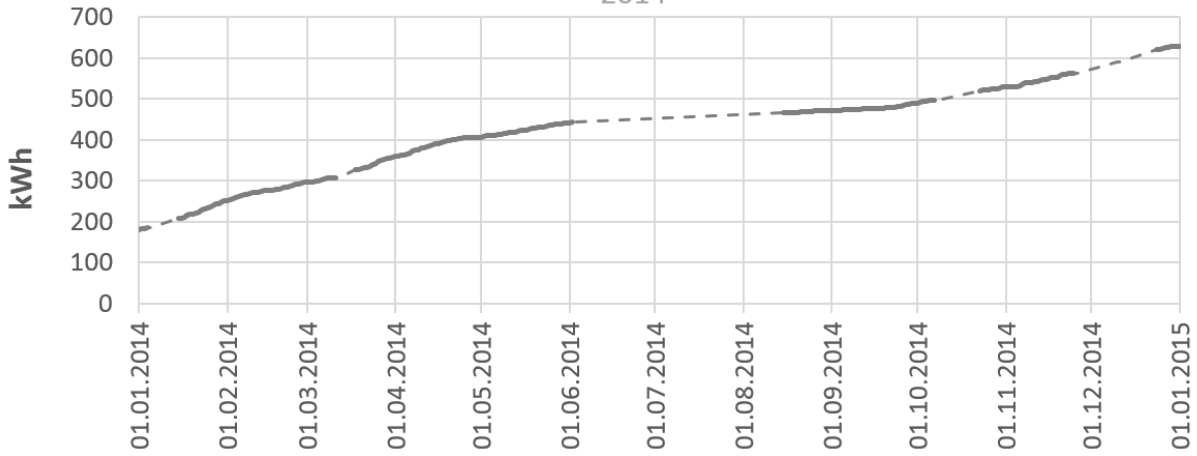
\*1 m<sup>3</sup> water =1000 l

Measured DHW consumption 2014



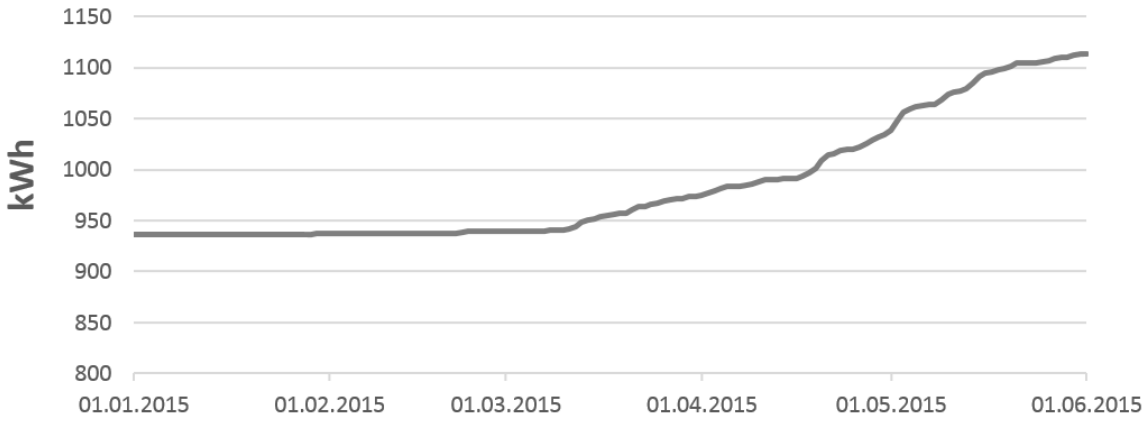
### Measure heat demand for floor heating

2014



### Measured solar energy supplied to tank

01.01.15 - 01.06.15



### Measured auxiliary energy supplied to tank

01.01.15 - 01.06.15

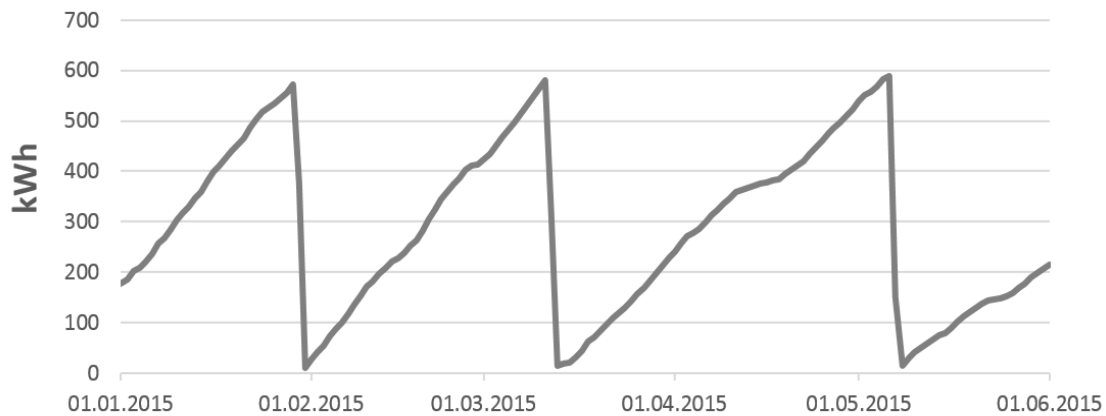


Figure A. 1 Remote readings 2014 and 2015



## A.2 Direct readings

Table A. 3: Direct readings of the meter displays during six plant visits

Date	Radiator consumption [kWh]	Floor heating consumption [kWh]	Solar energy supplied to tank [kWh]	DHW consumption [m <sup>3</sup> ]
13.05.2013	7,5	0,5	-	0,768
15.05.2013	7,5	0,5	-	0,768
11.11.2013	28,3	83,6	236	10,77
19.11.2014	292,9	558,4	613	32,336
29.01.2015	458,4	673,3	613	37,025
10.03.2015	597,2	734,5	617	39,987
04.06.2015	677,4	837,7	793	45,907

Table A. 4: Extracted values from Table A.3: Direct readings 11.11.13 – 19.11.14

Radiator [kWh]	Floor heating [kWh]	DHW consumption [m <sup>3</sup> ]	Electrical heating element (tank) [kWh]	Solar collector yield [kWh]
264,6	474,8	21,566	<i>Direct reading not possible</i>	377

Table A. 5: Measurements from a second passive house dwelling (28.05.2013 – 18.06.2014)

	Space heating	DHW	Electrical heating element (tank)	Solar collector yield
kWh	2216,8	2688,6	-	1080,0
kWh/(m <sup>2</sup> year)	29,6	35,8	-	14,4

### A.3 Weather data for 2014 and 2015

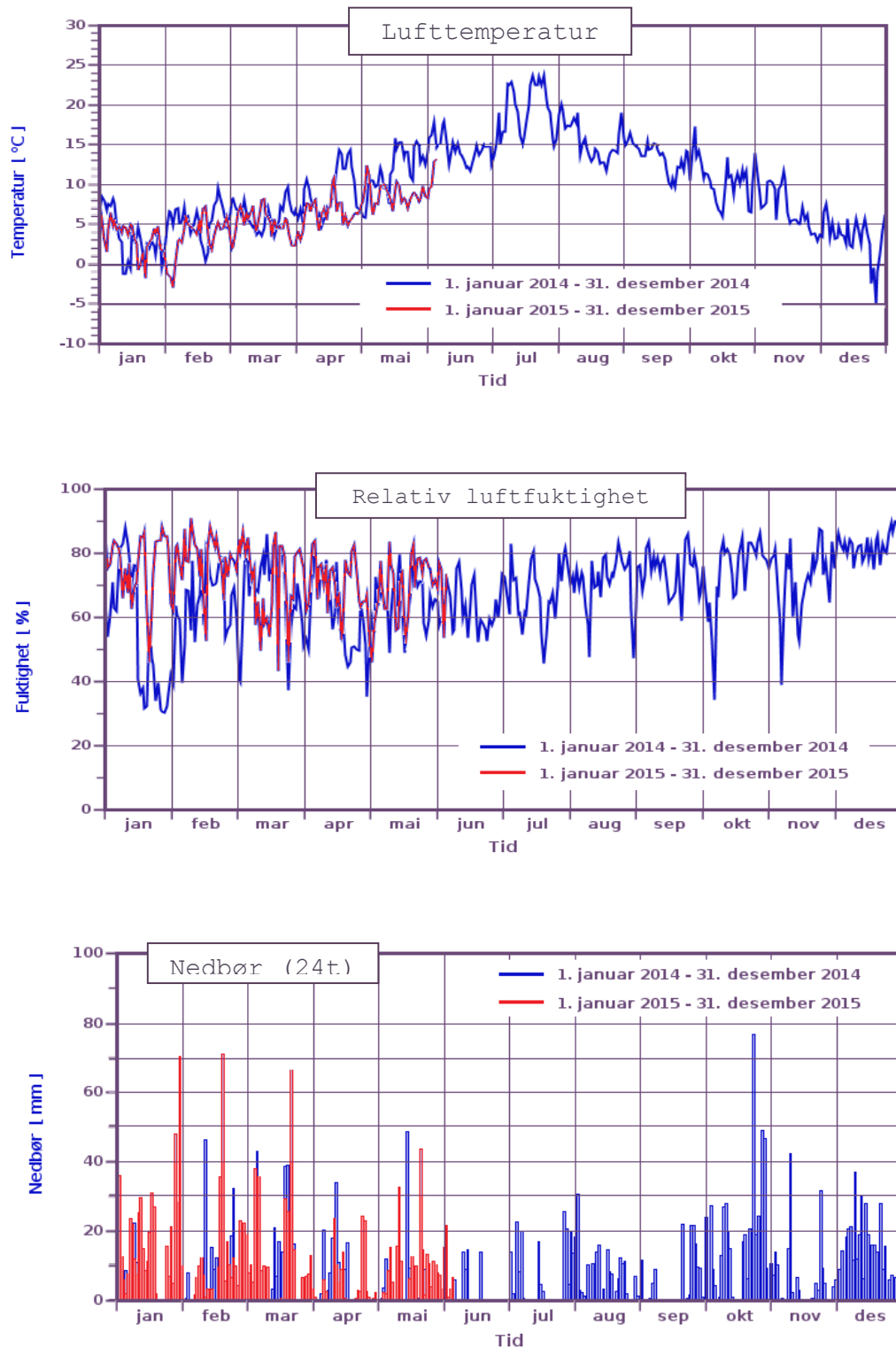



Figure A. 2: Daily mean air temperature, daily mean air humidity (%) and daily precipitation in Bergen for 2014 (blue) and 2015 (red) *Source: Meteorologisk institutt*


# Appendix B - Detailed component specifications

## B.1 Collector

### Technical specifications for Apricus AP-20



**Solar Collector Factsheet: SPF-Nr. C632**



<b>Model</b>	<b>AP-20</b>
<b>Type</b>	Tube collector
<b>Manufacturer</b>	Focus Technology Co., Ltd
<b>Address</b>	13th Floor Unicom Mansion 32 Zhong Yang Road CN-210008 Jiangsu
<b>Telephone</b>	+86 (0)25 3606934
<b>Fax</b>	+86 (0)25 3213395
<b>E-Mail</b>	sales@apricus-energy.com
<b>Internet</b>	www.apricus-energy.com
<b>Sales area</b>	CH,EU,US,CA,AU,ME,NZ

Performance test EN 12975  
 Quality test EN 12975

**Dimensions**

<b>Total length</b>	1.929 m
<b>Total width</b>	1.496 m
<b>Empty weight with glass</b>	63 kg
<b>Liquid content</b>	0.58 l
<b>Aperture area</b>	1.876 m <sup>2</sup>
<b>Absorber area</b>	1.606 m <sup>2</sup>
<b>Gross area</b>	2.886 m <sup>2</sup>

**Technical data**

<b>Minimum volume flow rate</b>	120 l/h
<b>Recommended volume flow rate</b>	120 l/h
<b>Maximum volume flow rate</b>	600 l/h
<b>Maximum operating pressure</b>	6 bar
<b>Maximum operating temperature</b>	250 °C
<b>Stagnation temperature</b>	245 °C
(Ta = 30°C, G = 1000 W/m <sup>2</sup> )	

**Types of mounting**

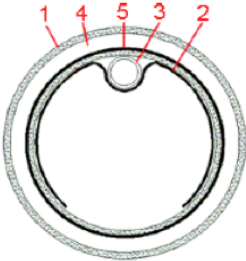
Construction for flat roof  
 Integration into sloped roof  
 Construction for sloping roof  
 Front mounting

**Further data**

Variable module size  
 Glazing replaceable

**Hydraulic connections**  
Copper pipe, nominal diameter 22 mm

**Construction**



**Element list and Nomenclature**

- 1 Glazing
- 2 Heat-conducting metal sheet
- 3 Heat pipe
- 4 Vacuum
- 5 Absorber

Institut für Solartechnik SPF, HSR Hochschule für Technik Rapperswil, Oberseestrasse 10, CH-8640 Rapperswil, Switzerland  
05.05.04 www.solarenergy.ch Page 1 of 2

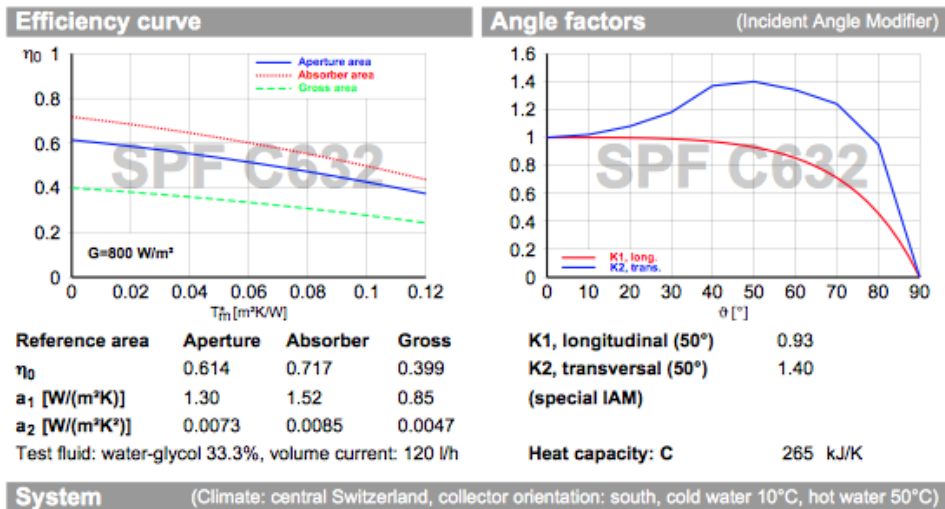


Figure B. 1: Test report for the Apricus AP-20 collector (SPF, 2004)

## B.2 Storage tank

Table B. 1: Technical specification for the storage tank and the two coils

Storage tank		
Volume	290	l
Height	1,6	m
Wall		
Material	Stainless steel (1.4521)	
Wall thickness	1,5	mm
Insulation		
Material	Mineral wool	
Insulation thickness	40	mm
Solar heat exchanger (internal coil)		

Pipe diameter		
Inner diameter	22	mm
Outer diameter	25	mm
Pipe length	9	m
Pipe surface area	0,8	m <sup>2</sup>
Bending radius	140	mm
Material	Stainless steel 1.4401	
<b>Space heating coil</b>		
Pipe diameter		
Inner diameter	22	mm
Outer diameter	25	mm
Pipe length	3	m
Pipe surface area	0,28	m <sup>2</sup>
Bending radius	140	mm
Material	Stainless steel 1.4401	

**Table B. 2: Thermal properties of selected stainless steel types. Source: Norwegian Standard NS-EN 10088-1:2004, Stainless steels - Part 1: List of stainless steels**

	Material		Density [kg/dm <sup>3</sup> ]	Thermal conductivity at 20°C [W/(mK)]	Specific thermal capacity at 20°C [J/(kgK)]
	Type	Designation number			
<b>Tank</b>	Stainless steel	1.4521	7,7	23	430
<b>Internal coils</b>	Stainless steel	1.4401	8	15	500

## B.3 Solar circuit

### B.3.1 Solar pump

**Table B. 3: Extract of technical pump data for Wilo Star ST 20/6 (Wilo, 2004)**

<b>Operating modes</b>	Speed-stage switching
<b>Manual functions</b>	Adjustment of speed (manual setting mode) Adjustment of speed stages: 3
<b>Approved fluids</b>	Water/glycol mixtures (max 1:1; mixtures with more than 20% glycol content require rechecking of the pumping data)
<b>Performance</b>	
Max. delivery head	6 m
Flow rate max.	3,5 m <sup>3</sup> /h
Speed range	1500 – 2500 rpm

---

**Permitted field of application**

Temperature range for use in heating,  
ventilation and A/C systems at max.  
ambient temperature of +40°C

-10 to 110 (short-time duty 2h: +120)

Standard version for operating pressure

10 bar

$p_{\max}$ :

---

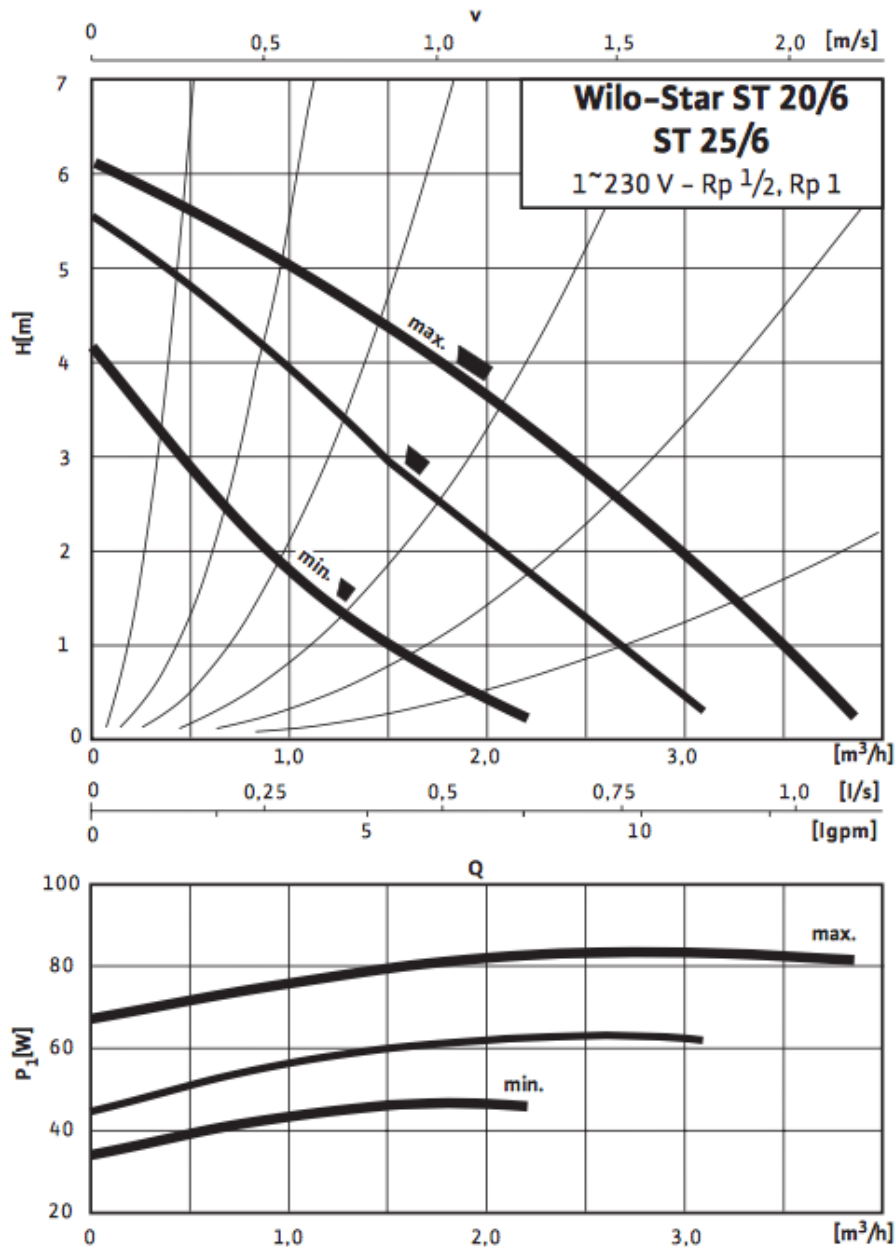


Figure B. 2: Pump curves for Wilo Star ST 20/6. 3 levels: high (max.), medium and low (min.) (Wilo, 2004)

### B.3.2 Pipelines

The solar loop consists of pre-insulated copper pipes of the type Armaflex DuoSolar Cu with HT/Armaflex protected with an outer film (made of polyolefin copolymer). An illustration of this particular type and some of its benefits according to the manufacturer is shown in Figure B.3.

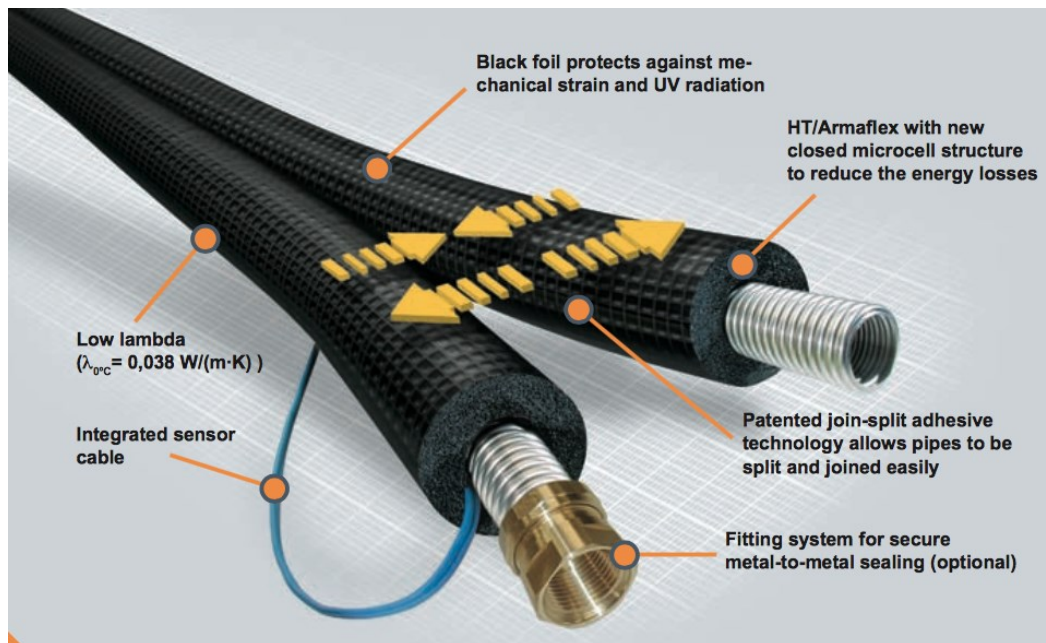


Figure B. 3: Pre-insulated pipes (Armacell, n.d)

Table B. 4: Properties of Armaflex DuoSolar Cu (Armacell, n.d)

Properties	Value/Assessment
<b>Temperature range</b>	
Max. service temperature	+ 150°C (+175°C)
Min. service temperature	-50°C
<b>Thermal conductivity <math>\lambda</math></b>	
At 0°C	$\leq 0,038 \text{ W/(mK)}$
At 40°C	$\leq 0,042 \text{ W/(mK)}$
<b>Reaction to fire</b>	Material class B2
<b>Water vapour diffusion resistance factor <math>\mu</math></b>	$\geq 4000$
<b>Special features</b>	Halogen free, resistant to UV radiation, CFC and HCHC-free, fulfills DIN 1988 Parts 2 and 7

### B.3.3 Solar liquid

**Table B. 5: Thermal properties of Tyfocor L (Tyforop, 2009)**

<b>Tyfocor L content [% vol.]</b>	<b>Density at 20°C [g/cm<sup>3</sup>]</b>	<b>Refractive index nD20</b>	<b>Frost protection [°C]</b>
<b>25</b>	1,023	1,3627	-10
<b>30</b>	1,029	1,3690	-14
<b>35</b>	1,033	1,3747	-17
<b>40</b>	1,037	1,3801	-21
<b>45</b>	1,042	1,3855	-26
<b>50</b>	1,045	1,3910	-32
<b>55</b>	1,048	1,3966	-40



# Appendix C – Parametric study

## C.1 Design parameters

### C.1.1 Effect of inclination and orientation angle of the investigated collectors

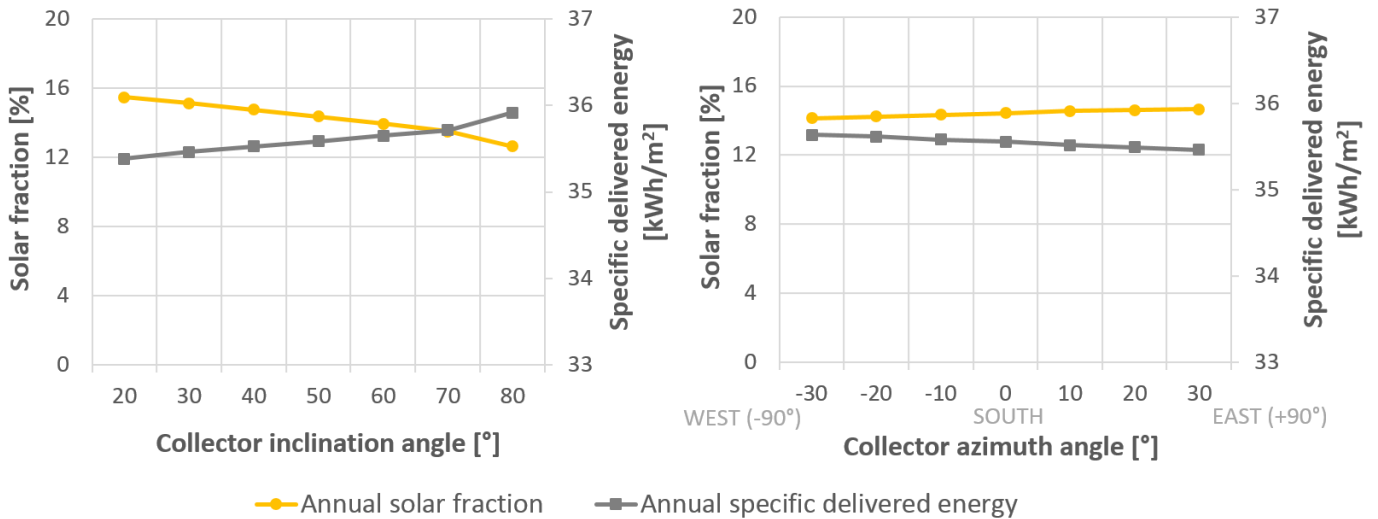


Figure C. 1: The effect of collector orientation (left) and inclination (right) angle on system performance

### C.1.2 Effect of solar coil material

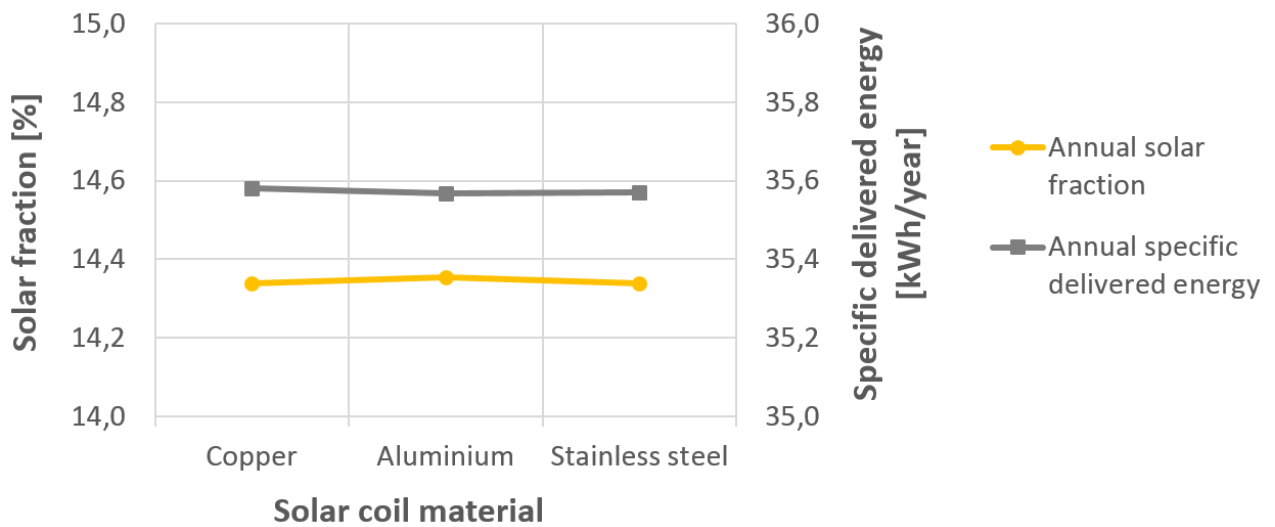


Figure C. 2: Effect of solar coil material on system performance

### C.2.3 Effect of propylene glycol concentration in solar liquid

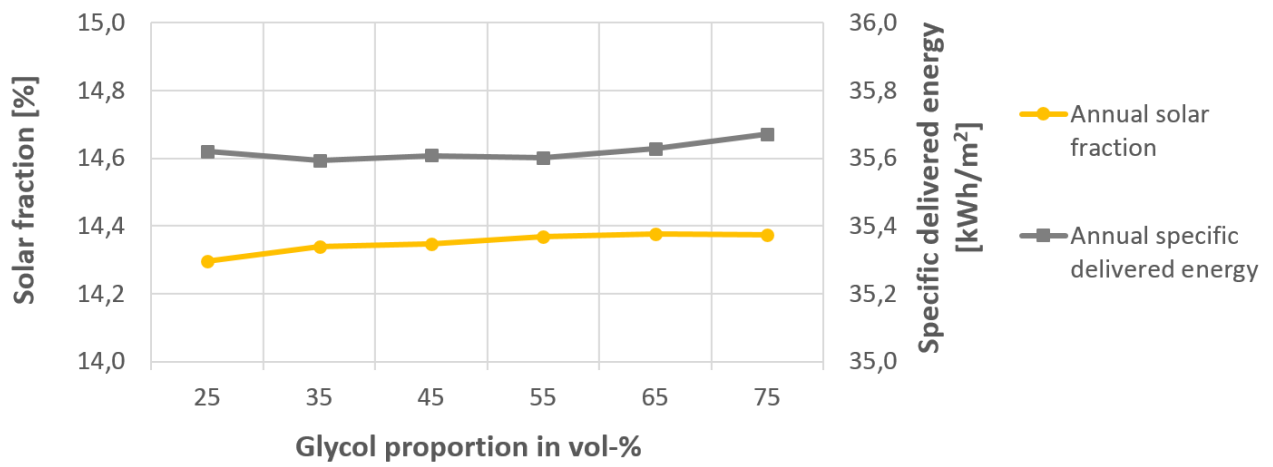


Figure C. 3: Effect of glycol percentage in solar liquid on system performance